

Copyright

by

Martin Joseph Donovan

2011

**The Dissertation Committee for Martin Joseph Donovan Certifies that this is the approved version of the following dissertation:**

**Influence of Carrier Particle Size and Surface Roughness on the Aerosol Performance of DPI Formulations**

**Committee:**

---

Hugh D.C. Smyth, Supervisor

---

Robert O. Williams

---

Jason T. McConville

---

Nathan Wiederhold

---

Venkatramanan Raman

**Influence of Carrier Particle Size and Surface Roughness on the  
Aerosol Performance of DPI Formulations**

**by**

**Martin Joseph Donovan, B.S.**

**Dissertation**

Presented to the Faculty of the Graduate School of

The University of Texas at Austin

in Partial Fulfillment

of the Requirements

for the Degree of

**Doctor of Philosophy**

**The University of Texas at Austin**

**August 2011**

**Dedication**

*Para mi mama y mi papa*

## ACKNOWLEDGEMENTS

First and foremost, I would like to express an extreme debt of gratitude to my advisor, Hugh Smyth, for his considerable and continued support throughout my (prolonged) tenure in his lab. Our ‘excellent pharmaceutical adventure’ that commenced in New Mexico and concluded in Texas had its share of frustrating and aggravation-inducing moments, but overall it was thoroughly enjoyable (at least I speak for myself) and informative; I sincerely doubt it would have turned out as successful had I joined anyone else’s lab at UNM.

I would also like to acknowledge Professor Venkat Raman and Shaun Kim, for their expertise and considerable efforts using computational fluid dynamics to visualize carrier particle trajectories through DPIs (Chapter 5). This was a very informative study, mostly I think, due to their contribution. Additionally, this project was advanced considerably by the extensive contributions of both Vincent Agustin at UNM and Y Vo at UT, both of whom greatly facilitated many of the studies and expedited the completion of this research. I would also like to express my gratitude to Respira Therapeutics in general for granting me the opportunity to continue working on the large carrier project, and to Dr. Jack Pappo in particular for his continued support and advice throughout my tenure with the company.

Last and certainly not least, I would like to thank Stephen Marek, for taking time off from climbing rocks and corralling cats to apply his instrumental expertise to greatly facilitate collecting the vast array of physicochemical data that is presented herein. His help expedited these extremely tedious measurements, allowing me to return to the aspect of research I found most enjoyable: performing a mind-numbing amount of cascade impactions, which for some strange reason, most people consider the height of tedium.

# **Influence of Carrier Particle Size and Surface Roughness on the Aerosol Performance of DPI Formulations**

Martin Joseph Donovan, Ph.D.

The University of Texas at Austin, 2011

Supervisor: Hugh Smyth

The influence of the size and morphology of carrier particles on drug dispersion performance from passive dry powder inhalers has been extensively studied topic, and a consensus has been reached regarding the adverse effect that larger carrier particle diameters impart to aerosol performance. However, previous studies have generally employed only a few carrier particle size fractions, generally possessing similar surface characteristics. Accordingly, theories developed to explain the influence of the physical characteristics of carrier particles on performance relied heavily on both extrapolation and interpolation. To fill in the gaps from the literature and simultaneously evaluate the influence of carrier particle size and morphology, a comprehensive study was undertaken using 4 lactose grades, each sieved into 13 contiguous sizes, to prepare 52 formulations incorporating a unique lactose grade-size population. The aerosol performance results indicated that large carrier particles possessing extensive surface roughness can improve drug dispersion, in contrast to what has been previously reported. It is proposed that this may be attributed to mechanical detachment forces arising from collisions between the carrier particle and inhaler during actuation.

Based on these observations, a novel dry powder inhaler platform was developed, employing carrier particles much larger ( $> 1$  mm) than previously explored in both the scientific and patent literature. Optimization of this technology required the judicious selection of a carrier material, and following an extensive screening process, low-density polystyrene was selected as a model candidate. Given its low mass, diameters in excess of 5-mm could be employed as carriers while still generating high detachment forces. To minimize drug particle aggregation, a novel drug-coating method employing piezo-assisted particle dispersion was developed to compensate for the reduced surface area of the novel carrier particles. In addition, the selection of a suitable inhalation device prototype was instrumental to the overall performance of the technology. *In vitro* testing of the novel large carrier particles yielded emitted fractions in excess of 85%, and overall drug delivery of up to 69% of the loaded dose.

# Table of Contents

<b>TABLE OF FIGURES</b>	<b>xii</b>
<b>TABLE OF TABLES</b>	<b>xvi</b>
<b>CHAPTER 1</b>	<b>1</b>
1. Introduction.....	1
1.1. Pulmonary Drug Delivery.....	1
1.2. Dry Powder Inhalers.....	2
1.3. Traditional DPI Formulations.....	3
1.4. Particle Engineering Technologies.....	4
1.5. Parameters Governing Performance of Binary Blends.....	5
1.6. Mechanism of Drug Detachment From Carrier Particles.....	7
1.7. Mechanical Detachment Forces.....	7
1.8. Detrimental Influence of Large Carrier Particles to Aerosol Performance.....	8
1.9. Theoretical Particle-Particle Adhesion Forces.....	8
1.10. Press-on Forces.....	10
1.11. Surface Roughness.....	14
1.12. Surface Area.....	15
1.13. Reduction in Fraction of Fine Lactose.....	16
1.14. Surface Energy.....	18
1.15. Summary.....	19
1.16. Mechanisms of DPI Performance.....	19
1.17. Turbulence Inducement.....	20

1.18. Mechanical Forces .....	21
1.19. Pneumatic Forces.....	22
1.20. Sustained Exposure to Flow Stream .....	23
1.21. Vibration Induced Dispersion .....	26
1.22. Electric and Magnetic Fields .....	28
1.23. Device Resistance and Flow Rate.....	29
1.24. Meshes and Screens .....	31
1.25. Summary .....	32
1.26. Conclusion.....	33
1.27. REFERENCES.....	34
<b>CHAPTER 2</b>	<b>45</b>
2. Research Objectives.....	45
<b>CHAPTER 3</b>	<b>51</b>
3. Comprehensive Study on the Influence of Size and Morphology of Lactose Carrier Particles on the Aerosol Performance of Binary DPI Formulations.....	51
3.1. INTRODUCTION.....	51
3.2. EXPERIMENTAL .....	53
3.3. RESULTS AND DISCUSSION .....	56
3.4. CONCLUSION.....	64
3.5. REFERENCES.....	65



<b>CHAPTER 4</b>	<b>80</b>
4. Influence of Carrier Particle Diameter and Surface Roughness on the Performance of Binary DPI Formulations .....	80
4.1. INTRODUCTION.....	80
4.2. EXPERIMENTAL .....	81
4.3. RESULTS .....	83
4.4. DISCUSSION .....	86
4.5. CONCLUSIONS.....	95
4.6. References .....	97
 <b>CHAPTER 5</b>	 <b>112</b>
5. Performance of Dry Powder Inhalers as a Function of the Diameter and Surface Roughness of the Carrier Particle Population .....	112
5.1. INTRODUCTION.....	112
5.2. EXPERIMENTAL .....	114
5.3. RESULTS AND DISCUSSION .....	117
5.4. CONCLUSION.....	126
5.5. References .....	128
 <b>CHAPTER 6</b>	 <b>145</b>
6. Influence of Flow Rate on Binary DPI Formulations as a Function of Carrier Particle Diameter and Surface Roughness.....	145
6.1. INTRODUCTION.....	145
6.2. EXPERIMENTAL .....	147
6.3. RESULTS AND DISCUSSION .....	149
6.4. CONCLUSION.....	155

6.5. References .....	156
<b>CHAPTER 7</b>	<b>166</b>
7. Development of a Novel Dry Powder Dispersion Mechanism for Pulmonary Drug Delivery Part 1: Carrier Particle Material Selection .....	166
7.1. INTRODUCTION .....	166
7.2. EXPERIMENTAL .....	171
7.3. RESULTS AND DISCUSSION .....	173
7.4. CONCLUSION .....	179
7.5. REFERENCES .....	181
<b>CHAPTER 8</b>	<b>194</b>
8. Development of a Novel Dry Powder Dispersion Mechanism for Pulmonary Drug Delivery, Part 2: Optimization of the Dispersion Mechanism and Coating Method	194
8.1. INTRODUCTION .....	194
8.2. EXPERIMENTAL .....	198
8.3. RESULTS AND DISCUSSION .....	200
8.4. Piezo-Assisted Coating (PAC) .....	204
8.5. Modulating Drug Coating .....	205
8.6. CONCLUSIONS .....	206
8.7. REFERENCES .....	208
<b>CHAPTER 9</b>	<b>220</b>
9. Refinement and Optimization of Large Carrier Particle Dispersion Technology ..	220
9.1. INTRODUCTION .....	220
9.2. EXPERIMENTAL .....	221

9.3. RESULTS AND DISCUSSION .....	226
9.4. CONCLUSION.....	231
9.5. REFERENCES.....	233
<b>CHAPTER 10</b>	<b>250</b>
10. Design, Development, and Testing of Prototype Inhaler Devices to Optimize Aerosol Performance from Drug-Coated Polystyrene Carrier Particles .....	250
10.1. INTRODUCTION.....	250
10.2. EXPERIMENTAL .....	253
10.3. RESULTS AND DISCUSSION .....	256
10.4. CONCLUSION.....	264
10.5. REFERENCES.....	265
<b>CHAPTER 11</b>	<b>285</b>
11. Final Conclusions .....	285
<b>APPENDIX</b>	<b>288</b>
1. Reported Literature Values of DPI Performance .....	288
1.1. Appendix References .....	298
<b>REFERENCES</b>	<b>308</b>
<b>VITA</b>	<b>319</b>

## TABLE OF FIGURES

Figure 1.1. Influence of Carrier Particle Size on Theoretical van der Waals Forces .....	44
Figure 3.1. SEM Images of $\alpha$ -lactose monohydrate. ....	69
Figure 3.2. SEM Images of anhydrous lactose.....	70
Figure 3.3. SEM Images of spray dried lactose.....	71
Figure 3.4. SEM Images of granulated lactose. ....	72
Figure 3.5. <i>In vitro</i> Aerosol Performance from the Fractionated Lactose Carrier Particle Populations.....	73
Figure 4.1. SEM Images of Anhydrous and Granulated Lactose Carrier Populations .....	100
Figure 4.2. SEM Images of Uncoated and Coated Carrier Particles .....	101
Figure 4.3. Decline in Specific Surface Area as Carrier Particle Size is Increased.....	102
Figure 4.4. AFM Images of Anhydrous Lactose Carrier Particles.....	103
Figure 4.5. RF values from Anhydrous Lactose Carrier Particles.....	104
Figure 4.6. RF values from Granulated Lactose Carrier Particles .....	105
Figure 4.7. Mechanisms of Drug Particle Detachment from 'Smooth' and 'Rough' Carriers.....	106
Figure 4.8. Aerosol Performance of AN and GR Formulations .....	107
Figure 4.9. MMAD Values of Budesonide Dispersed from Anhydrous and Granulated Carriers	108
Figure 5.1. SEM Images of Anhydrous and Granulated Lactose Carrier Particle Populations ...	133
Figure 5.2. Schematic views of the Handihaler® (left) and Aerolizer® dry powder inhalers.....	134
Figure 5.3. Contour of Velocity Magnitude Inside Handihaler (left) and Aerolizer (right).....	135
Figure 5.4. Carrier particle trajectory inside the Aerolizer at 60 L min <sup>-1</sup> .....	136
Figure 5.5. Carrier particle trajectory inside the Handihaler at 60 L min <sup>-1</sup> .....	137
Figure 5.6. Ratio of Fine Particle Fraction Values from the Aerolizer and Handihaler.....	138

Figure 5.7. <i>In vitro</i> Performance of Anhydrous and Granulated Carrier Formulations.....	139
Figure 5.8. MMAD Values of Budesonide Dispersed from the Handihaler and Aerolizer .....	140
Figure 6.1. SEM Images of $\alpha$ -Lactose Monohydrate and Granulated Lactose Carrier Particles	158
Figure 6.2. Aerosol Performance of Salbutamol Sulphate Blends with Increasing Flow Rate ...	159
Figure 6.3. Aerosol Performance of Budesonide Blends with Increasing Flow Rate .....	160
Figure 6.4. Aerosol Performance as a Function of Carrier Particle Surface Roughness.....	161
Figure 6.5. Slope of Respirable Fraction Improvement with Increasing Flow Rate .....	162
Figure 7.1. Predicted Mesh Interactions for Small and Large Carrier Particles.....	184
Figure 7.2. <i>In vitro</i> Aerosol Performance of Budesonide-Coated Polystyrene Beads .....	185
Figure 7.3. <i>In vitro</i> Aerosol Performance of Budesonide-Coated Sucrose Beads .....	186
Figure 7.4. <i>In vitro</i> Aerosol Performance of Budesonide-Coated Silica Beads.....	187
Figure 7.5. <i>In vitro</i> Aerosol Performance of Budesonide-Coated Glass Beads.....	188
Figure 7.6. Influence of Flow Rate on the Performance of Drug-Coated Beads .....	189
Figure 7.7. Blending-Time Studies of Budesonide-Coated Polystyrene, Silica, and Glass Beads	190
Figure 7.8. Blending Additive Studies of Budesonide-Coated Polystyrene Beads .....	191
Figure 8.1. Illustration of Powder Motion during Blending in a Turbula® Orbital Mixer. ....	211
Figure 8.2. Aerosol Performance of Budesonide-Coated Polystyrene Beads from the Aerolizer and Handihaler DPIs .....	212
Figure 8.3. Sudden Expansion of a Flow Stream (Adapted from Gupta, et al, 1984).....	213
Figure 8.4. Static Pressure Contours Across the Handihaler Dispersion Chamber at 30, 45, and 60 L min <sup>-1</sup> . ....	214
Figure 8.5. Illustration of Piezo-Assisted Coating (PAC) Process for Coating Polystyrene Beads	215
Figure 8.6. SEM Images of Uncoated Polystyrene Beads, and Beads Coated with Budesonide via Standard Blending or with the PAC Method. ....	216

Figure 8.7. <i>In Vitro</i> Aerosol Performance of the PAC Method. ....	217
Figure 8.8. Coating Time Studies using the PAC Method .....	218
Figure 9.1. SEM Images of ML006 Lactose Binary Blends .....	235
Figure 9.2. SEM Images of Drug Coated Polystyrene Beads.....	236
Figure 9.3. Device Resistance Measurement of the Handihaler with a Capsule or Bead .....	237
Figure 9.4. Illustration Depicting Relative Capsule and Bead Motions in the Handihaler .....	238
Figure 9.5. Image Series of Polystyrene Bead Oscillations.....	239
Figure 9.6. Long Exposure Photographs of Capsule and Bead Motion. ....	240
Figure 9.7. <i>In Vitro</i> Performance of Salbutamol and Budesonide Formulations.....	241
Figure 9.8. Illustration Depicting a Stationary Bead Configuration.....	242
Figure 9.9. <i>In vitro</i> Performance of Stationary and Oscillating Budesonide-Coated Polystyrene Beads .....	243
Figure 10.1. Archetypal Design of a Single Dispersion Chamber Prototype Inhaler .....	268
Figure 10.2. Prototype Designs with Varying Mouthpiece Length.....	269
Figure 10.3. Performance of Prototypes with Varying Mouthpiece Length .....	270
Figure 10.4. Prototype Designs with Tapered Device Outlet Channels.....	271
Figure 10.5. Performance of Tapered Mouthpiece Channel Prototypes .....	272
Figure 10.6. Prototype Designs with Varying Mouthpiece Channel Diameters .....	273
Figure 10.7. Performance of Varying Mouthpiece Channel Diameters .....	274
Figure 10.8. Designs Possessing Flow Bypass and Sheath Flow Channels .....	275
Figure 10.9. Performance of Flow Bypass and Sheath Flow Mouthpiece Designs.....	276
Figure 10.10. Design of a Dual Dispersion Chamber Prototype Inhaler .....	277
Figure 10.11. Pressure Drop Across the Dual Chamber Prototype at Various Flow Rates .....	278
Figure 10.12. Performance of Dual Chamber Prototype Inhaler .....	279

Figure 10.13. Stage Deposition from Dual Chamber Prototype ..... 280

## TABLE OF TABLES

Table 2.1. Chapter 3: Comprehensive Study of Lactose Carrier Particles in Binary Blends .....	47
Table 2.2. Chapter 4: Influence of Carrier Particle Diameter and Surface Roughness on Aerosol Performance .....	48
Table 2.3. Chapter 5: Influence of DPI Device on Aerosol Performance as a Function of Carrier Particle Diameter and Surface Roughness .....	49
Table 2.4. Chapter 6: Influence of Flow Rate on Aerosol Performance as a Function of Carrier Particle Diameter and Surface Roughness .....	50
Table 3.1. Measured Specific Surface Areas of Fractionated Lactose Carrier Particles .....	74
Table 3.2. Particle Sizing Data of Fractionated $\alpha$ -Lactose Monohydrate Carrier Particle Populations .....	75
Table 3.3. Particle Sizing Data of Fractionated Anhydrous Lactose Carrier Particle Populations .	76
Table 3.4. Particle Sizing Data of Fractionated Spray Dried Lactose Carrier Particle Populations	77
Table 3.5. Particle Sizing Data of Fractionated Granulated Lactose Carrier Particle Populations	78
Table 3.6. Drug Content Uniformity Measurements of the Experimental 1% (w/w) Salbutamol Binary Formulations .....	79
Table 4.1. Specific surface areas (SSA) of anhydrous and granulated lactose carrier particles..	109
Table 4.2. Aerosol Performance Values of Anhydrous and Granulated Lactose Formulations ..	110
Table 4.3. MMAD Values of Budesonide Particles Dispersed from Anhydrous and Granulated Lactose Carrier Particles .....	111
Table 5.1. Specific surface areas (SSA) of Anhydrous and Granulated lactose carrier particles by sieve fraction .....	141
Table 5.2. Average Simulated Collisions Experience by Carrier Particles in Aerolizer and Handihaler .....	142
Table 5.3. In vitro Aerosol Performance Data from Anhydrous Lactose Carrier Particle Formulations .....	143



Table 5.4. In vitro Aerosol Performance Data from Granulated Lactose Carrier Particle Formulations. ....	144
Table 6.1. Physical Properties of $\alpha$ -Lactose Monohydrate and Granulated Carrier Particle Populations.....	163
Table 6.2. Aerosol Performance Values of Salbutamol Sulphate Blends .....	164
Table 6.3. Aerosol Performance Values of Budesonide Blends .....	165
Table 7.1. Collected Bead Size Ranges Following Fractionation .....	192
Table 7.2. Measured Densities of Bead Materials.....	193
Table 8.1. Drug Coating as a Function of Bead Distance.....	219
Table 9.1. Stage Cut-off Sizes for the NGI at 15, 30 and 45 L min <sup>-1</sup> .....	244
Table 9.2. Physical Characterization of ML006 Lactose Carrier Particles and Large Porous Polystyrene Beads .....	245
Table 9.3. Device Resistance of Handihaler with the Inclusion of a Capsule or Bead.....	246
Table 9.4. <i>In vitro</i> Aerosol Performance of Budesonide Formulations .....	247
Table 9.5. <i>In vitro</i> Aerosol Performance of Salbutamol Formulations .....	248
Table 9.6. Acoustic Profile Data of Polystyrene Beads.....	249
Table 10.1. Resistances of Marketed DPIs and Devices Presently in Development .....	281
Table 10.2. Device Resistances of Handihaler and Single Chamber Prototype.....	282
Table 10.3. Resistances for Flow Bypass and Sheath Flow Channel Configurations.....	283
Table 10.4. Measured Device Resistance for Dual Chamber Prototype Device.....	284

# CHAPTER 1

## 1. Introduction

### 1.1. PULMONARY DRUG DELIVERY

The overall performance of a therapeutic inhalation regimen is a complex interplay between the physiology and anatomy of the patient's pulmonary system and disease state, the physicochemical properties of the drug formulation, and the device employed to aerosolize and deliver the dose. With regards to the patient, proper training and instruction on the use of their prescribed inhaler, though often neglected, can produce a marked improvement in performance. However, apart from the performance boon provided through education, the anatomy of a patient's airways will dictate both the inspiratory force they will produce and the duration over which it is sustained, and the formulation and device must compensate for any shortcomings in the patient's inspiratory output.

Evolving from a common ancestor, the development of therapeutic inhalation devices has diverged into three distinct classes: nebulizers, pressurized metered-dose inhalers (pMDIs) and dry powder inhalers, with the latter being the most recent addition to the family [1]. Given their bulkiness, external power requirements, and time required for inhalation, nebulizers lack portability and are generally confined to the home or clinic, although hand-held nebulizers have been introduced [2]. In contrast, pMDIs employing a pressurized gas propellant to aerosolize the dose, are highly portable and inexpensive. Inaugurated in the 1950s, pMDIs dominated the portable inhalation drug delivery market for many years, essentially running unopposed until the unveiling of the first DPI late the following decade (Spinhaler<sup>TM</sup>, Aventis) [3]. Even then, nascent DPIs were characterized by low efficiency, and delivered a dose from a capsule that had to be manually loaded prior to each actuation; a sharp contrast to pMDIs and their 200 dose capacity. However, pMDIs were not without their drawbacks, and chief among them was their use of the ozone-depleting chlorofluorocarbons (CFCs) as propellants [4]. In 1987, members of the international community, recognizing the irreparable damage CFCs have on the

environment, signed the Montreal Protocol pledging to phase out production of CFCs by 1996 [2]. In need of an alternative propellant, CFCs have been replaced by hydrofluoroalkanes (HFAs), although the transition has not proven seamless, as density and solubility differences between the propellants have led to reformulation issues. The high velocity of the emitted dose from a pMDI also requires coordination between patient inhalation and device actuation to avoid deposition in the throat, which many patients find difficult [5]. In addition, advanced therapeutics, including peptides, proteins and gene vectors, exhibit poor stability at room temperature when formulated into the aqueous solutions delivered by pMDIs [6].

## **1.2. DRY POWDER INHALERS**

Developed as an alternative to the pMDIs, dry powder inhalers have their own unique advantages and limitations, and can be broadly categorized into either passive or active devices [3]. Passive DPIs are breath-actuated, deriving the energy for powder dispersion and aerosol formation solely from the patient's inspiratory maneuver, alleviating the coordination of actuation and inhalation that many patients find problematic with pMDIs [4]. However, patients can produce a wide range of flow rates, which is reflected in the high inter-patient variability in the dose delivered from these devices. Additionally, some patients can only generate flow rates too low to produce an aerosol cloud, and treatment with DPIs can be ineffectual. In light of this, many DPI developers have concluded that the best strategy lies in decoupling powder dispersion from inhalation and, following the path of pMDIs, have designed active DPIs incorporating an assortment of auxiliary energy sources to aerosolize the dose.

DPIs can be further classified as either single dose or multi-dose devices, the latter being delineated into multi-unit dose or reservoir inhalers. The single-dose inhalers represent the first generation of DPIs (Spinhaler<sup>TM</sup>, Rotahaler<sup>TM</sup>), although some devices in this category are still currently marketed (Aerolizer<sup>TM</sup>, Handihaler<sup>TM</sup>). These inhalers generally deliver the dose from a gelatin capsule inserted into the device prior to each actuation. The multi-unit dose inhalers disperse individual doses pre-metered by the device manufacturer into blisters, while reservoir DPIs contain enough powder for multiple doses (typically 60 - 200) within the device, metering individual doses prior to actuation. Advantages of DPIs employing factory-metered doses

include environmental protection of the powder and consistency of the dose relative to their reservoir counterparts. However, a drawback is the higher cost of these devices, stemming from the multi-component designs and dedicated factory production lines [4]. Regardless of how the dose is provided, all DPIs contain a de-agglomeration principle to address the challenges inherent to producing aerosols from a dry powder.

### **1.3. TRADITIONAL DPI FORMULATIONS**

To be effectively delivered into the lung, drug particles are generally required to fall in the size range between 1 - 5  $\mu\text{m}$ ; particle size reduction is typically performed through “top down” processes such as jet milling, which yields highly cohesive particles with ill-defined size distributions and morphologies [5]. Particle engineering, a “bottom up” approach to producing respirable size particles at the initial particle formation step, holds promise in addressing the drawbacks of attrition processes such as jet milling. However, few technologies have been industrialized at least in part due to the increased cost of goods for these nascent techniques [7]. The cohesive interactions between the powder particles arise from a combination of electrostatic, capillary, and van der Waals forces, although by allowing the particles time to dissipate excess electric charges, and in the absence of high relative humidity, it is the latter that are most important [8]. Individually weak, but collectively robust, van der Waals interactions are the dominant attractive forces in particles with diameters under 10  $\mu\text{m}$ , exerting a 'velcro effect' that impedes powder dispersion. To aid in the entrainment and deagglomeration of these cohesive particles, dry powder formulations are generally binary, or interactive, blends, with the bulk, > 95% (w/w), comprised of large inert carrier particles (50 - 100  $\mu\text{m}$ ), to improve the flowability and metering properties of the formulation [9]. However, while the addition of the large carrier particles allows the powder to be readily entrained in a flow stream, the adhesive interactions between the drug and carrier hinders the formation of an aerosol comprised of primary drug particles. Consequently, drug particles that fail to detach from the carriers are deposited in the throat and upper airways [10].

#### 1.4. PARTICLE ENGINEERING TECHNOLOGIES

In lieu of developing inhalers that can enhance the de-agglomeration forces, an alternative approach is to reduce the cohesive and adhesive interactions within the powder through modifications to both drug and carrier particles [1]. For micronized drug, one strategy is to increase the diameter of the particle, thereby lowering the surface area-to-volume ratio, without compromising its aerodynamic diameter. The aerodynamic diameter of particle ( $d_a$ ) governs how it behaves in a flow stream, and is related to its true diameter ( $d_p$ ) and density ( $\rho_p$ ) as:

$$d_a = d_p \sqrt{\frac{\rho_p}{\rho_o}}$$

where  $\rho_o$  is the unit density, and  $\rho_p/\rho_o$  is the specific gravity of the particle [8]. From the above, it can be seen that an increase in the diameter of a particle can be balanced by a concomitant reduction in its density, an approach embodied by the large porous particles [11]. Additional developments in powder dispersion performance include smaller porous particles, Pulmospheres, and the use of supercritical fluid technology. However, in comparison to unmodified drug, these particles can be costly to manufacture, requiring the use of spray drying or spray-freeze drying [1]. Moreover, given their increased volume, larger reservoir systems must be developed to accommodate the formulation, requiring the production of devices specific to the powder [1]. Thus, while particle engineering technologies have demonstrated the ability to markedly improve aerosol performance from traditional dry powder inhalers, at present, marketed DPI formulations are generally binary formulations that exhibit poor dispersion properties relative to the aforementioned particle technologies. Accordingly, to improve performance of a DPI therapeutic regimen, strategies to optimize both the formulation and device are required. What follows is a detailed discussion of the physicochemical properties of binary DPI formulations, particularly the parameters of the carrier particle population that have been examined in the literature and found to either enhance, or impair performance through various mechanisms. Following this, the mechanisms by which dry powder inhalers are designed to improve drug delivery will be discussed in detail.

## 1.5. PARAMETERS GOVERNING PERFORMANCE OF BINARY BLENDS

As mentioned above, therapeutic formulations administered via dry powder inhalers are typically interactive mixtures, comprised of the active pharmaceutical ingredient and a coarse carrier material blended together to produce a homogeneous powder. Delivery to the deep lung requires drug particles possessing aerodynamic diameters between 1 and 5  $\mu\text{m}$ . However, given the high surface area-to-volume ratio of particles in this size range, van der Waals forces dominate the interactions, producing highly cohesive powders that flow poorly and are consequently resistant to re-dispersing back into primary particle sizes during inhalation. Drug agglomerates that fail to de-aggregate sufficiently deposit in the mouth and throat, reducing the therapeutic efficacy of the treatment and increasing the potential of unwanted side effects. To improve powder flow and dispersion, as well as assist in dose metering, a population of coarse particles (50 – 100  $\mu\text{m}$ ) are incorporated into the formulation, typically in excess of 95% (w/w) to serve as carriers onto which the drug particles adhere during blending, and from which they are subsequently detached during inhalation [10]. Carrier particles must be inert, possess a physical and chemical stability compatible with the drug substance, and be readily available and inexpensive [12]. While a variety of materials, primarily sugars, have been evaluated in the literature for their suitability to serve as carrier particles,  $\alpha$ -lactose monohydrate is the only material currently approved by the FDA for inhalation purposes [13-16].

The previous two decades have borne witness to extensive research on dry powder inhalation systems, revealing the influence that the patient, formulation and device have on dispersion performance, coupled with the understanding that a judicious selection of both drug and carrier particle properties are crucial parameters in optimizing performance. Production of a stable and homogeneous powder blend requires the interaction between drug and carrier particles be balanced, with forces strong enough such that drug preferentially adheres to the carrier during mixing, yet sufficiently tenuous to facilitate re-dispersion of drug particles during inhalation [17, 18]. Formulation factors affecting overall performance include the drug substance and concentration, mixing rate, mixing time, batch size, and the carrier particle population [19-21]. Studies focused specifically on the physical properties of carriers have

examined the particle size, size distribution, morphology, surface roughness, surface area, and surface energy of carrier particle populations [9, 22-28]. However, the absence of a uniform experimental methodology between research groups inhibits direct comparison of dispersion studies employing different drugs, carrier particle size fractions, and dry powder inhalers. Additionally, variations in blending method, time, batch size, and mixing container can significantly influence the forces experienced by the formulation during mixing, introducing further confounding factors [29, 30]. However, in spite of these caveats, reports from the literature have reached a general consensus on the detrimental effect larger carrier particles impart to overall aerosol performance.

To account for this phenomenon, multiple theories have been proposed in the literature. The following list will be examined in greater scrutiny below, but is presented now to illustrate the variety of adverse effects attributed to large carriers:

1. Increasing the diameter of carrier particles enhances the van der Waals forces between drug and carrier.
2. Larger carrier particle populations possess greater surface asperities and discontinuities.
3. Blends with larger carrier particles increase drug-carrier adhesion forces during mixing.
4. Higher carrier particle populations have a reduced surface area, below the threshold required for a drug particle monolayer (dependent on API concentration).
5. Surface impurities and high energy sites increase with carrier particle diameter.
6. Large carrier particle populations possess a lower fraction of fine particles (< 10  $\mu\text{m}$ ) relative to smaller carrier particles.

## **1.6. MECHANISM OF DRUG DETACHMENT FROM CARRIER PARTICLES**

It is important to note that these theories are not mutually exclusive, and the extent to which one predominates over another may vary as experimental parameters are altered. At this moment, let us briefly shift from our discussion of carrier particles and consider the mechanisms of drug dispersion in a dry powder inhaler. Detachment of drug from the carrier particle surface occurs through three distinct pathways [8, 9, 31, 32]:

1. Dispersion by acceleration flow or shear flow
2. Dispersion by impaction of drug aggregates on a target
3. Dispersion by mechanical forces

The importance of carrier surface morphology is evident in the first two mechanisms. For detachment by acceleration flow, drug particles must be exposed to the flow stream on the carrier surface, with larger drug particles and agglomerates possessing a greater surface area for interaction with the flow stream. Detachment by impaction of aggregates onto a target, where the drug is scraped off from the carrier during collisions with the inhaler and/or other carrier particles, similarly requires the drug be exposed on the surface. The final mechanism, dispersion by mechanical forces, occurs when carrier particles impact with the inhaler walls as they exit the device, transferring the momentum of the collision to the adhered drug particles.

## **1.7. MECHANICAL DETACHMENT FORCES**

If the force generated by the abrupt momentum change is both greater than the adhesion between the particles, and in a direction favorable for detachment (that is, if the particle is not oriented on the carrier so that the collision pushes the drug onto the carrier), the drug is dispersed [8, 9]. Of the three, the latter mechanism is largely independent of carrier particle shape, but directly proportional to carrier particle size, as larger carriers achieve higher momentums over smaller carriers traveling with comparable velocities [9]. As with the proposed theories accounting for the adverse effect of large carriers, the mechanisms of drug detachment are not mutually exclusive, and undoubtedly work in concert to promote dispersion. Additionally, the relative contribution of any one mechanism to total drug



detachment can vary significantly between formulation, inhaler, and flow rate, which varies considerably across a patient population. It is not surprising then that studies aimed at elucidating the predominant mechanism of drug particle detachment have yielded conflicting results [31-38].

While lacunae abound in our understanding of the precise forces governing drug particle detachment within a given inhaler, examining the list of proposed theories by which carrier particles influence formulation performance, and comparing it to the mechanisms of drug detachment, it is evident that dispersion by mechanical forces would seem incompatible with the requirements for good aerosol performance. In other words, increasing the contribution of mechanical forces in detachment requires larger carrier particles, but evidence suggests larger carrier particles are detrimental to formulation performance. Consequently, this mode of drug detachment from carrier particles has been traditionally overlooked, if not dismissed entirely [22]. However, given the dependence of impaction forces on the cube of the carrier diameter, we propose that forces generated from mechanical impactions between carrier particles in the inhaler can potentially overwhelm adhesion forces, significantly outweighing their proposed detrimental influences on dry powder formulation [8]. Accordingly, prior to presenting the case for large carrier particles, the case against them must be carefully cross-examined.

#### **1.8. DETRIMENTAL INFLUENCE OF LARGE CARRIER PARTICLES TO AEROSOL PERFORMANCE**

#### **1.9. THEORETICAL PARTICLE-PARTICLE ADHESION FORCES**

Increasing carrier particle size is believed to enhance the van der Waals forces between drug and carrier. Due to the high degree of asperities and surface roughness of pharmaceutical powders, an exact solution for the expected van der Waals forces between a drug particle and carrier particle has proven impossible to obtain. However, to simplify the problem and arrive at an approximate value, the drug and carrier particles are often represented as perfectly smooth spheres, allowing the theoretical van der Waals forces to be then calculated by:

$$F_{vdW} = \frac{A}{12D^2} \left( \frac{d_d d_c}{d_d + d_c} \right)$$

where A is the Hamaker constant ( $\sim 10^{-19}$  J), D is the inter-particle separation distance ( $\sim 0.4$  nm), and  $d_d$  and  $d_c$  are the respective diameters of the drug and carrier particles [8]. The Hamaker value is constant between two materials, and the inter-particle distance is also considered to be unchanged as the size of the drug and carrier particles are altered. Thus, holding the size of the drug particle constant, increasing the diameter of the carrier particle will theoretically produce an accompanying increase in adhesion force. However, a closer examination of the increase in the predicted van der Waals forces within the carrier particle populations of interest ( $> 50 \mu\text{m}$ ), reveals that the price exacted by larger carrier particles, in terms of higher van der Waals forces, is not as costly as presumed. To illustrate this, consider the interactions between a drug particle and carrier particle as the diameter of the latter is increased. As mentioned previously, the Hamaker constant and inter-particle distance are assumed constant, so variations in the equation depend entirely on the diameters of the drug and carrier

$$F_{vdW} = \frac{d_d d_c}{d_d + d_c}$$

Beginning with a drug particle and carrier particle both  $5 \mu\text{m}$  in diameter, the size of the carrier is doubled to  $10 \mu\text{m}$ , then increased five-fold to  $50 \mu\text{m}$ , and once more up to  $250 \mu\text{m}$  (Figure 1.1) Inserting the diameter values into the above equation reveals that while the adhesion force is increased by 32% when the carrier particle is doubled from  $5$  to  $10 \mu\text{m}$ , the next size increase is not accompanied by a commensurate raise, as the difference in adhesion force between  $10 \mu\text{m}$  and  $50 \mu\text{m}$  is roughly the same as the difference between  $5 \mu\text{m}$  and  $10 \mu\text{m}$ . Finally, raising the diameter of the carrier up to  $250 \mu\text{m}$  brings with it an even smaller

difference with the preceding carrier particle; less than 10% between 50  $\mu\text{m}$  and 100  $\mu\text{m}$ . The last comparison is the most relevant, as carrier particles are typically 50 – 100  $\mu\text{m}$ .

Thus, the cost of raising the size of the carrier particle is incurred primarily at smaller carrier particle diameters; much smaller than commonly employed in dry powder formulations. Another thing to note is that the value of the adhesive force begins to trend to a constant number, and it is not by coincidence that value is the same as the diameter of the drug particle. As the value of the carrier particle becomes much larger than that of the drug, the denominator is approximated simply as the value of the carrier particle, and the carrier diameter is eliminated entirely from the expression:

$$\text{as } d_c \gg d_d$$
$$F_{vdw} = \frac{d_d d_c}{d_d + d_c} \rightarrow \frac{d_d d_c}{d_c} = d_d$$

Accordingly, as the size of the carrier become sufficiently large, the theoretical van der Waals forces between drug and carrier will become constant and depend solely on the diameter of the drug particle. In conclusion, at the size ranges relevant to our discussion, increasing carrier particle size has a relatively low effect on the theoretical van der Waals forces.

#### **1.10. PRESS-ON FORCES**

Due to both their greater mass and improved flowability relative to their smaller counterparts, larger carrier particle populations can increase the press-on forces between the drug and carrier during blend preparation. Blending of drug and carrier particles into a homogeneous powder is primarily performed with an orbital mixer. During blending, the container holding the powder is rotated continuously, forcing the powder to slide back and forth between the ends of the container, repeatedly pressing against the particles below.

Accordingly, larger particles with greater mass and good flowability will collide against both the container walls and the particles underneath them, with greater force than smaller particles with poor flow [20]. Drug particles that are sandwiched between two carriers during a collision will be pressed against the carrier surface with high relative force, increasing the contact area between drug and carrier and thus the adhesion force between the two particles [9]. Consequently, a greater force will be required to detach the drug during inhalation, potentially yielding a formulation with poor dispersion performance.

However, examining the previous paragraph by the light of the proposed theories of large carrier particle performance reveals a dissonance between them. Press-on forces requires the presence of a drug particle located between two lactose particles. However, larger carriers have been associated with greater surface asperities and higher rugosity than smaller particles [9, 12, 29, 39]. Particles with rugged surfaces might then be expected to provide shelter to drug particles against press-on forces.

The possibility that this occurs was noted by de Boer and coworkers [9]. However, they believed this effect was dependent on drug concentration in the formulation, and that increasing drug concentrations would expose more particles to press-on forces, eliminating the potential benefit high rugosity would impart to formulations [20]. To address this, an additional study was undertaken to examine drug detachment of three lactose carrier size fractions, 45 – 63  $\mu\text{m}$ , 150 – 200  $\mu\text{m}$  and 250 – 350  $\mu\text{m}$ , at two different flow rates, as the drug concentration was increased from 0.4% (w/w) up to 6 % (w/w)[20]. As the drug concentration was elevated, the fraction of the drug particles detached from the surface of the 45 – 63  $\mu\text{m}$  carrier particles increased. This could be explained by the increased drug-drug agglomeration as the amount of drug in the formulation was raised, and as carrier particles of this size range would have a relatively low mass and hence very low press-on forces, it was not surprising detachment increased with drug concentration. In contrast, for the large carrier fractions, 250 – 350  $\mu\text{m}$ , increasing drug concentration inhibited drug detachment, although the difference was almost negligible as the concentration was doubled from 3% (w/w) to 6% (w/w).

The authors concluded that at higher drug concentrations, drug particles are not afforded shelter from the press-on forces, and hence the overall adhesion between drug and carrier populations increases with concentration. However, their assumption was based on a previous study by Podczek, showing that micronized salmeterol sulphate particles exhibit an adhesive nature when mixed with lactose carriers, i.e. lactose-salmeterol interactions are favored over salmeterol-salmeterol interactions [40]. Dickhoff, et al., assumed that budesonide would exhibit a similar adhesive tendency, and cited this as evidence that larger carrier particle fractions increased press-on forces between the drug particles and the carriers during blending, because the drug would preferentially attach to the carrier. However, a subsequent independent study examining the adhesive and cohesive tendencies of lactose with different drugs, concluded budesonide has strong cohesive properties, resulting in potential drug separation upon blending [17]. This finding was corroborated in a study examining the blending dynamics between budesonide and crystalline lactose, revealing the tendency of budesonide to both blend and segregate from the carrier as a function of time; a tendency attributed to a poor interaction between the drug and carrier [18]. Given the likelihood of budesonide to associate with itself in the presence of lactose, increasing the drug concentration would increase the extent of agglomeration at the expense of drug-carrier adhesion. If the large carrier lactose had a smooth surface, and possessed insufficient rugosity to shelter the budesonide agglomerates as the drug concentration was raised, it would be expected that drug detachment would increase with concentration (as observed for smaller carriers), as larger drug aggregates would possess a greater surface area, making them more susceptible to detachment by flow. However, this was not observed, and given the reported cohesive nature of budesonide, it is possible that the low detachment was a combination of the particles being sheltered from both the flow stream and detachment due to aggregate impactions, coupled with insufficient carrier particle-inhaler collisions at the low flow rate of 30 L min<sup>-1</sup>.

As the flow rate was doubled, it was observed that the larger carrier particles detach a greater fraction of drug than the smaller carrier particles at all drug concentration levels (0.4%, 1.6%, 3.0% and 6.0%). Thus, smaller carrier particles, with low press-on forces, detached a smaller fraction of drug compared to large carrier particles, where high press-on forces coupled

with asperities would be expected to inhibit performance relative to the smaller carriers. To reconcile this discrepancy, let us assume that both carrier particle populations have smooth surfaces and would be exposed to identical flow detachment forces and aggregate collision forces as they experience the same inhalation flow rate. It would be expected that both formulation would behave similarly. We now consider press-on forces, and the assumption that larger carrier would experience press-on forces to a greater extent the smaller carriers. It would now be expected that the small carriers would outperform the larger carrier, i.e. the smaller carriers would detach a greater fraction of drug. Finally, include the high surface rugosity of carriers, and now detachment forces by flow and aggregate impaction would be diminished in the large carriers, and the small carrier would be expected to significantly detach more drug. However, the opposite occurs. What then would account for the improved detachment properties of the larger carrier at higher flow rates? This difference must then be attributed to the increased mechanical forces experienced by larger carrier particles as the velocity is raised. In this case, impaction forces begin to overwhelm adhesion forces as noted by the ability of the large carriers to detach up to 95% of the drug. By contrast, for smaller carrier particles where impaction forces would not be as significant, the detachment forces that predominate, i.e. detachment by flow and aggregate impaction, are not as potent, lending support to our claim that detachment by mechanical forces is potentially the most dominant of the three. That the fraction of detached drug increased with drug loading at each concentration provides evidence of budesonide agglomeration, refuting the authors' assumption that budesonide would prefer to attach to the carrier, and that the extent of attachment would increase with higher drug concentrations. The availability of drug dispersion data (FPF, FPD, etc.) in addition to the detachment data would have been a welcome inclusion, as high drug detachment but low FPD would correspond to a cohesive drug.

In conclusion, the influence of press-on forces depends not only on the carrier particle size, but on the rugosity of the surface and the properties of the drug substance. Accordingly, a general statement associating increased press-on forces simply with particle size would be disputable.

### **1.11. SURFACE ROUGHNESS**

Carrier particles with larger diameters possess greater surface roughness, affording drug particles shelter from detachment mechanisms relying on acceleration flow or impaction of drug aggregates on a surface [9]. Drug particles will accumulate in the discontinuities on the carrier particle surface, and a rougher surface potentially affords multiple contact points between the drug and carrier, increasing the adhesive force between the particles [41]. This view is supported by studies investigating the influence of carrier morphology, where smoother lactose carriers produced higher fractions of fine particle deposition [12]. An additional role of surface roughness was proposed by Podczek, who believed that detachment of fine drug particles from the surface of coarse carriers occurs laterally to the surface, where the drug will slide until it reaches the edge of the carrier and fall-off [22]. The adverse influence of carrier particle size is then obvious, as it will extend the distance the drug particle must travel prior to detachment, requiring greater aerodynamic drag forces relative to a smaller carrier particle. However, this theory is contested by reports indicating that elongated lactose carrier particles can improve dispersion performance [42]. The authors attributed this beneficial influence to the enhanced aerodynamic properties of the elongated particles, allowing them to travel longer distances than their equivalent volume-spherical counterparts and prolong the exposure of adhered drug particles to drag forces.

Examining the detachment mechanisms, it is evident that smoother particles allow for greater detachment by flow and aggregate impaction, whereas detachment by mechanical forces is largely independent of carrier particle surface rugosity. Accordingly, for rough surfaces detachment becomes less dependent on flow and aggregate impaction, relying more on mechanical forces. Thus, it is not that high surface rugosity would inhibit detachment entirely, but rather it shifts the detachment mechanism to rely more on mechanical forces. As such, it could then be theorized that the size ranges examined (63 – 90  $\mu\text{m}$ ) in the study investigating surface roughness might be too small to permit a significant contribution of detachment to arise from carrier particle collisions [41, 42]. As mentioned previously during the discussion of press-on forces, impaction forces require both sufficiently high flow rates coupled with a relatively

large carrier particle diameter. As an example, consider two spherical carrier particles, one 90  $\mu\text{m}$  and the other 350  $\mu\text{m}$  (the respective upper limits of the Zeng, et al., and Dickhoff, et al., studies), moving with comparable velocity, impacting directly with a surface. In this case, the momentum difference between the two particles is entirely dependent on their mass, which is related to the diameter:

$$m = \frac{\rho\pi d^3}{6}$$

Increasing the carrier particle size from 90 to 350  $\mu\text{m}$ , could potentially produce impaction forces 59-fold greater in the latter carrier particle; assuming similar particle velocities. In summary, carrier particle roughness may inhibit performance by causing a shift to a detachment mechanism highly dependent on mechanical forces. Small carrier particles may possess insufficient mass for these forces to be effective at a given flow rate. In contrast, surface roughness of very large carriers is less debilitating when compared against smaller carriers, as the mechanical forces generated may potentially dominate over the detachment mechanisms that require a smooth carrier surface for optimal performance.

#### **1.12. SURFACE AREA**

For a constant mass of carrier particles, increasing carrier diameter can significantly lower the available surface area to which drug can adhere during blending. Consequently, drug particle agglomerates will form, and while they may be more readily detached by the flow stream relative to primary drug particles, dispersion performance will be reduced if the inhaler is unable to de-aggregate the flocculated particles. For example, a study evaluating the relationship between specific surface of lactose particles with increasing carrier particle diameter noted that increasing the diameters of the carrier particle population from < 32  $\mu\text{m}$  up to 63 – 90  $\mu\text{m}$  and 125 – 180  $\mu\text{m}$  markedly lowered the SSA of the carriers, from a high of 0.68



$\text{m}^2/\text{g}$  for the smallest lactose size fraction to  $0.36 \text{ m}^2/\text{g}$  for the mid-range particles and down to  $0.19 \text{ m}^2/\text{g}$  for the largest diameter carriers [19].

Thus, for a constant powder mass, the surface area available for drug attachment is halved as the carrier fraction is raised from 0 – 32  $\mu\text{m}$  to 63 – 90  $\mu\text{m}$ , and then halved again as the carrier particle diameter is increased to 125 – 180  $\mu\text{m}$ . In their studies examining the influence of drug concentration on drug detachment from carriers, Dickhoff, et al., calculated (using a simplified model where drug and carriers were presumed perfect spheres with mono-disperse populations equal to their respective  $d_{50}$ ) that for a population of 32 – 45  $\mu\text{m}$  carriers, 0.4% (w/w) drug concentration would correspond to 4.6% surface coverage, and increasing the drug concentration 4-fold to 1.6% (w/w) would cover 18.4% percent of the available surface area. By contrast, a 250 – 350  $\mu\text{m}$  carrier particle population would have 36.2% percent surface coverage at 0.4% (w/w) concentration and 145% when the drug particle concentration is raised to 1.6% (w/w). This latter concentration exceeds the threshold of a theoretical drug monolayer, increasing drug-drug interaction and leading to agglomerates. It should be noted that the tendency of drugs to form agglomerates varies with substance, but lowering the available surface area undoubtedly increases if not the extent, then at least the frequency, of interactions between drug particles [16].

### **1.13. REDUCTION IN FRACTION OF FINE LACTOSE**

Studies have repeatedly observed that as the diameter of the carrier particle population is increased, the amount of fine lactose particles (< 10  $\mu\text{m}$ ) in the powder is reduced [22, 24, 26, 43-47]. Intrinsic to the formulation, these fine lactose particles are produced during micronization, and adhere to the coarse carrier particles; during subsequent powder processing they can detach from the carrier surface [27]. The lactose fines are believed to modulate drug detachment by two distinct mechanisms:

1. Lactose fines form agglomerates with drug particles, and the increased surface area of these aggregates increases their susceptibility to detachment by flow

2. Lactose fines occupy high energy sites on the surface of the coarse carriers, allowing drug to adhere to lower energy sites

While both of these pathways can improve aerosol performance, the differences between them are not insubstantial. For the first mechanism, the formation of fine lactose-drug agglomerates with greater surface areas relative to primary drug particles would benefit dispersion by the flow stream, which dominates with smoother and smaller carriers. For the latter mechanism, the ability of lactose fines to occlude high energy sites on the carrier surface would affect drug detachment by all three of the proposed mechanisms. However, these high energy sites are thought to be located primarily in surface asperities and discontinuities, and thus attributed more to larger carriers [9, 27]. Furthermore, as high energy sites are primarily located in regions of high surface roughness, detachment by mechanical forces could play the major role in dislodging drug from high energy sites. Correspondingly, that larger carriers possess a lower amount of fine particles could be balanced by their (theorized) improved detachment potential against drug adhered to high energy sites, as carrier particle size is increased. However, this detachment potential depends on multiple factors, including inhaler, flow rate, drug substance and concentration and carrier particle morphology.

Of the two mechanisms, is not known which one dominates for a given formulation. Support for the first hypothesis is provided by studies revealing mixing order between fine lactose and drug particles (to prepare ternary blends of coarse lactose/fine lactose/drug) is unimportant, contesting the supposition that fine particles must adhere first to high energy sites [24]. Additionally, Louey, et al., also noted an increase in the surface energy of coarse lactose carriers following mixing with fine lactose particles. As the lactose fines are proposed to passivate the carrier surface, this result is inconsistent with the theory that lactose fines would expose lower energy sites to the drug. However, the theory that lactose fines strongly adhere to the carrier surface is supported by an in vivo deposition study reporting higher concentrations of fine particles in carrier population do not produce a concomitant increase in deep-lung fine particle deposition [48]. The authors attributed this observation to the formation of a stable

mixture between coarse and fine lactose particles, as would be assumed if the lactose fines principally interact with the high energy sites on the carriers.

#### **1.14. SURFACE ENERGY**

Given the numerous publications supporting the positive influence of lactose fines on dispersion, their overall ability to improve aerosol performance is uncontested. However, it is worth examining if larger carrier particle populations do indeed possess higher surface energies; or alternatively, that lactose with high energies exhibit reduced performance comparable to low energy carriers. Evidence conflicting with both of these theories has been observed in the literature, and raises doubts on the perceived relationship between surface energy and drug detachment. Studies employing atomic force microscopy (AFM) and inverse gas chromatography (IGC) to probe the surface energies of inhalation-grade lactose carriers (Respitose<sup>®</sup>, DMV-Fonterra) found that the milled (ML) and sieved carriers have very similar surface energies, in spite of the wide differences in particle size distribution between milled and sieved Respitose<sup>®</sup> carriers [27]. Additionally, milled lactose was found to have a greater degree of surface roughness, and would be expected to lower dispersion performance.

However, the observation of Louey, et al., that addition of fine particles actually increased the surface energies of carrier particles, precludes a direct relationship between surface energy and particle size [24]. In the case of the fine lactose, it is believed that the comminution process required to generate particles < 10 $\mu$ m would leave the resulting fines with a very high surface energy. Accordingly, if the surface energy of lactose is believed to increase at low particle sizes, and then again at high particle sizes, where would the trend reverse? That is, at what size ranges could we expect reduced surface energies as the particle size is lowered?

Alternatively, lactose powder with higher relative surface energy would be expected to perform worse than lower energy populations. However, Cline and Dalby observed the opposite trend, with improved dispersion performance associated with higher surface energies [28]. The authors attributed this correlation to the requirement of a minimum interaction energy, sufficient to pull apart highly cohesive drug aggregates into primary particles; lactose with a

higher energy will then be better able to attract drug particles onto the carrier surface, such that the drug is now found in its primary particle size. Accordingly, while it is intuitive to think lower carrier particle surface energies would improve dispersion by lowering adhesive interactions, the relationship appears ambiguous at best.

#### **1.15. SUMMARY**

In addressing the different mechanisms by which large carrier particles are perceived to be detrimental to dry powder formulations, it becomes clear that the role of large carrier particles is not as clearly defined as the literature might lead us to believe. Specifically, carrier particles with large diameters and high surface rugosity could potentially deviate from the expected trend, highlighting the incomplete nature of the proposed theories, while simultaneously illustrating the role of mechanical forces in the delivery of dry powder formulations.

#### **1.16. MECHANISMS OF DPI PERFORMANCE**

As was mentioned earlier, in addition to modifying the formulation, optimizing the performance of the DPI through which the formulation is dispersed is an additional pathway to enable improvements in DPI therapy.

From a pragmatic viewpoint, the development of a novel dry powder inhaler (DPI) is centered on two objectives: creating a device that can efficiently entrain and disperse a powdered drug formulation for inhalation therapy, while utilizing a design and function sufficiently novel to avoid patent infringement. Accordingly, this has produced no shortage of prospective designs, prototypes and devices incorporating a diverse array of powder dispersion strategies and de-agglomeration principles. Running the gamut from cyclones, baffles, and impellers, to the inclusion of external energy sources applying mechanical, electrical and pneumatic forces to the powdered dose, this abundance reflects the *carte blanche* at an inventor's disposal when conceptualizing a new inhaler. However, while the harvest from the patent literature may be bountiful, very few patented DPI designs reach the market, as an array

of factors including development cost, manufacturability, portability, and ease of use distinguish between a design that is plausible and one that is practical. The objective of this review is to provide a survey of the plurality of dispersion strategies employed in DPIs, drawing on examples from both the scientific and patent literature, and is not intended to compare the relative merits of one specific device to another.

#### **1.17. TURBULENCE INDUCEMENT**

In its most basic form, a dry powder inhaler is comprised of three regions: an air inlet port through which outside air enters the device during inhalation, a powder-holding chamber, and an outlet port delivering the dose to the patient. However, simply passing a flow stream across a static powder bed does not provide sufficient shear forces to effectively aerosolize the dose. When a particle is in a flow stream, it is subjected to two types of forces. The first of these are the body forces, such as gravity and electromagnetism, which act throughout the bulk of the particle and are described in terms of force per unit mass. The second category are the surface forces, generally provided as force per unit area and consisting of normal and shear, or tangential, stresses; it is the tangential stresses that are most important in powder de-agglomeration [49].

Turbulent flows are marked by highly irregular and rapid fluctuations of velocity in both time and space, containing high energy eddies that continuously buffet the drug particles, subjecting them to shear stresses through accelerations in different directions [8]. When these accelerations generate forces of sufficient magnitude, the drug can detach from an aggregate particle or carrier. A frequently encountered mode of inducing turbulence in an inhaler is to supply spiraling channels for the dose as it exits the device; a design popularized by the Turbuhaler™ [50]. However, while effective at generating turbulence, spiral paths also increase the surface area of the flow channel, enhancing the amount of particle deposition within the device. An example of this can be seen in the Turbuhaler™, where over 20% of the dose may be retained in the mouthpiece. By comparison to the Diskhaler™, possessing a straight-channel mouthpiece with a much smaller surface area, approximately 5% of the nominal dose is lost [51].

In lieu of spiraling flow channels, many DPIs of more recent vintage contain tangential inlets opening into a cylindrical chamber to generate a high energy cyclone within the device. As an example, the NEXT™ DPI, a reservoir inhaler, contains a cyclone chamber composed of two non-concentric arcs (US Patent No. 7,107,988). CFD analysis was used to optimize the design and dimensions of the chamber, and the resulting geometry was shown to eliminate 'dead spots' where drug deposition may have occurred [52]. An alternate example is found in the Conix™ inhaler, using a patented reverse cyclone technology. When the patient inhales, air is drawn into a cyclone chamber, establishing a vortex. As the flow stream travels down the cyclone, it encounters a blocked path at the bottom of the chamber, inducing the air flow to reverse direction and travel back up through a circular outlet [53].

#### **1.18. MECHANICAL FORCES**

In contrast to providing swirl channels or cyclone chambers, other inhalers incorporate designs applying mechanical forces to the powder. An example is the Spiros™ inhaler, where a powder-laden flow stream is carried through a battery-driven impeller to form an aerosol. An alternative embodiment (US Patent No. 6,237,591) uses a turbine to drive the impeller, labeling it a passive DPI, as the turbine is propelled when the patient inhales.

Apart from impellers, mechanical forces are provided by low density beads contained within the dispersion chamber (US Patent No. 6,971,384). When the patient inhales, the lightweight beads are driven by the entrained flow, repeatedly colliding with each other and the walls of the inhaler. As the dose is carried through the chamber, the powder is de-agglomerated as it is caught between the bead-bead and bead-wall impactions. Additionally, powder can be dispersed by employing a spring-driven hammer to strike a blister containing the dose (US Patent No. 5,655,523)[54].

When compared to inhalers that rely on turbulence, mechanically driven devices are more complex, requiring additional moving parts that may be prone to failure. However, an alternate strategy to generate mechanical impaction forces, without overly increasing the complexity of a device, is through the use of baffles (US Patent No. 5,724,959). Located

downstream of the powder-holding chamber, a narrow channel opens into a larger volume region containing an impactor plate, producing an abrupt change in the flow path. Due to their increased stopping distance, larger particles will be unable to follow the flow stream and navigate around the plate, colliding with the impactor and detaching drug from both aggregates and carriers. The width of the plate and the distance between it and the narrow-channel opening alters the cut-off size of the particles that will be intercepted.

## **1.19. PNEUMATIC FORCES**

### **1.19.1. Compressed Gas**

The most straightforward way to impart pneumatic forces to a powder bed is via a compressed gas source. However, while dry powder inhalers have been designed that utilize an external compressed gas source (US Patents, No. 5,875,776, and 5,775,320 as examples), more recent designs incorporate a method to compress air within the device through a manual pump. The most notable example is the Nektar Pulmonary Inhaler used to deliver Exubera (previously known as the Inhale DPI, Inhale Therapeutic Systems, US Patent No. 6,257,233). The DPI, which decouples device actuation from inhalation, is comprised of a lower pressurization chamber where the compressed air is generated, and an upper receiving chamber that holds the aerosolized powder following actuation. The air is compressed when the patient manually primes a handle coupled to a piston within the lower chamber. When actuated, the compressed air is discharged past the dose, drawing the powder into the upper chamber from where the patient subsequently inhales. Another example is the Vectura Aspirair™, employing a bolus of air that is manually compressed by the patient via a corkscrew-type manual pump, and discharged into the powder bed upon inhalation.

### **1.19.2. Vacuum**

An alternative approach to pneumatically driven dispersion is provided in US Patent No. 6,138,673, illustrating a reservoir DPI that creates a vacuum within the body of the device. The inhaler body can be extended by twisting the top portion relative to the lower portion two

revolutions, expanding the volume of the container from 550 mL to 750 mL, and creating a vacuum inside when the body is closed to the atmosphere. The device is manually actuated by the patient, inhaling while pressing a trigger that opens a valve within the body, exposing it to ambient air which enters the device through the dose holding chamber and aerosolizes the powder.

### **1.19.3. Synthetic Jetting Technology**

The application of synthetic jets to powder dispersion is another means of applying pneumatic forces and is described in US Patent No. 7,334,577. Synthetic jetting may be produced in a chamber bounded on one end by a wave generating device and on the opposite end by a rigid wall with a small orifice [55]. When acoustic waves are emitted at high frequency and amplitude from the generator, a jet of air, directed outward from the chamber, is produced. This 'synthetic' jet is comprised of vortical air puffs corresponding to the generator's frequency, which may be a piezoelectric element (discussed in detail below) or an electrodynamic transducer. When actuated, a dry powder dose located in the jet-producing chamber and resting above the generator, is levitated and dispersed by the high frequency vibrations. As the aerosolized powder nears the orifice, it is expelled from the chamber by the synthetic jet and into a flow channel where it is carried to the patient.

### **1.20. SUSTAINED EXPOSURE TO FLOW STREAM**

One of the drawbacks commonly cited with passive DPIs is that their reliance on the patient's inspiratory flow rate can render them incapable of providing sufficient energy to effectively aerosolize and deagglomerate the dose [31]. However, when considering that the duration of an inspiratory maneuver can last well beyond three seconds, and that the majority of the powder departs the inhaler within the first second of inhalation (well before the peak inspiratory flow rate is reached), it becomes clear that much of the energy available in the flow stream is never allowed the opportunity to interact with the dose [56]. Accordingly, the poor performance that plagues these devices cannot be solely attributed to an inadequate supply of energy, but also to an inefficient application of the available energy. To address this problem,



inhalers have been developed incorporating designs that can lengthen the time through which the dose interacts with the flow stream, sustaining the energy transfer between the air and powder. Alternatively, the device can delay the exposure of the dose to the flow stream until a pre-determined flow rate through the device has been attained, exposing the powder to the maximum energy levels of the flow.

#### **1.20.1. Delayed Exposure**

An example of this design incorporates a diverting flow channel in parallel with a secondary channel passing through the dosing chamber (US Patent No. 6,561,186). The flow channels share a common occluding mechanism connected by a rotatable vane, such that when one channel is open, the other is closed. When the flow rate reaches a pre-determined level, the vane closes, occluding the first channel, while simultaneously opening the second channel and allowing the flow access to the dose. In the Skyehaler™ (US Patent No. 6,182,655) a valve shield is moved within the inhaler in response to the suction generated from inhalation. When this force is sufficiently strong ( $> 1.5$  kPa) the valve shield opens a shutter, exposing the dose cavity to the flow stream. While these examples are from passive devices, the use of more complex air flow sensors is becoming a common feature in many active DPIs under development to automatically coordinate aerosol production with inhalation.

#### **1.20.2. Air Classifier Technology**

A vector quantity, the detachment forces acting on a drug particle adhered to a carrier are characterized by both a magnitude and a direction. When holding the magnitude constant, detachment forces exert their maximum effect when they act in a direction directly opposite to the adhering force [8]. However, due to the short duration of time to which a dose is subjected to separation forces in a typical DPI, coupled to the random nature of the detachment forces, only a small fraction of the drug particles will be correctly aligned to experience a force having a favorable combination of magnitude and direction sufficient to detach them from the carrier particle surface.

Air classifier technology was developed as a particle de-aggregation principle to sustain the interaction between the dose and the flow stream. A basic classifier is comprised of a cylindrical chamber, containing at least one tangential air inlet and a discharge outlet beginning at the center of one of the circular ends of the chamber [9]. Named for its ability to segregate, or classify, particles according to their size, it operates as a balance between centrifugal and drag forces. The drag force is proportional to the first power of the particle diameter and dominates for fine particles, while proportional to the cube of the particle diameter, larger carrier particles will experience a greater centrifugal force. When the powder is carried into the classifier through the tangential inlet, the large carrier particles, subjected to strong centrifugal forces, will be confined to the edge of the chamber, repeatedly impacting against the inner wall. As smaller drug particles are detached from the carriers through either drag forces or inertial forces arising from the carrier collisions, they will be pulled into the center of the chamber, under the discharge outlet, and removed from the classifier. Aggregated drug particles are broken up through collisions with both carrier particles and the classifier wall; the geometry of the classifier can be modified to alter the cut-off diameter of particle exiting the chamber [9, 57].

While the major fraction of drug that will detach does so within the first half-second of inhalation, these are the particles that are subjected to the strongest removal forces, generally drug aggregates and large primary particles [21]. As the dose continues circumnavigating the classifier, a secondary population, primarily smaller drug particles located in higher sites on the carrier and less susceptible to removal forces, is further released; studies indicate that the amount of drug exiting the classifier over the time interval from 0.5 to 2 seconds following inhalation can exceed 50% of the amount released within the first half-second [58]. Moreover, low flow rates can be compensated by sustaining the detachment forces acting on the dose, and produce fine particle fractions comparable to higher flow rates. Examples of DPIs incorporating air classifiers as their de-agglomeration principle are provided by the Twincer™ and Novolizer™ [57, 59].

The Twincer™ is a single-dose device containing two air classifiers in parallel; a design that permits a large dose, up to 25 mg, for delivering antibiotics as treatment for cystic fibrosis [59]. Delivering the dose from a blister, the powder is entrained and divided between two separate channels, each feeding into a discreet classifier; two additional tangential air inlets per classifier provide the necessary turbulence to detach the drug from the carrier. That the carrier particles are retained within the classifier following actuation is of no consequence, as the inhaler is a low-cost device, formed from three layered, molded plastic plates, and is intended to be disposable following each use. In contrast, the Novolizer™ is a reservoir inhaler, and eliminating the deposition of drug and carrier within the classifier following inhalation becomes important [57]. To achieve this, the Novolizer™ employs an eight-sided classifier, where each opening is a tangential air inlet. In addition, the classifier walls are not isometric, consisting of four long sides to accelerate the carriers and four short sides to generate impactions, and distributed in an alternating pattern. Using this arrangement the Novolizer™ can expel upwards of 95% of the dose from the device following each actuation.

## **1.21. VIBRATION INDUCED DISPERSION**

### **1.21.1. Capsule Vibrations**

Though not always explicit, inhalers that employ capsules to deliver a pre-metered dose rely heavily on mechanical vibrations to facilitate powder de-agglomeration. An example of a DPI that induces rapid capsule oscillations is the Handihaler™. When a patient inhales through this device, the airflow enters the DPI opposite the mouthpiece, passing through a short, narrow inlet tube and abruptly opening into a larger volume capsule chamber [60]. As the flow stream emerges from the narrower passage into the larger, the flow decelerates, causing the boundary layer to separate from the inner walls of the inhaler and re-attaching further upstream. This produces an annular region in the interim where fluid does not flow downstream, instead recirculating as a turbulent eddy resulting in a low pressure area [49]. The Handihaler exploits this phenomenon to rapidly vibrate the capsule during inhalation; the flow stream entering the larger chamber pushing the capsule forward while the low pressure region pulls its back. The capsule chamber was designed to be ample enough to allow the capsule room to oscillate, but

sufficiently confined to prevent the capsule from tilting on its side and inadvertently occluding the inlet. As shown in studies with the Aerolizer™, the rapid capsule vibrations, coupled with the shear forces produced from passing the powder through the narrow perforations in the capsule wall, provides an effective means of powder deaggregation [35].

### **1.21.2. Aeroelastic Vibrations**

An alternative form of vibration-induced dispersion is a passive DPI (US Patent No. 11,713,180) that operates on the aerodynamic principle of 'flutter.' When an aeroelastic object is placed within the path of a flow stream, it begins to oscillate, the energy of which in turn feeds further oscillations, rapidly intensifying the amplitude and frequency of its vibration. When a powdered dose is placed on an aeroelastic film, it is effectively aerosolized, requiring very low threshold flow rates to induce flutter in the film [61].

### **1.21.3. Piezoelectric Driven Dispersion**

The piezoelectric effect was initially observed in 1880 by the Curie brothers, who noticed that anisotropic crystals, i.e. crystals absent a center of symmetry, emit an electrical signal when stressed. Conversely, the application of an electrical signal produces mechanical deformation in the crystal; when this electrical stimulus is supplied in the form of an oscillating potential, rapid crystal vibrations are generated [62]. Piezoelectric polymers have long found wide application in numerous fields, including as components of nebulizers for pulmonary drug delivery, and have recently been introduced as a dispersion mechanism in dry powder inhalers.

An example of the piezoelectric de-agglomeration principle is found in the Microdose inhaler (US Patent No. 5,687,710), where a drug-containing blister is brought into contact with a piezoelectric vibrator housed within the device. The DPI includes an air flow sensor that activates the piezoelectric element as the patient inhales, transferring mechanical energy to the blister and imparted into the dry powder formulation within to disperse the dose through the blister openings [63]. Additionally, the frequency at which the piezoelectric element operates is not arbitrary, but set to match the blister's resonance frequency. Briefly explained, the acoustic

resonance of a system is its tendency to absorb more energy when oscillated at one of its own natural frequencies of vibration. By matching the frequency of the piezoelectric element to the resonance frequency of the blister, stronger oscillations can be generated without augmenting the effort required from the energy source.

An alternative application of the piezoelectric effect has been developed by Oriel Therapeutics, Inc. (US Patent No. 6,889,690), disclosing a multi-dose inhaler wherein the blisters containing the powder are comprised of a piezoelectric polymer material, incorporating the piezoelectric element into the blister itself. During inhalation, an electrical stimulus is provided to the blister, prompting the piezoelectric substrate to oscillate rapidly, vibrating the blister and ejecting the dose into the flow stream. Adjusting the shape of the blister can yield specific oscillation frequencies tailored to the flow characteristics of the formulation contained within; vibrating the blister to match the resonance frequency of the powder can optimize the dispersion potential [64]. Both of the above inhalers are active devices, requiring a self-contained power source to stimulate piezoelectric element.

#### **1.22. ELECTRIC AND MAGNETIC FIELDS**

While less common, de-agglomeration principles capitalizing on the high charge-to-mass ratio of micronized powders are found in the patent literature. In one example (US Patent No. 6,089,227), a DPI is comprised of two separate chambers, the barrier between them containing a rotating cylinder with a portion of its perimeter located in each chamber. One chamber is a powder reservoir, and the other is in fluid communication with an air inlet and outlet. When an electric field is generated in the reservoir, the charged powder is attracted to the surface of the electrically neutral cylinder, which slowly rotates, exposing the adhered drug particles to a second electric field, opposite in polarity from the first, in the adjacent chamber. This prompts the drug to detach from the dosing drum and flock to the electrode producing the field, although as this detachment is coordinated with inhalation, the particles are carried to the patient.

US Patent No. 6,328,033 also discloses an inhaler that utilizes an electric field, albeit an oscillating one. In this device, the electric field is oscillated between the top and bottom of the powder-holding chamber, entraining the drug particles as they are rapidly drawn from one side to the other. The electric field is maintained while the patient inhales through the device, and the flow passing through the chamber conveys the dose downstream. An additional embodiment of this design relies on a magnetic field for de-agglomeration, wherein the dry powder formulation is coated onto particles having a magnetic core. Upon actuation, a rapidly oscillating magnetic field is applied between the upper and lower sections of the dose package, causing the larger magnetic particles to rapidly vibrate, expelling the powder from their surfaces where the flow stream carries the dose to the patient. The magnetic field is sustained throughout the duration of the inhalation maneuver, confining the magnetic particles within the device.

### **1.23. DEVICE RESISTANCE AND FLOW RATE**

The role of resistance in DPIs, and the extent to which it influences device performance, is ambiguous. The equation relating flow rate (Q), device resistance (R), and the pressure drop ( $\Delta P$ ) across an inhaler was provided by Clark and Hollingsworth [65]:

$$\sqrt{\Delta P} = QR$$

For a given pressure drop, a higher flow rate will be generated through a lower resistance device. But how does device resistance translate into performance? When increasing the resistance in a DPI, either the air inlet is narrowed, or there is a constriction along the flow path, usually at the point where the fluid stream encounters the dose. As known from the flow continuity equation, reducing the cross sectional area increases the flow velocity, which in turn increases the kinetic energy carried by the flow stream; accordingly it seems intuitive that increased resistance would improve performance [49]. However, high resistance is not the only determinant of device performance. A comparison between the high resistance Pulvinal<sup>TM</sup> and the lower resistance Turbuhaler<sup>TM</sup>, both passive inhalers, demonstrated better dispersion performance in the latter DPI [66]. Equally important is the method in which the kinetic energy

from the flow rate is employed; in other words, the efficiency of the powder de-agglomeration principle. However, the importance of device resistance is being diminished through the introduction of inhalers that no longer rely solely on a brief, almost instantaneous interaction between the flow stream and powder (ACT, cyclones), and active DPIs providing external energy sources.

Studies comparing low and high resistance passive inhalers generally conclude that while low resistance devices allow a much wider range of flow rates, the performance of high resistance inhalers exceeds that of its low resistance counterparts [67, 68]. However, high resistance devices show significant flow rate dependence, and the amount of delivered drug varies widely across the spectrum of generated flow rates. In contrast, low resistance devices provide a more consistent dose across a wider range of inspiratory efforts. Additionally, a significant patient population, especially children and the elderly, have difficulty generating a sufficient flow rate through the higher resistance devices [69].

Closely related to resistance, is the flow rate through the device. While higher flow rates improve the kinetic energy levels imparted to the dose, increasing the flow rate through an inhaler does not improve performance ad infinitum. As shown in studies with the Aerolizer there is a flow rate where the fine particle fraction is maximized and throat deposition is minimal; increasing the flow rate beyond this point hinders performance as a larger fraction of the dose will deposit in the throat and mouth [36]. Accordingly, while high flow streams are desirable when encountering the dose, they are counterproductive if the velocity is not dampened as it exits the inhaler. One strategy to accomplish this is to widen the flow path in the mouthpiece, which significantly lowers the axial velocity of the flow stream as it exits the device, reducing throat and mouth deposition without comprising the turbulence levels [38]. Alternatively, other DPIs employ a co-axial sheath of air produced by flow bypass channels to form a buffer that surrounds the aerosol as it exits the device (Novolizer™), or incorporate baffles and curved paths to reduce flow velocity (Skyehaler™), although particle deposition may become problematic in these designs.

#### **1.24. MESHES AND SCREENS**

Ubiquitous to many commercial DPIs is a mesh, or screen, situated between the powder holding chamber and the inhaler exit, commonly tasked with performing the often overlooked, yet vital role of preventing the escape of the capsule, and capsule fragments, from the device during inhalation. However, it is also noted that meshes are integral components of inhalers that do not employ capsules, but rather disperse powder from blisters packs or reservoirs. The presence of the mesh can influence the flow field generated within an inhaler, both upstream and downstream of its location, and accordingly impact the overall performance of the device.

A mesh can be thought of as a distributed resistance that can effect a change in the flow direction of a fluid stream, coupled with a reduction in pressure [70], and can act as both a suppressor and generator of turbulence. In its role as a suppressor, the turbulence downstream of the mesh has been dampened in both scale and intensity subsequent to its passage through the mesh. In this case, the aim is obtaining a spatially uniform flow to both avoid generating further turbulence, and to remove existing turbulence from the flow stream. Meshes can also serve to increase the turbulence downstream of their location up to 10% relative of the upstream value. In this case, the meshes are commonly coarse, with porosities exceeding 45% of the total area.

Reports in the literature examining the influence of meshes on inhaler performance are at odds with each other, casting meshes in the role of both spectator and active participant in affecting device performance. A study investigating the influence of a mesh on carrier particle dispersion concluded that no benefit to overall performance (as measured by the  $FPF_{total}$ ) was obtained when powder was passed through a mesh, compared to the absence of the mesh [31]. Any small improvement in particle deaggregation the mesh may have provided was offset by the drug retained on the mesh ( $\approx 5\%$  of the nominal dose), resulting in no significant difference in performance. In contrast, Coates, et al., examining the effect of the grid inside the Aerolizer™ DPI, concluded that the grid does significantly affect overall inhaler performance. For these studies, dispersion performance of the Aerolizer™ outfitted with three different grids (the original grid geometry and two grids of increasing porosity) was compared, showing that the



original Aerolizer grid yielded no significant differences in the fine particle fraction of the emitted dose. This implies that the mesh had no effect on drug deaggregation, as noted in Voss and Finlay, but rather exerted its influence through reducing the number of impactions between the mouthpiece and the inhaler, as a significantly higher fraction of drug deposits inside the inhaler mouthpiece with increasing grid voidage. In the Aerolizer™, the grid serves as a turbulence suppressor, straightening the flow by reducing the level of tangential flow generated in the device [34]. As the turbulence is suppressed downstream of the powder dispersion chamber, overall performance is unaffected. In reconciling these opposing views, the length of the inhaler downstream of the mesh becomes important, and the dispersion apparatus used by Voss and Finlay was not a commercial inhaler, but an experimental set up with an extended flow path downstream of the grid. In this case, the laminar flow created by the mesh may have degenerated into turbulence flow prior to exiting the device.

#### **1.25. SUMMARY**

A diverse array of technologies have been designed to address the challenges of effectively aerosolizing a dry powder formulation. Recent years have seen an increase in the number of active DPIs in development, although passive devices, with their low costs and simple designs, will undoubtedly remain an active area of inhaler research, as they are especially attractive as disposable platforms for dry powder vaccine delivery. However, while much effort has been devoted to improving the powder dispersion performance of inhalers, the ability of the device to optimize inhalation therapy must be placed into perspective, as no matter how cleverly designed and masterfully crafted an inhaler may be, it cannot overcome patient misuse or a poorly prepared formulation. Future developments in DPIs will benefit greatly from parallel advancements in patient education and powder formulation technology. It is noted that the devices presented here were generally those that have been commercialized, which represent a small fraction of inhalers encountered in the patent literature.

## **1.26. CONCLUSION**

Despite the myriad designs that have been developed to improve device performance overall delivery remains low, as typically less than 30% of the total dose is delivered to the deep lung (for reported performance values, see Appendix). This is attributed to both the formulation and the inhaler, and thus accordingly, improving the performance of both will be the objective of this research.

## 1.27. REFERENCES

1. Frijlink, H.W. and A.H. de Boer, Trends in the technology-driven development of new inhalation devices. *Drug Discovery Today: Technologies*, 2005. 2(1): p. 47-57.
2. Smyth, H.D.C., and Leach, C.L., Alternative propellant aerosol delivery systems. *Critical Reviews in Therapeutic Drug Carrier Systems*, 2005. 22(6): p. 493 - 534.
3. Islam, N. and E. Gladki, Dry powder inhalers (DPIs)—A review of device reliability and innovation. *International Journal of Pharmaceutics*, 2008. 360(1-2): p. 1-11.
4. Ashurst, I., et al., Latest advances in the development of dry powder inhalers. *Pharmaceutical Science & Technology Today*, 2000. 3(7): p. 246-256.
5. Crowder, T.M., Louey, M.D., Sethuraman, V.V., Smyth, H.D.C., and Hickey, A.J, An odyssey in inhaler formulation and design. *Pharmaceutical Technology*, 2001. 7: p. 99 - 107.
6. Frijlink, H.W. and A.H. De Boer, Dry powder inhalers for pulmonary drug delivery. *Expert Opinion on Drug Delivery*, 2004. 1(1): p. 67-86.
7. Chow, A., et al., Particle Engineering for Pulmonary Drug Delivery. *Pharmaceutical Research*, 2007. 24(3): p. 411-437.
8. Finlay, W.H., *The Mechanics of Inhaled Pharmaceutical Aerosols*. 2001, London, UK: Academic Press.
9. de Boer, A., et al., Air classifier technology (ACT) in dry powder inhalation Part 1. Introduction of a novel force distribution concept (FDC) explaining the performance of a basic air classifier on adhesive mixtures. *International Journal of Pharmaceutics*, 2003. 260(2): p. 187-200.

10. Hickey, A.J., ed. *Pharmaceutical Inhalation Aerosol Technology*. 2nd ed. 2004, Marcel Dekker, Inc.: New York, NY.
11. Edwards, D.A., et al., Large Porous Particles for Pulmonary Drug Delivery. *Science*, 1997. 276(5320): p. 1868-1872.
12. Zeng, X.M., Martin, G.P., Marriott, C., and Pritchard, J., Lactose as a carrier in dry powder formulations: The influence of surface characteristics on drug delivery. *Journal of Pharmaceutical Sciences*, 2001. 90(9): p. 1424 - 1434.
13. French, D.L., Edwards, D.A., and Niven, R.W., The influence of formulation on emission, deaggregation and deposition of dry powders for inhalation. *Journal of Aerosol Science*, 1996. 27(5): p. 769 - 783.
14. Tee, S.K., Marriott, C., Zeng, X.M., and Martin, G.P., The use of different sugars as fine and coarse carriers for aerosolised salbutamol sulphate. *International Journal of Pharmaceutics*, 2000. 208: p. 111 - 123.
15. Steckel, H., Alternative sugars as potential carriers for dry powder inhalations. *International Journal of Pharmaceutics*, 2004. 270(1-2): p. 297-306.
16. Hooton, J.C., M.D. Jones, and R. Price, Predicting the behavior of novel sugar carriers for dry powder inhaler formulations via the use of a cohesive–adhesive force balance approach. *Journal of Pharmaceutical Sciences*, 2006. 95(6): p. 1288-1297.
17. Begat, P., Morton, D.A.V., Staniforth, J.N., and Price, R., Dry powder inhaler formulations I: Direct quantification by atomic force microscopy. *Pharmaceutical Research*, 2004. 21(9): p. 1591 - 1597.
18. Saleem, I., H. Smyth, and M. Telko, Prediction of Dry Powder Inhaler Formulation Performance From Surface Energetics and Blending Dynamics. *Drug Development and Industrial Pharmacy*, 2008. 34(9): p. 1002-1010.

19. Steckel, H., and Muller, B.W., In vitro evaluation of dry powder inhalers II: influence of carrier particle size and concentration on in vitro deposition. *International Journal of Pharmaceutics*, 1997. 154: p. 31 - 37.
20. Dickhoff, B., The effect of carrier surface and bulk properties on drug particle detachment from crystalline lactose carrier particles during inhalation, as function of carrier payload and mixing time. *European Journal of Pharmaceutics and Biopharmaceutics*, 2003. 56(2): p. 291-302.
21. de Boer, A.H., et al., The Mode of Drug Particle Detachment from Carrier Crystals in an Air Classifier-Based Inhaler. *Pharmaceutical Research*, 2004. 21(12): p. 2167-2174.
22. Podczec, F., The relationship between physical properties of lactose monohydrate and the aerodynamic behaviour of adhered drug particles. *International Journal of Pharmaceutics*, 1998. 160: p. 119 - 130.
23. Louey, M.D., Mulvaney, P., and Stewart, P.J., Characterisation of adhesional properties of lactose carriers using atomic force microscopy. *Journal of Pharmaceutical and Biomedical Analysis*, 2001. 25: p. 559 - 567.
24. Louey, M.D., and Stewart, P.J., Particle interactions involved in aerosol dispersion of ternary interactive mixtures. *Pharmaceutical Research*, 2002. 19(10): p. 1524 - 1531.
25. Louey, M.D., Razia, S., and Stewart, P.J., Influence of physico-chemical carrier properties on the in vitro aerosol deposition from interactive mixtures. *International Journal of Pharmaceutics*, 2003. 252: p. 87 - 98.
26. Guenette, E., et al., Understanding the effect of lactose particle size on the properties of DPI formulations using experimental design. *International Journal of Pharmaceutics*, 2009. 380(1-2): p. 80-88.

27. Hickey, A.J., et al., Physical characterization of component particles included in dry powder inhalers. I. Strategy review and static characteristics. *Journal of Pharmaceutical Sciences*, 2007. 96(5): p. 1282-1301.
28. de Boer, A., et al., Air classifier technology (ACT) in dry powder inhalation Part 2. The effect of lactose carrier surface properties on the drug-to-carrier interaction in adhesive mixtures for inhalation. *International Journal of Pharmaceutics*, 2003. 260(2): p. 201-216.
29. Cline, D., and Dalby, R., Predicting the quality of powder for inhalation from surface energy and area. *Pharmaceutical Research*, 2002. 19(9): p. 1274 - 1277.
30. Dickhoff, B., et al., The interaction between carrier rugosity and carrier payload, and its effect on drug particle redispersion from adhesive mixtures during inhalation. *European Journal of Pharmaceutics and Biopharmaceutics*, 2005. 59(1): p. 197-205.
31. Selvam, P., et al., Micronized Drug Adhesion and Detachment from Surfaces: Effect of Loading Conditions. *Aerosol Science and Technology*, 2011. 45(1): p. 81-87.
32. Voss, A., and Finlay, W.H., Deagglomeration of dry powder pharmaceutical aerosols. *International Journal of Pharmaceutics*, 2002. 248: p. 39 - 50.
33. Nichols, S.C., and Wynn, E., New Approaches to Optimizing Dispersion in Dry Powder Inhalers – Dispersion Force Mapping and Adhesion Measurements. *Respiratory Drug Delivery 2008*, 2008. 1: p. 175 - 184.
34. Chew, N.Y.K., Chan, H.K., Bagster, D.F., and Mukhraiya, Characterization of pharmaceutical powder inhalers: estimation of energy input for powder dispersion and effect of capsule device configuration. *Aerosol Science*, 2002. 33: p. 999 - 1008.

35. Coates, M.S., et al., Effect of design on the performance of a dry powder inhaler using computational fluid dynamics. Part 1: Grid structure and mouthpiece length. *Journal of Pharmaceutical Sciences*, 2004. 93(11): p. 2863-2876.
36. Coates, M.S., et al., The Role of Capsule on the Performance of a Dry Powder Inhaler Using Computational and Experimental Analyses. *Pharmaceutical Research*, 2005. 22(6): p. 923-932.
37. Coates, M.S., et al., Influence of Air Flow on the Performance of a Dry Powder Inhaler Using Computational and Experimental Analyses. *Pharmaceutical Research*, 2005. 22(9): p. 1445-1453.
38. Coates, M.S., et al., Effect of design on the performance of a dry powder inhaler using computational fluid dynamics. Part 2: Air inlet size. *Journal of Pharmaceutical Sciences*, 2006. 95(6): p. 1382-1392.
39. Coates, M.S., et al., Influence of Mouthpiece Geometry on the Aerosol Delivery Performance of a Dry Powder Inhaler. *Pharmaceutical Research*, 2007. 24(8): p. 1450-1456.
40. Larhrib, H., Characterisation and deposition studies of engineered lactose crystals with potential for use as a carrier for aerosolised salbutamol sulfate from dry powder inhalers. *European Journal of Pharmaceutical Sciences*, 2003. 19(4): p. 211-221.
41. Podczeck, F., Evaluation of the Adhesion Properties of Salbutamol Sulphate to Inhaler Materials. *Pharmaceutical Research*, 1998. 15(5): p. 806-808.
42. Kawashima, Y., Serigano, T., Hino, T., Yamamoto, H., and Takeuchi, H., Effect of surface morphology of carrier lactose on dry powder inhalation property of pranlukast hydrate. *International Journal of Pharmaceutics*, 1998. 172: p. 179 - 188.

43. Zeng, X.M., Martin, G.P., Marriott, C., and Pritchard, J., The influence of carrier morphology on drug delivery by dry powder inhalers. *International Journal of Pharmaceutics*, 2000. 200: p. 93 - 106.
44. Srichana, T., Martin, G.P, and Marriott, C., On the relationship between drug and carrier deposition from dry powder inhalers in vitro. *International Journal of Pharmaceutics*, 1998. 167: p. 13 - 23.
45. Zeng, X.M., Martin, G.P., Tee, S.K., and Marriott, C., The role of fine particle lactose on the dispersion and deaggregation of salbutamol sulphate in an air stream in vitro. *International Journal of Pharmaceutics*, 1998. 176: p. 99 - 110.
46. Zeng, X.M., Martin, G.P., Tee, S.K., Ghoush, A.A., and Marriott, C., Effects of particle size and adding sequence of fine lactose on the deposition of salbutamol sulphate from a dry powder formulation. *International Journal of Pharmaceutics*, 1999. 182: p. 133 - 144.
47. Staniforth, J.N., Performance-modifying influences in dry powder inhalation systems. *Aerosol Science and Technology*, 1995. 22(4): p. 346 - 353.
48. Islam, N., Stewart, P., Larson, I., and Hartley, P., Lactose surface modification by decantation: are drug-fine lactose ratios the key to better dispersion of salmeterol xinafoate from lactose-interactive mixtures? *Pharmaceutical Research*, 2004. 21(3): p. 492 - 499.
49. Karhu, M., Kuikka, J., Kauppinen, T., Bergstrom, K., and Vidgren, M., Pulmonary deposition of lactose carriers used in inhalation powders. *International Journal of Pharmaceutics*, 2000. 196: p. 95 - 103.
50. Gupta, V., and Gupta, S.K., *Fluid Mechanics and Its Applications*. 1984, New Delhi: New Age International.



51. Wetterlin, K., Turbuhaler: A new powder inhaler for administration of drugs to the airways. *Pharmaceutical Research*, 1988. 5(8): p. 506 - 508.
52. de Boer, A.H., Gjaltema, D., and Hagedoorn, P., Inhalation characteristics and their effects on in vitro drug delivery from dry powder inhalers Part 2: Effect of peak flow rate (PIFR) and inspiration time on the in vitro drug release from three different types of commercial dry powder inhalers. *International Journal of Pharmaceutics*, 1996. 138: p. 45 - 56.
53. Brambilla, G., Cocconi, D., Armani, A., Smith, S., Lye, E., and Burge, S., Designing a novel dry powder inhaler: The NEXT™ DPI (Part 1). *Respiratory Drug Delivery*, 2006. 2: p. 553 - 555.
54. Needham, M., Fradley, G., and Cocks, P., Investigating the efficiency of reverse cyclone technology for DPI drug delivery. *Respiratory Drug Delivery*, 2010. 2: p. 369 - 372.
55. Stein, S., Hodson, D., Alband, T., Sitz, R., Robison, T., Wang, Z., Chiou, H., Simons, J., McNally, R., and Ganser, J., The 3M taper dry powder inhaler device. *Respiratory Drug Delivery*, 2010. 2: p. 377 - 380.
56. Aydin, M., Akouka, H., Merrill, T., Reynolds, E., Becker, D., Shukla, R., Weitzel, D., and Byron, D., Application of synthetic jetting for pulmonary delivery of drug candidates.
57. Bisgaard, H., et al., Fine particle mass from the Diskus inhaler and Turbuhaler inhaler in children with asthma. *European Respiratory Journal*, 1998. 11(5): p. 1111-1115.
58. de Boer, A., et al., Air classifier technology (ACT) in dry powder inhalation Part 3. Design and development of an air classifier family for the Novolizer® multi-dose dry powder inhaler. *International Journal of Pharmaceutics*, 2006. 310(1-2): p. 72-80.

59. de Boer, A.H., Hagedoorn, P., Gjaltema, D., Lambregts, D., Iringarter, M., and Frijlink, H.W., The rate of drug particle detachment from carrier crystals in an air classifier-based inhaler. *Pharmaceutical Research*, 2004. 21(12): p. 2158 - 2166.
60. de Boer, A., et al., Design and in vitro performance testing of multiple air classifier technology in a new disposable inhaler concept (Twincer®) for high powder doses. *European Journal of Pharmaceutical Sciences*, 2006. 28(3): p. 171-178.
61. Wachtel, H., Ertunc, O., Koksoy, C., and Delgado, A., Aerodynamic Optimization of Handihaler and Respimat: The Roles of Computational Fluid Dynamics and Flow Visualization. *Respiratory Drug Delivery 2008*, 2008. 1: p. 165 - 174.
62. Selvam, P., et al., A novel dry powder inhaler: Effect of device design on dispersion performance. *International Journal of Pharmaceutics*, 2010. 401(1-2): p. 1-6.
63. Eiggins, B.R., *Chemical Sensors and Biosensors*. 2002, West Sussex, England: John Wiley & Sons Ltd.
64. Brown, B., Rasmussen, J., Becker, D., and Friend, D.R., A piezo-electronic inhaler for local and systemic applications. *Drug Delivery Technology*, 2004. 4(8): p. 90 - 93.
65. Crowder, T. and A. Hickey, Powder specific active dispersion for generation of pharmaceutical aerosols. *International Journal of Pharmaceutics*, 2006. 327(1-2): p. 65-72.
66. Clark, A.R., and Hollingworth, A.M., The relationship between powder inhaler resistance and peak inspiratory conditions in healthy volunteers - implications for in vitro testing. *Journal of Aerosol Medicine*, 1993. 6(2): p. 99 - 110.
67. MEAKIN, B.J., et al., The Effect of Flow Rate on Drug Delivery from the Pulvinal, a High-Resistance Dry Powder Inhaler. *Journal of Aerosol Medicine*, 1998. 11(3): p. 143-152.

68. Srichana, T., G.P. Martin, and C. Marriott, Dry powder inhalers: The influence of device resistance and powder formulation on drug and lactose deposition in vitro. *European Journal of Pharmaceutical Sciences*, 1998. 7(1): p. 73-80.
69. Mendes, P., J. Pinto, and J. Sousa, A non-dimensional functional relationship for the fine particle fraction produced by dry powder inhalers. *Journal of Aerosol Science*, 2007. 38(6): p. 612-624.
70. Johannes, H.W., et al., Inhalation therapy in asthma: Nebulizer or pressurized metered-dose inhaler with holding chamber? In vivo comparison of lung deposition in children. *The Journal of pediatrics*, 1999. 135(1): p. 28-33.
71. Laws, E.M., and Livesey, J.L., Flow through screens. *Annual Reviews in Fluid Mechanics*, 1978. 10: p. 247 - 266.

#### Patents

US Patent No. 11,713,180

US Patent No. 6,889,690

US Patent No. 6,138,673

US Patent No. 7,107,988

US Patent No. 6,237,591

US Patent No. 6,971,384

US Patent No. 5,655,523

US Patent No. 5,724,959

US Patent No. 5,875,772

US Patent No. 5,775,320

US Patent No. 6,257,233

US Patent No. 7,354,577

US Patent No. 6,561,180

US Patent No. 6,182,655

US Patent No. 5,087,710

US Patent No. 6,089,277

US Patent No. 6,328,033

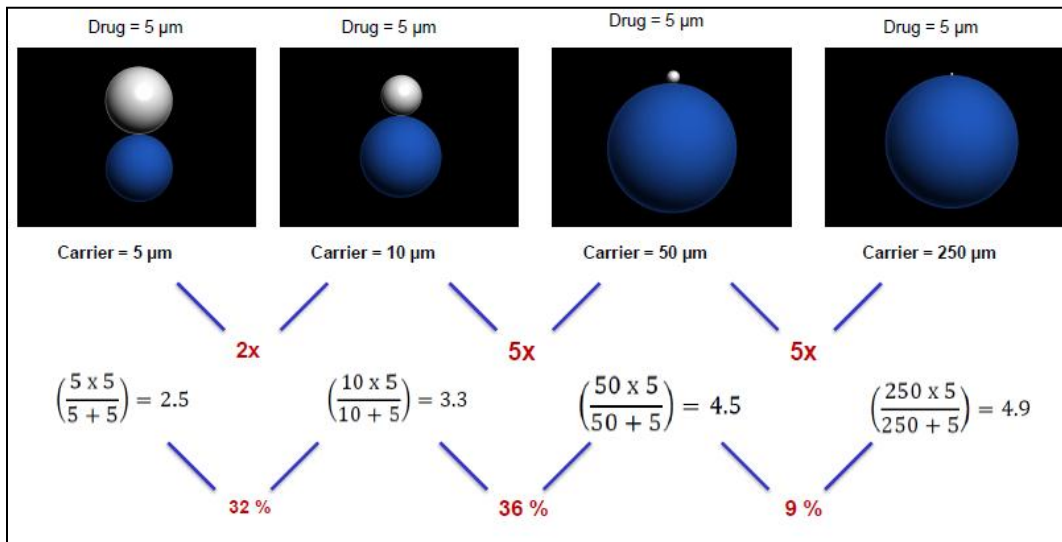


Figure 1.1. Influence of Carrier Particle Size on Theoretical van der Waals Forces

Variation in theoretical van der Waals forces as carrier particle size is increased and the drug particle diameter is held constant.

## CHAPTER 2

### 2. Research Objectives

The main objective of this Ph.D. thesis was to understand the mechanisms of drug detachment from carrier particles in binary DPI formulations, which generally deliver less than 30% of the dose to the deep lung (Appendix). As highlighted in the previous chapter, while the influence that carrier particle physical properties impart to the aerosol performance of a formulation has been an extensively examined topic, much of the previous research has focused primarily on similar particle diameters (typically  $< 100 \mu\text{m}$ ) and morphologies ( $\alpha$ -lactose monohydrate). Accordingly, the theories that were developed to explain and predict performance of DPI formulations were based upon observations obtained from limited data sets, and much of the carrier particle landscape, in terms of size and surface roughness, has remained unexplored.

We proposed that given the underlying physical equations governing momentum and collision forces, large carrier particles may prove more beneficial to performance than previously believed. Accordingly, the specific aims of this thesis were to:

1. Provide a comprehensive study evaluating the influence of carrier particle diameter and morphology on the aerosol performance of binary DPI formulations.
2. Examine the mechanism by which the surface roughness of the carrier particle population affects performance as a function of the diameter of the carrier particle.
3. Investigate the influence that the diameter and surface roughness of the carrier particle population impart to the performance of a dry powder inhaler. Specifically, this will evaluate the performance from different inhalers as a function of the size and surface roughness of the carrier particle population.

4. The final study will assess the influence of the volumetric flow rate through a DPI as a function of the diameter and surface roughness of the carrier particle population.

These topics will be addressed in Chapters 3 through 6, and the experimental outlines of these studies are shown in Tables 1 – 4. The observations gleaned from these experiments will then guide the development of a novel mechanism of dry powder dispersion, which will be the focus of Chapters 7 through 10.

Table 2.1. Chapter 3: Comprehensive Study of Lactose Carrier Particles in Binary Blends

Carrier Particle Material	Carrier Particle Size Fractions ( $\mu\text{m}$ )	API	Concentration	Volumetric Flow Rate ( $\text{L min}^{-1}$ )	DPI
$\alpha$ -Lactose Monohydrate	< 20	Salbutamol	1 % (w/w)	60	Aerolizer*
Anhydrous Lactose	20 – 32				
Spray Dried Lactose	32 – 45				
Granulated Lactose	45 – 63				
	63 – 75				
	75 - 90				
	90 – 106				
	106 – 125				
	125 - 150				
	150 – 180				
	180 – 212				
	212 – 250				
	250 - 300				



Table 2.2. Chapter 4: Influence of Carrier Particle Diameter and Surface Roughness on Aerosol Performance

Carrier Particle Material	Carrier Particle Size Fractions ( $\mu\text{m}$ )	API	Concentration	Volumetric Flow Rate ( $\text{L min}^{-1}$ )	DPI
Anhydrous Lactose	< 32	Budesonide	2 % (w/w)	60	Aerolizer*
Granulated Lactose	32 – 45				
	45 – 63				
	63 – 75				
	75 - 90				
	90 – 125				
	125 - 150				
	150 – 180				
	180 – 212				
	212 – 250				
	250 - 300				

Table 2.3. Chapter 5: Influence of DPI Device on Aerosol Performance as a Function of Carrier Particle Diameter and Surface Roughness

Carrier Particle Material	Carrier Particle Size Fractions ( $\mu\text{m}$ )	API	Concentration	Volumetric Flow Rate ( $\text{L min}^{-1}$ )	DPI
Anhydrous Lactose	< 32	Budesonide	2 % (w/w)	60	Aerolizer*
Granulated Lactose	32 – 45				Handihaler*
	45 – 63				
	63 – 75				
	75 - 90				
	90 – 125				
	125 - 150				
	150 – 180				
	180 – 212				
	212 – 250				
250 - 300					

Table 2.4. Chapter 6: Influence of Flow Rate on Aerosol Performance as a Function of Carrier Particle Diameter and Surface Roughness

Carrier Particle Material	Carrier Particle Size Fractions ( $\mu\text{m}$ )	API	Concentration	Volumetric Flow Rate ( $\text{L min}^{-1}$ )	DPI
$\alpha$ -Lactose Monohydrate	45 – 63	Salbutamol Sulphate	1 % (w/w)	30	Aerolizer*
Granulated Lactose	125 - 150	Budesonide		60	
	250 - 300			90	

## CHAPTER 3

### 3. Comprehensive Study on the Influence of Size and Morphology of Lactose Carrier Particles on the Aerosol Performance of Binary DPI Formulations

#### 3.1. INTRODUCTION

Dry powder formulations for pulmonary delivery are generally binary blends, comprised of micronized drug particles with aerodynamic diameters between 1 – 5  $\mu\text{m}$  and coarse, inert carrier particles that comprise the bulk (> 98% (w/w)) of the formulation. The carrier particles assist in powder entrainment and fluidization during inhalation, as the cohesive forces between micronized drug particles are too strong to allow adequate dispersion. Additionally, the carrier particles facilitate dose metering, as typically 10 – 200 mcg of drug are required per dose, and such small quantities are difficult to measure accurately and reproducibly. However, while carrier particles are beneficial to the performance of dry powder systems, detachment of drug particles from the surface of the carriers remains problematic, and drug that remains adhered to the coarse carriers will deposit in the throat and upper airways, exerting no therapeutic effect and inducing unwanted side effects. Consequently, commercially available dry powder inhalers are inefficient, delivering only approximately 20 – 30% of the total dose to its intended target of the deep lung.

The understanding that a judicious selection of both drug and carrier particle properties are crucial parameters in optimizing performance is universally acknowledged. Production of a stable and homogeneous powder blend requires the interaction between drug and carrier particles be balanced, with forces strong enough such that drug preferentially adheres to the carrier during mixing, yet sufficiently tenuous to facilitate re-dispersion of drug particles during inhalation. Studies focused on the physical properties of carriers have examined the particle size, size distribution, morphology, surface roughness, surface area, and surface energy of carrier particle populations [1-11]. The influence that the physical properties of the carrier

particles can impart to the aerosol performance of the formulation has been well documented in the literature, and a general consensus has been reached in the field that increasing the diameter of the carrier particle population hinders drug dispersion performance.

As discussed in chapter 1, to account for this observation multiple explanations have been proposed in the literature, and the previous two decades have witness extensive research on the various physicochemical properties of lactose carrier particles that most influence aerosol performance. However, when one examines these studies, it quickly becomes apparent that while the conclusions are intended to be predictive for a wide range of carrier particle physical properties, the sample size upon which they are based is generally limited, consisting of only a few experimental formulations.

Specifically, studies that focus on examining the influence of carrier particle diameter on aerosol performance have tended to employ only a single lactose grade, specifically  $\alpha$ -lactose monohydrate, characterized by relatively flat surfaces and a morphology commonly described as a 'tomahawk' shape. Conversely, studies that focus on evaluating the influence of surface roughness have employed only a single carrier particle size fraction; typically well below 100  $\mu\text{m}$ . From these relatively small sample sizes, theories predicting the performance of a wide range of carrier particle sizes and surface roughness levels have been developed, thus relying extensively on interpolation and extrapolation to account for the broad swathes of terra incognita that remain unexplored on the carrier particle landscape.

#### *Specific Aim*

Accordingly, the aim of this chapter is to fill in the gaps from the literature by performing a comprehensive study using 4 lactose grades fractionated into narrow and contiguous particle diameter populations up to 300  $\mu\text{m}$ . In addition to evaluating the aerosol performance of the resulting DPI formulations, the physicochemical parameters of the carrier particle populations that have been previously cited as being important to performance were measured to examine their influence on dispersion from the lactose carriers. These parameters include the particle size distribution, concentration of lactose fines, specific surface areas, and

surface energies of the carrier particles, and also the blend uniformities of the resulting formulations.

## **3.2. EXPERIMENTAL**

### **3.2.1. Materials**

Salbutamol was purchased in bulk (Jinhua Chemical Company, China) and micronized with a high energy jet-mill with pusher and grinding pressures of 80 and 110 PSI, respectively (Aljet; Fluid Energy Processing and Equipment Co., PA, USA). 500 g samples of lactose monohydrate (Pharmatose® 80 Mesh), anhydrous lactose (SuperTab® 21AN), spray-dried lactose (SuperTab® 14SD), and granulated lactose (SuperTab® 30GR) were provided by DMV-Fonterra (New Zealand). Size-3 HPMC capsules (VCaps®) were gifted by Capsugel (NJ, USA). Analytical grade ethanol was purchased from Sigma (Sigma-Aldrich, Corp., MO, USA).

### **3.2.2. Fractionation of Carrier Particle Populations**

Samples of each lactose batch were fractionated on an Autosiever® vibrating sieve shaker (Gilson Company Inc., OH, USA) with a sieve intensity, or amplitude, setting of 40 for 5 minutes through the following sieves: 300 µm, 250 µm, 212 µm, 180 µm, 150 µm, 125 µm, 106 µm, 90 µm, 75 µm, 63 µm, 45 µm, 32 µm, and 20 µm. Following the initial fractionation, the lactose carriers were sieved two additional times, at 3-minute sieving intervals, to obtain narrow particle size distributions. In total, lactose was obtained to produce binary blends of 13 size fractions each for α-lactose monohydrate, anhydrous lactose, spray-dried lactose and granulated lactose for a total of 52 formulations.

### **3.2.3. Preparation of Binary Blends**

Approximately 5 mg of salbutamol were mixed with 495 mg of the fractionated lactose populations via geometric dilution to obtain 500 mg of a 1% binary blend. The formulations were prepared in 30 mL glass vials and blended with a Turbula® orbital mixer (Glen Mills, NJ, USA) for 40 minutes at 46 RPM. Following blending, the formulations were stored in a

desiccator at least 5 days prior to use. The drug content uniformity of the resulting blends was assessed by randomly selecting eight 20-mg samples from each mixture, and analyzing the drug content in the powder. The blend uniformity for each formulation is provided as the coefficient of variation; the percent ratio of the standard deviation to the mean for N = 8 samples.

#### **3.2.4. Physical Characterization of the Powders**

The size distribution and surface roughness of the lactose carrier particle populations were visually examined by scanning electron microscopy (SEM; Supra 40VP, Zeiss, Germany). Prior to SEM, approximately 20 nm of a platinum::palladium (80::20) mixture was deposited onto the particles via sputter coating.

The drug and carrier particles were sized via laser diffraction using a Sympatec HELOS (Sympatec GmbH, Germany) apparatus equipped with a 6-mL cuvette dispersing system. Mineral oil was used as the dispersing fluid, which included 1% Span 85 to aid in particle de-aggregation. The powders were suspended in the mineral oil and, if physically stable, sonicated for 60 seconds to disrupt aggregates. Measurements were collected following elimination of all visible air bubbles. The ‘forced stability’ option was used to ignore the signal from errant dust or residual air bubbles. The span of the carrier particle size was obtained according to the following formula:

$$\text{Span} = \frac{d_{50}}{d_{90} - d_{10}}$$

To evaluate the concentration of fine lactose particles present in each carrier particle population, the percent volume of lactose particles below 10  $\mu\text{m}$  in each of the fractionated lactose samples was also measured by laser diffraction.

The specific surface area of the lactose carrier particle populations was evaluated via nitrogen adsorption with a single-point BET method with a Monosorb<sup>®</sup> surface area analyzer (Quantachrome Instruments; FL, USA). Samples were outgassed under nitrogen at 40 °C for 24 hours prior to each measurement.

### **3.2.5. Inverse Gas Chromatography (IGC)**

Inverse Gas Chromatography (IGC) was employed to measure the surface energy of three different size fractions of each lactose type. A Hewlett Packard (now Agilent) 5890 Series II gas chromatograph with a flame ionization detector (FID) was converted to IGC by removing the internals of the oven and replacing them with glass tubing (ID 5 mm). A piece of glass tubing (L = 8 in) was packed with between 1-2 g of powder, and plugged with silanized glass wool on either end. All glass tubing pieces were silanized by soaking in a 0.5% (v/v) dichloromethyl silane solution in toluene, rinsing in toluene and ethanol. Glass tubing was stored in a desiccator prior to use.

To determine the dispersive component of the powder surface energy, a series of injections of the normal alkanes from n-hexane to n-decane were used. THF, chloroform, acetone, ethanol, ethyl ether, and ethyl acetate were employed as polar probes to determine the specific component of the surface energy. All injections were performed at infinite dilution. The original enthalpy method was used instead of assuming constant entropy (which, experimentally, was shown to not occur); thus, each powder was subjected to three temperatures: 60 deg C, 48 deg C, and 36 deg C. Lower temperatures were not possible to control with the built-in oven of the IGC.

### **3.2.6. *In vitro* Aerosol Performance**

20 ( $\pm$  1) mg of powder were loaded into size-3 HPMC capsules and dispersed through an Aerolizer® (Plastiapae S.p.A., Italy) DPI into a next generation cascade impactor (MSP Corporation, MN, USA) at a volumetric flow rate of 60 L min<sup>-1</sup>. HPMC capsules were selected instead of traditional gelatin capsules as the latter have a tendency to fracture when their walls are perforated by the piercing mechanism of the inhaler. Accordingly, when the capsule fractures the size of the perforations are altered, and it has been demonstrated that the size of the perforations can alter performance through the Aerolizer. HPMC capsules perforated reproducibly, such that deviations in aerosol performance were not attributed to variations in the capsule. Actuation time was set to 4 seconds to allow 4 L of air to pass through the device.



To inhibit particle re-entrainment upon deposition, the NGI stages were coated with a 2% (v/v) solution of silicon oil in hexane and allowed to air dry prior to each impaction. Before each actuation 15 mL of EtOH were added to the pre-separator and collected following powder dispersion from each capsule. Drug depositing in the capsule, inhaler, mouthpiece adaptor, and induction port were collected by rinsing each component with 10 mL of EtOH, while the NGI stages were each rinsed with 5 mL.

Drug content was assessed using UV-VIS absorption spectroscopy at 230 nm. The emitted fraction was calculated as the ratio of the drug mass depositing in the mouthpiece, induction port, pre-separator, and impactor stages over the cumulative mass of drug collected following actuation (total drug deposited in the capsule, inhaler, mouthpiece, induction port, pre-separator and stages). The fine particle fraction (FPF) of each dose was the ratio of the drug mass depositing on stages 3 through 8 (corresponding to an aerodynamic diameter less than 4.46  $\mu\text{m}$ ) of the impactor over the emitted dose [12]. The respirable fraction (RF) was the ratio of the drug mass depositing on stages 3 – 8 over the entire dose recovered following each actuation.

### **3.2.7. Statistics**

Statistical significance between performance values was determined with one-way ANOVA with Post Hoc tests between groups according to the Bonferroni method ( $P < 0.05$ ).

## **3.3. RESULTS AND DISCUSSION**

### **3.3.1. Physical Characterization of Lactose Particles**

From the SEM images depicted in Figure 3.1 - Figure 3.4, it is noted that the four lactose grades possess markedly diverse morphologies and surface characteristics. Lactose monohydrate and anhydrous lactose are characterized by relatively low surface roughness. Spray dried lactose and granulated lactose exhibit extensive surface roughness with increasing carrier particle size; it is noted that the surface asperities are more pronounced for the granulated carrier particles, specifically as diameter is increased.

Table 3.1 lists the measured specific surface areas (SSA). For both the lactose monohydrate and anhydrous populations, SSA values generally exhibited a progressive decline with increasing carrier particle size, diminishing from 0.98 m<sup>2</sup>/g to 0.18 m<sup>2</sup>/g for the former, and 0.79 to 0.31 m<sup>2</sup>/g for the latter between the < 20 μm and 250 – 300 μm particle size fractions. It is noted that for anhydrous carriers the drop in surface area was not as steep, nor continuous, by comparison with lactose monohydrate. Indeed, a small increase in SSA was observed for larger carrier particle size ranges relative to the preceding size fraction. Additionally, there was a marked disparity in SSA values at the largest size fractions for anhydrous lactose when compared to lactose monohydrate, suggesting that larger carrier particles of anhydrous lactose possess some degree of surface roughness.

SSA values from the spray dried lactose were erratic, as overall performance between the 20 – 32 μm and 250 – 300 μm size fractions declined from 0.42 m<sup>2</sup>/g down to 0.34 m<sup>2</sup>/g. However, in between these size ranges the specific surface area fluctuated between 0.31 m<sup>2</sup>/g and 0.43 m<sup>2</sup>/g, indicating that small spray dried particles possessed relatively low surface areas (as would be expected based on their spherical morphology), and large carrier particles were characterized by extensive surface roughness. The SSA values from granulated particles initially diminished between the 20 – 32 μm and 75 – 90 μm carrier particle populations. However, following this size range the SSA of the particles increased up to 0.43 m<sup>2</sup>/g for the 250 – 300 μm size fraction, indicating that large granulated particles possess extensive surface roughness, with values generally comparable to those of the spray dried carriers.

### **3.3.2. Fine Lactose Concentration**

Of the four lactose grades, the respective size fractions of α-lactose monohydrate generally contained the highest concentration of fine lactose particles (diameters < 10 μm) (Tables 3.2 – 3.5). Moreover, in contrast to the other lactose grades, only α-lactose monohydrate populations possessed a noticeable concentration of fines for the larger diameter size fractions. As the carrier particle populations were triple-sieved, fines that remained were likely very strongly adhered to the surface of the large carriers. This may be indicative of the high surface energy of the lactose monohydrate carriers relative to the other lactose grades, as

the strong attachment between the fines and carriers could be due to the 'active' sites on the carrier surface.

Extensive research has repeatedly demonstrated that formulations with higher concentrations of fine particles typically outperform formulations possessing a lower amount of lactose fines [13-15]. To explain this observation two principle theories have been presented in the literature. The 'active site' theory proposes that fine excipient particles will predominately adhere to regions on the surface of the lactose carrier particles possessing the highest energies, or active sites, thereby promoting strong interparticle interactions [14]. Accordingly, if the high energy sites on the coarse carriers are already occupied by excipient fines, when the micronized drug particles are blended with the carrier population the API will then occupy lower energy sites, facilitating detachment from the carriers during inhalation. An alternate theory proposes that during blending the fine excipient particles and micronized drug can form loose aggregates, termed 'multiplets,' that promote detachment from the carrier surface due to their larger diameter, and thus surface area, relative to individual drug particles [7, 13, 16]. The greater surface area increases the force exerted on the multiplets by the flow stream, allowing them to be more readily liberated from the carrier surface compared to primary API particles. The multiplets formed between the adhesive forces of the drug and excipient are predicted to be less stable than aggregates comprised solely of drug particles and held together via cohesive interactions.

Accordingly, from the previous theories it would be expected that lactose monohydrate carriers, specifically the smaller size fractions possessing extensive lactose fines concentrations, would produce relatively high aerosol performance due to passivation of active sites on the carrier particles or the formation of readily detached multiplets. It is noted that anhydrous, spray dried and granulated lactose populations exhibited some degree of lactose fines, though for these three lactose grades only smaller size fractions possessed a measurable amount. Studies examining the potential of anhydrous lactose to serve as carrier particles in binary DPI formulations have noted a relatively high concentration of fine particles following jet sieving, which was attributed to the relatively brittle nature of this lactose grade [17]. For spray-dried

and granulated carriers, fine lactose particles were not observed in the SEM images, in contrast to the lactose monohydrate and the anhydrous lactose grades. However, it is likely that these fines were primarily located within the surface asperities, where multiple contact points between the fine particle and the coarse carrier would induce strong adhesive interactions.

### **3.3.3. Blend Uniformity**

Production of a stable and homogeneous binary DPI formulation requires the adhesive interaction between the drug and carrier be sufficiently robust such that the drug particles preferentially bind to the carrier during blending, and then remain adhered to the carrier from its production, through transit, and until used by the patient. However, good aerosol performance dictates that the drug-carrier interaction be sufficiently tenuous to permit drug detachment and re-dispersion during inhalation [18]. The inability to satisfactorily balance these competing conditions yields the low drug delivery efficiency traditionally associated with binary DPI blends [2]. Indeed, studies evaluating blend stability and uniformity have noted an inverse relationship with aerosol performance, where binary blends demonstrating excellent drug content homogeneity displayed significantly reduced aerosol performance relative to counterparts with comparatively lower blend uniformity [19].

Governing the relative strength of these adhesive interactions are the physicochemical properties of the carrier particle population, including carrier particle size, size distribution, mass, surface roughness, available surface area, and surface energy. In addition to the physicochemical properties of the carrier particle population, content uniformity may also be influenced by the API in the blend [18, 20, 21]. Furthermore, the drug-carrier interactions may be modified by the drug concentration (% w/w) and blending parameters, including mixing times, blending speeds, and batch size [9, 22].

As the surface area available for drug binding is diminished, the potential for drug-drug interactions increases, promoting the formation of stable drug agglomerates that may be resistant to dispersion during inhalation. Accordingly, it was not unexpected that the largest carrier size fraction of lactose monohydrate would exhibit low blend uniformity (%CV = 9.3%), as

it possessed the lowest SSA values of all the carrier particle populations. However, it was surprising that the smallest size fractions of lactose monohydrate would also exhibit poor blend uniformity. Indeed, the < 20  $\mu\text{m}$  lactose monohydrate fraction produced the least uniform blend despite possessing the greatest overall surface area available for drug binding.

To explain this apparent contradiction, it is necessary to examine the theories describing the blending of binary formulations. As noted by de Boer, there are two types of drug agglomerates encountered during blending; the 'natural' agglomerates and the 'blending' agglomerates [5]. The natural agglomerates are initially present in the drug powder when it is added to the formulation, and these must be broken down via abrasion by the coarse carriers during blending. This abrasion process requires that the carrier particles be sufficiently heavier than the drug particles, otherwise the contact between drug and carrier will be insufficient to disrupt these natural agglomerates.

Conversely, blending agglomerates are formed during mixing due to repeated and extensive contact between drug particles. Blending agglomerates would be expected to arise when insufficient carrier particle surface area is available, thus inducing extensive drug-drug interactions. It is expected that the formation of agglomerates would be especially problematic when using a cohesive drug such as budesonide. Accordingly, it is speculated that despite its high surface area, the < 20  $\mu\text{m}$  fraction possesses insufficient mass and surface roughness to disrupt drug agglomerates, resulting in the observed poor blend uniformity (Table 3.6). Of the four lactose grades, anhydrous carriers produced the most consistently uniform blends, with coefficients of variation < 5% for nearly all size fractions and indeed, typically below 2%.

#### **3.3.4. Surface Energies of the Carrier Particles**

The values of the dispersive component of the surface area of each lactose sample was plotted versus the temperature, and the slope of each of these plots was analyzed [23]. There was a general trend with the slope; a more negative slope was indicative of a formulation which performed better (higher RF) for the size fractions 32 - 45  $\mu\text{m}$  and 106 - 125  $\mu\text{m}$ . This trend, however, broke down for the 250 - 300  $\mu\text{m}$  size fraction. The relative acid and base constants,

$K_a$  and  $K_b$ , yielded no discernable trend. Ultimately, given the relatively large amount of sample required per run, following sieving there was insufficient lactose from many of the carrier particle populations to permit analysis of replicates during IGC testing. Accordingly, while it has been previously noted in the literature that surface energy measurements of the carrier particle populations may be predictive of aerosol performance, in the present study no direct relationship between this parameter and drug dispersion was observed.

### **3.3.5. In Vitro Aerosol Performance**

Performance values from the DPI formulations dispersed at  $60 \text{ L min}^{-1}$  are presented in Figure 3.5. All four lactose grades displayed unique performance profiles as would be expected considering their diverse physicochemical properties. Of the four carrier grades,  $\alpha$ -lactose monohydrate exhibited a performance trend most consistent with that predicted from the literature, as increasing carrier particle diameters progressively diminished overall performance, with RF values declining from 48% for  $< 20 \mu\text{m}$  to 21% for the largest carrier population. Similarly, anhydrous lactose exhibited its highest RF value from the smallest size fraction, with performance then declining sharply from 40% to approximately half this level (22%) for the  $45 - 63 \mu\text{m}$  carriers. However, following the  $45 - 63 \mu\text{m}$  formulation, performance values exhibited a slight increase and plateaued between 25 – 30% for the remaining carrier size fractions. Thus, in contrast to the  $\alpha$ -lactose monohydrate formulations, performance did not progressively decline with increasing carrier size.

As with the previous two lactose grades, the smallest size fraction produced the highest dispersion performance for spray dried carriers. This was followed by a sharp decline as the respirable fraction diminished from 44% at the  $< 20 \mu\text{m}$  size fraction to 42%, 34%, 26%, and 17% for successive carrier diameters. Performance continued to diminish for the  $75 - 90 \mu\text{m}$  carriers, as RF declined to a low of 11%. However, following this size fraction a significant improvement was observed, and in contrast to anhydrous lactose, deposition performance doubled as carrier particle diameter increased, reaching 24% at  $125 - 150 \mu\text{m}$ , and remaining above 20% up through the  $250 - 300 \mu\text{m}$  size range.

Granulated lactose also exhibited a performance profile that deviated markedly from that of  $\alpha$ -lactose monohydrate. In contrast to the other lactose grades, the highest RF values were not produced by the  $< 20 \mu\text{m}$  formulation, as performance statistically similar to the smallest carrier population was observed for all size ranges following the  $75 - 90 \mu\text{m}$  carrier population. However, this is not because the granulated carriers failed to exhibit a performance decline. To the contrary, RF significantly declined immediately following the  $< 20 \mu\text{m}$  blend, as performance dropped to 26% for the  $20 - 32 \mu\text{m}$  carriers. However, RF values proceeded to increase slightly, fluctuating between 28 – 33%, and then exhibited a significant improvement to 37% for the  $90 - 106 \mu\text{m}$  size range, remaining above 33% through the largest size fraction.

It was not unexpected that  $\alpha$ -lactose monohydrate and anhydrous lactose would produce similar performance trends given their morphological similarities. While  $\alpha$ -lactose monohydrate carriers have been extensively examined in the literature, there are only a few published studies for anhydrous carriers, despite their use in the commercial Asmanex<sup>®</sup> formulation delivered via the Twisthaler<sup>®</sup>[24]. One such study examined the performance of anhydrous and  $\alpha$ -lactose monohydrate carrier particle populations fractionated with an air-jet sieve to obtain size fractions between  $63 - 90 \mu\text{m}$ , and it was speculated that the improved performance observed from the anhydrous carriers may be due to the higher concentration of fine lactose particles for this grade relative to lactose monohydrate [17]. The authors attributed this to the increased friability of anhydrous lactose, which induced extensive fragmentation during air-jet sieving. By comparison, in the present study the carrier particles were fractionated in triplicate, and via a milder process than air-jet sieving, to obtain narrow size distributions and remove as much of the lactose fines from the coarse carrier populations as possible. Accordingly, anhydrous lactose did not possess a markedly higher concentration of fines, as noted from the particle sizing data. Anhydrous lactose carriers displayed performance comparable to  $\alpha$ -lactose monohydrate beginning from the  $106 - 125 \mu\text{m}$  size fraction, with the latter grade significantly outperforming the former for all preceding sizes. However, at the  $250 - 300 \mu\text{m}$  fraction a significantly higher RF value was observed from the anhydrous carrier formulations, as it did not exhibit the progressive decline in performance seen with  $\alpha$ -lactose monohydrate. Previous studies in our lab employing anhydrous carriers to disperse budesonide

from the Aerolizer at  $60 \text{ L min}^{-1}$  also noted a similar plateau as performance (again measured by RF) declined significantly from 15% (45 – 63  $\mu\text{m}$ ) to 10% for the following size fraction (63 – 75  $\mu\text{m}$ ), and generally remained between 8% - 10% for the larger diameter carrier populations [25].

As with anhydrous carrier particles, reported studies with spray dried and granulated lactose are sparse. One notable study that examined both of these lactose grades using sieved size fraction of 63 – 90  $\mu\text{m}$  concluded that granulated lactose exhibited the worst overall performance due to its extensive surface roughness, which would enhance the adhesive interaction with micronized drug particles by providing multiple contact points relative to smoother surfaces [3]. In the present study, it is noted that the smallest granulated particles did indeed produce performance significantly lower than the other lactose carriers, however performance soon improved from the granulated carriers such that by the 75 – 90  $\mu\text{m}$  size fraction, RF values were no longer significantly lower compared to the other grades.

Overall, the highest RF value was produced by  $\alpha$ -lactose monohydrate, specifically the < 20  $\mu\text{m}$  diameter size fraction, with 48% of the recovered dose depositing on the lower stages of the NGI. As was noted earlier, this size fraction corresponded to both the formulation with the highest surface area, and the greatest concentration of fine lactose particles. Additionally, this lactose grade exhibited the poorest blend uniformity, which has been speculated to be a predictor of good dispersion performance. Accordingly, it is noted that this particular size fraction conformed to essentially every theory developed to predict carrier particle performance. Overall,  $\alpha$ -lactose monohydrate carrier particles matched well with the predicted theories, as performance progressively declined with increasing carrier particle diameter.

However, when the experimental parameters were broadened to include lactose grades and size ranges that have not been as extensively studied as  $\alpha$ -lactose monohydrate, these theories are no longer applicable. This is especially true for large carrier particle size fractions possessing extensive surface roughness. Accordingly, while trends matching well with the literature were observed for certain carrier particle subpopulations, there did not appear to be a direct link between the examined physicochemical properties and aerosol performance across all tested particle populations.



### 3.4. CONCLUSION

In this chapter a comprehensive study was undertaken to evaluate the *in vitro* aerosol performance of binary DPI formulations with carrier particle populations derived from four lactose grades fractionated into 13 narrow particle size ranges. The results from this study indicate that for a given particle size fraction, the physicochemical properties and aerosol performance of lactose carriers may vary considerably, deviating from the predicted trend that smaller carrier particle diameters generally outperform their larger diameter counterparts. Indeed, this trend was only observed in two of the four lactose grades examined, as the other two grades did not exhibit a progressive decline in performance. Specifically, for lactose grades with relatively low surface roughness ( $\alpha$ -lactose monohydrate and anhydrous lactose) the results generally followed the predicted trend that performance diminishes as the diameter of the carrier particle population is increased. However, for lactose grades possessing extensive surface roughness, *in vitro* deposition deviated considerably from the predicted trend, especially for granulated carriers, as the performance of the largest fractions was comparable to the smallest carrier particle size fraction.

The results of this study imply that large carrier particles possessing extensive surface roughness may potentially aid dispersion performance, though at present the mechanism by which this occurs remains unknown. Accordingly, it will be the focus of the following chapter to explore this mechanism in greater detail.

### 3.5. REFERENCES

1. Podczek, F., The relationship between physical properties of lactose monohydrate and the aerodynamic behaviour of adhered drug particles. *International Journal of Pharmaceutics*, 1998. 160: p. 119 - 130.
2. Steckel, H., and Muller, B.W., In vitro evaluation of dry powder inhalers II: influence of carrier particle size and concentration on in vitro deposition. *International Journal of Pharmaceutics*, 1997. 154: p. 31 - 37.
3. Kawashima, Y., Serigano, T., Hino, T., Yamamoto, H., and Takeuchi, H., Effect of surface morphology of carrier lactose on dry powder inhalation property of pranlukast hydrate. *International Journal of Pharmaceutics*, 1998. 172: p. 179 - 188.
4. Louey, M.D., Razia, S., and Stewart, P.J., Influence of physico-chemical carrier properties on the in vitro aerosol deposition from interactive mixtures. *International Journal of Pharmaceutics*, 2003. 252: p. 87 - 98.
5. de Boer, A., et al., Air classifier technology (ACT) in dry powder inhalation Part 2. The effect of lactose carrier surface properties on the drug-to-carrier interaction in adhesive mixtures for inhalation. *International Journal of Pharmaceutics*, 2003. 260(2): p. 201-216.
6. Cline, D., and Dalby, R., Predicting the quality of powder for inhalation from surface energy and area. *Pharmaceutical Research*, 2002. 19(9): p. 1274 - 1277.
7. Islam, N., Stewart, P., Larson, I., and Hartley, P., Lactose surface modification by decantation: are drug-fine lactose ratios the key to better dispersion of salmeterol xinafoate from lactose-interactive mixtures? *Pharmaceutical Research*, 2004. 21(3): p. 492 - 499.

8. Islam, N., et al., Surface roughness contribution to the adhesion force distribution of salmeterol xinafoate on lactose carriers by atomic force microscopy. *Journal of Pharmaceutical Sciences*, 2005. 94(7): p. 1500-1511.
9. Dickhoff, B., The effect of carrier surface and bulk properties on drug particle detachment from crystalline lactose carrier particles during inhalation, as function of carrier payload and mixing time. *European Journal of Pharmaceutics and Biopharmaceutics*, 2003. 56(2): p. 291-302.
10. Dickhoff, B., et al., The interaction between carrier rugosity and carrier payload, and its effect on drug particle redispersion from adhesive mixtures during inhalation. *European Journal of Pharmaceutics and Biopharmaceutics*, 2005. 59(1): p. 197-205.
11. Hickey, A.J., et al., Physical characterization of component particles included in dry powder inhalers. I. Strategy review and static characteristics. *Journal of Pharmaceutical Sciences*, 2007. 96(5): p. 1282-1301.
12. Marple, V.A., Roberts, D.L., Romay, F.J. and Hochrainer, D., Next generation pharmaceutical impactor (A new impactor for pharmaceutical inhaler testing). Part I: Design. *Journal of Aerosol Medicine*, 2003. 16(3): p. 283 - 299.
13. Louey, M.D., and Stewart, P.J., Particle interactions involved in aerosol dispersion of ternary interactive mixtures. *Pharmaceutical Research*, 2002. 19(10): p. 1524 - 1531.
14. Jones, M.D. and R. Price, The Influence of Fine Excipient Particles on the Performance of Carrier-Based Dry Powder Inhalation Formulations. *Pharmaceutical Research*, 2006. 23(8): p. 1665-1674.
15. Lucas, P., Anderson, K., and Staniforth, J.N., Protein Deposition from Dry Powder Inhalers: Fine Particle Multiplets as Performance Modifiers. *Pharmaceutical Research*, 1998. 15(4): p. 562 - 69.

16. Louey, M.D., Mulvaney, P., and Stewart, P.J., Characterisation of adhesional properties of lactose carriers using atomic force microscopy. *Journal of Pharmaceutical and Biomedical Analysis*, 2001. 25: p. 559 - 567.
17. Larhrib, H., Zeng, X.M., Martin, G.P., Marriott, C., and Pritchard, J., The use of different grades of lactose as a carrier for aerosolised salbutamol sulphate. *International Journal of Pharmaceutics*, 1999. 191: p. 1 - 14.
18. Begat, P., Morton, D.A.V., Staniforth, J.N., and Price, R., Dry powder inhaler formulations I: Direct quantification by atomic force microscopy. *Pharmaceutical Research*, 2004. 21(9): p. 1591 - 1597.
19. Flament, M., The influence of carrier roughness on adhesion, content uniformity and the in vitro deposition of terbutaline sulphate from dry powder inhalers. *International Journal of Pharmaceutics*, 2004. 275(1-2): p. 201-209.
20. Saleem, I., H. Smyth, and M. Telko, Prediction of Dry Powder Inhaler Formulation Performance From Surface Energetics and Blending Dynamics. *Drug Development and Industrial Pharmacy*, 2008. 34(9): p. 1002-1010.
21. Saintlorant, G., et al., Influence of carrier on the performance of dry powder inhalers. *International Journal of Pharmaceutics*, 2007. 334(1-2): p. 85-91.
22. Selvam, P., et al., Micronized Drug Adhesion and Detachment from Surfaces: Effect of Loading Conditions. *Aerosol Science and Technology*, 2011. 45(1): p. 81-87.
23. Telko, M.J. and A.J. Hickey, Critical assessment of inverse gas chromatography as means of assessing surface free energy and acid-base interaction of pharmaceutical powders. *Journal of Pharmaceutical Sciences*, 2007. 96(10): p. 2647-2654.
24. Pitchayajittipong, C., et al., Characterisation and functionality of inhalation anhydrous lactose. *International Journal of Pharmaceutics*, 2010. 390(2): p. 134-141.

25. Donovan, M.J. and H.D.C. Smyth, Influence of size and surface roughness of large lactose carrier particles in dry powder inhaler formulations. *International Journal of Pharmaceutics*, 2010. 402(1-2): p. 1 - 9.

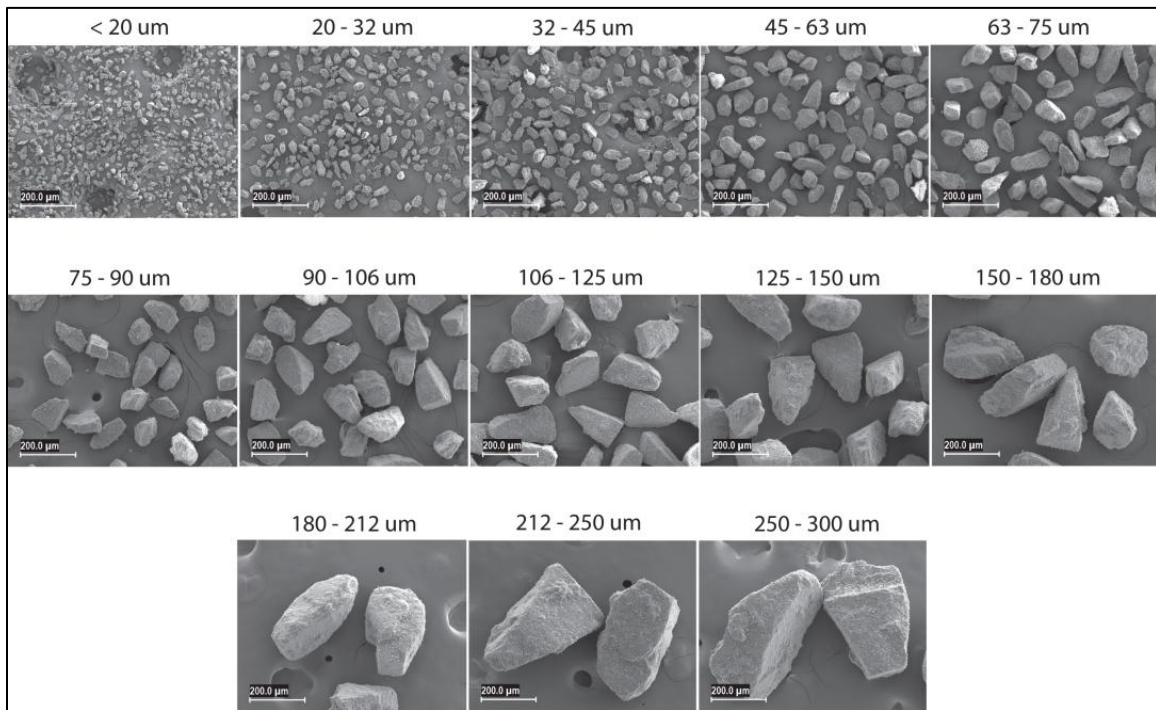


Figure 3.1. SEM Images of  $\alpha$ -lactose monohydrate.

Scale bars denote 200  $\mu\text{m}$

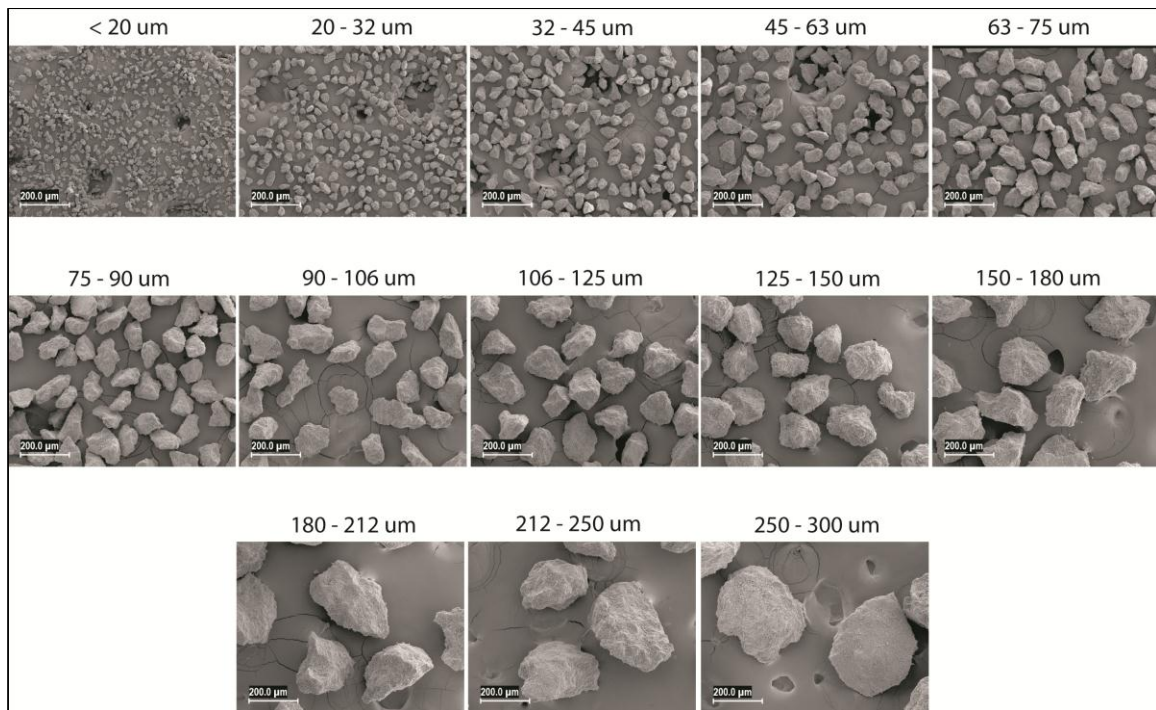


Figure 3.2. SEM Images of anhydrous lactose.

Scale bars denote 200 μm

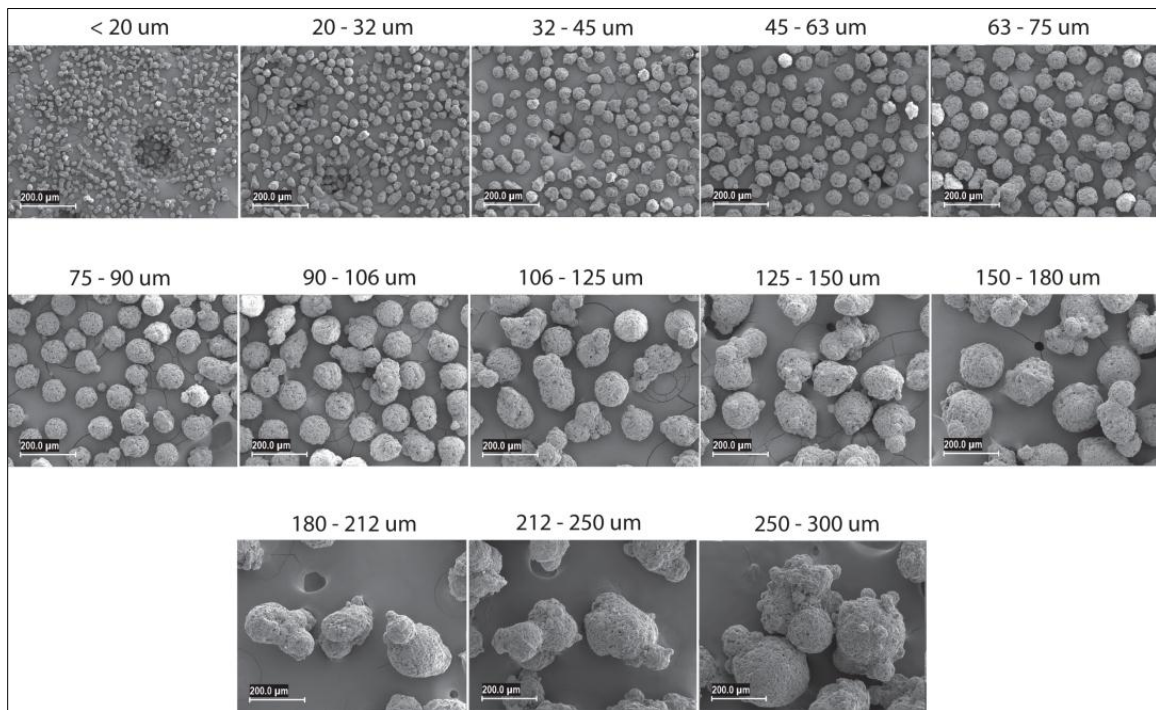


Figure 3.3. SEM Images of spray dried lactose.

Scale bars denote 200 μm



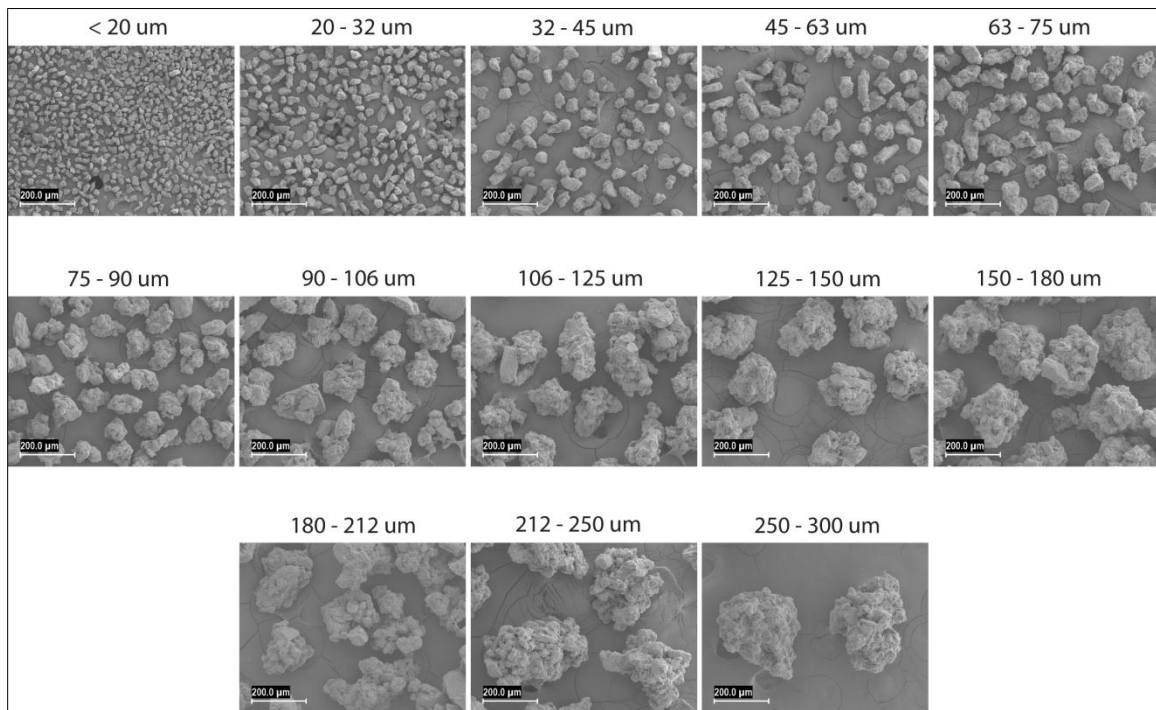


Figure 3.4. SEM Images of granulated lactose.

Scale bars denote 200 μm

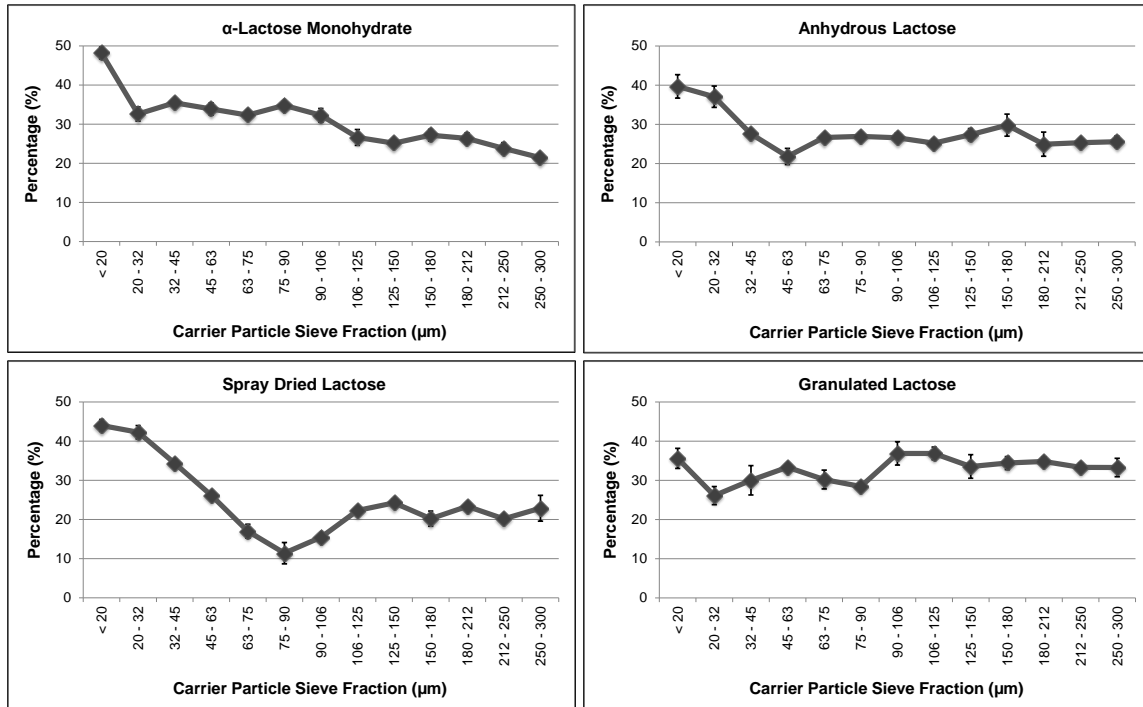


Figure 3.5. *In vitro* Aerosol Performance from the Fractionated Lactose Carrier Particle Populations

Aerosol performance was evaluated at  $60 \text{ L min}^{-1}$ . Values are given as mean ( $\pm$  stdev) for N = 3 replicates.

Table 3.1. Measured Specific Surface Areas of Fractionated Lactose Carrier Particles

Sieve Fraction ( $\mu\text{m}$ )	Specific Surface Area ( $\text{m}^2/\text{g}$ )			
	LMH	AN	SD	GR
< 20	0.98	0.79	---	----
20 – 32	0.63	0.54	0.42	0.88
32 – 45	0.57	0.43	0.31	0.63
45 – 63	0.39	0.42	0.37	0.52
63 – 75	0.39	0.34	0.32	0.36
75 – 90	0.35	0.34	0.31	0.34
90 – 106	0.29	0.32	0.37	0.35
106 – 125	0.27	0.29	0.31	0.37
125 – 150	0.25	0.32	0.40	0.37
150 – 180	0.24	0.30	0.40	0.39
180 – 212	0.20	0.28	0.43	0.41
212 – 250	0.19	0.26	0.39	0.41
250 – 300	0.18	0.31	0.34	0.43

Specific surface areas of  $\alpha$ -lactose monohydrate (LMH), anhydrous lactose (AN), spray dried lactose (SD) and granulated lactose (GR) carrier particle populations. It noted that for SD and GR carrier populations < 20  $\mu\text{m}$ , there was insufficient sample recovered following sieving to both prepare the formulations and measure the specific surface area in triplicate.

Table 3.2. Particle Sizing Data of Fractionated  $\alpha$ -Lactose Monohydrate Carrier Particle Populations

Carrier Sieve Fraction ( $\mu\text{m}$ )	$\alpha$ -Lactose Monohydrate				
	$d(10)$	$d(50)$	$d(90)$	Span	% Fines
< 20	4.3 (0.4)	18.2 (0.8)	33.5 (1.8)	1.6	25.8 (2.0)
20 – 32	16.1 (0.2)	31.2 (0.2)	44.3 (0.8)	1.1	14.1 (0.6)
32 – 45	30.6 (0.7)	43.6 (0.4)	63.6 (1.6)	1.2	9.8 (0.5)
45 – 63	40.8 (1.5)	65.3 (1.5)	90.9 (4.6)	0.8	5.0 (0.3)
63 – 75	54.9 (2.2)	85.5 (1.7)	122.3 (3.8)	0.8	5.0 (1.4)
75 – 90	61.1 (2.7)	94.8 (1.9)	128.7 (5.5)	1.2	3.5 (0.1)
90 – 106	84.0 (1.9)	128.3 (2.4)	182.2 (9.4)	0.8	3.1 (0.3)
106 – 125	104.5 (2.5)	158.3 (6.7)	224.4 (14.6)	0.8	2.6 (0.3)
125 – 150	115.9 (6.9)	183.3 (3.5)	250.3 (5.3)	0.7	2.9 (0.6)
150 – 180	147.5 (8.7)	231.2 (6.2)	333.9 (12.3)	0.8	2.3 (0.7)
180 - 212	178.6 (12.1)	270.0 (9.8)	409.7 (21.9)	0.9	1.1 (0.4)
212 – 250	203.3 (13.9)	311.0 (6.7)	443.3 (15.0)	0.8	1.9 (0.5)
250 – 300	230.0 (6.5)	352.8 (6.2)	479.9 (13.8)	0.7	2.4 (0.4)

Table 3.3. Particle Sizing Data of Fractionated Anhydrous Lactose Carrier Particle Populations

Carrier Sieve Fraction ( $\mu\text{m}$ )	Anhydrous Lactose				
	<i>d</i> (10)	<i>d</i> (50)	<i>d</i> (90)	<i>Span</i>	<i>% Fines</i>
< 20	3.7 (0.1)	20.2 (0.2)	32.8 (0.3)	1.4	20.5 (0.4)
20 – 32	16.0 (0.4)	33.6 (0.3)	48.7 (0.4)	1.0	8.0 (0.1)
32 – 45	32.2 (0.3)	48.5 (0.4)	65.8 (1.2)	0.7	3.9 (0.1)
45 – 63	43.5 (0.4)	64.7 (1.2)	85.0 (2.2)	0.6	3.4 (0.1)
63 – 75	49.0 (2.5)	79.5 (0.8)	106.4 (3.2)	0.7	4.6 (0.9)
75 – 90	65.3 (5.8)	97.9 (2.1)	130.0 (6.4)	0.7	3.1 (0.2)
90 – 106	90.8 (2.3)	121.9 (2.2)	165.5 (7.6)	0.6	---
106 – 125	101.9 (7.6)	142.7 (1.5)	184.9 (6.5)	0.6	---
125 – 150	121.6 (4.5)	168.2 (2.6)	218.5 (7.2)	0.6	---
150 – 180	146.9 (6.5)	205.5 (6.7)	287.7 (14.0)	0.7	---
180 - 212	169.7 (14.9)	243.3 (3.0)	335.0 (11.1)	0.7	---
212 – 250	199.7 (9.3)	277.1 (6.0)	349.6 (9.4)	0.5	---
250 – 300	239.7 (13.2)	318.0 (4.4)	404.9 (15.6)	0.5	---

Table 3.4. Particle Sizing Data of Fractionated Spray Dried Lactose Carrier Particle Populations

Carrier Sieve Fraction ( $\mu\text{m}$ )	Spray Dried Lactose				
	<i>d</i> (10)	<i>d</i> (50)	<i>d</i> (90)	<i>Span</i>	<i>% Fines</i>
< 20	4.5 (0.1)	20.6 (0.1)	30.8 (0.3)	0.8	14.1 (0.1)
20 – 32	16.1 (0.6)	31.2 (0.2)	44.3 (0.8)	1.1	8.3 (0.1)
32 – 45	30.6 (0.1)	44.8 (0.2)	59.1 (0.4)	1.6	5.0 (0.1)
45 – 63	42.5 (0.3)	57.7 (0.6)	71.4 (0.3)	2.0	3.5 (0.1)
63 – 75	51.4 (1.9)	69.2 (0.5)	87.8 (0.9)	1.9	6.5 (0.5)
75 – 90	65.3 (1.2)	84.7 (0.6)	104.1 (1.2)	2.2	5.2 (0.2)
90 – 106	81.9 (2.0)	94.8 (1.9)	127.4 (4.0)	2.1	3.1 (0.4)
106 – 125	98.9 (1.3)	128.8 (1.6)	172.4 (4.6)	1.8	5.0 (0.2)
125 – 150	118.9 (0.5)	166.0 (2.5)	234.2 (14.4)	1.4	---
150 – 180	144.4 (4.0)	204.6 (4.1)	298.0 (11.7)	1.3	---
180 - 212	166.1 (3.5)	254.7 (11.8)	362.3 (14.9)	1.3	---
212 – 250	188.9 (8.7)	278.8 (12.5)	367.5 (19.9)	1.6	---
250 – 300	219.4 (2.6)	313.1 (4.3)	396.5 (8.8)	1.8	---

Table 3.5. Particle Sizing Data of Fractionated Granulated Lactose Carrier Particle Populations

Carrier Sieve Fraction ( $\mu\text{m}$ )	Granulated Lactose				
	<i>d</i> (10)	<i>d</i> (50)	<i>d</i> (90)	<i>Span</i>	<i>% Fines</i>
< 20	5.3 (0.4)	22.4 (0.6)	35.3 (1.7)	1.3	14.7 (0.4)
20 – 32	20.4 (0.3)	35.8 (0.4)	51.0 (1.2)	0.9	7.5 (0.2)
32 – 45	32.8 (0.3)	52.5 (0.5)	73.5 (2.1)	0.8	4.7 (0.1)
45 – 63	35.4 (1.2)	62.9 (0.9)	87.6 (2.8)	0.8	4.9 (0.1)
63 – 75	45.3 (0.9)	77.1 (0.9)	108.7 (2.5)	0.8	3.5 (0.2)
75 – 90	44.0 (2.7)	87.7 (1.1)	136.4 (4.5)	1.1	4.1 (0.5)
90 – 106	82.7 (2.0)	123.9 (1.6)	175.1 (4.8)	0.7	---
106 – 125	105.6 (1.1)	147.5 (1.5)	202.2 (6.8)	0.7	---
125 – 150	125.7 (1.9)	176.4 (2.2)	265.0 (14.4)	0.8	---
150 – 180	151.2 (2.7)	207.0 (4.0)	277.5 (13.7)	0.6	---
180 - 212	160.7 (4.2)	231.4 (4.9)	297.8 (10.3)	0.6	---
212 – 250	198.3 (7.3)	279.8 (3.8)	353.0 (6.1)	0.6	---
250 – 300	230.3 (8.1)	303.8 (10.9)	364.9 (20.0)	0.4	---

Table 3.6. Drug Content Uniformity Measurements of the Experimental 1% (w/w) Salbutamol Binary Formulations

Carrier Particle Sieve Fraction ( $\mu\text{m}$ )	LACTOSE GRADE			
	$\alpha$ -Lactose Monohydrate	Anhydrous	Spray Dried	Granulated
< 20	13.7 %	5.3 %	6.6 %	2.6 %
20 – 32	10.6 %	3.8 %	2.8 %	5.3 %
32 – 45	6.0 %	2.3 %	2.1 %	2.7 %
45 – 63	1.2 %	1.4 %	2.9 %	1.9 %
63 – 75	3.7 %	0.3 %	1.6 %	2.7 %
75 – 90	2.1 %	0.7 %	2.7 %	6.4 %
90 - 106	2.2 %	2.2 %	3.9 %	8.4 %
106 – 125	1.9 %	0.8 %	2.7 %	5.1 %
125 – 150	2.7 %	1.4 %	1.4 %	6.2 %
150 – 180	2.5 %	2.3 %	3.2 %	4.7 %
180 – 212	4.2 %	1.9 %	1.5 %	6.1 %
212 – 250	6.3 %	1.2 %	3.0 %	2.7 %
250 - 300	9.3 %	1.7 %	1.6 %	4.3 %

The drug content uniformity of each blend is expressed as the percent coefficient of variation for N = 8 replicates.



## CHAPTER 4

### 4. Influence of Carrier Particle Diameter and Surface Roughness on the Performance of Binary DPI Formulations

#### 4.1. INTRODUCTION

Therapeutic formulations administered via dry powder inhalers are typically interactive mixtures, comprised of the active pharmaceutical ingredient and a coarse carrier material blended together to produce a homogeneous powder. Delivery to the deep lung requires drug particles possessing aerodynamic diameters between 1 and 5  $\mu\text{m}$  [1]. However, given the high surface area-to-volume ratio of particles in this size range, the ubiquitous van der Waals forces dominate the interactions, producing highly cohesive powders that flow poorly and are consequently resistant to dispersing into primary particle sizes during inhalation [2, 3].

Previous studies investigating the physical properties of lactose carriers on aerosol performance have generally been limited to broad particle size distributions, and/or carrier particle fractions below 200  $\mu\text{m}$  [4-6]. In addition, examination of larger carrier particles have focused primarily on a single particle morphology, that of  $\alpha$ -lactose monohydrate, while studies investigating the role of surface roughness are restricted to a single particle size range [7-9].

In the previous chapter, a comprehensive analysis of the influence of carrier particle diameter and morphology was performed. The *in vitro* deposition profiles from 52 formulations prepared with 13 narrow size fractions of four lactose grades were evaluated. The results indicated that performance can deviate markedly from the predicted trend, especially for larger carrier particle populations of both spray dried and granulated lactose. It was speculated that the increased surface roughness of the spray dried and granulated particles relative to  $\alpha$ -lactose monohydrate and anhydrous carriers was in part responsible for the observed differences in performance. However, the mechanism by which the combination of large carrier particle diameters and extensive surface roughness modulates drug detachment is presently not known.

### *Specific Aim*

It was therefore the specific aim of this chapter to concurrently evaluate the influence of carrier particle size and surface roughness on the aerosol performance of binary dry powder formulations. To this end, 2% (w/w) budesonide blends were prepared incorporating 11 carrier particle size fractions ranging up to 300  $\mu\text{m}$  and derived from two morphologically distinct lactose grades (anhydrous and granulated). *In vitro* drug deposition was used to assess the aerosol performance of the dry powder formulations. It is noted that both the drug and concentration differed from that of the previous study, when the formulations were prepared to possess an API concentration of 1% (w/w) with salbutamol. This difference was designed to determine if the aerosol performance trends of the previous study were due in larger part to the carrier particle population, or to the influence of the API.

## **4.2. EXPERIMENTAL**

### **4.2.1. Materials**

Micronized budesonide (EP) was purchased from Spectrum Chemicals (CA, USA) and used as received. Analytical grade ethanol was supplied by Sigma Chemical Company (MO, USA). As inhalation grade lactose is processed to yield particles predominately below 200  $\mu\text{m}$ , lactose grades typically employed in tablet preparation were used as carrier particles. Samples of anhydrous (SuperTab<sup>®</sup> 22AN), and granulated (SuperTab<sup>®</sup> 30GR) lactose were provided by DMV-Fonterra (New Zealand). Size 3 gelatin capsules were obtained courtesy of Capsugel<sup>®</sup> (NJ, USA).

### **4.2.2. Fractionation of Lactose Carrier Particles**

Samples of each lactose batch were fractionated on a vibrating sieve shaker (Gilson Company Inc., OH, USA) for 5 minutes through the following sieves: 300  $\mu\text{m}$ , 250  $\mu\text{m}$ , 212  $\mu\text{m}$ , 180  $\mu\text{m}$ , 150  $\mu\text{m}$ , 125  $\mu\text{m}$ , 90  $\mu\text{m}$ , 75  $\mu\text{m}$ , 63  $\mu\text{m}$ , 45  $\mu\text{m}$ , and 32  $\mu\text{m}$ . Following the initial fractionation, the lactose carriers were again sieved for an additional 5 minutes to obtain narrow particle size distributions.

#### **4.2.3. Preparation of Budesonide/Lactose Binary Blends**

Budesonide and lactose were mixed in a ratio of 1:50 (w/w) via geometric dilution to obtain 500 mg of a 2% binary blend. The formulations were blended with a Turbula® orbital mixer (Glen Mills, NJ, USA) for 40 minutes at 46 RPM. Samples were stored in a desiccator at least 5 days prior to use. Blend uniformity was determined by randomly selecting eight 20-mg samples from each mixture, and assessing the drug content in the powder. Formulations were considered well blended if the coefficient of variation (% CV) between the samples for a given blend was below 5%.

#### **4.2.4. Scanning Electron Microscopy**

Carrier particle size and surface roughness were visually assessed by scanning electron microscopy (SEM; Supra 40VP, Zeiss, Germany). Prior to SEM, approximately 20 nm of platinum were deposited onto the particle surfaces via sputter coating.

#### **4.2.5. Surface Area Analysis**

Specific surface areas of the lactose carrier particle populations were determined via nitrogen adsorption with a single-point BET method using a Monosorb® surface area analyzer (Quantachrome, FL, USA).

#### **4.2.6. Atomic Force Microscopy**

Atomic Force Microscopy was performed on a Multimode SPM NanoScope IIID (Veeco Instruments, CA, USA) in tapping mode using RTESP cantilevers with a nominal spring constant of 40 N/m. AFM settings were tuned to provide the best topographical image. Image processing and analysis was done in NanoScope Analysis software (v1.10, Veeco Instruments).

#### **4.2.7. Density of Lactose Carriers**

The true densities of the lactose carrier particles were determined with a helium pycnometer (Quantachrome, FL, USA).

#### **4.2.8. In Vitro Drug Deposition**

Size 3 gelatin capsules filled with 20 ( $\pm$  1) mg of powder were dispersed through an Aerolizer® DPI (Plastiaple S.p.A., Italy) into a next generation cascade impactor (Copley Scientific, UK) at a volumetric flow rate of 60 L min<sup>-1</sup> actuated for 4-second intervals. Prior to each actuation the pre-separator was loaded with 15 mL of ethanol, which was collected following powder dispersion from each capsule. Additionally, the drug deposited in the capsule, inhaler, adaptor mouthpiece, throat, and NGI stages was collected by rinsing with ethanol. Drug content was assessed via UV-VIS absorption spectroscopy at 244 nm. The emitted fraction was calculated as the ratio of the drug mass depositing in the throat, pre-separator, and impactor stages over the cumulative mass of drug collected following actuation (total drug deposited in the capsule, inhaler, mouthpiece, throat, pre-separator and stages). The fine particle fraction (FPF) of each dose was the ratio of the drug mass depositing on stages 3 - 8 (corresponding to an aerodynamic diameter less than 4.46  $\mu$ m) of the impactor over the emitted dose. The respirable fraction was the ratio of the drug mass deposited on stages 3 – 8 over the entire dose recovered following each actuation.

#### **4.2.9. Statistics**

Statistical significance between performance values was determined with one-way ANOVA with Post Hoc tests between groups according to the Bonferroni method ( $P < 0.05$ ).

### **4.3. RESULTS**

#### **4.3.1. Physical characterization of Lactose Carrier Particles**

Narrow lactose carrier particle fractions were generated by the double-sieving technique (Figure 4.1). Although the vast majority of studies examining binary dry powder formulations are restricted to only  $\alpha$ -lactose monohydrate carriers, different grades of lactose have been employed as carrier particles in the literature. These include both granulated lactose and anhydrous lactose [41, 75, 84]. Granulated lactose is  $\alpha$ -lactose monohydrate generated via fluidized bed granulation, producing particles with extensive surface rugosity (Figure 4.1 and

Figure 4.2). Anhydrous lactose is a form of  $\beta$ -lactose, absent the water of crystallization of the monohydrate form, and is characterized by relatively flat particle surfaces. The increased surface roughness of the granulated lactose carriers becomes increasingly evident at the larger particle size ranges, though at the smaller fractions the distinction between anhydrous and granulated carriers is less apparent. Notably, the anhydrous carriers exhibited a greater degree of fine particles on their surface (Figure 4.2).

The specific surface areas (SSA) of all 11 carrier fractions, for both anhydrous and granulated lactose, are listed in Table 4.1. The extensive surface roughness of the granulated particles yielded SSA values up to four-fold higher than the anhydrous particles. Additionally, the SSA of the granulated particles does not diminish with increasing carrier particle size to the same extent as the anhydrous carriers.

#### **4.3.2. Surface Roughness of Carrier Particles**

Theoretically, given the higher surface area-to-volume ratio of smaller particles, the specific surface area (SSA) of a carrier powder diminishes as the diameter of the particles is increased. For a constant mass of carrier particles (e.g. 20 mg), the surface area available for drug binding is reduced for larger carriers, potentially leading to drug-drug particle agglomeration which can hinder aerosol performance. Practically, surface area may be significantly influenced by the extent of surface roughness, particularly as the carrier particle size is varied [9, 11]. Therefore, surface area can be effectively used as a relative measure of surface roughness for a series of size fractions of the lactose carriers. The experimentally observed SSA for each size fraction of each lactose grade was determined and was compared to the theoretical SSA for equivalent sized spheres possessing a diameter corresponding to the mean particle diameter of the sieve fraction. For example, the mono-disperse spherical particle population for the carrier sieve fraction 63 – 75  $\mu\text{m}$  possesses a theoretical diameter of 69  $\mu\text{m}$ . To facilitate comparison, the SSA was normalized to that of the smallest size fraction of each population (spherical, anhydrous, and granulated); the SSA of each subsequent carrier particle fraction (CPF) was divided by that of its smallest size fraction (< 32  $\mu\text{m}$ ):

$$\frac{SSA_{CPF}}{SSA_{<32}}$$

Figure 4.3 depicts the decline in SSA as particle diameter is increased, normalized to the SSA of the < 32  $\mu\text{m}$  particles for each population. This plot allows the direct comparison of how closely each lactose grade follows the theoretical relationship between particle size and surface area, and provides excellent insight into the degree of surface roughness. The theoretical SSA of the perfectly spherical particles declines as an exponential function. However, in reality lactose has significant surface roughness coupled with the presence of fine particles. Thus, the observed decline in SAA of the lactose particles is not as severe as that of the spherical particles (Figure 4.3). For anhydrous lactose, the SSA begins to noticeably deviate from theoretical at the 45 – 63  $\mu\text{m}$  carrier fraction, and converges to approximately 40% of the < 32  $\mu\text{m}$  SSA value over the remaining size ranges. By contrast, the SSA of the granulated lactose is within 80%, and in a few instances over 90%, of the smallest particle size fraction despite large increases in particle size. Accordingly, given the higher rugosity of granulated particles relative to their anhydrous counterparts, increasing carrier particle size does not severely diminish the surface area available for drug attachment during blending. This difference may be important for limiting the extent of drug-drug particle agglomerate formation that occurs during blending for formulations with granulated carriers relative to anhydrous.

To supplement SSA data on surface roughness, Atomic Force Microscopy (AFM) studies were performed on selected lactose size fractions. Figure 4.4 shows representative examples of the surface topography of both small anhydrous carrier particles (75 - 90  $\mu\text{m}$ ) and larger anhydrous carrier particles (250 – 300  $\mu\text{m}$ ). Statistical differences in surface roughness were identified in the root mean square (RMS) value of the roughness between large and small carriers. RMS surface roughness values of the 250 – 300  $\mu\text{m}$  anhydrous samples was 568 ( $\pm$  31) nm compared to 385 ( $\pm$  60) nm for the 75 – 90  $\mu\text{m}$  samples for three replicates. The surface roughness of granulated lactose was difficult to measure using AFM due to the large and abrupt changes in the surface structures, particularly in the z-direction. Therefore, AFM results for

granulated lactose should be interpreted with caution, as the successful imaging attempts will bias the results in favor of smoother surfaces.

#### **4.3.3. *In vitro* Aerosol Performance**

Aerosol performance is governed by the combined influence of both carrier particle size and surface roughness, and the results of the present study reveal that poor dispersion performance is not a property inherent to larger carrier particles. For anhydrous carrier formulations, performance did not progressively decline with carrier size (Figure 4.5). Three distinct plateaus in RF values were noted as the size of the carriers was increased, with performance abruptly dropping off as carrier size increased to 32 - 45  $\mu\text{m}$  (RF decreased from 18.4% to 13.7%), and once more at the transition to the 63 – 75  $\mu\text{m}$  size range (14.6% compared to 10.4%) (Table 4.2). Additionally, following a drop in performance at the 150 – 180  $\mu\text{m}$  size range (RF = 7.5%), a slight but statistically significant improvement was seen as RF values climbed for the three largest carrier size fractions, ranging from 8.7% to 9.9%. The observation that performance did not continually decline with carrier size, but rather exhibited a minor resurgence at the largest size ranges, was unexpected in the context of the current literature.

In contrast to anhydrous formulations, the drug deposition performance of granulated carriers exhibited a distinct overall trend (Figure 4.6). Although the smallest three fractions demonstrated a decline in performance, with RF values progressively dropping from 11.2% to 6.6%, dispersion improved markedly for larger carriers. A progressive increase in RF was observed beginning with the 90 – 125  $\mu\text{m}$  size range, eventually surpassing the performance of even the < 32  $\mu\text{m}$  carrier population, such that the three largest carriers significantly outperformed all but the 125 – 150  $\mu\text{m}$  size fraction.

#### **4.4. DISCUSSION**

The influence of carrier particle surface roughness on drug dispersion performance has been previously examined in the literature [7 - 9, 11, 12]. It has been observed that there are two distinct types of roughness, differing by the scale of the carrier surface asperities relative to

the drug particles [7]. Micro-scale rugosity refers to carrier surfaces with asperities smaller than the drug particles, reducing the contact surface area between drug and carrier. By providing a corrugated surface for drug particle attachment, micro-scale rugosity has been demonstrated to benefit dispersion performance by diminishing the adhesive interaction with the carrier particle [7, 13, 14]. However, carriers with micro-scale surface asperities have also been observed to inhibit aerosol performance relative to smooth lactose by enhancing friction forces between rougher carriers, to the detriment of powder flow properties [8].

In contrast to the corrugated surface, macro-scale rugosity describes surface features larger than the drug particles, which are believed to increase the extent of contact with the carrier [11, 12]. Furthermore, drug particles located within these large surface asperities are sheltered from the flow stream during inhalation, limiting the detachment forces acting on them. Consequently, carrier particles with macro-scale rugosity have been shown to hinder aerosol performance [7, 11]. However, previous work specifically examining the influence of surface roughness has been limited to a single carrier size range. Accordingly, the effect of surface roughness on aerosol performance over a wide range of carrier particle sizes had to be extrapolated in previous studies, with speculation that the greater degree of surface roughness on larger carriers was a major contributor to their reduced dispersion performance relative to smaller carriers [7, 11, 12]. Our results indicate that surface roughness influences performance by altering the relative contributions of the mechanisms governing drug detachment from carrier particles. Moreover, as the detachment potential of these mechanisms can vary greatly with carrier particle size, the view that large carrier particles are detrimental to aerosol performance is re-evaluated in light of the present study.

#### **4.4.1. Mechanisms of Drug Detachment from Carrier Particles**

Drug detachment and dispersion from carrier particles during inhalation is thought to proceed through two major mechanisms: detachment by the flow stream (fluid forces) and detachment by impaction (mechanical forces) [15, 16]. While these mechanisms are not mutually exclusive, they are distinct and depend on different physical characteristics of the drug and carrier particles to maximize their potential to cause detachment. Detachment by flow



requires a relatively flat carrier particle surface, with minimal asperities, allowing the flow stream an unobstructed path to access and remove the drug particles. Additionally, detachment by flow is facilitated for larger drug particles (either drug agglomerates or primary particles) due to the increased surface area available for interaction with the flow stream [11].

Mechanical forces arise from the abrupt momentum transfer that occurs when a carrier particle contacts the inhaler wall [3, 16]. As momentum is dependent on the mass of the particle, detachment by mechanical forces are proportional to the cube of the carrier particle diameter, such that large particles will generate greater detachment forces (assuming constant velocity between carrier particle size fractions) [17]. Moreover, detachment by mechanical forces is not inhibited by carrier particle surface roughness to the same degree as detachment by flow, and all drug particles adhered to a carrier will equally experience the carrier-inhaler collision force [16]. However, only those drug particles for which the detachment force both exceeds the adhesive interaction with the carrier, and is in a direction favorable to detachment, will be dislodged from the carrier.

Although drug particles are simultaneously subjected to both flow and mechanical forces, they do not begin to act upon the drug at the same instant. In order for a drug particle to experience mechanical forces the carrier to which it is attached must be in motion, and this motion is generated by the flow stream acting on the carrier particle. However, the instant that the flow stream begins to influence the carrier, it has begun to exert fluid detachment forces on drug particles on the carrier surface. Thus, drug particles are exposed to fluid forces prior to mechanical forces. This distinction is important, as drug particles readily exposed on the surface will likely be detached by the flow stream at the onset of inhalation, prior to the existence of mechanical forces. Accordingly, mechanical forces do not influence all of the drug particles on the carrier, but rather those that still remain adhered to the carrier following fluid detachment, when the carrier-inhaler impactions occur.

#### **4.4.2. Surface Roughness and Particle Size Influence the Predominant Mechanism of Detachment**

Figure 4.7 schematically illustrates the distinction between detachment by flow and mechanical forces in carriers with different surface roughness. For carriers with low surface roughness, the drug is readily exposed to the flow stream. Thus, for smoother carriers detachment by flow may be effective at drug detachment, and is likely the dominant mechanism. With increasing carrier surface roughness, drug is sheltered within asperities, and drug detachment becomes less dependent on the flow stream and more reliant on mechanical forces. Accordingly, when examining the carriers from the two lactose grades used in this study, it is speculated that detachment by flow will predominate for the relatively smoother anhydrous particles while mechanical forces will dominate for the granulated carriers where surface roughness will shelter drug particles from the flow stream to a greater degree (e.g. Figure 4.2).

The wide disparity in aerosol performance between the lactose types is therefore attributed to their diverse surface roughness characteristics. The influence of surface roughness on aerosol performance is evidenced by the divergent trends in RF values between the two lactose types as carrier size is increased (Figure 4.8). Anhydrous lactose exhibits a decline in overall performance with increasing particle size, whereas the granulated carriers yielded the opposite trend. The overall reduction in performance observed in the formulations with anhydrous carrier particles is consistent with detachment by flow. From the literature, it has been noted that smaller carrier particles possess smoother surfaces relative to larger size fractions [11, 12]. It is then proposed that more drug particles are sheltered within asperities on larger carriers, and thus less susceptible to detachment by the flow stream. Additionally, the reduction in available surface area for larger anhydrous size fractions would lead to more extensive drug agglomeration, hindering aerosol performance (Table 4.1). Thus, with larger anhydrous carriers not only are fewer drug particles dislodged from the surface, much of the detached drug is aggregated (as measured by MMAD and discussed below). Consequently, most of the drug that can be removed by the forces generated within a given inhaler at a specific flow rate is likely detached rapidly by the initial fluid forces, and a limited number of

drug particles remain available for detachment by the mechanical forces that occur subsequent to the flow forces.

Conversely, it is proposed that drug detachment from granulated particles was primarily dependent on mechanical forces. As the magnitude of mechanical detachment forces increases with carrier particle size, the larger granulated carrier particles significantly outperformed the smaller size fractions (Figure 4.8). The relatively high performance of  $< 32 \mu\text{m}$  granulated particles can be attributed to the small surface roughness of this size fraction, which enabled detachment by flow to predominate.

#### **4.4.3. Evidence for Mechanical Detachment Mechanisms for Larger Carrier Particles: Flow Rate Dependent Detachment**

Mechanical detachment forces rely on the abrupt momentum transfer generated by carrier-inhaler collisions [3]. Thus, as both the mass and velocity of the carrier particle are important, the performance would depend on carrier particle size and inhalation flow rate, all other factors being equal. Accordingly, the influence of flow on the performance of large carrier particles is an area that remains to be fully explored. However, while only a single volumetric flow rate was examined in this study, evidence for improved drug detachment from large carriers with increasing flow can be found in the literature. In their studies with  $\alpha$ -lactose monohydrate carrier particles, Dickhoff and coworkers observed the drug detachment from particle size fractions including both a small ( $32 - 45 \mu\text{m}$ ) and large ( $250 - 355 \mu\text{m}$ ) population [18]. For 1.6% (w/w) budesonide formulations at 30 Lpm, smaller carriers detached approximately half of the drug adhered to their surface, while the  $250 - 355 \mu\text{m}$  size range dislodged only 42%. Doubling the flow to 60 Lpm, the large carrier particles outperformed their smaller counterparts, detaching 93% compared to 81%.

For smaller carrier particles with low surface rugosity, the drug is readily exposed to the flow stream, and increasing the flow rate would augment the magnitude of the pneumatic detachment forces. However, it is known that large carriers possess greater surface roughness, allowing drug particles to be sheltered from the flow stream [11]. Supposing drug dispersion is

governed solely by detachment due to flow, two particles with equally smooth surfaces would be expected to perform comparably, regardless of carrier particle size. The observations made in these studies that larger, higher rugosity particles outperformed the smaller, smoother carriers at 60 Lpm provides evidence for additional detachment mechanisms other than flow forces [18]. Moreover, while this mode of detachment benefits larger carrier particles, its influence is not observed at lower flow rates. Accordingly, a mechanism that enhances detachment forces with increasing carrier particle size (i.e. mass) and velocity strongly supports the role of mechanical forces arising from carrier particle-inhaler collisions. In fact, these forces may be stronger in magnitude than fluid forces and provide more efficient methods of detaching particles from carrier surfaces.

#### **4.4.4. Relationship Between Carrier Particle Size Fraction and Detached Drug Particle Size**

Given their increased detachment potential due to mechanical forces, larger carriers may dislodge drug particles resistant to the flow stream. These “detachment-resistant” drug particles may be smaller drug particles (less susceptible to flow-related detachment due to their small surface area) or drug particles attached to high energy sites on the carriers. When attached to larger carriers, these may be available for detachment via mechanical impactions. In addition, drug particles located within small surface asperities in a depth sufficient to obstruct their interaction with the flow stream would have more potential for detachment. Indeed, a study examining the relationship between impact forces and particle detachment revealed that greater impaction magnitudes were required to separate particles from a surface as the diameter of the particles decreased [19]. It follows then that the diameter of drug particles depositing in the cascade impactor would be smaller from formulations with larger carriers, as they will be able to generate greater impaction forces. Our observations are consistent with this theory (Figure 4.9), for both anhydrous and granulated carriers, where the mass median aerodynamic diameter (MMAD) of the deposited budesonide particles exhibited a decreasing trend with increasing carrier particle size.

Examining only the MMAD values for the carrier particle fractions, it might be concluded that large carriers would demonstrate the best performance across both lactose types. This was true for granulated lactose, but for anhydrous lactose decreases in SSA likely lead to drug-drug aggregates as carrier size increased. Indeed, with the exception of the 45 - 63  $\mu\text{m}$  size range, the SSA plateau is also reflected in the respirable fractions (Table 2), where values initially drop-off significantly from the smallest particle size range, and again following the 45 – 63  $\mu\text{m}$  fraction.

#### **4.4.5. Transition from Flow Detachment to Mechanical Detachment**

To reconcile the opposing trends of MMAD and overall drug deposition performance for anhydrous carriers with particle size, it is proposed that the drug aggregates formed during blending are readily detached by the flow stream due to their augmented surface area but they are not dispersed into primary particles (accounting for the diminished RF values). However, larger carriers increased the mechanical forces arising from particle-inhaler collisions, and drug particles impervious to detachment by flow were eventually dislodged. As these are believed to be smaller primary drug particles, detachment correlates with deep lung deposition, contributing to the RF values. At precisely what size range this shift in detachment mechanism occurs is unclear, but as noted previously from Figure 4.5, aerosol performance of anhydrous particles deviates from the declining trend at the 180 – 212  $\mu\text{m}$  carrier fraction, where a slight but significant improvement in RF value is observed. From Table 3, this coincides with the carrier particle fraction when MMAD begins to trend to smaller values, supporting the theory that mechanical detachment forces generated by larger carriers dislodge drug particles resistant to the flow stream.

An alternative explanation for the MMAD decline is the ability of larger carriers to comminute aggregated drug particles during blending. It has been observed that two types of drug agglomerates exist in dry powder formulations: natural agglomerates present in the pure drug powder, and mixing agglomerates that arise as drug and carrier particles are blended [9]. While the lower SSA of larger carriers can induce mixing agglomerates, their greater mass and flowability improves their potential to breakup natural agglomerates during blending, allowing them to potentially aid and hinder performance simultaneously. Whether disruption of natural

agglomerates surpasses the formation of mixing agglomerates depends not only on formulation conditions such as drug (w/w) concentration, blending time and batch size, but also on the drug itself. For the beneficial aggregate disruption to dominate, the interaction between drug and carrier must be stronger than that amongst drug particles, such that drug dislodged from agglomerates will adhere to the lactose, and remain attached throughout blending. Conversely, aggregate formation prevails when the drug possesses a high cohesive tendency, preferentially associating with other drug particles over the carriers [20].

Begat and colleagues have previously demonstrated the cohesive nature of budesonide, the model drug employed in the present study [20]. We also observed similar phenomena when we previously performed dynamic blending studies with budesonide and different lactose types [21]. Accordingly, it is speculated that agglomerate formation may predominate during blending, accounting for the decline in aerosol performance for larger anhydrous carriers. The reduction in MMAD is also observed with granulated lactose, where the high surface rugosity would shelter drug particles and inhibit the breakup of natural drug agglomerates. This supports the view that larger carriers can potentially dislodge smaller primary drug particles that would generally resist fluid detachment, as the increased amount of natural agglomerates with larger granulated carriers (due to increased surface roughness) would be expected to shift MMAD values higher, but they are instead compensated by a number of smaller detached drug particles, such that MMAD actually trends lower with carrier size. The difference between the two lactose types, where granulated carriers generally produced smaller MMAD values at each carrier size fraction, may be explained by the greater SSA of granulated particles, which can limit the extent of drug-drug particle interaction relative to the anhydrous carriers, reducing formation of blending agglomerates.

#### **4.4.6. Effects of Increasing Carrier Particle Diameter and Mass**

Aerosolization performance can be improved by increasing the size of the carrier particles, thereby increasing the mechanical impaction forces that can be very efficient at detaching drug particles from the carrier surface. However, the improvement to aerosol performance imparted by large carrier particles will not continue indefinitely, as the mass of

carriers (and gravitational forces acting upon them) eventually become prohibitively large. The benefit to momentum that is conferred by the increased mass of the carrier particle will be countered by a reduction in particle velocity, as the carriers' inertia will resist the flow stream, resulting in a diminishing force of the carrier-inhaler impactions. In our studies, the RF values of the 250 – 300  $\mu\text{m}$  formulations for both lactose types were not significantly different from those of the size fraction immediately preceding them (212 – 250  $\mu\text{m}$ ) (Table 4.2). Therefore it is unclear precisely when the mass of carrier begins to inhibit drug dispersion. The maximum particle size employed in this study was limited to 300  $\mu\text{m}$ , as at the next largest size range a fraction of the carrier particles were retained within the capsules following actuation from the Aerolizer®, due to some particles being too broad to pass through the capsule perforations. It is speculated that the performance of size ranges greater than 300  $\mu\text{m}$  would not increase significantly from those of the 250 – 300  $\mu\text{m}$  fractions given the density of the carrier particles (between 1.54 – 1.56  $\text{g}/\text{cm}^3$ , data not shown).

#### **4.4.7. Previous Studies Examining Anhydrous and Granulated Lactose**

As stated earlier, both granulated and anhydrous lactose have been employed as carrier particles previously in the literature. Granulated lactose particles were used by Kawashima and colleagues, who studied the influence of carrier particle surface morphology on the dispersion of pranlukast hydrate [7]. Particles with high surface roughness were produced via fluidized bed granulation, and sieved between 63 – 90  $\mu\text{m}$ . Their results demonstrated that the granulated particles yielded the lowest aerosol performance of the experimental carrier populations. This was attributed to the high adhesive force between the drug and granulated carrier particles, as a consequence of the increased number of contact points resulting from the high surface roughness of the carriers. That the authors concluded that granulated particles were poor carriers is understandable, as the fraction they employed fell into a size range that was not sufficiently large to generate high mechanical forces, as demonstrated by our observations. Consequently, detachment relied on the flow stream, which was unable to interact extensively with the drug particles due to the high surface roughness of the carriers. In comparison with the present study, the 63 – 75  $\mu\text{m}$  and 75 – 90  $\mu\text{m}$  granulated carriers exhibited relatively low

performance relative to the larger carriers. By contrast, Dickhoff and coworkers employed 250 – 355  $\mu\text{m}$  granulated lactose carriers in their studies on surface roughness, and observed that granulated carriers could detach a higher fraction of drug from their surface relative to crystalline lactose carrier particles [9]. The authors proposed that the increased surface roughness of the granulated carrier particles allowed drug particles to be shielded within surface asperities from press-on forces during mixing, which hindered drug dispersion from the crystalline carriers. Our results were in agreement with those of Dickhoff, where the largest granulated carriers outperformed their smoother anhydrous counterparts.

Studies including a 63 – 90  $\mu\text{m}$  anhydrous lactose fraction observed a significantly greater dispersion performance by comparison to  $\alpha$ -lactose monohydrate carriers of comparable size [10]. The authors attributed this enhanced performance to the higher content of fine lactose on the surface of anhydrous particles relative to the other carriers. However, the performance of anhydrous carriers as their size fraction was altered was not examined. Thus, although both anhydrous and granulated lactose have been previously studied, including both small (63 – 90  $\mu\text{m}$ ) and large (250 – 355  $\mu\text{m}$ ) granulated fractions, the influence of carrier size on the two lactose types was not investigated until the present study.

#### **4.5. CONCLUSIONS**

The work described here continued in part from Chapter 3, as the influence of carrier particle size and surface roughness was evaluated by employing a drug and concentration that differed from that of the previous study. This was done to ensure that the performance was reproducible irrespective of API, indicating that the observed profiles through the Aerolizer at 60  $\text{L min}^{-1}$  depended primarily on the carrier population rather than the drug. Although differences were noted, specifically between the overall performance levels of salbutamol and budesonide, with the former producing markedly high RF values, overall deposition followed a similar pattern to that observed in Chapter 3, as performance from large carriers with extensive surface roughness again exhibited levels at least comparable to the smallest size fraction.



As was noted in Chapter 1, the prevailing theories in the literature have been proposed to account for a relatively narrow carrier particle size distribution, and have focused primarily on a single particle morphology; the 'tomahawk' shape of  $\alpha$ -lactose monohydrate. Indeed, for anhydrous lactose carrier particles with relatively flat surfaces, the results in our studies generally followed the expected trend with dispersion performance diminishing with increasing carrier particle diameter. However, improvements in aerosol performance were observed with larger size fractions in the formulations with granulated carrier particles, which were characterized by a high degree of surface roughness. Additionally, even the largest anhydrous carrier sizes were also seen to improve drug dispersion, possibly by dislodging smaller primary drug particles that were less susceptible to detachment by the flow stream, as indicated by the decline in MMAD of deposited budesonide. The present study strongly suggests that surface roughness may influence aerosol performance by shifting the detachment mechanism to rely heavily on the mechanical forces generated from collisions between the carrier particle and the inhaler walls. Given that mechanical forces can potentially increase with larger carrier particles, the role of carrier particle size on dispersion performance was shown to vary markedly with surface roughness.

The aerosol performance of a given formulation may be strongly dependent on the inhaler through which it is dispersed. Thus, it is recognized that the performance trends observed in Chapters 3 and 4 may deviate appreciably if the powder is dispersed through a device that does not promote either carrier particle-inhaler interactions or interparticle collisions to the same extent as the Aerolizer. Accordingly, the following chapter will focus on the influence that the selected DPI can have on dispersion performance as the size and surface roughness of the carrier particles are altered. Furthermore, the use of two inhalers will allow us to simultaneously evaluate how the physical properties of the lactose carrier population can affect performance from a dry powder inhaler, which to our knowledge, has not been previously investigated in detail.

#### 4.6. REFERENCES

1. Hickey, A.J., ed. *Pharmaceutical Inhalation Aerosol Technology*. 2nd ed. 2004, Marcel Dekker, Inc.: New York, NY.
2. Visser, J., *Van der Waals and other cohesive forces affecting powder fluidization*. Powder Technology, 1989. **58**: p. 1 - 10.
3. Finlay, W., *The Mechanics of Inhaled Pharmaceutical Aerosols, An Introduction* 2001, New York, NY: Academic Press.
4. Steckel, H., and Muller, B.W., *In vitro evaluation of dry powder inhalers II: influence of carrier particle size and concentration on in vitro deposition*. International journal of pharmaceutics, 1997. **154**: p. 31 - 37.
5. Podczeczek, F., *The relationship between particulate properties of carrier materials and the adhesion force of drug particles in interactive mixtures*. Journal of Adhesion Science and Technology, 1997. **11**: p. 1089 - 1104.
6. Louey, M.D., Razia, S., and Stewart, P.J., *Influence of physico-chemical carrier properties on the in vitro aerosol deposition from interactive mixtures*. International journal of pharmaceutics, 2003. **252**: p. 87 - 98.
7. Kawashima, Y., Serigano, T., Hino, T., Yamamoto, H., and Takeuchi, H., *Effect of surface morphology of carrier lactose on dry powder inhalation property of pranlukast hydrate*. International journal of pharmaceutics, 1998. **172**: p. 179 - 188.
8. Zeng, X.M., Martin, G.P., Marriott, C., and Pritchard, J., *Lactose as a Carrier in Dry Powder Formulations: The Influence of Surface Characteristics on Drug Delivery*. Journal of Pharmaceutical Sciences, 2001. **90**(9): p. 1424 - 1434.

9. Dickhoff, B.H., et al., *The interaction between carrier rugosity and carrier payload, and its effect on drug particle redispersion from adhesive mixtures during inhalation.* European journal of pharmaceutics and biopharmaceutics : official journal of Arbeitsgemeinschaft fur Pharmazeutische Verfahrenstechnik e.V, 2005. **59**(1): p. 197-205.
10. Larhrib, H., Zeng, X.M., Martin, G.P., Marriott, C., and Pritchard, J., *The use of different grades of lactose as a carrier for aerosolised salbutamol sulphate.* International journal of pharmaceutics, 1999. **191**: p. 1 - 14.
11. De Boer, A., et al., *Air classifier technology (ACT) in dry powder inhalation Part 2. The effect of lactose carrier surface properties on the drug-to-carrier interaction in adhesive mixtures for inhalation.* International journal of pharmaceutics, 2003. **260**(2): p. 201-216.
12. Podczec, F., *The relationship between physical properties of lactose monohydrate and the aerodynamic behaviour of adhered drug particles.* International journal of pharmaceutics, 1998. **160**: p. 119 - 130.
13. Chew, N.Y.K., et al., *How Much Particle Surface Corrugation Is Sufficient to Improve Aerosol Performance of Powders?* Pharmaceutical research, 2005. **22**(1): p. 148-152.
14. Adi, S., et al., *Micro-particle corrugation, adhesion and inhalation aerosol efficiency.* European journal of pharmaceutical sciences : official journal of the European Federation for Pharmaceutical Sciences, 2008. **35**(1-2): p. 12-8.
15. Voss, A., and Finlay, W.H., *Deagglomeration of dry powder pharmaceutical aerosols.* International journal of pharmaceutics, 2002. **248**: p. 39 - 50.
16. De Boer, A., et al., *Air classifier technology (ACT) in dry powder inhalation, Part 1. Introduction of a novel force distribution concept (FDC) explaining the performance of a*

- basic air classifier on adhesive mixtures*. International journal of pharmaceutics, 2003. **260**(2): p. 187-200.
17. Donovan, M., and Smyth, H.D., *A New Method of Improving Dry Powder Dispersions using Large Carrier Particles*. Respiratory Drug Delivery, Lisbon, Portugal, 2009. **2**: p. 429 - 32.
  18. Dickhoff, B.H.J., et al., *The effect of carrier surface and bulk properties on drug particle detachment from crystalline lactose carrier particles during inhalation, as function of carrier payload and mixing time*. European Journal of Pharmaceutics and Biopharmaceutics, 2003. **56**(2): p. 291-302.
  19. Concessio, N.M., VanOort, M.M., Knowles, M.R., and Hickey, A.J., *Pharmaceutical Dry Powder Aerosols: Correlation of Powder Properties with Dose Delivery and Implication for Pharmacodynamic Effect*. Pharmaceutical research, 1999. **16**(6): p. 828 - 834.
  20. Begat, P., Morton, D.A.V., Staniforth, J.N., and Price, R., *The cohesive-adhesive balances in dry powder inhaler formulations I: Direct quantification by atomic force microscopy*. Pharmaceutical research, 2004. **21**(9): p. 1591 - 1597.
  21. Saleem, I., H. Smyth, and M. Telko, *Prediction of dry powder inhaler formulation performance from surface energetics and blending dynamics*. Drug development and industrial pharmacy, 2008. **34**(9): p. 1002-10.

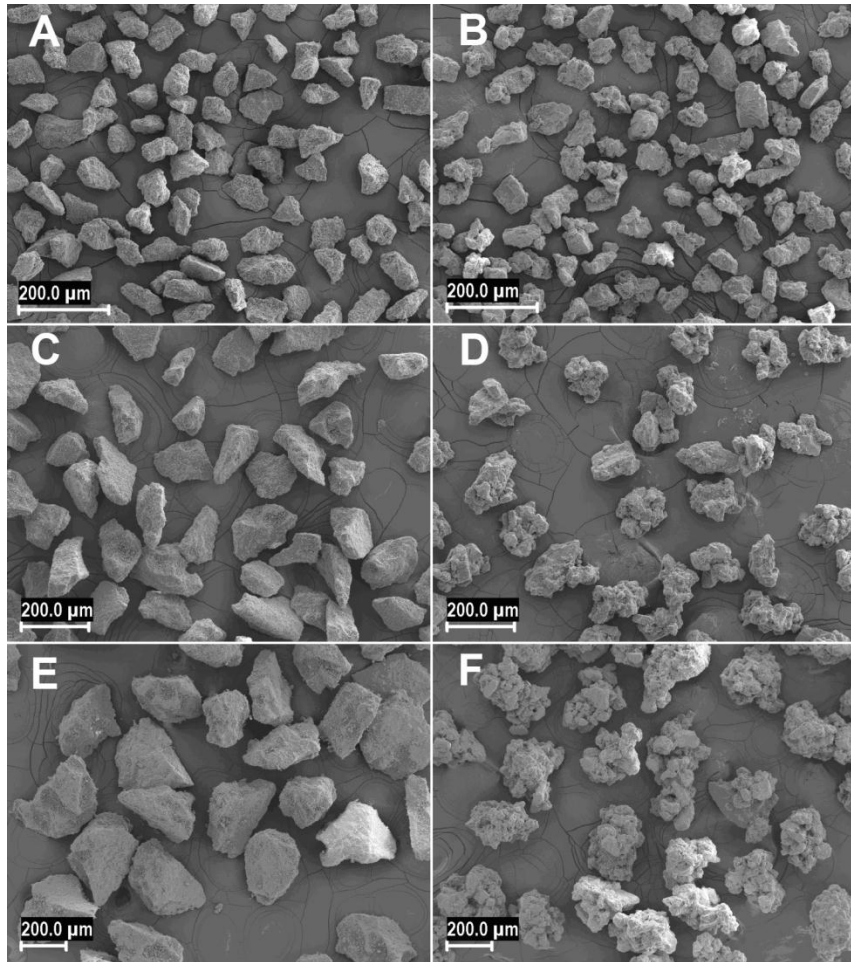


Figure 4.1. SEM Images of Anhydrous and Granulated Lactose Carrier Populations

SEM micrographs of uncoated (A) 45 – 63  $\mu\text{m}$  anhydrous lactose (B) 45 – 63  $\mu\text{m}$  granulated lactose (C) 90 – 125  $\mu\text{m}$  anhydrous lactose (D) 90 – 125  $\mu\text{m}$  granulated lactose (E) 212 – 250  $\mu\text{m}$  anhydrous lactose (F) 212 – 250  $\mu\text{m}$  granulated lactose sieve fractions. Scale bars denote 200  $\mu\text{m}$ .

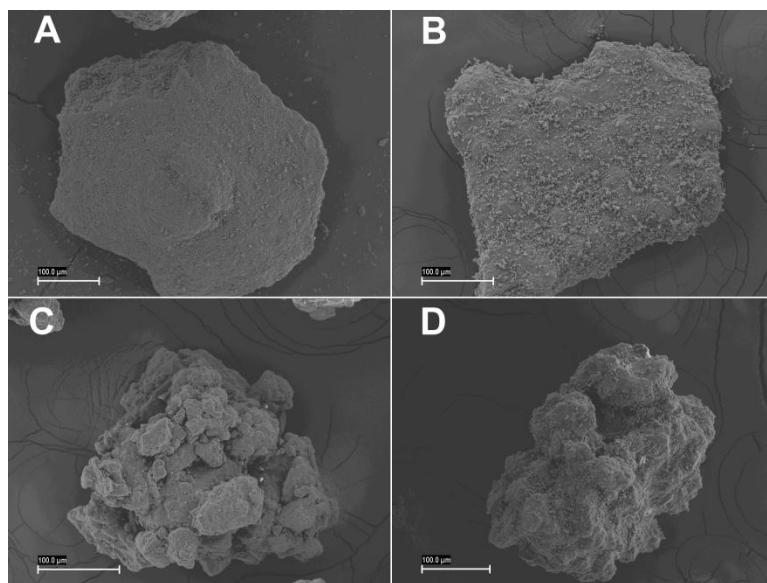


Figure 4.2. SEM Images of Uncoated and Coated Carrier Particles

SEM micrographs of 250 – 300  $\mu\text{m}$  (A) anhydrous lactose carrier particles without drug (B) anhydrous lactose carrier particles with 2% (w/w) budesonide (C) granulated lactose carrier particles without drug, and (D) granulated lactose with 2% (w/w) budesonide. Scale bars denote 100  $\mu\text{m}$ .

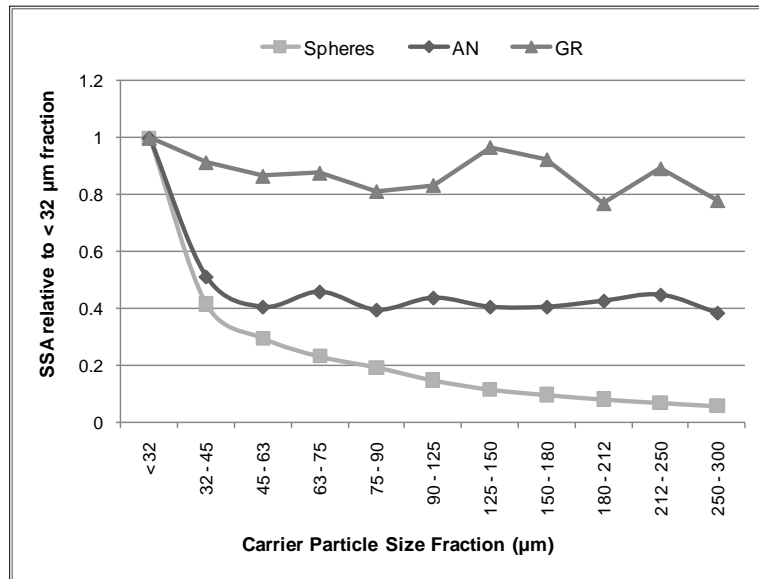


Figure 4.3. Decline in Specific Surface Area as Carrier Particle Size is Increased

Reduction in specific surface area (SSA) with increasing carrier particle size for anhydrous (AN) and granulated (GR) lactose carrier particles, as compared to populations of mono-disperse spherical particles.

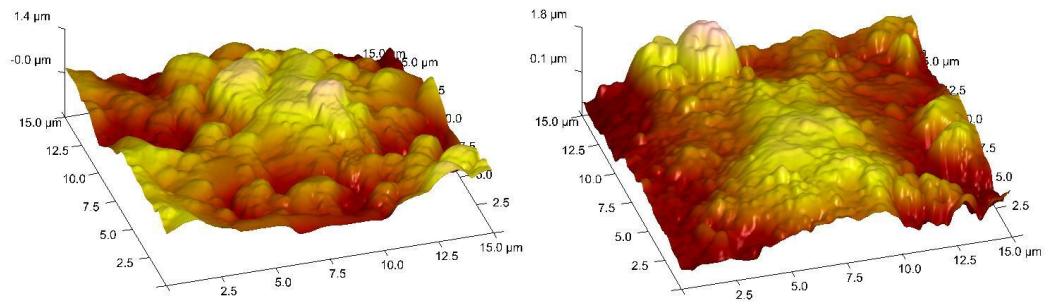


Figure 4.4. AFM Images of Anhydrous Lactose Carrier Particles

Surfaces of uncoated 75 – 90 μm (left) and 250 – 300 μm (right) anhydrous lactose particles determined by tapping mode atomic force microscopy.



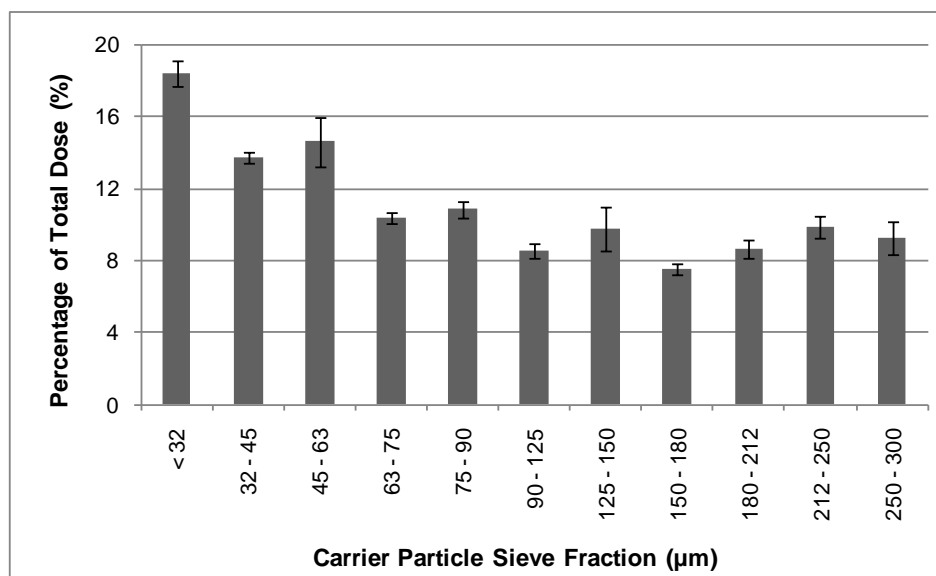


Figure 4.5. RF values from Anhydrous Lactose Carrier Particles

*In vitro* drug deposition results for 2% (w/w) budesonide formulations employing anhydrous lactose carrier particles. Values are given as mean ( $\pm$  standard deviation) for N = 3 replicates.

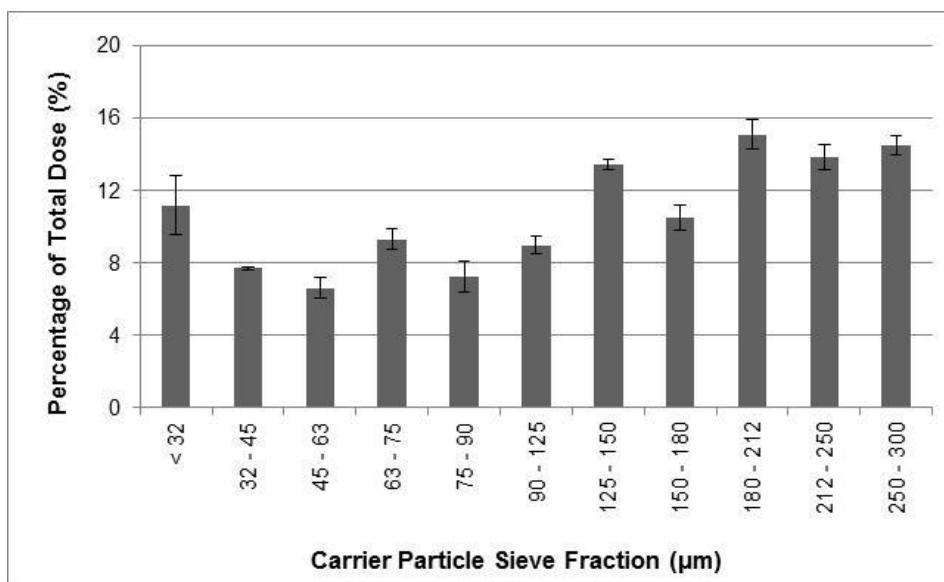


Figure 4.6. RF values from Granulated Lactose Carrier Particles

*In vitro* drug deposition results for 2% (w/w) budesonide formulations employing granulated lactose carrier particles. Values are given as mean ( $\pm$  standard deviation) for N = 3 replicates.

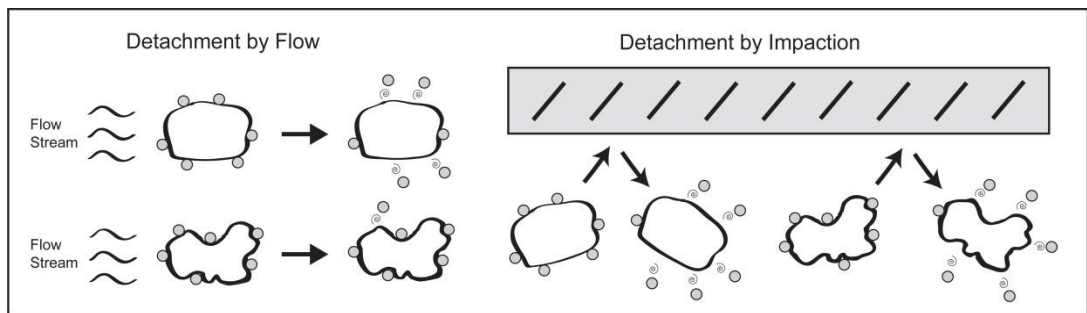


Figure 4.7. Mechanisms of Drug Particle Detachment from 'Smooth' and 'Rough' Carriers

Drug detachment occurs by the flow stream, or from mechanical forces arising from impactions between the carriers and inhaler as the particles exit the device during inhalation. The relative influence of the two mechanisms varies with surface roughness. Adapted from de Boer et al., 2003b.

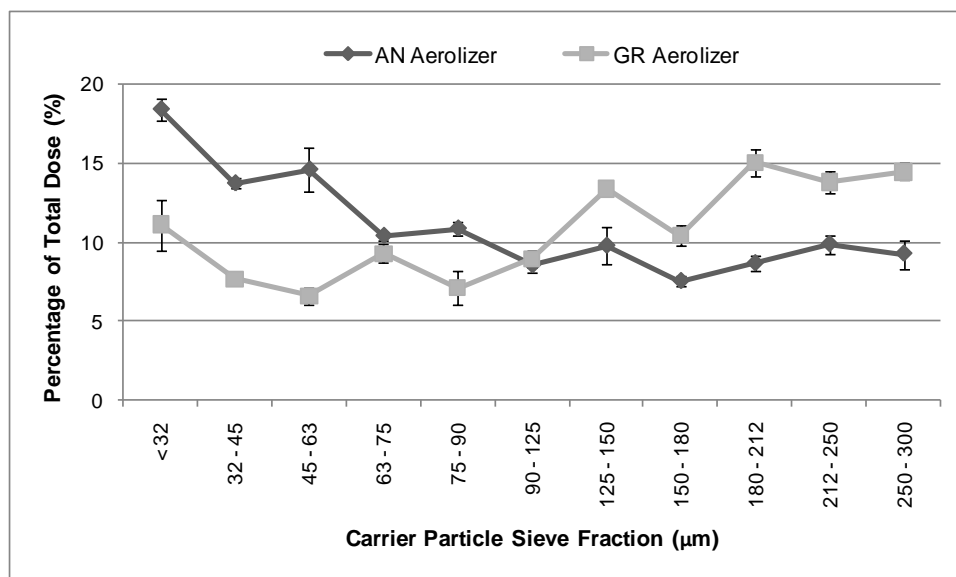


Figure 4.8. Aerosol Performance of AN and GR Formulations

Respirable fractions (RF) of 2% (w/w) budesonide formulations with anhydrous (AN) and granulated (GR) carrier particles following aerosolization at  $60 \text{ L min}^{-1}$ . Values are given as mean ( $\pm$  standard deviation) for  $N = 3$  replicates.

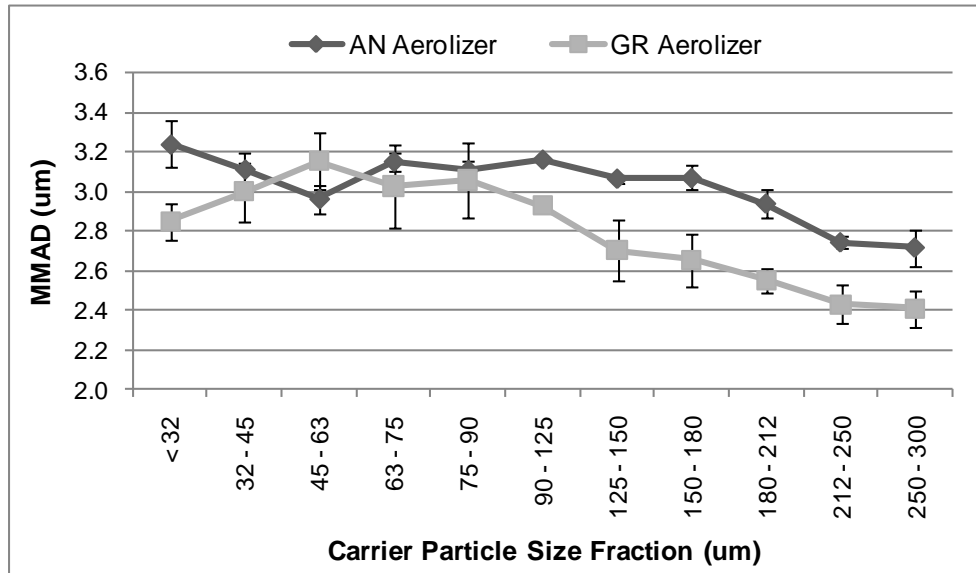


Figure 4.9. MMAD Values of Budesonide Dispersed from Anhydrous and Granulated Carriers

Mass median aerodynamic diameters (MMAD) of budesonide particles deposited from anhydrous (AN) and granulated (GR) carriers. Values are given as mean ( $\pm$  standard deviation) for N = 3 replicates.

Table 4.1. Specific surface areas (SSA) of anhydrous and granulated lactose carrier particles

Carrier Size Fraction ( $\mu\text{m}$ )	Anhydrous ( $\text{m}^2/\text{g}$ )	Granulated ( $\text{m}^2/\text{g}$ )	$\text{SSA}_{(\text{GR})} / \text{SSA}_{(\text{AN})}$
< 32	0.94	1.87	2.0
32 – 45	0.48	1.71	3.6
45 – 63	0.38	1.62	4.3
63 – 75	0.43	1.64	3.8
75 – 90	0.37	1.52	4.1
90 – 125	0.41	1.56	3.8
125 - 150	0.38	1.81	4.8
150 – 180	0.38	1.73	4.6
180 – 212	0.40	1.44	3.6
212 – 250	0.42	1.67	4.0
250 - 300	0.36	1.46	4.1

Measured specific surface areas (SSA) of anhydrous and granulated lactose by sieve fraction. The column on the right lists the SSA ratio of the granulated particles over anhydrous particles for a specific size range.

Table 4.2. Aerosol Performance Values of Anhydrous and Granulated Lactose Formulations

Carrier Sieve Fraction ( $\mu\text{m}$ )	Anhydrous (AN) Lactose			Granulated (GR) Lactose		
	% Emitted	FPF	RF	% Emitted	FPF	RF
> 32	63.5 (1.6)	29.1 (1.4)	18.4 (0.7)	57.0 (1.4)	18.5 (1.2)	11.2 (1.6)
32 – 45	64.5 (1.8)	21.3 (0.9)	13.7 (0.3)	69.1 (3.7)	11.1 (0.6)	7.7 (0.1)
45 – 63	63.2 (2.2)	23.1 (1.8)	14.6 (1.4)	74.4 (4.1)	8.9 (1.2)	6.6 (0.6)
63 – 75	68.9 (1.8)	15.1 (0.4)	10.4 (0.3)	73.9 (3.7)	12.7 (1.4)	9.3 (0.6)
75 – 90	71.9 (2.4)	15.2 (0.3)	10.9 (0.5)	73.9 (6.6)	9.7 ( 2.1)	7.1 (1.1)
90 – 125	62.3 (1.9)	13.7 (0.6)	8.5 (0.4)	77.8 (1.8)	11.6 (0.9)	9.0 (0.5)
125 - 150	62.7 (2.1)	15.6 (1.4)	9.8 (1.2)	71.3 (4.2)	18.9 (1.5)	13.4 (0.3)
150 – 180	62.3 (2.0)	12.1 (0.8)	7.5 (0.3)	73.8 (2.5)	14.2 (1.3)	10.5 (0.7)
180 – 212	61.8 (1.9)	14.1 (1.1)	8.7 (0.5)	72.6 (3.2)	20.8 (1.1)	15.1 (0.8)
212 - 250	63.5 (2.3)	15.5 (0.8)	9.9 (0.6)	68.7 (5.4)	20.2 (1.5)	13.8 (0.7)
250 - 300	61.6 (1.7)	15.0 (1.1)	9.3 (0.9)	68.5 (4.5)	20.2 (1.5)	14.5 (0.6)

*In vitro* drug deposition results for 2% (w/w) budesonide formulations employing anhydrous and granulated lactose carrier particles. Values are given as mean ( $\pm$  standard deviation) for N = 3 replicates.

Table 4.3. MMAD Values of Budesonide Particles Dispersed from Anhydrous and Granulated Lactose Carrier Particles.

	Anhydrous (AN) Lactose	Granulated (GR) Lactose
Carrier Sieve Fraction ( $\mu\text{m}$ )	MMAD ( $\mu\text{m}$ )	MMAD ( $\mu\text{m}$ )
< 32	3.24 (0.12)	2.85 (0.09)
32 – 45	3.11 (0.09)	3.00 (0.15)
45 – 63	2.96 (0.07)	3.15 (0.14)
63 – 75	3.15 (0.05)	3.03 (0.21)
75 – 90	3.11 (0.04)	3.06 (0.19)
90 – 125	3.16 (0.01)	2.93 (0.03)
125 – 150	3.07 (0.02)	2.70 (0.15)
150 – 180	3.07 (0.06)	2.66 (0.13)
180 – 212	2.94 (0.07)	2.55 (0.06)
212 – 250	2.74 (0.03)	2.43 (0.10)
250 - 300	2.72 (0.09)	2.41 (0.09)

Mass median aerodynamic diameters (MMAD) of micronized budesonide drug particles detached from anhydrous and granulated lactose carrier particles as determined by *in vitro* drug deposition. Values are given as mean ( $\pm$  stdev) for N = 3 replicates.



## CHAPTER 5

### 5. Performance of Dry Powder Inhalers as a Function of the Diameter and Surface Roughness of the Carrier Particle Population

#### 5.1. INTRODUCTION

Dry powder inhaler formulations are typically binary mixtures comprising micronized active agent blended with a coarse carrier particle population that constitutes the bulk of the formulation (> 95% w/w) [10]. When a patient inhales through a dry powder inhaler (DPI), the energy derived from their inspiratory effort fluidizes the powdered dose, detaching a fraction of the drug from the larger carrier particles and depositing it in the deep lung where it exerts its intended therapeutic effect [8]. It is well recognized that dry powder inhalers possess distinct mechanisms of powder dispersion [87]. Passive DPIs rely solely on the patient's inspiratory effort to fluidize and disperse the powdered formulation, and have evolved considerably from their inception, incorporating a diverse array of geometries, including vortices and cyclones, to induce turbulence and particle-inhaler collisions to maximize the detachment potential of the available flow stream[3, 6].

The use of computational fluid dynamics (CFD) to model the inhalation flow stream, pressure profiles, and particle trajectories within therapeutic inhalers has become increasingly prevalent, finding employment in the optimization of device parameters during development or, *ex post facto*, to elucidate the de-agglomeration principle of a commercially available inhaler [34-38, 60]. By coupling CFD simulations with *in vitro* aerosol performance, information on the relative contributions of device and formulation can be obtained. A notable example of this approach is a series of studies by Coates and colleagues on the Aerolizer<sup>®</sup> dry powder inhaler, where the device geometry (e.g. air inlet area, mouthpiece length) and operating parameters (volumetric flow rate, capsule size) were varied to assess their influence on *in vitro* aerosol performance [34-38].

Drug detachment from carrier particles is believed to proceed through two primary mechanisms: (1) aerodynamic, or fluid-based, detachment arising from the direct interaction of the flow stream with drug particles located on the carrier surface, and (2) mechanical, or impaction-based, detachment due to collisions between carrier particles and the inhaler walls during particle transit through the device [31, 87]. Although the diverse internal geometries of inhalers will vary the relative contributions between aerodynamic and mechanical detachment forces, it has been reported that the magnitude of impact-based events may exceed those of flow-based events, and could potentially be the dominating factor in drug detachment from carrier particles [9, 32, 87, 93].

Previous research in our laboratory has demonstrated that large lactose carrier particles ( $> 180 \mu\text{m}$ ) can improve drug deposition *in vitro* for both anhydrous and granular lactose populations, although the improvement with carrier particle size was more pronounced in formulations with granulated carrier particles [80]. It is speculated that the surface roughness of the granulated particles shifted the drug detachment mechanism from flow-based detachment for carrier particles with minimal surface roughness, to impaction-based detachment forces as carrier particle size and roughness increased. The aerosol performance improvement was thought to result from an increased incidence of carrier particle-inhaler collisions, given the higher inertia of larger carrier particles, which inhibit their ability to travel with the flow stream through the inhaler. However, it is recognized that the aerodynamic behavior of carrier particles can vary significantly based on the inhaler through which a formulation is dispersed, and improved performance may be observed if the carrier particle design matches the predominant mechanism(s) of detachment induced by specific inhaler types. Accordingly, the specific aim of this study was to assess the role of the DPI design on aerosol performance as the size and shape of the carrier particle population is varied. CFD simulations of carrier particle trajectories were coupled with *in vitro* drug deposition studies to investigate the combined influence of device and carrier on formulation performance.

## **5.2. EXPERIMENTAL**

### **5.2.1. Materials**

Micronized budesonide (EP) was purchased from Spectrum Chemicals (CA, USA) and used as received. Analytical grade ethanol was supplied by Sigma Chemical Company (MO, USA). Samples of anhydrous (SuperTab® 22AN), and granulated (SuperTab® 30GR) lactose were obtained from DMV-Fonterra (New Zealand). Size 3 gelatin capsules were provided by Capsugel® (NJ, USA).

### **5.2.2. Fractionation of Lactose Carrier Particles**

Samples of each lactose batch were fractionated on an Autosiever vibrating sieve shaker (Gilson Company Inc., OH, USA) with a sieve intensity, or amplitude, setting of 40 for 5 minutes through the following sieves: 300 µm, 250 µm, 212 µm, 180 µm, 150 µm, 125 µm, 90 µm, 75 µm, 63 µm, 45 µm, and 32 µm. Following the initial fractionation, the lactose carriers were again sieved to obtain narrow particle size distributions.

### **5.2.3. Preparation of Budesonide/Lactose Binary Blends**

Budesonide and lactose were mixed in a ratio of 1:50 (w/w) via geometric dilution to obtain 500 mg of a 2% binary blend. The formulations were blended with a Turbula® orbital mixer (Glen Mills, NJ, USA) for 40 minutes at 46 RPM. Samples were stored in a desiccator at least 5 days prior to use. Blend uniformity was determined by randomly selecting eight 20-mg samples from each mixture, and assessing the drug content in the powder. Formulations were considered well blended and ready for use if the coefficient of variation (% CV) between the samples for a given blend was below 5%.

### **5.2.4. Scanning Electron Microscopy**

The size and morphology of carrier particles were visually assessed by scanning electron microscopy (SEM; Supra 40VP, Zeiss, Germany). Prior to SEM, approximately 20 nm of platinum were deposited onto the particle surfaces via sputter coating.

### **5.2.5. Surface Area Analysis**

Specific surface areas of the lactose carrier particle populations were determined via nitrogen adsorption with a single-point BET method using a Monosorb® surface area analyzer (Quantachrome, FL, USA).

### **5.2.6. Density of Lactose Carriers**

The true densities of the lactose carrier particles were determined with a helium multipycnometer (Quantachrome, FL, USA).

### **5.2.7. *In Vitro* Drug Deposition**

20 ( $\pm$  1) mg of powder were loaded into size 3 gelatin capsules and dispersed through an Aerolizer® (Plastiap S.p.A., Italy) and Handihaler® (Boehringer Ingelheim Inc., CT, USA) DPI into a next generation cascade impactor (MSP Corporation, MN, USA) at a volumetric flow rate of 60 L min<sup>-1</sup> actuated for 4-second intervals. Prior to each actuation, 15 mL of EtOH were added to the pre-separator and collected following powder dispersion from each capsule. Drug depositing in the capsule, inhaler, mouthpiece adaptor, and induction port were collected by rinsing each component with 10 mL of EtOH, while the NGI stages were each rinsed with 5 mL. Drug content was assessed via UV-VIS absorption spectroscopy at 244 nm. The emitted fraction was calculated as the ratio of the drug mass depositing in the mouthpiece, induction port, pre-separator, and impactor stages over the cumulative mass of drug collected following actuation (total drug deposited in the capsule, inhaler, mouthpiece, induction port, pre-separator and stages). The fine particle fraction (FPF) of each dose was the ratio of the drug mass depositing on stages 3 through 8 (corresponding to an aerodynamic diameter less than 4.46  $\mu$ m) of the impactor over the emitted dose. The respirable fraction (RF) was the ratio of the drug mass deposited on stages 3 – 8 over the entire dose recovered following each actuation.

### 5.2.8. Computational Fluid Dynamics

CFD analysis was employed to study the flow field and assess carrier particle trajectories within the DPIs during actuation. The geometry of the Aerolizer was generously provided as a CAD file by the manufacturer (S.p.A. Italy); the computational mesh consisted of approximately 3.7 million unstructured computational volumes. By comparison, the Handihaler is composed of relatively simpler internal geometric features, which were modeled from measurements obtained with a caliper. The Handihaler geometry was modeled using 3 million unstructured computational volumes. The computational mesh, in each case, was clustered near the walls to provide better resolution of the near-wall turbulence. For instance, the  $y^+$  value, which is a normalized distance used to characterize the near-wall resolution with respect to the boundary layer, was roughly 15. For both the configurations, the incoming mass flow rate was set at  $60 \text{ L min}^{-1}$ . A size 3 capsule was placed in the capsule chamber. The flow inside the inhaler is turbulent, comprising of a range of length and time scales. To ensure computational tractability, this turbulent flow field is modeled using the Reynolds-averaged Navier Stokes (RANS) approach[94]. In this work, the commercial solver FLUENT® (ANSYS, Inc., Canonsburg, PA) is used to solve the RANS equations. The turbulence properties of the flow field are described using the shear-stress transport (SST) based  $k-\omega$  model. The flow equations were discretized using a first-order numerical scheme. Although a higher order scheme would provide better accuracy with lower number of computational volumes, it was found to significantly reduce the convergence characteristics. By using a large number of computational volumes, the dissipative errors associated with a first order scheme were minimized. Extensive grid convergence studies demonstrated that the mesh used here provides mesh-converged results. The RANS equations were solved until a steady state solution was reached. After this step, discrete particles corresponding to the drug carrier particles were introduced in the flow. The particles evolved using a drag law, with non-spherical corrections imposed to account for particle shape effects (Fluent Inc. (2006) Centerra Resource Park, Lebanon, NH). The flow rate is high enough for gravitational forces to be important. The initial locations of the particles were different for the two configurations (as shown in the particle trajectory images in the Results and Discussion section below). These locations were based on the assumption that the capsule was perforated

from one side, and the particles leave the capsule with identical velocities. Since the mass loading of the particles in relation to the local fluid mass is very small, the effect of the particles on the flow field is neglected. Three different particle diameters were simulated for each inhaler. The particles were assumed to be a monodisperse population of uniform spheres with diameters of 32, 108, and 275  $\mu\text{m}$ . In each simulation, roughly 1000 particles were initiated with zero velocity. Since the mass loading is small, collisions amongst the particles are neglected. The particles are evolved using discrete particle equations. The number of collisions that each particle experienced with different sections of the DPIs were tracked as the particles travelled through the inhaler. In order to ensure statistical convergence of the results, different particle numbers were considered. It was found that using 500 particles was sufficient to obtain converged statistics for the average number of collisions that the particles undergo with the inhaler walls.

#### **5.2.9. Statistics**

Statistical significance between performance values was determined with one-way ANOVA with Post Hoc tests between groups according to the Bonferroni method ( $P < 0.05$ ).

### **5.3. RESULTS AND DISCUSSION**

#### **5.3.1. Physical Characterization of Carrier Particle Populations**

The double-sieving technique yielded narrow particle size distributions (Figure 5.1). While  $\alpha$ -lactose monohydrate is typically used as the carrier particle population in binary dry powder formulations, other grades including anhydrous and granulated lactose have been studied, affording the opportunity to assess the influence of carrier morphology on aerosol performance [41, 75, 79, 80]. The disparity in surface roughness between the anhydrous and granulated lactose particles increases with particle size, as evidenced by the diminishing specific surface areas of the anhydrous particles relative to their granulated counterparts with increasing carrier sieve fraction (Table 5.1). Surface areas of larger granulated lactose did not diminish appreciably as particle sizes were increased (as would be expected for perfectly

smooth spherical particles). Instead, the increasing roughness (due to granulation) causes a relatively minimal decline in surface area as the size of the particles within the powder is increased. The true densities of all carrier particle size fractions in both grades of lactose ranged between 1.54 and 1.58 g/cm<sup>3</sup>.

### **5.3.2. CFD Analysis**

Internal geometries of the Handihaler and Aerolizer are illustrated in Figure 5.2. The flow stream enters the Aerolizer via two tangential inlets found on opposite sides of the capsule chamber [37]. The resulting turbulent flow field induces the capsule to rotate and rattle with high frequency during inhalation, assisting in ejecting and dispersing the powdered dose through the perforations in the capsule wall [35]. It is noted that although the motion of the capsule itself is not simulated in this work, it may affect particle release and transport in the fluid flow, and it has been speculated that the emitted powder particles may collide with the capsule, though a previous investigation concluded that impactions between the powder particles and the spinning capsule do not significantly contribute to dispersion performance in the Aerolizer[35]. However, those studies were performed on pure micronized mannitol, and the inclusion of carrier particles may potentially alter this result and is a topic that merits future study.

A key feature of the internal geometry of the Aerolizer is a grid dividing the capsule chamber and the mouthpiece to prevent capsule egress from the device during inhalation. Additionally, it is noted that the grid has been demonstrated to straighten the flow and suppress turbulence downstream of its location [34]. On the other hand, the mechanism of the Handihaler is based on the sudden expansion of the inhalation flow stream as it passes from the inlet into the larger capsule chamber. The abrupt opening from the smaller inlet chamber to the capsule chamber causes the boundary layer of the flow stream to separate at the corner of the expansion, creating an annular region where a portion of the flow re-circulates, resulting in a pressure loss in this region [49]. The incoming flow stream pushes the capsule toward the grid while the low pressure region simultaneously attracts the capsule toward the inlet, causing the capsule to spin and vibrate in the chamber [60]. Similar to the Aerolizer, the Handihaler also

contains a mesh between the capsule chamber and the mouthpiece. However, this grid is made of thinner wires and its effect on the flow field is comparably less significant than the grid located in the Aerolizer, as the blockage represented by the wires is a very small fraction of the total surface area.

Figure 5.3 depicts the velocity magnitude of the flow stream in the inhalers at  $60 \text{ L min}^{-1}$ . In the Handihaler, the maximum flow speed is found upstream of the capsule with very high shear flow around the capsule itself. In contrast, the Aerolizer exhibits a much more complex flow pattern, as the incoming flow generates a swirling motion inside the capsule chamber. The grid between the capsule chamber and the mouthpiece constricts the flow, and consequently the velocity magnitude is very high when the fluid exits the capsule chamber through the grid spacing. The grid also regulates the swirling flow generated by the capsule chamber [34].

Carrier particle trajectories were simulated through the DPIs to quantify the frequency of their collisions with the internal geometry of the inhaler (Table 5.2). It was expected that the distinct internal geometries of the inhalers would yield distinct particle trajectories. As seen in Figure 5.4, the fluid flow inside the Aerolizer actively promotes particle collisions with the inhaler wall. The tangential air inlets introduce a swirl component to the flow stream that is imparted to the powder as they exit the capsule, causing particles to swirl through the mouthpiece.

In contrast to the Aerolizer, carrier particles within the Handihaler experience markedly fewer collisions with the inhaler (Figure 5.5). The wake region downstream of the cavity causes the particles to accelerate and travel at an angle to the vertical direction, directing the particle trajectory towards the inhaler wall. As the particles have significant inertia (increasing with carrier particle size), once they are launched on this trajectory the fluid flow is unable to significantly alter the particle trajectory. The initial acceleration around the capsule introduces the collisional movement, pushing the particles downstream towards the inhaler exit.

Table 5.2 shows the influence of particle diameter on the number of collisions with the mouthpiece wall experienced by the particles. It should be noted that the fluid flow corresponds



to particles with zero diameter, or zero Stokes number. Increasing the particle diameter increases the Stokes number and causes a departure of the particle trajectory from the fluid trajectory. As the particles become larger, their response to changes in the fluid flow is slower. Consequently, larger particles can possess ballistic trajectories and undergo more collisions, and increasing the particle diameter increases the number of collisions. It is seen that the Aerolizer exhibits greater sensitivity to particle size relative to the Handihaler. This is primarily attributed to the fact that the Handihaler does not introduce a swirling motion inside the mouthpiece, which causes the particles to have a longer residence time (or trajectory length) inside the mouthpiece.

### **5.3.3. In vitro Aerosol Performance**

*In vitro* drug dispersion profiles for all experimental formulations are presented in Tables 5.3 to 5.4. The percentage of the nominal dose emitted from the Handihaler exceeded that emitted from the Aerolizer, yielding over 75% emitted fraction (EF) for all carrier particle sizes between both lactose grades. For anhydrous lactose formulations dispersed from the Handihaler, the enhanced EF did not correspond to improved drug deposition compared with the Aerolizer, as respirable fraction (RF) values were generally comparable between devices across most carrier particle size fractions. The disparity between EF and RF is reconciled by the higher fine particle fraction (FPF) values obtained from the Aerolizer, indicating that although for anhydrous formulations the Handihaler is more effective at emitting drug from the device, the Aerolizer demonstrates a greater tendency for detaching drug from the carrier particles. In contrast, granulated carrier particle formulations dispersed from the Handihaler outperformed those from the Aerolizer for all but the largest carrier particle size fractions.

From the drug dispersion profiles, it is observed that the increased number of collisions between the carrier particles and inhaler does not directly translate into improved aerosol performance, as measured by RF. For a given dry powder formulation, RF values reflect the combined EF and FPF, revealing an inhaler's potential to both emit the drug from the device and detach it from the carrier, such that it can travel to the deep lung[41]. By itself, EF is a metric describing the inhaler's ability to emit the drug from the device and deliver it to the patient, but

reveals nothing as to whether the drug is detached from the carrier, and drug that remains adhered to the coarse carrier particles will deposit in the mouth, throat and upper airways. Accordingly, FPF is a better measure of an inhaler's drug detachment potential, providing the fraction of detached drug exiting the device relative to the total amount that leaves the inhaler. A high EF coupled with a high FPF will generate excellent RF values, but opposing EF and FPF performance (e.g. high EF and low FPF) will only yield moderate respirable fractions.

Although significant differences in emitted dose were observed between the devices, this did not yield a consistent disparity in overall performance, as the relatively high EF from Handihaler was offset by the Aerolizer's enhanced tendency to emit drug particles detached from the carriers. To provide an approximate measure of the relative drug detachment potential of the DPIs, the ratio of FPF values from the Aerolizer over the Handihaler ( $FPF_{\text{Aerolizer}} / FPF_{\text{Handihaler}}$ ) against the carrier particle size fraction were plotted (Figure 5.6). Values > 1 indicate the Aerolizer may be more effective at drug detachment while a ratio less than unity gives the advantage to the Handihaler. It must be noted that detached drug particles may be agglomerates of primary drug particles, which due to their large size will deposit in the throat and conducting airways. This is especially relevant for the corticosteroid budesonide, which has been demonstrated to be a relatively cohesive drug [17, 18]. However, as the same formulation was used for each size fraction within a lactose grade, the extent of drug agglomeration was presumed constant between samples, with the inhaler as the variable. For the anhydrous carrier formulations, all but a single size fraction (90 – 125  $\mu\text{m}$ ) exceeded 1, indicating the ability of the Aerolizer to emit drug particles detached from the carrier outperforms the Handihaler. Conversely, most granulated carriers yielded better drug detachment from the Handihaler (ratios were less than 1). However, at carrier particle sizes greater than the 75 – 90  $\mu\text{m}$  and the 90 – 125  $\mu\text{m}$  fractions for the granulated and anhydrous carriers respectively, the FPF ratio began to increase, indicating an improvement in drug detachment potential of the Aerolizer relative to the Handihaler for large carrier particle formulations. It is speculated that the higher frequency of carrier-inhaler collisions within the Aerolizer as carrier size is increased may account for the observed improvement in drug detachment. In these larger carrier formulations, impaction-based forces may be a significant mechanism of drug detachment as discussed below.

#### 5.3.4. Influence of Device on Performance

Due to the marked variation in the internal geometries of the two inhalers, differences in aerosol performance were expected between the Aerolizer and Handihaler. Regarding device resistance, the Aerolizer and Handihaler reside on opposing ends of the spectrum, as the Aerolizer has less than half the resistance ( $0.072 \text{ (cmH}_2\text{O)}^{0.5} / (\text{L min}^{-1})$ ) of the Handihaler ( $0.158 \text{ (cmH}_2\text{O)}^{0.5} / (\text{L min}^{-1})$ ) [37, 95]. This increased resistance of the Handihaler arises from the narrow inlet tube at the base of the capsule chamber (Figure 5.2) [60]. It is noted that the flow rate selected for this study ( $60 \text{ L min}^{-1}$ ) is much higher than that typically generated through the Handihaler, but is readily attainable by > 90% of adult patients through an Aerolizer [95-97]. The relationship between inhaled resistance (R), volumetric flow rate (Q), and pressure drop ( $\Delta P$ ) across a device is  $(\Delta P)^{0.5} = QR$  [65]. For a fixed flow rate, a higher resistance device will produce a greater pressure drop, which has been found to correlate with improved aerosol performance [67, 68, 98]. Additionally, the overall energy passing through an inhaler can be approximated from the product of the pressure drop across the device, volumetric flow rate, and actuation time [33]. Thus, although the volumetric flow rate is the same through both inhalers (60 Lpm), a greater pressure drop, and hence a higher energy value is calculated for the Handihaler, which is predicted to improve performance from this DPI. However, despite the device differences, RF values exhibited minimal dependence on the inhaler for the anhydrous carrier particles, varying instead as a function of carrier particle size, with larger carrier particle diameters diminishing overall performance (Figure 5.7). By comparison, granulated lactose formulations showed some device dependency, notably in the smaller carrier particle size fractions, with both inhalers demonstrating comparable performance as carrier size increased.

For anhydrous lactose formulations, the relatively flat surfaces of the carriers permit direct interaction between the drug particles and inhalation flow stream. The overall dispersion performance between the devices is similar across all anhydrous carrier size fractions, indicating the comparable ability of the DPIs to detach drug readily accessible to the air flow. However, in granulated lactose formulations, where direct interaction between the drug and flow stream is inhibited by the surface roughness of the carriers, the Handihaler exhibited higher RF values up

to the largest size fractions, when it is speculated that increasingly larger mechanical forces allowed the Aerolizer to improve its detachment potential (as indicated by the increasing FPF ratio), and attain comparable RF values. The improved performance at smaller carrier sizes of granulated lactose in the Handihaler may be attributed to the greater overall aerodynamic energy passing through this device (as mentioned above). A previous study on the Handihaler revealed that a pressure gradient develops across the capsule chamber, pulling drug particles primarily from the lower capsule perforation located nearest the corner of the flow stream expansion[60]. This mechanism may enable drug within the surface asperities of the granulated particles to be pulled-off of the carriers, allowing performance to be relatively independent of carrier particle diameter and thus surface roughness, as the surface roughness of granulated carriers tended to increase with carrier size.

### **5.3.5. Interparticle Collisions**

In addition to carrier particles colliding with the inhaler walls, interparticle collisions between carriers during actuation may provide an additional source of mechanical detachment forces. For a fixed mass of powder, increasing the diameter of the carrier population diminishes the overall number of carrier particles in the dose, such that formulations with the largest lactose sizes contain a fraction of the number of carrier particles relative to the smallest carrier size ranges. Previous studies have reported that lactose fluidizes from capsules via two distinct mechanisms dependent upon the flowability, and hence the cohesiveness, of the powder [99-101]. Powders with good flowability are entrained by an 'erosion' mechanism, where the powder is fluidized by layers and exits the inhaler gradually as a continuous stream [100, 101]. By contrast, for poorly flowing powders fluidization occurs by the 'fracture' mechanism whereby the powder fluidizes as multiple agglomerates, and in extreme cases may fluidize as a single aggregated powder plug.

It has been proposed that smaller carrier particle size fractions, particularly those with a significant concentration of lactose fines, improve aerosol performance by coupling the fracture entrainment mechanism with an extensive number of carrier particles, thereby generating a high density aerosol cloud that promotes collisions between lactose carriers[100, 101]. In the

present study, only anhydrous formulations exhibited performance consistent with this mechanism, but performance from granulated carriers was incompatible with this theory, as the < 32  $\mu\text{m}$  carrier populations did not yield RF values significantly higher than the larger carriers. However, variables apart from carrier particle size can affect the extent to which interparticle collisions may occur. For instance, the DPI employed may influence interparticle collisions, as devices with more complex internal geometries may enhance the frequency and/or magnitude of interparticle collisions relative to inhalers with simpler internal geometries. Additionally, the cross-sectional area of the capsule perforation may likewise affect interparticle collisions, as smaller openings can prevent the powder from exiting the capsule as agglomerated plugs, thus limiting the density of the aerosol cloud. Thus, it is noted that the inhalers employed in these studies may not be ideal for promoting interparticle interactions, as the swirling particle trajectories in the capsule chamber of the Aerolizer may be offset by the small cross-sectional area of the capsule perforations, while the larger diameter capsule openings from the Handihaler are coupled with an internal geometry that may not induce extensive interparticle collisions relative to the Aerolizer. Accordingly, although interparticle collisions may influence aerosol performance under certain conditions, this detachment mechanism was not supported by the data for both lactose grades, and thus CFD simulations capturing carrier-carrier interactions were deemed beyond the scope of the present study.

#### **5.3.6. Mass Median Aerodynamic Diameter**

In contrast to the respirable fraction, the mass median aerodynamic diameter (MMAD) of drug depositing on the stages of the cascade impactor varies significantly between inhalers for both anhydrous and granulated lactose formulations (Figure 5.8). Furthermore, while the MMAD from the Aerolizer displayed an overall decreasing trend with increasing carrier particle size for both lactose populations, MMAD values obtained from the Handihaler were generally independent of the formulation. The disparity between the MMAD values for formulations dispersed through the inhalers were greatest at the smaller carrier particle formulations, and eventually converged on a mutual value for the largest carrier size fractions. In our previous study, it was postulated that the reduction in MMAD obtained from larger carrier particles

dispersed through the Aerolizer may be attributed to the increased detachment of smaller drug particles from the carrier surface [80]. As the collision force between a particle and inhaler is dependent on the mass, and thus the volume, of the carrier particle, the momentum generated from a collision increases with the cube of the carrier particle diameter, assuming a relatively constant particle velocity (as volume  $\propto$  diameter<sup>3</sup>)[8]. Thus, larger carrier particles can generate strong mechanical detachment forces, which can potentially exceed fluid-based forces [32, 87, 93].

These strong mechanical forces may dislodge drug particles resistant to fluid-based detachment, including small aggregates and primary drug particles located within carrier particle surface asperities, inhibiting their interaction with the flow stream. Accordingly, the size of drug particles depositing in the impactor would be expected to decrease with larger carrier particle populations, as observed in both the anhydrous and granulated formulations dispersed from the Aerolizer. Comparing MMAD values obtained from the Aerolizer with the corresponding RF values, the carrier particle size fraction when the MMAD markedly declined matched the carrier size when aerosol performance exhibited a local improvement; this corresponded to the 180 - 212  $\mu\text{m}$  size fraction for anhydrous carriers, and 90 - 125  $\mu\text{m}$  for granulated lactose ( $p < 0.05$ ). Conversely, MMAD values in the Handihaler were relatively consistent between carriers for both lactose grades, displaying no general trend with performance, although the MMAD from formulations dispersed through the Handihaler were consistently lower than from the Aerolizer, with the exception of the largest carrier sizes ( $> 180 \mu\text{m}$ ).

In combination with the particle trajectory simulations, the aerosol performance data suggest the presence of an impaction-based mechanism of drug detachment in the Aerolizer whereby the relatively numerous and high energy collisions between large carriers and the inhaler wall generate a force sufficient in both magnitude and direction to detach smaller drug particles immune to detachment by the flow stream. As discussed in detail elsewhere, this favors large carrier particles with extensive surface roughness, and accordingly the improvement in aerosol performance with larger carrier populations is more pronounced in

granulated lactose formulations[80]. However, it is noted that while the present studies were performed at a fixed flow rate, the velocity, and hence momentum, of the carrier particles may significantly affect performance, particularly for larger carrier populations.

#### **5.4. CONCLUSION**

In this chapter, the influence of carrier particle size and surface roughness on inhaler performance was investigated. Coupling the CFD particle trajectory simulations with the *in vitro* results, it is concluded that impaction-based forces are not a significant mechanism of detachment in the Handihaler, as reflected by both the absence of improved performance at the large carrier fractions and the minimal increase in simulated carrier particle-inhaler collisions with carrier diameter. In contrast, the internal geometry of the Aerolizer is capable of generating a higher number of particle-inhaler collisions, with the frequency of the collisions increasing with carrier diameter. Accordingly, aerosol performance from this DPI exhibited a dependence on the carrier particle size fraction which was not observed in the Handihaler to a similar extent. Additionally, performance was also significantly influenced by carrier particle morphology, and although granulated lactose is not commonly employed in dry powder inhaler formulations, the use of this lactose grade afforded greater insight into distinctions in DPI performance than relatively smooth surfaced anhydrous lactose. In conclusion, the results of this study suggest that matching the physical properties of the carrier population to the predominant detachment mechanism of the DPI may significantly influence aerosol performance.

Up to this point, all the *in vitro* deposition studies have been performed at a fixed flow rate, specifically 60 L min<sup>-1</sup>. It has been speculated that large carrier particles with extensive surface roughness promote drug detachment via mechanical forces that arise during collisions between the carrier particles and the inhaler walls, and that the greater mass of the larger particles increases their momentum relative to smaller carriers, inducing more forceful impactions.

Accordingly, as momentum is a function of both the mass and the velocity of the carrier particles, it is speculated that increasing the inhalation flow rate may prove more beneficial to particles that rely on mechanical detachment forces as opposed to particles that rely primarily on fluid forces, given that mechanical forces are thought to be more effective at particle detachment. Studies investigating the influence of flow rate on dispersion as the size and surface roughness of the lactose carriers are altered will be the focus of the next chapter.



## 5.5. REFERENCES

1. Hickey, A.J., ed. *Pharmaceutical Inhalation Aerosol Technology*. 2nd ed. 2004, Marcel Dekker, Inc.: New York, NY.
2. Finlay, W.H., *The Mechanics of Inhaled Pharmaceutical Aerosols* 2001, London, UK: Academic Press.
3. de Boer, A., et al., *Air classifier technology (ACT) in dry powder inhalation Part 1. Introduction of a novel force distribution concept (FDC) explaining the performance of a basic air classifier on adhesive mixtures*. *International Journal of Pharmaceutics*, 2003. 260(2): p. 187-200.
4. Frijlink, H.W. and A.H. De Boer, *Dry powder inhalers for pulmonary drug delivery*. *Expert Opinion on Drug Delivery*, 2004. 1(1): p. 67-86.
5. Islam, N. and E. Gladki, *Dry powder inhalers (DPIs)—A review of device reliability and innovation*. *International Journal of Pharmaceutics*, 2008. 360(1-2): p. 1-11.
6. Coates, M.S., et al., *Effect of design on the performance of a dry powder inhaler using computational fluid dynamics. Part 1: Grid structure and mouthpiece length*. *Journal of Pharmaceutical Sciences*, 2004. 93(11): p. 2863-2876.
7. Coates, M.S., et al., *The Role of Capsule on the Performance of a Dry Powder Inhaler Using Computational and Experimental Analyses*. *Pharmaceutical Research*, 2005. 22(6): p. 923-932.
8. Coates, M.S., et al., *Influence of Air Flow on the Performance of a Dry Powder Inhaler Using Computational and Experimental Analyses*. *Pharmaceutical Research*, 2005. 22(9): p. 1445-1453.

9. Coates, M.S., et al., *Effect of design on the performance of a dry powder inhaler using computational fluid dynamics. Part 2: Air inlet size*. Journal of Pharmaceutical Sciences, 2006. 95(6): p. 1382-1392.
10. Coates, M.S., et al., *Influence of Mouthpiece Geometry on the Aerosol Delivery Performance of a Dry Powder Inhaler*. Pharmaceutical Research, 2007. 24(8): p. 1450-1456.
11. Wachtel, H., Ertunc, O., Koksoy, C., and Delgado, A., *Aerodynamic Optimization of Handihaler and Respimat: The Roles of Computational Fluid Dynamics and Flow Visualization*. Respiratory Drug Delivery 2008, 2008. 1: p. 165 - 174.
12. Voss, A., and Finlay, W.H., *Deagglomeration of dry powder pharmaceutical aerosols*. International Journal of Pharmaceutics, 2002. 248: p. 39 - 50.
13. Nichols, S.C., and Wynn, E., *New Approaches to Optimizing Dispersion in Dry Powder Inhalers – Dispersion Force Mapping and Adhesion Measurements*. Respiratory Drug Delivery 2008, 2008. 1: p. 175 - 184.
14. Wong, W., et al., *Particle Aerosolisation and Break-up in Dry Powder Inhalers 1: Evaluation and Modelling of Venturi Effects for Agglomerated Systems*. Pharmaceutical Research, 2010. 27(7): p. 1367-1376.
15. de Boer, A., et al., *Air classifier technology (ACT) in dry powder inhalation Part 2. The effect of lactose carrier surface properties on the drug-to-carrier interaction in adhesive mixtures for inhalation*. International Journal of Pharmaceutics, 2003. 260(2): p. 201-216.
16. Donovan, M.J. and H.D.C. Smyth, *Influence of size and surface roughness of large lactose carrier particles in dry powder inhaler formulations*. International Journal of Pharmaceutics, 2010. 402(1-2): p. 1 - 9.

17. Pope, S.B., *Turbulent Flows*2000: Cambridge University Press.
18. Kawashima, Y., Serigano, T., Hino, T., Yamamoto, H., and Takeuchi, H., *Effect of surface morphology of carrier lactose on dry powder inhalation property of pranlukast hydrate*. International Journal of Pharmaceutics, 1998. 172: p. 179 - 188.
19. Larhrib, H., Zeng, X.M., Martin, G.P., Marriott, C., and Pritchard, J., *The use of different grades of lactose as a carrier for aerosolised salbutamol sulphate*. International Journal of Pharmaceutics, 1999. 191: p. 1 - 14.
20. Pitchayajittipong, C., et al., *Characterisation and functionality of inhalation anhydrous lactose*. International Journal of Pharmaceutics, 2010. 390(2): p. 134-141.
21. Gupta, V., and Gupta, S.K., *Fluid Mechanics and Its Applications*1984, New Delhi: New Age International.
22. Begat, P., Morton, D.A.V., Staniforth, J.N., and Price, R., *Dry powder inhaler formulations I: Direct quantification by atomic force microscopy*. Pharmaceutical Research, 2004. 21(9): p. 1591 - 1597.
23. Saleem, I., H. Smyth, and M. Telko, *Prediction of Dry Powder Inhaler Formulation Performance From Surface Energetics and Blending Dynamics*. Drug Development and Industrial Pharmacy, 2008. 34(9): p. 1002-1010.
24. Alshowair, R., et al., *Can all patients with COPD use the correct inhalation flow with all inhalers and does training help?* Respiratory Medicine, 2007. 101(11): p. 2395-2401.
25. Chodosh, S., et al., *Effective Delivery of Particles with the HandiHaler® Dry Powder Inhalation System over a Range of Chronic Obstructive Pulmonary Disease Severity*. Journal of Aerosol Medicine, 2001. 14(3): p. 309-315.

26. Bronsky, E.A., et al., *Inspiratory flow rates and volumes with the Aerolizer dry powder inhaler in asthmatic children and adults*. Current Medical Research and Opinion, 2004. 20(2): p. 131-137.
27. Clark, A.R., and Hollingworth, A.M., *The relationship between powder inhaler resistance and peak inspiratory conditions in healthy volunteers - implications for in vitro testing*. Journal of Aerosol Medicine, 1993. 6(2): p. 99 - 110.
28. Mendes, P., J. Pinto, and J. Sousa, *A non-dimensional functional relationship for the fine particle fraction produced by dry powder inhalers*. Journal of Aerosol Science, 2007. 38(6): p. 612-624.
29. Srichana, T., G.P. Martin, and C. Marriott, *Dry powder inhalers: The influence of device resistance and powder formulation on drug and lactose deposition in vitro*. European Journal of Pharmaceutical Sciences, 1998. 7(1): p. 73-80.
30. Louey, M., M. Vanoort, and A. Hickey, *Standardized entrainment tubes for the evaluation of pharmaceutical dry powder dispersion*. Journal of Aerosol Science, 2006. 37(11): p. 1520-1531.
31. Chew, N.Y.K., Chan, H.K., Bagster, D.F., and Mukhraiya, *Characterization of pharmaceutical powder inhalers: estimation of energy input for powder dispersion and effect of capsule device configuration*. Aerosol Science, 2002. 33: p. 999 - 1008.
32. Tuley, R., et al., *Experimental observations of dry powder inhaler dose fluidisation*. International Journal of Pharmaceutics, 2008. 358(1-2): p. 238-247.
33. Watling, C.P., J.A. Elliott, and R.E. Cameron, *Entrainment of lactose inhalation powders: A study using laser diffraction*. European Journal of Pharmaceutical Sciences, 2010. 40(4): p. 352-358.

34. Shur, J., et al., *The Role of Fines in the Modification of the Fluidization and Dispersion Mechanism Within Dry Powder Inhaler Formulations*. *Pharmaceutical Research*, 2008. 25(7): p. 1631-1640.

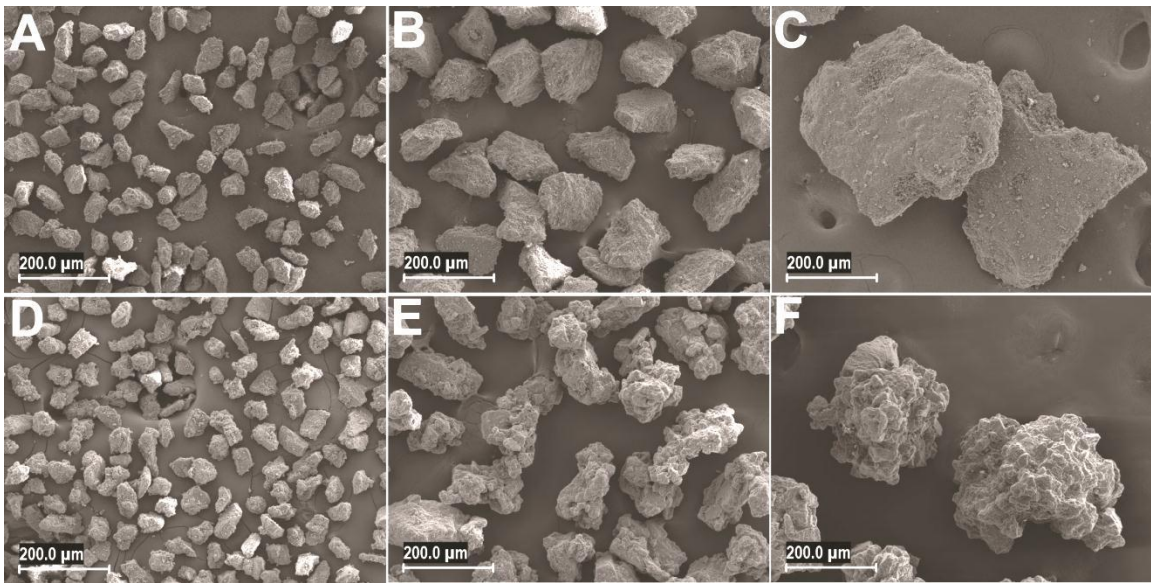


Figure 5.1. SEM Images of Anhydrous and Granulated Lactose Carrier Particle Populations

SEM micrographs of uncoated (A) 32 - 45  $\mu\text{m}$  anhydrous lactose, (B) 90 - 125  $\mu\text{m}$  anhydrous lactose, (C) 250 - 300  $\mu\text{m}$  anhydrous lactose, (D) 32 - 45  $\mu\text{m}$  granulated lactose, (E) 90 - 125  $\mu\text{m}$  granulated lactose, and (F) 250 - 300  $\mu\text{m}$  granulated lactose sieve fractions. Scale bars denote 200  $\mu\text{m}$ .

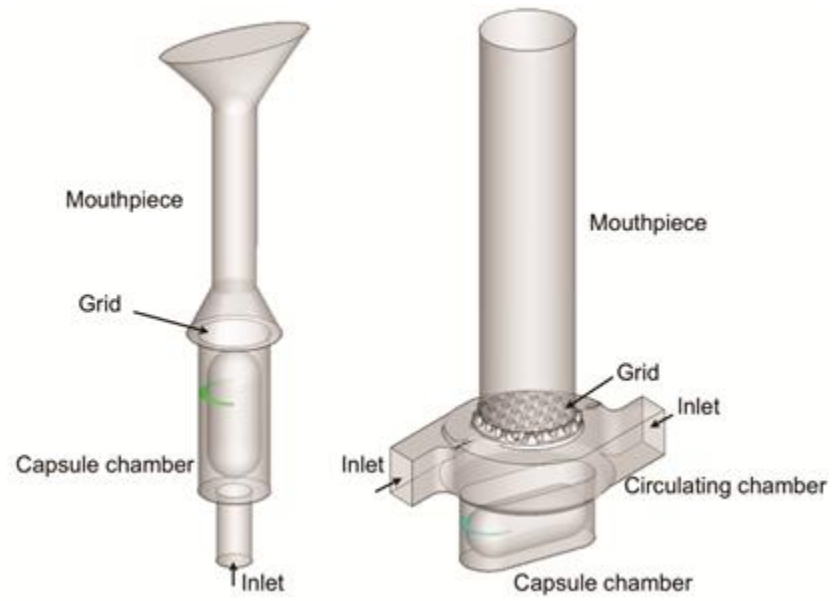


Figure 5.2. Schematic views of the Handihaler® (left) and Aerolizer® dry powder inhalers.

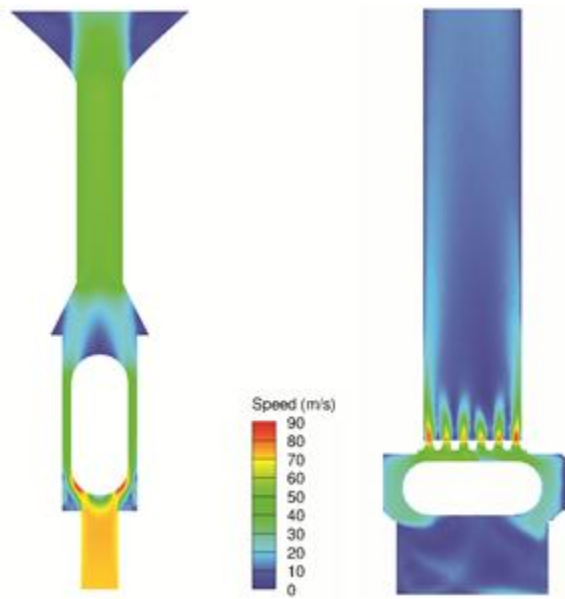


Figure 5.3. Contour of Velocity Magnitude Inside Handihaler (left) and Aerolizer (right).



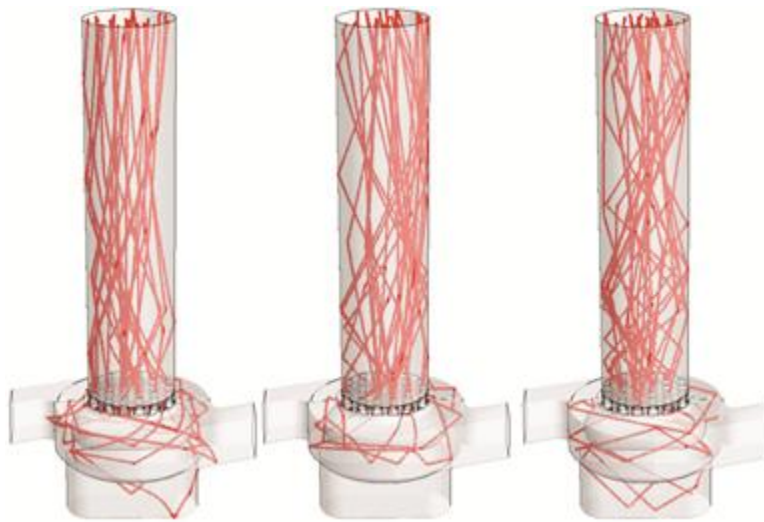


Figure 5.4. Carrier particle trajectory inside the Aerolizer at  $60 \text{ L min}^{-1}$

The particles were modeled as spherical, mono-disperse populations. From left, article diameter = 32, 108, and 275  $\mu\text{m}$ .

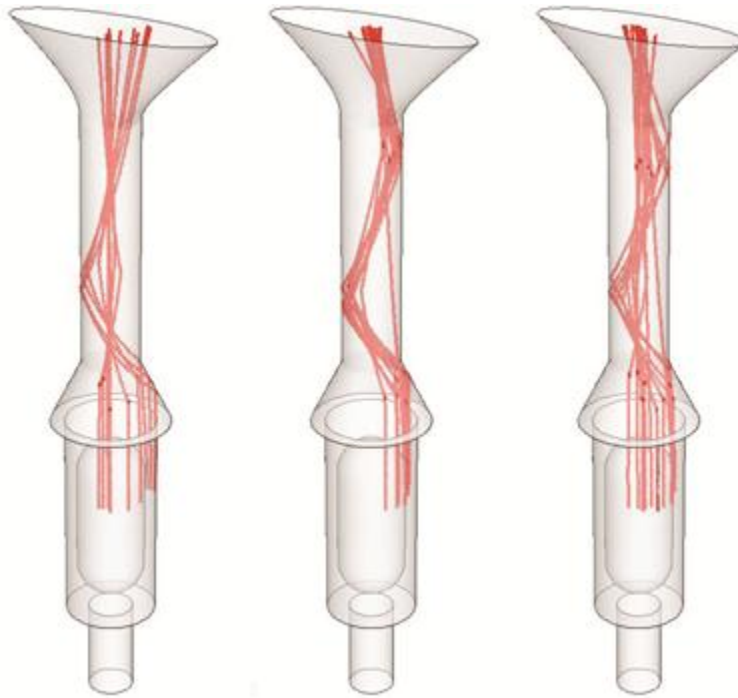


Figure 5.5. Carrier particle trajectory inside the Handihaler at 60 L min<sup>-1</sup>

The particles were modeled as spherical, mono-disperse populations. From left, particle diameter = 32, 108, and 275 μm.

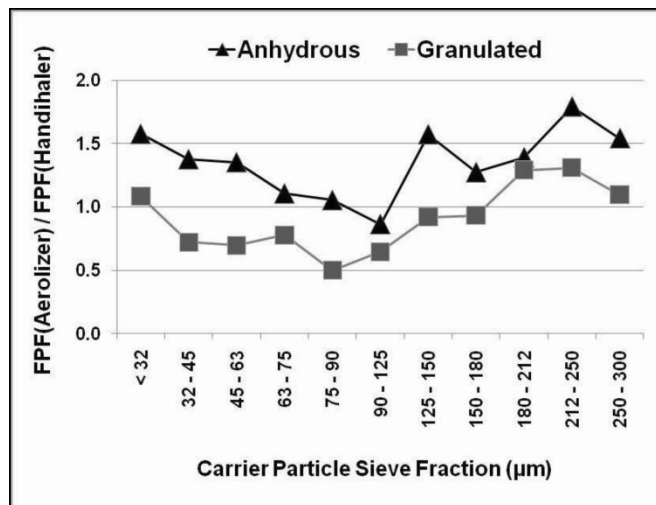


Figure 5.6. Ratio of Fine Particle Fraction Values from the Aerolizer and Handihaler

Ratio of the FPF values obtained from the Aerolizer over the Handihaler for both anhydrous and granulated lactose formulations as a function of carrier particle size.

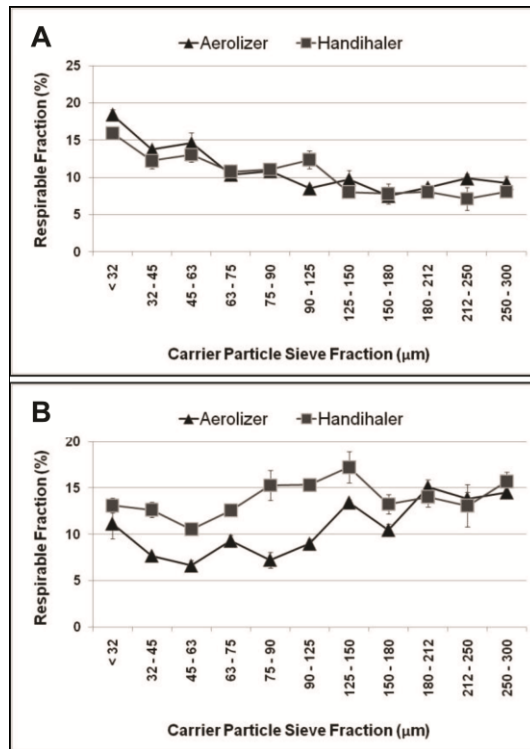


Figure 5.7. *In vitro* Performance of Anhydrous and Granulated Carrier Formulations

Respirable fraction (RF) values of (A) anhydrous and (B) granulated lactose carrier particles dispersed from the Aerolizer and Handihaler at  $60 \text{ L min}^{-1}$ . Values are given as the mean of  $N = 3$  replicates, with error bars representing the standard deviation for  $N = 3$  replicates.

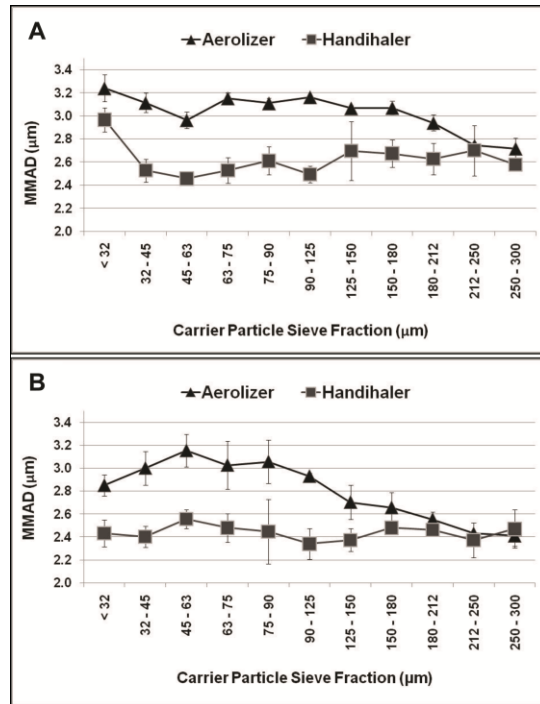


Figure 5.8. MMAD Values of Budesonide Dispersed from the Handihaler and Aerolizer

Mass median aerodynamic (MMAD) of budesonide particles following dispersion of 2% (w/w) formulations with (A) anhydrous lactose, and (B) granulated lactose carrier particles at 60 L min<sup>-1</sup> from both the Aerolizer and Handihaler DPIs. Values are given as the mean of N = 3 replicates, with error bars representing the standard deviation for N = 3 replicates.

Table 5.1. Specific surface areas (SSA) of Anhydrous and Granulated lactose carrier particles by sieve fraction

Carrier Sieve Fraction ( $\mu\text{m}$ )	Anhydrous (AN) ( $\text{m}^2/\text{g}$ )	Granulated (GR) ( $\text{m}^2/\text{g}$ )
< 32	0.94	1.87
32 – 45	0.48	1.71
45 – 63	0.38	1.62
63 – 75	0.43	1.64
75 – 90	0.37	1.52
90 – 125	0.41	1.56
125 - 150	0.38	1.81
150 – 180	0.38	1.73
180 – 212	0.40	1.44
212 - 250	0.42	1.67
250 - 300	0.36	1.46

Table 5.2. Average Simulated Collisions Experience by Carrier Particles in Aerolizer and Handihaler

Carrier Particle Sieve Fraction ( $\mu\text{m}$ )	Aerolizer			Handihaler		
	32 ( $\mu\text{m}$ )	107.5 ( $\mu\text{m}$ )	275 ( $\mu\text{m}$ )	32 ( $\mu\text{m}$ )	107.5 ( $\mu\text{m}$ )	275 ( $\mu\text{m}$ )
Inhale-Carrier Collisions	2.3	3.6	4.0	1.7	2.2	2.3

Average number of collisions between a carrier particle and the inhaler as it exits the device during actuation from the Aerolizer and Handihaler at  $60 \text{ L min}^{-1}$ .

Table 5.3. In vitro Aerosol Performance Data from Anhydrous Lactose Carrier Particle Formulations

Carrier Particle Sieve Fraction ( $\mu\text{m}$ )	Aerolizer®			Handihaler®		
	EF	FPF	RF	EF	FPF	RF
< 32	63.5 (1.6)	29.1 (1.4)	18.4 (0.7)	86.4 (1.1)	18.5 (0.7)	15.9 (0.4)
32 – 45	64.5 (1.8)	21.3 (0.8)	13.7 (0.3)	79.0 (8.0)	15.5 (0.7)	12.2 (1.1)
45 – 63	63.1 (2.2)	23.1 (1.8)	14.6 (1.4)	76.3 (1.2)	17.1 (1.2)	13.0 (0.9)
63 – 75	68.9 (1.8)	15.1 (0.4)	10.4 (0.3)	79.2 (2.5)	13.7 (0.3)	10.8 (0.2)
75 – 90	71.8 (2.4)	15.2 (0.3)	10.9 (0.5)	77.1 (1.3)	14.4 (0.7)	11.1 (0.4)
90 - 125	62.3 (1.9)	13.7 (0.6)	8.5 (0.4)	80.0 (8.1)	15.9 (0.8)	12.4 (1.2)
125 – 150	62.7 (2.1)	15.6 (1.4)	9.8 (1.2)	81.1 (4.7)	9.9 (0.5)	8.0 (0.8)
150 – 180	62.3 (2.0)	12.1 (0.8)	7.5 (0.3)	82.3 (1.9)	9.5 (1.6)	7.8 (1.3)
180 – 212	61.8 (1.9)	14.1 (1.1)	8.7 (0.5)	79.9 (1.8)	10.1 (0.2)	8.1 (0.2)
212 – 250	63.4 (2.3)	15.5 (0.8)	9.9 (0.6)	82.3 (0.8)	8.7 (1.9)	7.1 (1.5)
250 - 300	61.6 (1.7)	15.0 (1.1)	9.3 (0.9)	80.2 (0.4)	9.8 (0.3)	8.1 (0.6)

Emitted fraction (EF), fine particle fraction (FPF), and respirable fraction (RF) for 2% (w/w) budesonide formulations with anhydrous lactose carrier particles characterized *in vitro* from the Aerolizer® and Handihaler® dry powder inhalers at 60 L min<sup>-1</sup>. Values are given as the mean of N = 3 replicates, and values within parentheses represent the standard deviation for N = 3 replicates.



Table 5.4. In vitro Aerosol Performance Data from Granulated Lactose Carrier Particle Formulations.

Carrier Particle Sieve Fraction ( $\mu\text{m}$ )	Aerolizer®			Handihaler®		
	EF	FPF	RF	EF	FPF	RF
< 32	57.0 (1.4)	18.5 (1.2)	11.1 (1.6)	76.9 (1.6)	17.1 (1.4)	13.1 (0.8)
32 – 45	69.1 (3.7)	11.1 (0.6)	7.7 (0.1)	82.0 (0.5)	15.4 (1.0)	12.6 (0.8)
45 – 63	74.4 (4.1)	8.9 (1.2)	6.6 (0.6)	82.1 (1.9)	12.8 (0.2)	10.5 (0.3)
63 – 75	73.8 (3.7)	12.6 (1.4)	9.3 (0.6)	78.4 (2.7)	16.2 (0.7)	12.6 (0.2)
75 – 90	73.9 (6.6)	9.7 (2.1)	7.2 (0.8)	78.7 (1.9)	19.4 (2.4)	15.3 (1.6)
90 - 125	77.8 (1.8)	11.6 (0.9)	9.0 (0.5)	86.1 (2.0)	17.9 (0.8)	15.3 (0.4)
125 – 150	71.3 (4.2)	18.9 (1.5)	13.4 (0.3)	84.3 (3.4)	20.5 (2.5)	17.2 (1.7)
150 – 180	73.8 (2.5)	14.2 (1.3)	10.5 (0.7)	87.3 (1.4)	15.2 (1.5)	13.3 (1.1)
180 – 212	72.6 (3.2)	20.8 (1.1)	15.1 (0.8)	87.1 (1.6)	16.1 (1.4)	14.0 (1.1)
212 – 250	68.7 (5.4)	20.2 (1.5)	13.8 (0.7)	84.3 (1.1)	15.4 (2.8)	13.1 (2.3)
250 - 300	68.5 (4.5)	20.1 (1.5)	14.5 (0.5)	85.5 (0.6)	18.4 (1.0)	15.7 (1.0)

Emitted fraction (EF), fine particle fraction (FPF), and respirable fraction (RF) for 2% (w/w) budesonide formulations with granulated lactose carrier particles characterized *in vitro* from the Aerolizer® and Handihaler® dry powder inhalers at 60 L min<sup>-1</sup>. Values are given as the mean of N = 3 replicates, and values within parentheses represent the standard deviation for N = 3 replicates.

## CHAPTER 6

### 6. Influence of Flow Rate on Binary DPI Formulations as a Function of Carrier Particle Diameter and Surface Roughness

#### 6.1. INTRODUCTION

The studies detailed in the preceding three chapters have demonstrated that large diameter carrier particles may prove beneficial to aerosol performance by promoting drug detachment via mechanical forces. In chapter 4, it was speculated that drug detachment from carrier particles with extensive surface roughness would rely less on fluid forces and more on mechanical forces, as the rugosity of the carrier surface would inhibit the flow stream from direct interaction with the drug particles. It was also theorized that the magnitude of the impaction forces generated by carrier particle-device collisions would be enhanced for larger diameter carriers relative to smaller particles due to their potentially higher momentum. This was supported by the observed aerosol performance profiles of formulations prepared with granulated lactose carriers, where drug deposition improvements were observed as the size of the carrier particle increased [80]. This contrasts with the performance of carrier particles with less extensive surface roughness, as drug deposition generally diminished with increasing carrier particle diameter.

To further examine the potential of carrier particle-device collisions to promote drug detachment, the performance of formulations prepared with carrier particle populations of varying size and surface roughness was examined through two commercial DPIs possessing markedly different internal geometries, and thus distinct powder de-agglomeration mechanisms. These studies were combined with computational fluid dynamics (CFD) to simulate the particle trajectories through the device as the diameter of the carrier particle was altered. The results indicated that coupling an inhaler that promotes particle-device collisions to carrier particle populations with physical properties that would most benefit from impactions (e.g. large carriers with high surface roughness), can yield improvements in performance relative to

carrier particle populations where collisions are less frequent. Conversely, for inhalers with internal geometries that do not promote carrier particle-inhaler collisions, no significant improvements in drug deposition were observed as carrier diameter was increased.

In the previous work, the flow rate was maintained at a constant value, specifically 60 L min<sup>-1</sup>. In Chapter 4 it was speculated that the higher momentum arising from larger carriers (assuming comparable particle velocities) would induce more forceful collisions with the inner walls of the device as the particle travels through the inhaler during actuation. As momentum is a function of both the mass and velocity of the carrier particle, it is speculated that increasing the flow rate through an inhaler may provide increased dispersion improvements from larger diameter carriers relative to their smaller counterparts.

#### *Specific Aim*

Accordingly, the specific aim of this chapter was to evaluate the influence of flow rate on the performance of binary DPI blends as the size and surface roughness of the carrier particle population is altered. For this purpose, two morphologically distinct lactose grades were selected to serve as carriers, specifically  $\alpha$ -lactose monohydrate and granulated lactose, and aerosol performance was evaluated *in vitro* via cascade impaction at 30, 60 and 90 L min<sup>-1</sup>. As it is noted that increasing the flow rate through the device will enhance the magnitude of both the fluid forces and mechanical forces experienced by the powder, the use of lactose grades possessing either low or high surface roughness will allow discernment of which force plays a more significant role in improving performance, as the influence of fluid forces are expected to be mitigated for granulated carriers relative to  $\alpha$ -lactose monohydrate. Additionally, to ensure that any observed performance differences were attributable to the carrier particles rather than the drug, the blends were prepared with both budesonide and salbutamol sulphate.

## **6.2. EXPERIMENTAL**

### **6.2.1. Materials**

Micronized salbutamol sulphate (USP grade) was purchased from Letco Medical (AL, USA) and used as received. Budesonide was purchased in bulk (JinHuo Chemical Company, China) and micronized with a high energy jet mill (Aljet; Fluid Energy Processing and Equipment Co., PA, USA). Analytical grade ethanol was purchased from Sigma (Sigma-Aldrich Chemical Co. MO, USA). As carrier particle populations,  $\alpha$ -lactose monohydrate (Pharmatose® 80 Mesh) and granulated lactose (SuperTab® 30GR) were provided by DMV-Fonterra (New Zealand). Size-3 HPMC capsules (VCaps®) were provided by Capsugel (NJ, USA).

### **6.2.2. Carrier Particle Fractionation**

Samples of  $\alpha$ -lactose monohydrate and granulated lactose were fractionated using an Autosiever® vibrating sieve shaker (Gilson Company Inc., OH, USA). The sieving intensity (amplitude) was set to 40, and samples were fractionated for 5 minutes through sieves with the following mesh sizes: 300  $\mu\text{m}$ , 250  $\mu\text{m}$ , 150  $\mu\text{m}$ , 125  $\mu\text{m}$ , 63  $\mu\text{m}$ , and 45  $\mu\text{m}$ . Following the initial fractionation, the lactose carriers were sieved two additional times, at 3-minute sieving intervals, to obtain narrow particle size distributions.

### **6.2.3. Preparation of Binary Blends**

1% (w/w) binary formulations were prepared by mixing 5 mg of drug with 495 mg of each lactose carrier particle population via geometric dilution. The formulations were blended with a Turbula™ orbital mixer (Glen Mills, NJ) for 40 minutes at 46 RPM. The blend uniformity of each formulation was evaluated by randomly selecting eight 20-mg samples from each blend and assessing the drug content. The blend uniformity is provided as the percent coefficient of variation for N = 8 replicates.

#### **6.2.4. Physical Characterization**

The size distribution and surface roughness of the lactose carrier particle populations were visually examined by scanning electron microscopy (SEM; Supra 40VP, Zeiss, Germany). Prior to SEM, approximately 20 nm of a platinum::palladium (80::20) mixture was deposited onto the particles via sputter coating.

Sizing of the drugs and the carrier particle populations were performed using laser diffraction with a Sympatec HELOS (Sympatec GmbH, Germany) apparatus equipped with a 6-mL cuvette dispersing system. Mineral oil was used as the dispersing fluid, which included 1% Span 85 to aid in particle de-aggregation. The powders were suspended in the mineral oil and, if physically stable, sonicated for 60 seconds to disrupt aggregates. Measurements were collected following elimination of all visible air bubbles. The 'forced stability' option was used to ignore the signal from errant dust or residual air bubbles.

The specific surface area of the lactose carrier particle populations was evaluated via nitrogen adsorption with a single-point BET method using a Monosorb<sup>®</sup> surface area analyzer (Quantachrome Instruments; FL, USA). Samples were outgassed under nitrogen at 40 °C for 24 hours prior to each measurement.

#### **6.2.5. In Vitro Aerosol Performance**

20 ( $\pm$  1) mg of powder were loaded into size-3 HPMC capsules and dispersed through an Aerolizer<sup>®</sup> (Plastiap S.p.A., Italy) DPI into a next generation cascade impactor (MSP Corporation, MN, USA) at volumetric flow rates of 30, 60 and 90 L min<sup>-1</sup>. The actuation time was adjusted to allow 4 L to flow through the inhaler. To inhibit particle re-entrainment, the NGI stages were coated with a 2% (v/v) solution of silicon oil in hexane and allowed to air dry before each impaction. Prior to each actuation, 15 mL of sample solvent (H<sub>2</sub>O for salbutamol sulphate and EtOH for budesonide) were added to the pre-separator and collected following powder dispersion from each capsule. Drug depositing in the capsule, inhaler, mouthpiece adaptor, and induction port were collected by rinsing each component with 10 mL of sample solvent, while the NGI stages were each rinsed with 5 mL.

The drug content was evaluated using UV-VIS absorption spectroscopy at 230 nm and 244 nm for salbutamol sulphate and budesonide, respectively. The emitted fraction was calculated as the ratio of the drug mass depositing in the mouthpiece, induction port, pre-separator, and impactor stages over the cumulative drug mass collected following actuation (total drug deposited in the capsule, inhaler, mouthpiece, induction port, pre-separator and stages). At 30 and 60 L min<sup>-1</sup>, the fine particle fraction (FPF) of each dose was the ratio of the drug mass depositing on stages 3 - 8 (corresponding to an aerodynamic diameter less than 6.4 µm and 4.46 µm for 30 and 60 L min<sup>-1</sup>, respectively) of the impactor over the emitted dose [72]. The respirable fraction (RF) was the ratio of the drug mass depositing on stages 3 – 8 over the entire dose recovered following each actuation. At 90 L min<sup>-1</sup>, the same performance metrics were evaluated, with the exception that the drug collected from stages 2 - 8 was considered to be respirable as the cut-off diameter of stage 1 at 90 L min<sup>-1</sup> is 6.48 µm.

#### **6.2.6. Statistics**

Statistical significance between performance values was determined with one-way ANOVA with Post Hoc tests between groups according to the Bonferroni method ( $P < 0.05$ ).

### **6.3. RESULTS AND DISCUSSION**

#### **6.3.1. Physical Characterization**

The sizing data and specific surface area measurements for each carrier particle population are presented in Table 6.1. For α-lactose monohydrate, increasing the diameter of the carrier particles resulted in a progressive reduction in SSA, with values declining from 0.39 to 0.18 m<sup>2</sup>/g between the 45 – 63 µm carriers and the 250 – 300 µm fraction. This contrasts with the granulated carriers, where the overall decline between the smallest (0.52 m<sup>2</sup>/g) and largest (0.43 m<sup>2</sup>/g) carrier fractions was only 17%, as compared to the 54% SSA reduction observed between lactose monohydrate carriers. Additionally, the granulated carriers did not display a progressive SSA decline with larger particles, as the SSA measured from the largest size fraction

exceeded that of the 125 – 150  $\mu\text{m}$  carriers. The increasing disparity in surface roughness between the two grades as a function of carrier particle diameter is seen in Figure 6.1.

### **6.3.2. *In vitro* Aerosol Performance**

The complete aerosol performance data for the salbutamol sulphate and budesonide formulations are presented in Tables 6.2 and 6.3, respectively. Given that multiple parameters were altered throughout this study, the influence that carrier particle size and surface roughness had on performance as a function of flow rate will be examined separately. It is noted that the Aerolizer is a relatively low resistance device, and 90 L  $\text{min}^{-1}$  corresponds to approximately a 4 kPa pressure drop through this inhaler [34, 97, 102]. Accordingly, this is a flow rate that is readily achieved by most patients through this DPI [97].

### **6.3.3. Influence of Carrier Particle Size (Salbutamol Sulphate)**

Figure 6.2 depicts the flow rate performance of the salbutamol sulphate formulations as a function of carrier particle size. For  $\alpha$ -lactose monohydrate, increasing the diameter of the carrier particle population inhibited performance for all flow rates examined. At 30 L  $\text{min}^{-1}$ , the disparity between the smallest and largest size fractions was most pronounced, with respective RF values of 22% and 8%. As the flow is increased to 90 L  $\text{min}^{-1}$  the 45 – 63  $\mu\text{m}$  formulation still outperformed its 250 – 300  $\mu\text{m}$  counterpart, however the difference between them was less stark than at the lower flow rate, as the 250 – 300  $\mu\text{m}$  carriers produced an RF value of 30% relative to 38% from the small carriers.

For the granulated carriers, 30 L  $\text{min}^{-1}$  proved most detrimental to performance from the 250 – 300  $\mu\text{m}$ , as RF was only 9% compared to 19% from the 45 – 63  $\mu\text{m}$  carriers. As with lactose monohydrate, the largest carriers exhibited the greatest relative improvement in performance with increasing flow rate. However, at 90 L  $\text{min}^{-1}$  the largest carrier size fraction demonstrated comparable performance to the 45 – 63  $\mu\text{m}$  carriers. Additionally, the 125 – 150  $\mu\text{m}$  carriers also exhibited performance comparable to the smaller size fraction at both

60 L min<sup>-1</sup> and 90 L min<sup>-1</sup>, in contrast to lactose monohydrate, where the smallest size fraction continually produced higher RF values across the three flow rates.

#### **6.3.4. Influence of Carrier Particle Size (Budesonide)**

The flow rate performance of the budesonide formulations as a function of carrier particle size is provided in Figure 6.3. For lactose monohydrate, performance was comparable across the carrier size ranges for the tested flow rates. A slightly greater improvement in performance with flow rate was noted for the 250 – 300 µm carriers as RF values ranged from 9 - 24% compared against 13 – 24% for the 45 – 63 µm particle size fraction.

As with the lactose monohydrate carriers, the granulated lactose formulations exhibited comparable performance at the lower flow rate. However, performance differed between the particle sizes as flow rate was increased. Interestingly, it was the two largest size fractions that demonstrated both the greatest performance increase, and the highest RF values, while the 45 – 63 µm carriers provided significantly lower performance at 60 and 90 L min<sup>-1</sup>. For the 45 – 63 µm size fraction, the respirable fraction doubled from 11% up to 22% as flow was increased from 30 to 90 L min<sup>-1</sup>. In contrast, performance from the 250 – 300 µm carriers more than tripled across the same flow rate span, as RF values increased from 12% to 37%.

#### **6.3.5. Influence of Surface Roughness**

The flow rate performance of the formulations as a function of particle surface roughness is presented in Figure 6.4. As was noted previously, the different APIs generally resulted in markedly different dispersion profiles for a given lactose grade-size fraction combination. The exception to this was the 125 – 150 µm and 250 – 300 µm granulated carrier particles.

However, when aerosol performance was evaluated comparing different lactose grades of the same carrier particle size fraction, it was observed that the overall performance trends were similar between APIs. Performance was essentially comparable for the 45 – 63 µm carriers at all flow rates (with budesonide at 60 L min<sup>-1</sup> being the lone exception). For the two larger



carrier fractions, both lactose grades produced similar RF values at 30 L min<sup>-1</sup>. However, as the flow rate was increased disparities were noted, as the granulated carriers outperformed their lactose monohydrate counterparts with the exception of the 125 – 150 µm/salbutamol formulations, where performance differences were slight but not significant ( $p < 0.05$ ). Overall, the greatest performance disparity between carriers was observed for the 250 – 300 µm/budesonide blends, as the granulated carriers produced an average respirable fraction of 37% compared to 24% for the lactose monohydrate carriers.

### **6.3.6. Combined Influence of Size and Surface Roughness**

To assess the combined influence of carrier particle size and surface roughness on performance, the slope of the improvement in RF with increasing flow rate is shown for both drugs in Figure 6.5. Of the three size fractions, the 45 – 63 µm exhibit the least flow rate dependent performance, as the performance improvements across the studied flow rates were not as stark relative to the larger carriers. For the larger carriers, the typically lower performance at 30 L min<sup>-1</sup> coupled to their greater overall improvement with increasing flow rate resulted in larger values for the RF slope. It is noted that the relative values between carrier size fractions for a given lactose grade were similar as the drug was varied, indicating that despite producing significant differences in terms of absolute aerosol performance, the relative differences in performance were generally independent of the drug employed. Of the six carrier particle populations examined, the 250 – 300 µm granulated carriers produced the greatest performance improvement with flow rate. Given that the high surface roughness would be expected to inhibit detachment by the flow stream, the enhanced performance of these carriers may be attributed to increased mechanical impaction forces.

### **6.3.7. Influence of API**

The use of two APIs resulted in marked variations in aerosol performance among lactose grades. Overall, salbutamol sulphate formulations tended to produce significantly greater performance values relative to budesonide. However, for the 125 -150 µm and 250 – 300 µm granulated carriers, RF values were comparable between drugs at 90 L min<sup>-1</sup>, indicating that in

contrast to the other tested carrier particle populations, performance from these carrier particles is relatively independent of the drug employed at the higher flow rate. This may suggest that for these carrier particle populations, the detachment forces exceed adhesion forces at higher flow rates.

The influence that the API material can impart to aerosol performance has been reported previously and is speculated to be due to the distinct physicochemical properties of the drug materials, specifically their respective adhesive and cohesive forces [17, 19]. Previous research examining these properties for salbutamol sulphate and budesonide concluded that budesonide possesses a high cohesive tendency while salbutamol sulphate is characterized as relatively adhesive, indicating that in a binary blend salbutamol particles may preferentially bind with lactose rather than form drug agglomerates via cohesive interactions, as would be predicted for budesonide [17]. It is noted that these adhesive and cohesive properties of the API described the relative affinity, or lack thereof, between the drug and lactose, and thus the described properties may differ as the frame of reference is altered. However, as the carriers in the present study were also lactose, it was assumed that budesonide was cohesive and salbutamol sulphate was adhesive.

The granulated lactose particles were selected in part for their potential to mitigate the role of fluid forces in drug detachment, thereby allowing the influence of mechanical detachment forces to be more clearly evaluated. However, it is noted that the greater surface area of the granulated carriers relative to  $\alpha$ -lactose monohydrate (especially for the 250 – 300  $\mu\text{m}$  fraction) may aid aerosol performance by inhibiting the formation of drug aggregates (for high drug concentrations), and also by sheltering drug particles within surface asperities and thus limiting the extent of the press-on forces between drug and carrier particles that arise during mixing. This is expected to lower the adhesion force between the drug and carrier surface, as the press-on forces can increase the contact area, and thus the magnitude of the interaction, between particles. This has been discussed in great detail previously, particularly by de Boer and colleagues [9, 29].

To summarize the blending theory, it is noted that two distinct types of drug agglomerates are encountered during blending. 'Natural' agglomerates are initially present in the drug powder, and during blending they may be broken up through abrasion as drug is continuously ground between coarse carrier particles. In contrast, 'blending' agglomerates are formed during powder mixing due to cohesive interactions between the drug particles [9]. Returning to the discussion of differing adhesive and cohesive APIs, it would be predicted that budesonide would prove most likely to form blending agglomerates, while salbutamol sulphate would be predicted to be distributed uniformly, given its reported high adhesive interaction with lactose [17].

Accordingly, for budesonide thorough blending, particularly to induce abrasion of the drug between carrier particles, would be required to disrupt agglomerates [18]. However, the high surface rugosity of the larger granulated carrier particles would be expected to shelter the budesonide agglomerates within their surface asperities, inhibiting the ability of these carriers to both disrupt natural agglomerates and prevent formation of blending agglomerates [9]. This in turn could be expected to impair delivery of budesonide from large granulated carriers relative to lactose monohydrate, as drug agglomerates typically deposit in the induction port and pre-separator.

Conversely, for an adhesive drug such as salbutamol sulphate, the opposite would be predicted as the formation of blending agglomerates would not be expected to be problematic, but large press-on forces could potentially augment the already strong adhesive interaction (relative to budesonide) between drug and carrier [29, 30]. These press-on forces would be larger for the lactose monohydrate carriers, as their low surface roughness would preclude drug sheltering in contrast to the granulated particles.

Accordingly, for a given size fraction, particles with low and high surface rugosity could potentially improve or impair performance, dependent upon the properties of the drug. Thus, two APIs with distinct adhesive and cohesive properties were selected to determine if the aerosol performance improvement previously observed from the large granulated carriers was due primarily to the drug or the carrier, as the primary benefit to performance imparted by

these carriers could potentially occur during blending rather than during dispersion. However, as noted above, while absolute performance values differed significantly between salbutamol and budesonide formulations, the relative differences as carrier particle size and surface roughness varied were independent of the API.

#### **6.4. CONCLUSION**

The present chapter evaluated the influence of the volumetric flow rate on the performance of binary DPI formulations prepared with multiple carrier particle size fractions possessing low and high surface roughness. It was noted that although both the fluid forces and mechanical forces are increasing with the flow stream, the use of carrier particles with extensive surface roughness would mitigate the influence of flow detachment forces relative to particles with a lower degree of surface asperities. The results from this study suggest that increasing flow is most beneficial to larger diameter carrier particles in general, and to large carrier particles with extensive surface roughness in particular. Accordingly, as mechanical forces would predominate for these carriers, it was proposed that increasing the flow stream promotes forceful collisions between the carrier particle and inhaler due to the increased momentum of larger particles relative to smaller size fractions.

The results of the present study, in combination with the previous three chapters, have demonstrated that under conditions where mechanical detachment forces are considerable, large carrier particles exhibit aerosol performance levels that deviate considerably from that predicted from many of the theories described in the literature. Specifically, dispersing large diameter carrier particles with extensive surface roughness through a low resistance device designed to promote carrier particle-device collisions yields excellent drug dispersion performance.

## 6.5. REFERENCES

1. Donovan, M.J. and H.D.C. Smyth, *Influence of size and surface roughness of large lactose carrier particles in dry powder inhaler formulations*. International Journal of Pharmaceutics, 2010. 402(1-2): p. 1 - 9.
2. Marple, V.A., Roberts, D.L., Romay, F.J. and Hochrainer, D., *Next generation pharmaceutical impactor (A new impactor for pharmaceutical inhaler testing). Part I: Design*. Journal of Aerosol Medicine, 2003. 16(3): p. 283 - 299.
3. Nielsen, K.G., et al., *Flow-dependent effect of formoterol dry-powder inhaled from the Aerolizerfi*. European Respiratory Journal, 1997. 10(9): p. 2105-2109.
4. Coates, M.S., et al., *Effect of design on the performance of a dry powder inhaler using computational fluid dynamics. Part 1: Grid structure and mouthpiece length*. Journal of Pharmaceutical Sciences, 2004. 93(11): p. 2863-2876.
5. Bronsky, E.A., et al., *Inspiratory flow rates and volumes with the Aerolizer dry powder inhaler in asthmatic children and adults*. Current Medical Research and Opinion, 2004. 20(2): p. 131-137.
6. Begat, P., Morton, D.A.V., Staniforth, J.N., and Price, R., *Dry powder inhaler formulations I: Direct quantification by atomic force microscopy*. Pharmaceutical Research, 2004. 21(9): p. 1591 - 1597.
7. Steckel, H., and Muller, B.W., *In vitro evaluation of dry powder inhalers II: influence of carrier particle size and concentration on in vitro deposition*. International Journal of Pharmaceutics, 1997. 154: p. 31 - 37.
8. de Boer, A., et al., *Air classifier technology (ACT) in dry powder inhalation Part 2. The effect of lactose carrier surface properties on the drug-to-carrier interaction in adhesive mixtures for inhalation*. International Journal of Pharmaceutics, 2003. 260(2): p. 201-216.

9. Dickhoff, B., et al., *The interaction between carrier rugosity and carrier payload, and its effect on drug particle redispersion from adhesive mixtures during inhalation*. *European Journal of Pharmaceutics and Biopharmaceutics*, 2005. 59(1): p. 197-205.
10. Saleem, I., H. Smyth, and M. Telko, *Prediction of Dry Powder Inhaler Formulation Performance From Surface Energetics and Blending Dynamics*. *Drug Development and Industrial Pharmacy*, 2008. 34(9): p. 1002-1010.
11. Selvam, P., et al., *Micronized Drug Adhesion and Detachment from Surfaces: Effect of Loading Conditions*. *Aerosol Science and Technology*, 2011. 45(1): p. 81-87.

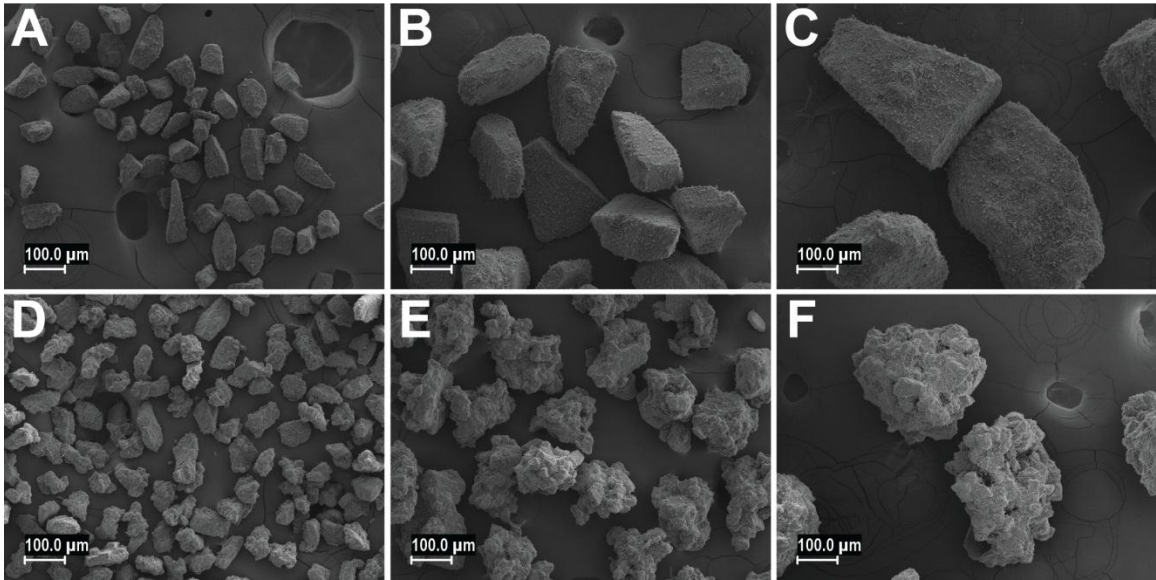


Figure 6.1. SEM Images of  $\alpha$ -Lactose Monohydrate and Granulated Lactose Carrier Particles

SEM images depicting both  $\alpha$ -lactose monohydrate carrier particles fractionated into (A) 45 – 63  $\mu\text{m}$ , (B) 125 -150  $\mu\text{m}$  and (C) 250 – 300  $\mu\text{m}$  size ranges. Granulated lactose carrier particles fractionated into (D) 45 – 63  $\mu\text{m}$ , (E) 125 -150  $\mu\text{m}$  and (C) 250 – 300  $\mu\text{m}$  size ranges are also shown.

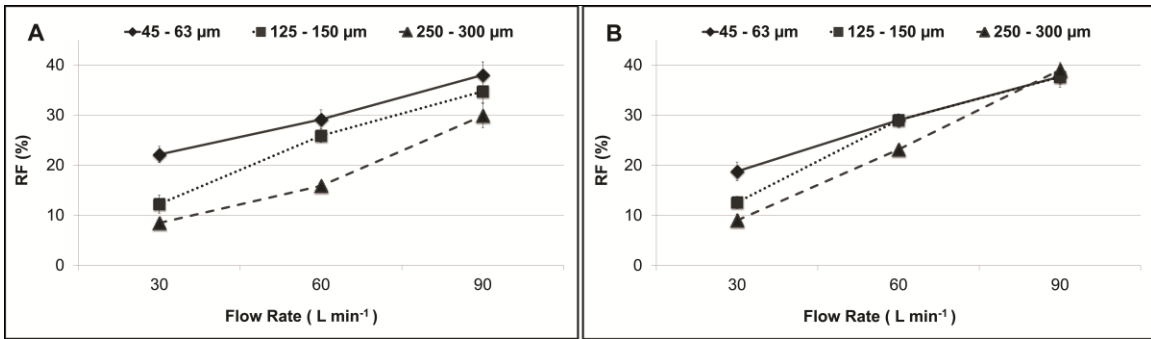


Figure 6.2. Aerosol Performance of Salbutamol Sulphate Blends with Increasing Flow Rate

Respirable fractions (RF) from 1% (w/w) salbutamol sulphate formulations blended with 45 – 63 μm, 125 – 150 μm, or 250 – 300 μm sieved size fractions of (A) α-lactose monohydrate or (B) granulated lactose carrier particles. Data are presented as the mean (± standard deviation) for N = 3 replicates.



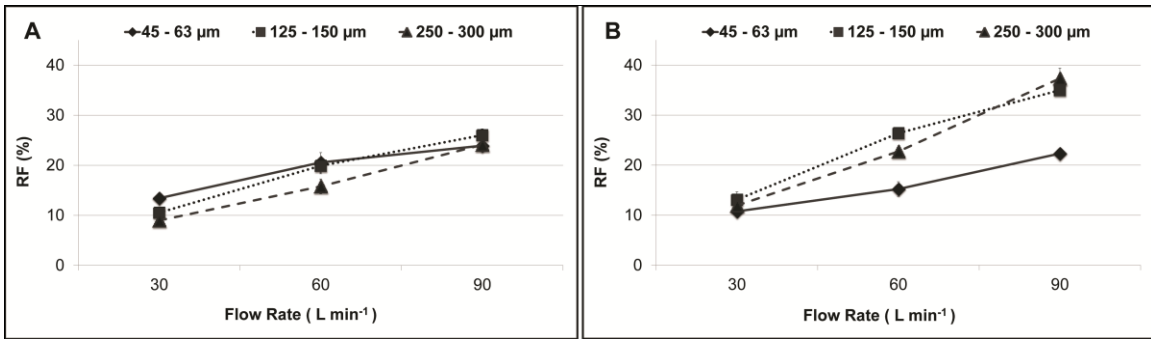


Figure 6.3. Aerosol Performance of Budesonide Blends with Increasing Flow Rate

Respirable fractions (RF) from 1% (w/w) budesonide formulations blended with 45 – 63 μm, 125 – 150 μm, or 250 – 300 μm sieved size fractions of (A) α-lactose monohydrate or (B) granulated lactose carrier particles. Data are presented as the mean (± standard deviation) for N = 3 replicates.

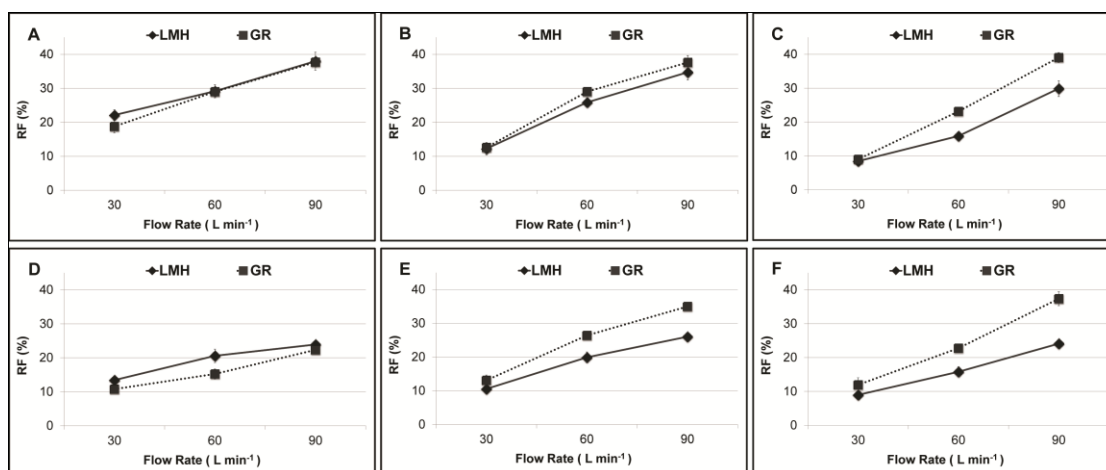


Figure 6.4. Aerosol Performance as a Function of Carrier Particle Surface Roughness

Respirable fractions (RF) from 1% (w/w) salbutamol sulphate formulations with either  $\alpha$ -lactose monohydrate or granulated lactose carrier particle populations with sieved size fractions of (A) 45 – 63  $\mu\text{m}$ , (B) 125 – 150  $\mu\text{m}$ , and (C) 250 – 300  $\mu\text{m}$ . Also depicted are RF values from 1% (w/w) budesonide formulations with either  $\alpha$ -lactose monohydrate or granulated lactose carrier particle populations with sieved size fractions of (D) 45 – 63  $\mu\text{m}$ , (E) 125 – 150  $\mu\text{m}$ , (F) 250 – 300  $\mu\text{m}$ . Data are presented as the mean ( $\pm$  standard deviation) for N = 3 replicates.

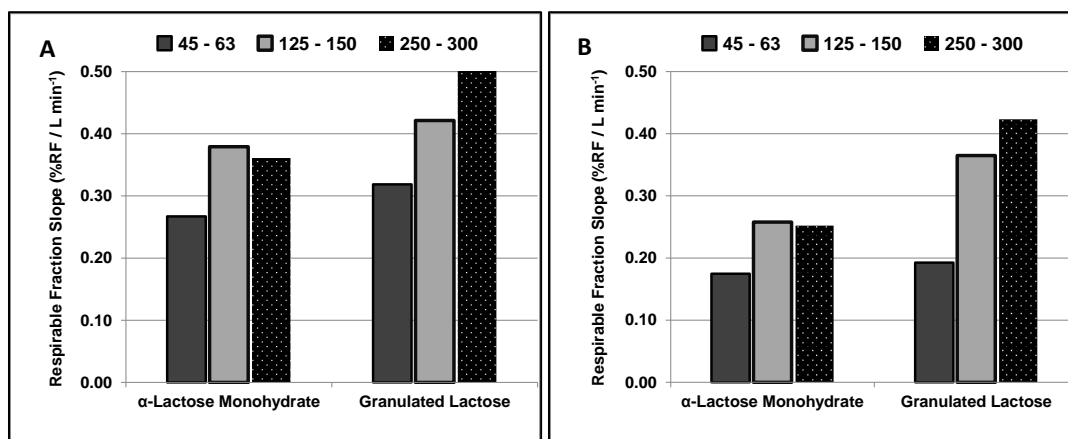


Figure 6.5. Slope of Respirable Fraction Improvement with Increasing Flow Rate

Slope of the respirable fraction (%RF) between 30 L min<sup>-1</sup> and 90 L min<sup>-1</sup> for 1% binary formulations with 45 – 63 μm, 125 – 150 μm, and 250 – 300 μm size fractions of α-lactose monohydrate or granulated carriers with (A) salbutamol sulphate or (B) budesonide as the active pharmaceutical ingredient.

Table 6.1. Physical Properties of  $\alpha$ -Lactose Monohydrate and Granulated Carrier Particle Populations

Carrier Particle Sieve Fraction ( $\mu\text{m}$ )	$d_{10}$	$d_{50}$	$d_{90}$	% Fines ( $< 10 \mu\text{m}$ )	Specific Surface Area ( $\text{m}^2/\text{g}$ )
<b><math>\alpha</math>-Lactose Monohydrate</b>					
45 – 63	41	65	91	5.0	0.39
125 – 150	116	184	250	2.9	0.25
250 – 300	230	353	480	2.4	0.18
<b>Granulated Lactose</b>					
45 – 63	35	63	88	4.9	0.52
125 - 150	126	176	265	---	0.37
250 - 300	230	304	365	----	0.43

Table 6.2. Aerosol Performance Values of Salbutamol Sulphate Blends

Carrier Particle Sieve Size Fraction ( $\mu\text{m}$ )	30 L min <sup>-1</sup>			60 L min <sup>-1</sup>			90 L min <sup>-1</sup>		
	EF (%)	FPF (%)	RF (%)	EF (%)	FPF (%)	RF (%)	EF (%)	FPF (%)	RF (%)
<b><math>\alpha</math>-Lactose Monohydrate</b>									
45 – 63 $\mu\text{m}$	81.6 (1.6)	26.9 (1.7)	22.0 (1.6)	81.3 (2.0)	35.8 (1.8)	29.1 (1.9)	78.2 (3.7)	48.6 (1.1)	38.0 (2.6)
125 – 150 $\mu\text{m}$	75.8 (1.9)	15.8 (2.1)	12.0 (1.8)	78.2 (1.3)	33.0 (1.7)	25.8 (1.4)	80.1 (1.8)	43.3 (2.1)	34.7 (2.3)
250 – 300 $\mu\text{m}$	80.5 (4.6)	10.2 (1.6)	8.1 (0.8)	75.1 (2.2)	20.9 (1.8)	15.7 (0.9)	77.5 (1.6)	38.5 (3.4)	29.8 (2.4)
<b>Granulated Lactose</b>									
45 – 63 $\mu\text{m}$	83.2 (1.9)	22.9 (1.0)	18.6 (1.9)	82.8 (3.8)	35.0 (2.1)	29.0 (0.9)	81.8 (0.5)	46.1 (0.5)	37.7 (0.2)
125 – 150 $\mu\text{m}$	86.4 (2.1)	14.3 (1.1)	12.4 (1.2)	82.6 (0.8)	35.1 (1.7)	29.0 (1.3)	81.0 (0.8)	46.5 (2.2)	37.6 (2.1)
250 – 300 $\mu\text{m}$	84.4 (2.6)	10.4 (1.6)	8.8 (1.3)	77.3 (3.6)	29.9 (1.7)	23.1 (0.3)	78.3 (1.6)	49.9 (0.9)	39.1 (1.5)

The *In vitro* aerosol performance of 1% (w/w) salbutamol sulphate binary blends prepared with 45 – 63  $\mu\text{m}$ , 125 – 150  $\mu\text{m}$ , or 250 – 300  $\mu\text{m}$  lactose monohydrate or granulated lactose carrier particle populations were evaluated at 30, 60 and 90 L min<sup>-1</sup>. Data are presented as the mean ( $\pm$  standard deviation) for N = 3 replicates.

Table 6.3. Aerosol Performance Values of Budesonide Blends

Carrier Particle Sieve Size Fraction ( $\mu\text{m}$ )	30 L min <sup>-1</sup>			60 L min <sup>-1</sup>			90 L min <sup>-1</sup>		
	EF (%)	FPF (%)	RF (%)	EF (%)	FPF (%)	RF (%)	EF (%)	FPF (%)	RF (%)
<b><math>\alpha</math>-Lactose Monohydrate</b>									
45 – 63 $\mu\text{m}$	69.4 (5.4)	19.3 (0.3)	13.4 (1.0)	73.4 (2.7)	28.0 (1.7)	20.6 (2.0)	73.3 (0.7)	32.6 (0.7)	23.9 (0.7)
125 – 150 $\mu\text{m}$	72.7 (1.5)	14.5 (0.6)	10.5 (0.6)	70.4 (2.9)	28.3 (1.3)	19.9 (1.6)	70.8 (0.8)	36.8 (2.0)	26.0 (1.3)
250 – 300 $\mu\text{m}$	73.9 (1.1)	12.2 (1.9)	9.0 (1.3)	69.8 (1.2)	22.6 (1.8)	15.8 (1.5)	71.9 (0.8)	33.5 (0.9)	24.1 (0.5)
<b>Granulated Lactose</b>									
45 – 63 $\mu\text{m}$	72.0 (3.3)	14.9 (0.1)	10.8 (0.6)	75.4 (1.1)	20.2 (2.2)	15.2 (1.5)	79.5 (2.0)	28.1 (1.3)	22.3 (0.7)
125 – 150 $\mu\text{m}$	82.7 (0.8)	15.8 (1.8)	13.1 (1.6)	79.2 (1.6)	33.3 (0.3)	26.4 (0.5)	79.6 (0.3)	44.0 (0.6)	35.0 (0.6)
250 – 300 $\mu\text{m}$	81.0 (3.4)	14.7 (2.0)	11.9 (2.1)	74.2 (1.6)	30.6 (0.1)	22.7 (0.6)	77.3 (1.7)	48.3 (1.6)	37.3 (2.0)

The *in vitro* aerosol performance of 1% (w/w) budesonide binary blends prepared with 45 – 63  $\mu\text{m}$ , 125 – 150  $\mu\text{m}$ , or 250 – 300  $\mu\text{m}$  lactose monohydrate or granulated lactose carrier particle populations were evaluated at 30, 60 and 90 L min<sup>-1</sup>. Data are presented as the mean ( $\pm$  standard deviation) for N = 3 replicates.

## CHAPTER 7

### 7. Development of a Novel Dry Powder Dispersion Mechanism for Pulmonary Drug Delivery Part 1: Carrier Particle Material Selection

#### 7.1. INTRODUCTION

##### 7.1.1. Lactose Carrier Particles

In Chapter 1, the different mechanisms by which large carrier particles are perceived to be detrimental to the aerosol performance of DPI formulations were reviewed. The unfavorable parameters of large diameter carrier particles include their relatively low surface area, the enhanced press-on forces during blending, their extensive surface roughness and the potential for increased van der Waals forces and higher surface energies relative to smaller carrier particles [1-12].

In Chapter 3, a comprehensive study was undertaken to evaluate the *in vitro* aerosol performance of binary DPI formulations with carrier particle populations derived from four grades of lactose fractionated into 13 narrow particle size ranges. The results from this study indicate for a given particle size fraction, the performance of lactose carriers can vary considerably, and may deviate from the predicted trend that smaller carrier particle diameters will outperform their larger carrier diameter counterparts. Specifically, it was observed that for lactose grades with relatively low surface roughness ( $\alpha$ -lactose monohydrate and anhydrous lactose) the results generally followed the predicted trend that performance diminishes as the diameter of the carrier particle population is increased. However, for lactose grades possessing extensive surface roughness, *in vitro* deposition deviated considerably from the predicted trend, especially for granulated carriers, as the performance of the largest fractions was comparable to the smallest carrier particle size fraction.

The mechanism governing drug particle detachment as the size and surface roughness of the carrier particle population varies was further investigated in Chapter 4 [13]. *In vitro* aerosol performance of multiple size fractions of anhydrous and granulated lactose carriers revealed a similar trend in deposition to that observed in Chapter 3, despite employing a different drug (budesonide) and concentration (2% (w/w)) than that employed in the initial comprehensive study (1% (w/w) salbutamol), indicating the deviation from the predicted trend observed with large carrier particles with extensive surface roughness was not an anomaly. It was proposed that the surface roughness of granulated carrier particle populations induces a shift in the drug detachment mechanism, as their extensive rugosity inhibits detachment by the flow stream, thus making them more dependent on detachment by mechanical impactions. Accordingly, this would then favor larger carrier particle diameters, as their larger relative mass enables them to impact against the inner walls of the inhaler with greater force, accounting for the improved performance observed with large granulated carrier particle populations.

In Chapter 5, the influence that the proposed carrier particle collisions with the inner walls of the inhaler have on aerosol performance was investigated by dispersing DPI formulations with carrier particle populations of diverging surface roughness through two commercial inhalers operating with different dispersion mechanisms. The *in vitro* experiments were coupled with particle trajectory simulations using computation fluid dynamics (CFD). It was observed that in the Aerolizer, increasing the diameter of the carrier particles tended to increase the predicted number of collisions the particle has with the inhaler walls as it exits the device. This was correlated to the improved aerosol performance observed *in vitro* with large granulated carrier particle formulations. Conversely, larger carrier particles did not increase the predicted number of carrier-inhaler collisions in the Handihaler to the same extent as seen in the Aerolizer. This was supported by the *in vitro* deposition studies through the Handihaler, where there was no significant improvement in performance with increasing carrier particle diameter. These results suggest that carrier particle-inhaler collisions may be a significant source of drug detachment, and for carriers with high surface roughness, larger particle diameters would be beneficial for detachment via this mechanism.



Chapter 6 examined the influence that the inhalation flow rate on the performance of large granulated carrier particles. As it was previously speculated that mechanical detachment forces predominate for these carriers, it is proposed that higher particle velocities, and hence momentums, would yield greater performance improvements with increasing flow rate relative to smaller carrier particle size fractions. Binary formulations of budesonide and salbutamol sulphate were prepared using relatively smooth ( $\alpha$ -lactose monohydrate), and rough (granulated) lactose grades as carrier particle populations. As the flow rate was increased from 30 to 60 L min<sup>-1</sup>, and then to 90 L min<sup>-1</sup>, the performance improvement from the largest carrier particle size, both lactose monohydrate and granulated, exceeded that of the smaller carriers, regardless of the API in the formulation. Additionally, at 90 L min<sup>-1</sup> the largest granulated carrier size fraction matched the performance of the smallest  $\alpha$ -lactose monohydrate carriers for salbutamol sulphate, and outperformed all other size fractions, for both lactose grades, when budesonide was the API. These results suggest that the improvement induced by larger flow rates is most beneficial for large carriers in general, and for large carriers with extensive surface roughness in particular, as would be expected if mechanical forces indeed played a significant role in drug detachment.

Taken together, the results from Chapters 3 – 6 suggest that the role of large carrier particles is not as clearly defined as implied from the literature. Specifically, carrier particles with large diameters and high surface roughness appear to deviate from the predicted trend, highlighting the incomplete nature of the proposed theories, while simultaneously illustrating the role of mechanical forces in the aerosol performance of dry powder formulations. Accordingly, we now examine the theory behind the hypothesis that larger carrier particles can enhance performance of DPI formulations.

### **7.1.2. Large Carrier Particles: Theory**

The premise that larger carriers assist in drug dispersion is based on the observation that as larger carrier particles possess a greater mass compared to smaller carrier populations, they will collide with greater momentum against the inhaler walls as they exit the device during inhalation. This increased momentum will enhance the mechanical detachment forces

experienced by the drug particles adhered to the carriers. The force,  $F$ , experienced during a collision is due to the change in particle momentum ( $\Delta p$ ) over the collision time,  $\Delta t_c$  (~100  $\mu$ s)[14]. Momentum is the mass of the carrier multiplied by its velocity:

$$F_{\text{mech}} = \frac{\Delta p}{\Delta t_c} = \frac{mv}{\Delta t_c}$$

The mass of a spherical particle is the density,  $\rho$ , multiplied by its volume,  $V$ :

$$m = \rho V$$

Since the volume of a sphere is given by:

$$V = \frac{\pi d^3}{6}$$

The overall linear momentum of a spherical particle possessing diameter,  $d$ , composed of a material with density,  $\rho$ , traveling at a velocity,  $v$ , and undergoing a collision time,  $t_c$ , would experience an impaction force:

$$F_{\text{mech}} = \frac{\rho \pi d^3}{6(\Delta t_c)}$$

As the mechanical forces vary with the cube of the carrier particle diameter, they have the potential to rapidly increase to values that can overwhelm the adhesive interaction between the drug and carrier. To estimate the carrier particle size threshold when impaction forces could theoretically begin to overwhelm adhesive forces, a model was developed using Microsoft Excel<sup>®</sup> that allowed a range of factors, including drug and carrier diameters, densities, and inhalation flow rate to be adjusted. The simplistic and rudimentary nature of the model is readily acknowledged, and limitations of the model include:

1. The assumption of spherical and mono-disperse drug and carrier populations,
2. The assumption that the carrier particle velocity equals that of the flow stream,

3. The interactions between the carrier and the inhaler are modeled as head-on collisions, where the trajectory of the carrier particle is perpendicular to that surface against which it collides, such that the entire momentum of the carrier particle is transferred to the drug particle.

Adhesive forces were calculated using the theoretical van der Waals forces, with a 5  $\mu\text{m}$  drug particle diameter [14]:

$$F_{\text{vdW}} = \frac{A}{12D^2} \left( \frac{d_d d_c}{d_d + d_c} \right)$$

Given the limitations of the model, the generated values of adhesive and carrier particle impaction forces are far from exact, however the general trend is nevertheless interesting, where due to the reliance of the mechanical forces on the cube of the carrier particle diameter it is predicted that these detachment forces can potentially overwhelm adhesive interactions.

### **7.1.3. Novel Large Carrier Particles**

As previously discussed, the results of Chapters 3 - 6 supported the hypothesis that large carrier particle diameters are not inherently deleterious to performance. However, given that mechanical forces have the potential to rapidly exceed the strength of the adhesive interaction between drug and carrier, the ability to enhance the forces generated by the carrier-inhaler collisions may improve the performance already observed in the lactose studies. Revisiting the limitations of the theory cited earlier, it was noted that in our initial calculations we assumed a direct, head-on collision between the carrier and inhaler. However, glancing collisions would most likely be the norm, as the carrier particle caroms off the inhaler wall [15]. In this case, the mechanical forces would be a fraction of what was predicted when the model was developed assuming perpendicular trajectories and head-on collisions. Accordingly, if carrier particles with diameters much greater than the mesh openings within an inhaler were employed, a direct collision would be guaranteed (Figure 7.1). Furthermore, the use of carrier particles with large diameters ensures that they are retained within the device throughout inhalation, thus allowing

materials other than lactose to be explored, as the carrier itself will not be delivered to the patient.

### *Specific Aim*

In this chapter, the potential for developing of a novel dispersion mechanism based upon macro carrier particles (> 500  $\mu\text{m}$ ) is explored. The aerosol performance of drug-coated beads composed of multiple materials, including polystyrene, sucrose, silica, and glass, were screened for their potential to serve as large carrier particles. In addition to varying the bead material, multiple size ranges of each material were also employed to assess the influence of bead diameter on drug delivery. The selected beads were coated with budesonide using the traditional blending protocol employed for binary lactose formulations, and their performance was evaluated *in vitro* via cascade impaction through the Aerolizer. Dispersion was performed at both 30 and 60  $\text{L min}^{-1}$ , to assess the flow rate dependence of the drug-coated beads.

## **7.2. EXPERIMENTAL**

### **7.2.1. Materials**

Micronized budesonide (EP grade) was purchased from Spectrum Chemical (CA, USA) and used as received. Porous polystyrene beads (Fairfield Processing Corp., CT, USA) were purchased locally. Samples of sucrose beads were provided by Colorcon (Colorcon, Inc., PA, USA) and silica beads were provided by Sud-Chemie (NM, USA). Glass beads and analytical grade ethanol was purchased from Sigma (Sigma-Aldrich Corp., MO, USA). For the blending additive studies, polypropylene and steel beads (Crosman Corporation, NY, USA) were purchased locally.

### **7.2.2. Screening of Carrier Particle Size**

The carrier particles were sorted using 12" diameter ASTM test sieves with the following mesh sizes: 0.595 mm (No. 30), 0.84 mm (No. 20), 1.17 mm (No. 16), 1.44 mm (No. 14), 2.36 mm (No. 8), 3.38 mm (No. 6), 4.38 mm (No. 5), and 5.38 mm (No. 3 1/2).

### **7.2.3. Blending of Beads and Drug Powder**

Approximately 5 mg of budesonide were weighed into a 30 mL glass vial, to which were added 5 beads (for diameters > 3.38 mm), or 10 beads (for diameters < 3.38 mm). The drug and beads were blended with a Turbula™ orbital mixer (Glen Mills, NJ) at 46 RPM for 40 minutes. Following blending, the beads were removed from the coating vial and stored in a desiccator for 72 hours prior to use.

### **7.2.4. Density**

The densities of the sucrose, silica, and glass beads were measured using a helium pycnometer (Quantachrome, FL, USA). The density of the porous polystyrene beads was obtained by weighing the beads individually, and then measuring the diameters of the beads with calipers and assuming the volume of sphere. The densities of 10 replicates were measured for the porous polystyrene beads.

### **7.2.5. *In vitro* Aerosol Performance**

The aerosol performance of the drug-coated polystyrene beads was evaluated *in vitro* using a next generation cascade impactor (NGI; MSP Corp., MN, USA) at 30 and 60 L min<sup>-1</sup>. To accommodate the beads within the inhaler, a capsule-based device was required, and accordingly the Aerolizer DPI (Plastiap S.p.A, Italy) was selected as the capsule chamber was sufficiently large to allow the beads adequate space to move within during inhalation. The actuation time was adjusted to allow 4 L of air to flow through the device at each flow rate. For bead diameters > 3.38 mm, a single bead was used per cascade impaction run. For smaller diameters, 3 beads were placed into the capsule chamber of the Aerolizer for each actuation. 15 mL of EtOH was added to the pre-separator prior to every run and collected following each impaction. The capsule, dispersion chamber, mouthpiece, mouthpiece adaptor, and induction port were each rinsed with 10 mL of EtOH, and the stages of the NGI were each rinsed with 5 mL.

Drug mass was quantified by UV-VIS spectroscopy at 244 nm using an Infinite M200 microplate reader equipped with a cuvette port (Tecan US, Inc., NC, USA). For each cascade impaction, the recovered dose is the cumulative drug mass collected from the bead, inhaler, mouthpiece adaptor, induction port, pre-separator, and NGI stages. The emitted fraction (EF) is provided as the percentage of the recovered dose collected from the mouthpiece adaptor, induction port, pre-separator, and NGI stages. The fine particle fraction (FPF) is the percentage of the emitted dose collected from stages 3 – 8 of the NGI, while the respirable fraction (RF) is the percentage of the recovered dose collected from stages 3 – 8. As the flow rate varies through the NGI, the particle cut-off diameters for each stage also varies. At 60 L min<sup>-1</sup> the cut-off diameter of stage 2 is 4.46 μm, shifting to 6.40 μm at 30 L min<sup>-1</sup> [16].

### **7.3. RESULTS AND DISCUSSION**

#### **7.3.1. Physical Characterization**

The sieve fractions collected for each material are presented in Table 7.1. For each material, at least two size fractions were obtained, allowing for the influence of particle size in addition to density to be assessed. The measured densities of all beads (those that will be drug-coated and those to be employed as blending additives in subsequent studies) are provided in Table 7.2. The polystyrene beads possessed a very low average density (0.027 g /cm<sup>3</sup>) by comparison to the sucrose (1.51 g /cm<sup>3</sup>), silica (1.84 g /cm<sup>3</sup>) and glass beads (2.48 g /cm<sup>3</sup>)

#### **7.3.2. Aerosol Performance of Drug-Coated Beads**

The *in vitro* performance of drug-coated polystyrene, sucrose, silica, and glass beads are presented in Figure 7.2 to Figure 7.5. The parameters evaluated were the ability of the bead to deliver the dose from the device (EF), coupled to the efficiency of powder dispersion (FPF). This first parameter is a combination of the effectiveness of the bead-inhaler collisions to detach the drug from the carrier; the latter assesses both the carrier's ability to prevent the formation of stable drug agglomerates during blending, coupled to the inhaler's capacity to de-aggregate the powder that is detached from the bead. It is noted that both EF and FPF will also be heavily

influenced by the blending process of the drug and carrier, and this will be discussed in detail below. Furthermore, the effectiveness of the collisions between the bead and device to detach the drug are specifically examined, and the fraction of the total dose that was retained on the beads following dispersion was evaluated, as was the fraction of the total dose retained on the inner walls of the inhaler.

For the polystyrene beads (Figure 7.2), diverging trends in bead and device retention were observed as the diameters of the carrier particle populations were enlarged. Bead retention increased significantly ( $p < 0.05$ ) from 4% with the 0.84 – 1.12 mm size fraction, up to approximately 14% of the total dose for the 4.38 – 5.38 mm carrier beads. In combination, the polystyrene beads yielded emitted fractions that were relatively constant for all bead size ranges examined, with 45 – 50% of the total dose delivered from the device. FPF exhibited a slight improvement with carrier diameter, increasing from an average of 55% (0.84 – 1.12 mm) up to 66% (3.38 – 4.38 mm) and 64% (4.38 – 5.38 mm).

For the sucrose, silica, and glass beads (Figure 7.3 to Figure 7.5), significantly lower dose emission was observed relative to the polystyrene, with EF values between 20 – 30% for silica, and 10 – 20% for the sucrose and glass beads. Interestingly, the dose retained on the bead decreased with larger bead sizes, despite the much greater press-on forces between the drug and carrier that could be expected during blending with larger, and thus heavier, beads. This suggests that collisions between the bead and device generated greater detachment forces with increasing bead size for a given material. As with the polystyrene, there was observed a trade-off between bead and device retention, with the drug mass collected from the device generally increasing with carrier particle size for the three denser materials. It was observed that bead retention was not directly related to bead density, as the silica material retained between 37 – 45% of the dose on the bead following dispersion, in contrast to the sucrose particles, which despite a lower density retained 45 – 60% for the 0.84 – 1.17 mm and 1.17 – 1.44 mm size ranges, indicating that the bead material plays a role in modulating the adhesive force between drug and carrier, which is likely a function of the physicochemical properties of both the drug and the bead. Overall, FPF values ranged from approximately 45% for the sucrose beads up to

69% for the glass beads, indicating that the powder emitted from the device is likely to be well dispersed.

The pattern of dose retention differed between the polystyrene carriers and the denser materials, as most of the retained dose was collected from the inner walls of the device for the former, while the majority of the non-emitted dose remained adhered to the bead surface following dispersion for the sucrose, silica, and glass beads. It is speculated that the retained dose from the polystyrene carriers was due to the collisions between the bead and inner surface of the device, causing powder to rub-off onto the inhaler walls with each collision. This indicates that the detachment forces of the polystyrene carriers are sufficient to remove upwards of 85% of the dose from the bead surface. In contrast, for the heavier beads the force of the collisions between the bead and inhaler appeared to be insufficient to effectively detach most of the dose, as observed with the polystyrene beads. Accordingly, while the denser beads exhibited FPF values comparable to, if not greater than, the polystyrene carriers, overall drug deposition was higher for the low density beads.

### **7.3.3. Flow Rate Dependent Performance**

To assess the flow rate dependent performance of the drug-coated beads, the volumetric flow rate was reduced by half, and dispersion performance of the different bead materials was evaluated at 30 L min<sup>-1</sup> (Figure 7.6). Polystyrene beads demonstrated excellent flow rate independent performance with no significant difference in RF values for the 0.84 – 1.17 mm size fraction, and only a slight decline for the larger 4.38 – 5.38 mm carriers, as the mean respirable fraction decreased from 28% to 24%. For silica, sucrose, and glass beads, the performance was significantly inhibited at the lower flow rate for all size fractions examined. Similar to the performance at 60 L min<sup>-1</sup>, the silica beads exhibited the best performance of the three remaining materials at 30 L min<sup>-1</sup>, but RF values were only 5%, a decline of approximately 60% from the performance at the higher flow rates. For the sucrose beads, performance was halved at 30 L min<sup>-1</sup>, while glass beads essentially ceased to function at the lower flow rate, delivering less than 2% of the dose to the ‘deep lung’ region of the NGI.



The flow rate independent performance of the polystyrene beads is likely due to the very low density of these particles, allowing these beads to be readily entrained at 30 L min<sup>-1</sup>, and thus producing sufficient momentums to yield effective collision/detachment forces. By comparison, for the much heavier sucrose, silica, and glass beads, the reduction in flow rate appeared to have adversely affected the velocity, and hence linear momentum, of the particles, resulting in diminished collision forces and thus significantly reducing the percentage of the dose detached from the bead surface.

#### **7.3.4. Blending Studies**

The beads were blended with the drug powder according the protocol employed to prepare traditional lactose-based binary DPI formulations. However, given the extremely low surface area of the beads relative to 20 mg of inhalation-grade lactose, coupled with the reported cohesive nature of budesonide, it was speculated that longer blending times may adversely affect aerosol performance by inducing the formation of drug agglomerates that typically deposit in the induction port and pre-separator.

As noted by De Boer and coworkers, during powder blending there are two competing processes that promote either excellent or poor drug content uniformity in the formulation[1, 3]. In one instance, the repeated abrasion of the drug particles by the coarse carriers can break-up agglomerates of drug that were initially present in the powder prior to blending. These are termed 'natural agglomerates,' and their disruption has long been noted to be an advantage of thorough powder blending. However, the repeated physical contact between drug particles may also induce formation of 'blending' agglomerates, which arise if the cohesive tendency of the drug particles exceeds the adhesive tendency between the drug and carrier material [17, 18]. Accordingly, to produce a blend with excellent drug content uniformity, natural agglomerates must be broken-down while the formation of agglomerates during blending must be prevented. The process that dominates for a given formulation depends on the physicochemical properties of both the drug and carrier, the overall concentration (% w/w) of each component, and the blending parameters employed, including blending speed, mixing time, and batch size.

Budesonide was selected as the model drug for these screening studies due in part to its cohesive nature, as the affinity between budesonide particles was reportedly much stronger than the adhesive interaction between budesonide and lactose, in contrast to salbutamol sulphate, which displayed the opposite trend, and adhered readily to the surface of the lactose. At the outset of these studies, it was recognized that one of the challenges of using large beads as carriers for pulmonary delivery would be to overcome the diminished surface area available for drug binding; a limitation of large diameter carrier particle populations that was discussed in Chapter 1. Accordingly, if the process could be optimized for budesonide, it is expected that performance from other API materials would be at least comparable to that of this cohesive powder.

#### **7.3.5. Blending Time**

To examine the influence of blending time, 0.84 – 1.17 mm beads of polystyrene, silica, and glass were mixed for short (8 minutes) or long (40 minutes) time intervals. Following blending, their aerosol performance was tested at 60 L min<sup>-1</sup> (Figure 7.7). From the theory describing blending of binary formulations, it was speculated that heavier particles could break-up drug agglomerates, thereby potentially improving dispersion. Conversely, denser beads could potentially also increase bead retention, as the press-on forces between the drug and carrier surface would be enhanced by the higher momentum of the heavier particles during blending.

The resulting RF values indicate that blending time and performance are not related solely by the density of the material, as increased mixing times improved performance from the heavier glass beads, while reducing overall drug deposition from the lighter silica beads. The observed improvement in performance with longer coating times for the glass beads contrasted with our initial hypothesis, as it was expected that these heavy particles would enhance the adhesive forces between drug and carriers by providing large press-on forces during blending. It was speculated that prolonged mixing times may cause the beads to detach drug from their surface due to the repeated collisions occurring during blending. As larger particles, especially agglomerates would be most susceptible to detachment due to their higher mass, a greater

concentration of fine particles may remain on the surface of the glass beads following blending at 40 minutes compared to 8 minutes. This was supported by the lower recovered doses observed from these carriers at 40 minutes relative to the 8-minute blending period, indicating that a lower drug mass remains adhered to the bead, potentially due to the detachment of the larger aggregates. In contrast to the silica and the glass material, the low density polystyrene beads exhibited no significant change in performance between the two blending periods.

### **7.3.6. Blending Additives**

During the blending-time studies, it was noted that the low mass of the polystyrene beads may be incapable of either disrupting natural agglomerates or preventing the formation of blending agglomerates. It was thus speculated that performance may be improved if higher density materials were incorporated into the formulation during blending, thereby providing the requisite abrasion to limit the extent of drug aggregates coating the bead surface. To test this theory, polystyrene beads were blended with budesonide alone, or with five polypropylene ( $\rho = 1.0 \text{ g/cm}^3$ ) or steel ( $\rho = 7.8 \text{ g/cm}^3$ ) beads included in the vial. The polypropylene and steel beads were monodisperse with 6 mm diameters. Following blending, the polystyrene beads were tested through the Aerolizer at  $60 \text{ L min}^{-1}$  and the resulting aerosol performance is presented in Figure 7.8.

While the inclusion of heavier beads was expected to disrupt drug agglomerates, the increased momentum of the denser particles during blending could potentially augment the press-on forces between the drug and carrier, increasing bead retention and lowering emitted fraction. However, the amount of the nominal dose that remained adhered to the bead surface following dispersion was not significantly different between the three samples, and emitted fraction was noted to improve with the inclusion of the polypropylene and steel blending additives. The addition of both the polypropylene and steel beads also yielded increased respirable fractions compared to polystyrene beads alone, although only the RF increase from the formulation with steel bead additives was found to be significant ( $p < 0.05$ ). For both EF and RF, the observed improvements correlated with the denser, and thus heavier, additive.

Accordingly, the inclusion of dense beads during blending could be a potential strategy to improve aerosol performance from low-density polystyrene carriers by providing a sufficient energy source to disrupt drug agglomerates.

#### **7.4. CONCLUSION**

In this chapter, the aerosol performance of large, drug-coated beads was evaluated to determine the potential of developing a novel dry powder dispersion mechanism based on the mechanical forces that occur when large carrier particles impact with the inner walls and mesh of a DPI. In contrast to the predicted theory, the low surface area of the large carriers did not cause extensive 'throat' deposition. Indeed, all materials and size fractions produced FPF values ranging from 45 - 70% at 60 L min<sup>-1</sup>. However, the ability of the beads to deliver the dose to the patient was rather low. For the sucrose, silica, and glass materials, a large fraction of the dose remained adhered to the bead surface following actuation, suggesting that the collisions forces generated by these materials were not sufficient in magnitude to detach the drug from the carriers. Consequently, when the flow rate was halved to 30 L min<sup>-1</sup>, these materials essentially ceased to function, delivering less than 5% of the total dose.

Similar to sucrose, silica, and glass beads, the low-density polystyrene were plagued by low dose emission, with EF values typically below 50%. However, in contrast to the denser materials, the majority of the retained dose was collected from the inner walls of the device rather than from the bead, indicating effective drug detachment. Additionally, of the tested materials only polystyrene demonstrated flow rate independent performance and thus polystyrene beads were selected for future studies.

The following chapter will focus on improving performance from the drug-coated beads by increasing the fraction of the dose that is delivered from the device. As it is speculated that the physical impactions between the carrier and inhaler are primarily responsible for the retained dose, an alternative dispersion mechanism will be investigated to limit the physical contact between the drug and carrier while maintaining their excellent drug detachment potential. Additionally, the blending studies indicated that due to their low mass, polystyrene

beads are ineffective at disrupting agglomerates, and mild improvements were observed when high density additives were included during blending. However, a more effective method to inhibit drug agglomerates is desired, and accordingly this will also be addressed in the following chapter.

## 7.5. REFERENCES

1. A. de Boer, P. Hagedoorn, D. Gjaltema, J. Goede, K. Kussendrager, and H. Frijlink. Air classifier technology (ACT) in dry powder inhalation Part 2. The effect of lactose carrier surface properties on the drug-to-carrier interaction in adhesive mixtures for inhalation. *Int J Pharm.* 260:201-216 (2003).
2. A. de Boer, P. Hagedoorn, D. Gjaltema, J. Goede, and H. Frijlink. Air classifier technology (ACT) in dry powder inhalation Part 1. Introduction of a novel force distribution concept (FDC) explaining the performance of a basic air classifier on adhesive mixtures. *Int J Pharm.* 260:187-200 (2003).
3. B. Dickhoff, A. Deboer, D. Lambregts, and H. Frijlink. The interaction between carrier rugosity and carrier payload, and its effect on drug particle redispersion from adhesive mixtures during inhalation. *Eur J Pharm Biopharm.* 59:197-205 (2005).
4. H. Steckel, and Muller, B.W. In vitro evaluation of dry powder inhalers II: influence of carrier particle size and concentration on in vitro deposition. *Int J Pharm.* 154:31 - 37 (1997).
5. D. Cline, and Dalby, R. Predicting the quality of powder for inhalation from surface energy and area. *Pharm Res.* 19:1274 - 1277 (2002).
6. M.D. Louey, and Stewart, P.J. Particle interactions involved in aerosol dispersion of ternary interactive mixtures. *Pharm Res.* 19:1524 - 1531 (2002).
7. M.D. Louey, Razia, S., and Stewart, P.J. Influence of physico-chemical carrier properties on the in vitro aerosol deposition from interactive mixtures. *Int J Pharm.* 252:87 - 98 (2003).
8. F. Podczec. The relationship between physical properties of lactose monohydrate and the aerodynamic behaviour of adhered drug particles. *Int J Pharm.* 160:119 - 130 (1998).

9. F. Podczek. Evaluation of the Adhesion Properties of Salbutamol Sulphate to Inhaler Materials. *Pharm Res.* 15:806-808 (1998).
10. Y. Kawashima, Serigano, T., Hino, T., Yamamoto, H., and Takeuchi, H. Effect of surface morphology of carrier lactose on dry powder inhalation property of pranlukast hydrate. *Int J Pharm.* 172:179 - 188 (1998).
11. N. Islam, Stewart, P., Larson, I., and Hartley, P. Lactose surface modification by decantation: are drug-fine lactose ratios the key to better dispersion of salmeterol xinafoate from lactose-interactive mixtures? *Pharm Res.* 21:492 - 499 (2004).
12. N. Islam, P. Stewart, I. Larson, and P. Hartley. Surface roughness contribution to the adhesion force distribution of salmeterol xinafoate on lactose carriers by atomic force microscopy. *J Pharm Sci.* 94:1500-1511 (2005).
13. M.J. Donovan and H.D.C. Smyth. Influence of size and surface roughness of large lactose carrier particles in dry powder inhaler formulations. *Int J Pharm.* 402:1 - 9 (2010).
14. W.H. Finlay. *The Mechanics of Inhaled Pharmaceutical Aerosols*, Academic Press, London, UK, 2001.
15. M.S. Coates, D.F. Fletcher, H.-K. Chan, and J.A. Raper. Effect of design on the performance of a dry powder inhaler using computational fluid dynamics. Part 1: Grid structure and mouthpiece length. *J Pharm Sci.* 93:2863-2876 (2004).
16. V.A. Marple, Roberts, D.L., Romay, F.J., Miller, N.C., Truman, K.G., Van Oort, M., Olsson, B., Holroyd, M.J., Mitchell, J.P., and Hochrainer, D. Next Generation Pharmaceutical Impactor (A New Impactor for Pharmaceutical Inhaler Testing). Part I: Design. *Journal of Aerosol Medicine.* 16:283 - 299 (2004).
17. P. Begat, Morton, D.A.V., Staniforth, J.N., and Price, R. Dry powder inhaler formulations I: Direct quantification by atomic force microscopy. *Pharm Res.* 21:1591 - 1597 (2004).

18. I. Saleem, H. Smyth, and M. Telko. Prediction of Dry Powder Inhaler Formulation Performance From Surface Energetics and Blending Dynamics. *Drug Dev Ind Pharm.* 34:1002-1010 (2008)



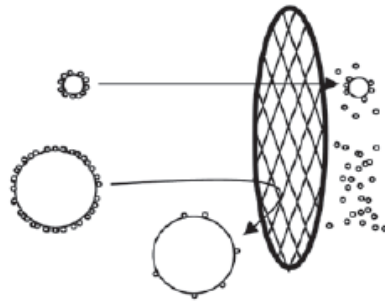


Figure 7.1. Predicted Mesh Interactions for Small and Large Carrier Particles

The smaller carrier particle will generally pass through perforations in the mesh, or experience glancing collisions. By contrast, the large carriers will experience direct collisions, maximizing the resulting impaction force.

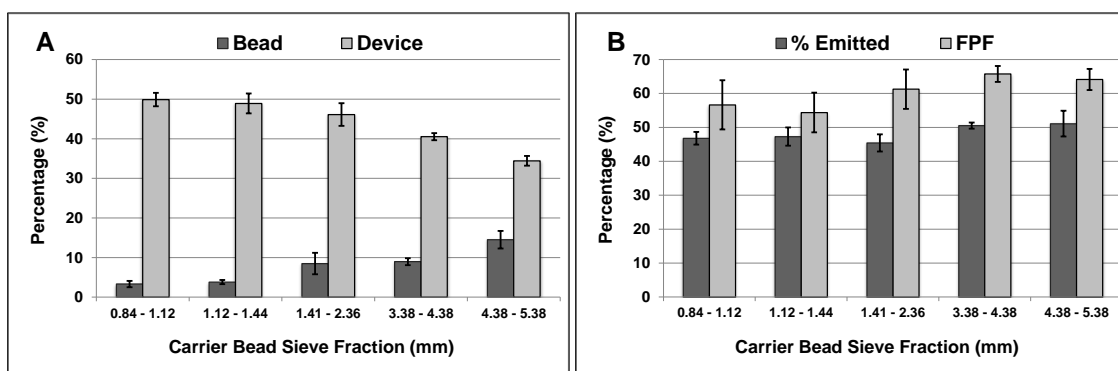


Figure 7.2. *In vitro* Aerosol Performance of Budesonide-Coated Polystyrene Beads

The *in vitro* aerosol performance of budesonide-coated polystyrene beads was evaluated through the Aerolizer at  $60 \text{ L min}^{-1}$ . The performance metrics evaluated were the (A) percentage of the recovered dose that remained adhered to the bead or device following actuation and (B) the emitted fractions (% emitted) and fine particle fractions (FPF). Values are provided as the mean ( $\pm$  standard deviation) for  $N = 3$  replicates.

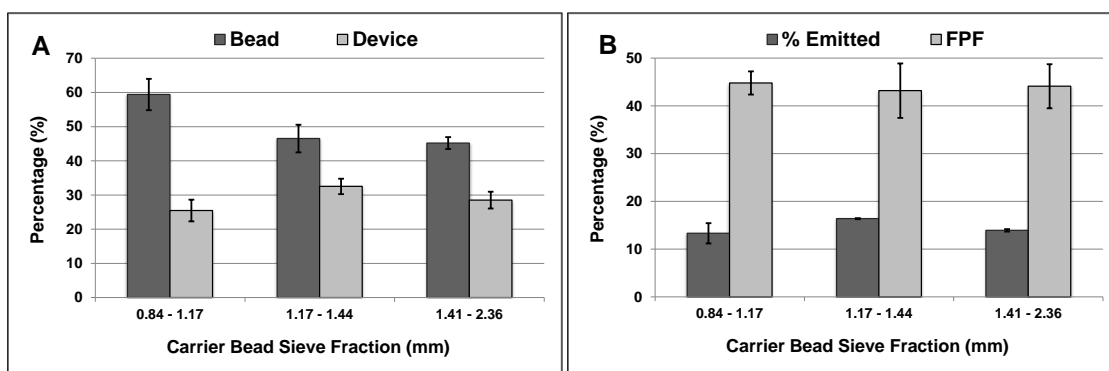


Figure 7.3. *In vitro* Aerosol Performance of Budesonide-Coated Sucrose Beads

The *in vitro* aerosol performance of budesonide-coated sucrose beads was evaluated through the Aerolizer at  $60 \text{ L min}^{-1}$ . The performance metrics evaluated were the (A) percentage of the recovered dose that remained adhered to the bead or device following actuation and (B) the emitted fractions (% emitted) and fine particle fractions (FPF). Values are provided as the mean ( $\pm$  standard deviation) for N = 3 replicates.

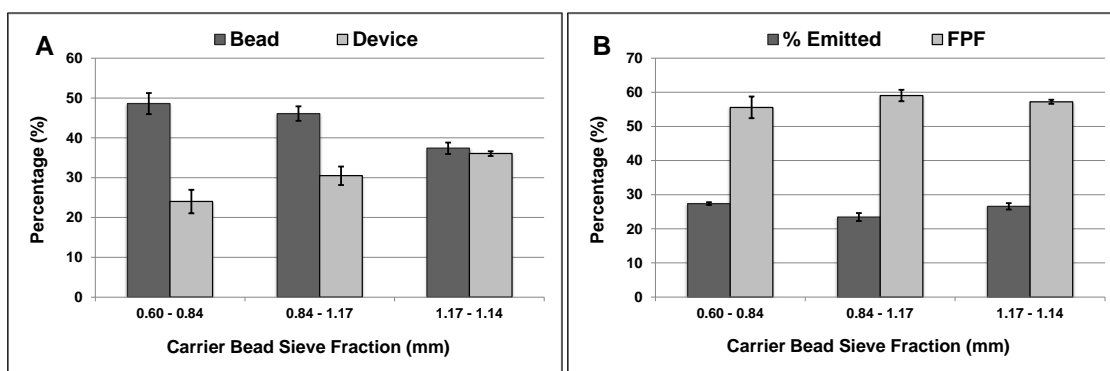


Figure 7.4. *In vitro* Aerosol Performance of Budesonide-Coated Silica Beads

The *in vitro* aerosol performance of budesonide-coated silica beads was evaluated through the Aerolizer at  $60 \text{ L min}^{-1}$ . The performance metrics evaluated were the (A) percentage of the recovered dose that remained adhered to the bead or device following actuation and (B) the emitted fractions (% emitted) and fine particle fractions (FPF). Values are provided as the mean ( $\pm$  standard deviation) for N = 3 replicates.

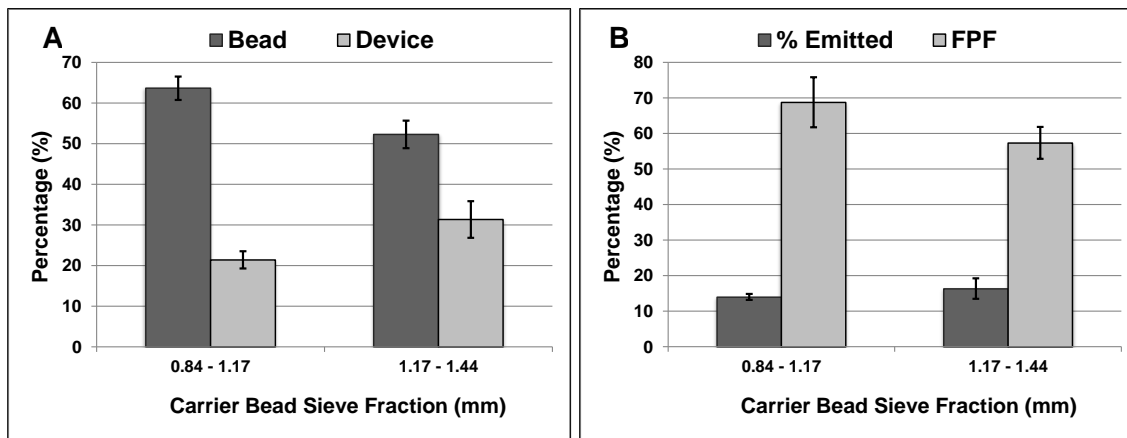


Figure 7.5. *In vitro* Aerosol Performance of Budesonide-Coated Glass Beads

The *in vitro* aerosol performance of budesonide-coated glass beads was evaluated through the Aerolizer at  $60 \text{ L min}^{-1}$ . The performance metrics evaluated were the (A) percentage of the recovered dose that remained adhered to the bead or device following actuation and (B) the emitted fractions (% emitted) and fine particle fractions (FPF). Values are provided as the mean ( $\pm$  standard deviation) for  $N = 3$  replicates.

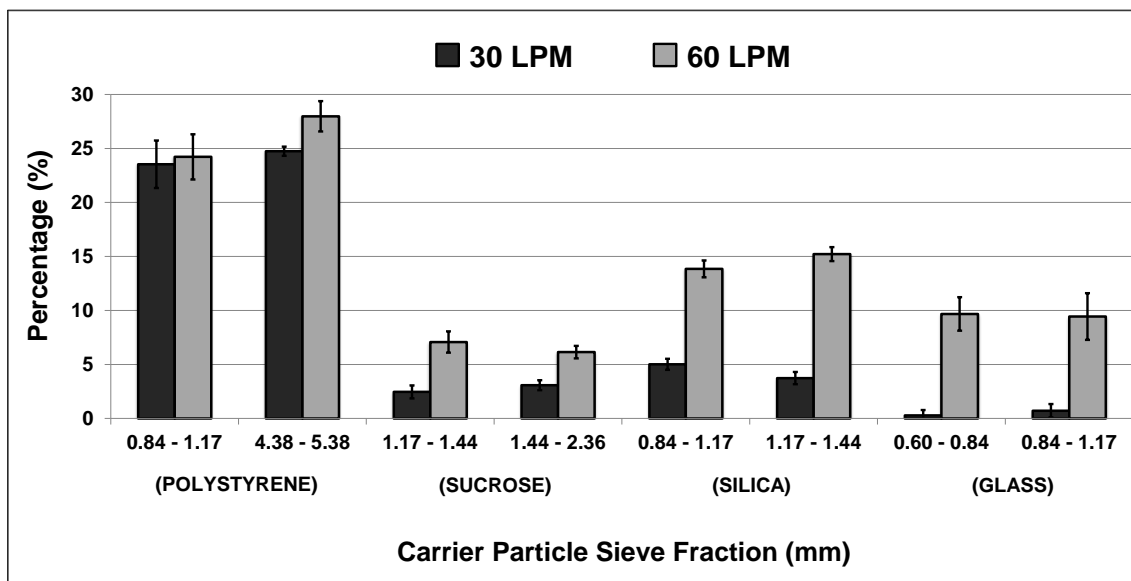


Figure 7.6. Influence of Flow Rate on the Performance of Drug-Coated Beads

To assess the relative flow rate dependence of the drug-coated beads, the *in vitro* aerosol performance was evaluated through the Aerolizer at 30 L min<sup>-1</sup> using beads of the different materials. The respirable fractions (RF) were compared against their respective values at 60 L min<sup>-1</sup>. Values are provided as the mean ( $\pm$  standard deviation) for N = 3 replicates.

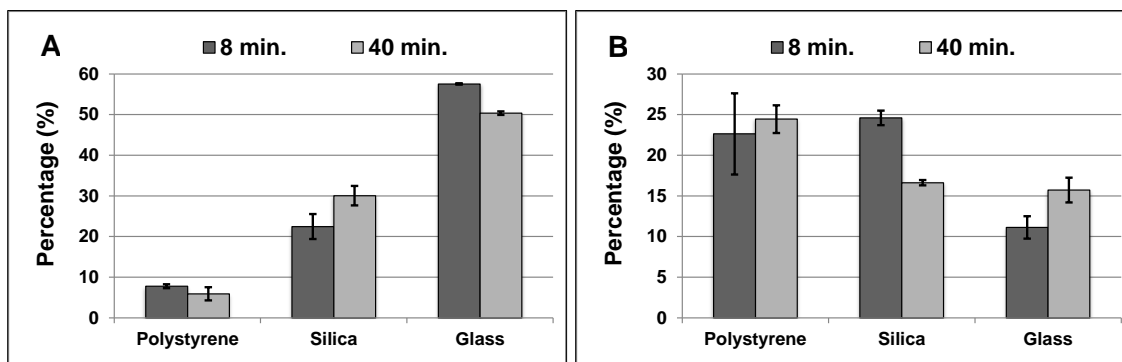


Figure 7.7. Blending-Time Studies of Budesonide-Coated Polystyrene, Silica, and Glass Beads

Polystyrene, silica, and glass beads with diameters between 0.84 – 1.17 mm were blended with budesonide for either 8 minutes or 40 minutes. Following blending they were dispersed at 60 L min<sup>-1</sup> through the Aerolizer. The performance metrics evaluated are (A) the percentage of the recovered dose that was retained on the beads following dispersion and (B) the respirable fractions from each formulation. Values are provided as the mean ( $\pm$  standard deviation) for N = 3 replicates.

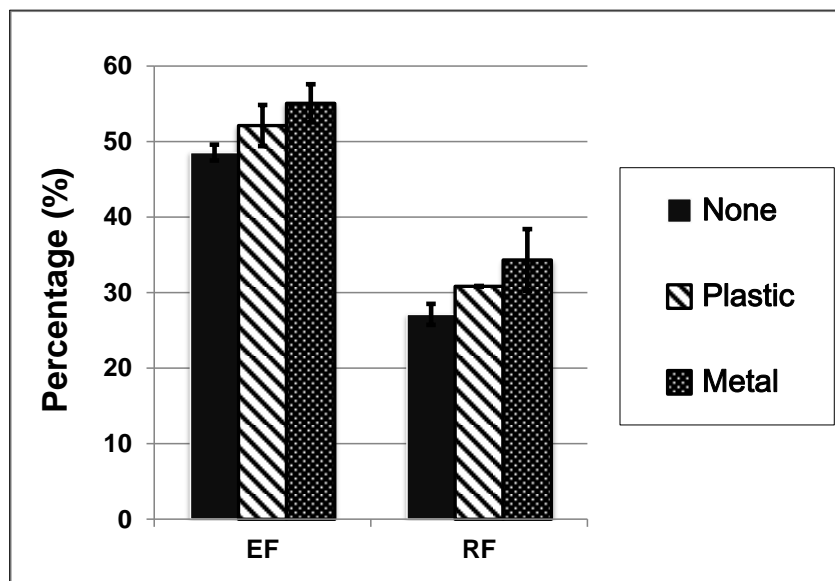


Figure 7.8. Blending Additive Studies of Budesonide-Coated Polystyrene Beads

Polystyrene beads (0.84 – 1.17 mm) were blended with budesonide either alone, or with polypropylene or steel beads added to the formulation during mixing to evaluate the ability of the denser beads to disrupt drug agglomerates. The formulations were blended for 40 minutes, and their aerosol performance was assessed at 60 L min<sup>-1</sup>. The emitted fractions (EF) and respirable fractions (RF) are reported as the mean ( $\pm$  standard deviation) for N = 3 replicates.



Table 7.1. Collected Bead Size Ranges Following Fractionation

<b>Bead Size Ranges (mm)</b>			
<b>Polystyrene</b>	<b>Sucrose</b>	<b>Silica</b>	<b>Glass</b>
0.84 – 1.17	0.84 – 1.17	0.60 – 0.84	0.60 – 0.84
1.17 – 1.44	1.17 – 1.44	0.84 – 1.17	0.84 – 1.17
1.44 – 2.36	1.44 - 2.36	1.17 – 1.44	
3.38 – 4.38			
4.38 – 5.38			

For each of the materials at least two size fractions were collected, allowing for the evaluation of both density and carrier particle diameter on aerosol performance.

Table 7.2. Measured Densities of Bead Materials

	Material	Density (g/cm <sup>3</sup> )
<b>Carriers</b>	Polystyrene	0.027
	Sucrose	1.51
	Silica	1.84
	Glass	2.48
<b>Additives</b>	Polypropylene	1.04
	Steel	7.65

## CHAPTER 8

### 8. Development of a Novel Dry Powder Dispersion Mechanism for Pulmonary Drug Delivery, Part 2: Optimization of the Dispersion Mechanism and Coating Method

#### 8.1. INTRODUCTION

In the previous chapter, a novel dry powder dispersion mechanism based upon collisions of large diameter drug-coated beads was introduced, and bead materials of various size ranges screened for their potential to serve in this capacity. Of the tested materials, the low density ( $0.027 \text{ g/cm}^3$ ) polystyrene beads demonstrated drug deposition levels comparable to the reported values from many commercial devices, coupled with excellent flow rate independent performance. Therefore, this material was selected as the most suitable candidate for future studies.

With the selection of the carrier particle material complete, the focus of this chapter will be to address the performance issues encountered during the initial screening studies. Particularly, the high fraction of the total dose retained within the device following actuation and the extensive formation of drug particle aggregates during blending will be addressed as a means to improve the aerosol performance of the drug-coated polystyrene beads.

##### 8.1.1. Device Retention

As discussed in Chapter 5, efficient delivery from dry powder inhalers requires high dose emission coupled with effective powder dispersion. Accordingly, devices that perform well at only one of these tasks will yield only moderate drug deposition levels relative to an inhaler that excels at both emission and dispersion. Many studies examining the performance of commercial DPIs have noted that there is generally a trade-off between dose emission and powder dispersion, as the design features that optimize one parameter typically do so to the detriment of the other. For example, DPIs that produce high emitted fractions tend to have very straight

flow paths that minimize the surface area of the powder flow channel through the inhaler. Alternatively, inhalers that employ more complex internal geometries to increase turbulence of the powder-laden flow stream and/or promote particle-particle and particle-device collisions, are more susceptible to higher levels of mouthpiece retention [1-4].

Examples of these opposing characteristics of DPI performance are illustrated in the Diskhaler and Turbuhaler, two marketed DPIs that have enjoyed considerable commercial success [5]. At comparable volumetric flow rates, the percentage of the nominal dose retained in the mouthpiece of the Diskhaler was typically below 5%, and tended to remain constant as flow rate was varied. In contrast, mouthpiece deposition was strongly dependent on flow rate through the Turbuhaler, as higher flow rates corresponded to lower device retention, with values ranging between 20 – 40% of the nominal dose. However, despite the greater emitted fraction values obtained through the Diskhaler, overall performance from the Turbuhaler was superior, with RF values of approximately 35% compared to an average of 23% from the Diskhaler.

Referring to the earlier discussion regarding the trade-off between device emission and powder dispersion, it is clear that the Diskhaler is superior at delivering the dose from the device, while the Turbuhaler excels at de-aggregation. Examining the internal geometries of these devices, it is noted that in contrast to the relatively simple internal mouthpiece geometry of the Diskhaler (essentially a straight channel from the powder bed to the exit of the device), the Turbuhaler incorporates a spiraling flow path in the mouthpiece to aid in drug dispersion [6, 7]. However, this design induces more drug particles to deposit in this region for the Turbuhaler. Accordingly, while the powder dispersion from this device is relatively high, with FPF values in excess of 50%, the lower emitted fractions result in RF values of 35%, as opposed to the higher deposition levels that could be achieved if the emitted fraction from the Turbuhaler matched that of the Diskhaler. However, it is noted that these inhalers employ different formulations, as the Diskhaler delivers a binary blend of coarse lactose carriers and micronized drug, while the Turbuhaler generally employs spheronized pellets of pure drug, and accordingly differences in performance may not be solely attributable to device design features.

In Chapter 7, *in vitro* aerosol performance studies from the drug-coated polystyrene beads actuated through the Aerolizer exhibited good powder dispersion, with FPF values of up to 70%. However, dose delivery was relatively low, as over 50% of the total dose was retained in the inhaler following actuation, yielding low emitted fractions and overall RF values between 25 – 30%. In contrast to the heavier sucrose, silica, and glass beads, where upwards of 80% of the dose remained adhered to the bead following dispersion, the majority of the retained dose from the polystyrene beads was collected from the inner walls and mesh of the device. Thus, it was speculated that the repeated collisions between the drug-coated beads and the inhaler induces a large fraction of the drug to rub-off onto the walls, where it remains adhered. Accordingly, despite the excellent powder dispersion profiles exhibited by the Aerolizer, an alternative dispersion mechanism using the Handihaler® DPI was explored as a means to enhance the dose emitted from the device.

#### **8.1.2. Drug Powder Aggregates**

In the previous chapter, coating of drug on the carrier beads was performed using the standard method employed in preparing lactose-based binary blends. Specifically, the drug and beads were mixed together for an extended period of time (typically 40 minutes) using a Turbula® orbital mixer where the vial containing the formulation is continuously rotated, causing the powder to tumble back-and-forth from one end to the other throughout the blending period (Figure 8.1). For traditional binary formulations with lactose carrier particles, the continuous tumbling allows coarse carriers to break down drug aggregates, producing a stable blend with excellent uniformity, as the drug particles are well distributed over the surface of the carriers. However, in order to perform this function, the carrier particles must be sufficiently heavy to disrupt drug aggregates via abrasion. As seen in chapter 3, despite the extremely large surface area available in the LMH < 20 µm carrier particle population, the blend uniformity was relatively poor, with a coefficient of variation above 10%. It was proposed that this resulted from the very low mass of these small carrier particles, rendering them ineffective at disrupting either the natural agglomerates initially present in the drug powder, or the blending agglomerates that form during mixing [6, 8-10].

Similarly, as was discussed in Chapter 7, the low mass of polystyrene beads inhibits their ability to break down drug agglomerates. Moreover, the much lower available surface area for drug binding of the beads relative to traditional lactose carrier particles would be expected to promote the formation of blending agglomerates. In addition to the carrier particle parameters that could induce aggregate formation, the adhesive and cohesive properties of drugs can vary extensively, as noted by Begat and coworkers, who developed an cohesive-adhesive balance (CAB) approach to characterizing the relative affinity of drug particle for lactose interface. In their study, it was noted that budesonide is a relatively cohesive material, and it would be expected that during blending agglomerates may be produced [11, 12]. Indeed, an investigation on the blending dynamics of a budesonide-lactose binary system indicated that content homogeneity does not increase with blending time, as might be expected with an adhesive drug. Instead, the system exhibits a erratic blend uniformity profile, where the coefficient of variation declines as drug particles are distributed over the carrier particle surface, only to increase as drug segregates from the carriers. Combined, the low mass and reduced surface area would result in considerable drug particle agglomerate formation during blending in a traditional orbital mixer. Consequently, when these drug particle aggregates are emitted from an inhaler possessing a powder dispersion mechanism incapable of disrupting the agglomerates, extensive ‘throat’ deposition would be expected to occur.

One possible method to combat the formation of agglomerates is to include high density additives to supply the requisite abrasion mechanism that the low density polystyrene beads cannot provide. This approach was examined in the previous chapter, where polypropylene (density =  $1.0 \text{ g/cm}^3$ ) and steel (density =  $7.6 \text{ g/cm}^3$ ) beads were added to the formulation prior to blending. Significant improvements in aerosol performance were observed for the steel bead additives relative to a control formulation that did not include any blending additives, as RF values increased from 28% to 34%. However, the performance enhancement was minimal, and a more effective approach was sought. Specifically, the potential of a novel coating method to deposit the micronized drug particles onto the surface of the bead in their primary particle size (1 – 5  $\mu\text{m}$ ) was explored.

## **8.2. EXPERIMENTAL**

### **8.2.1. Materials**

Micronized budesonide (EP grade) was purchased from Spectrum Chemical (CA, USA) and used as received. Porous polystyrene beads (Fairfield Processing Corp., CT, USA) were purchased locally. As described in Chapter 7, the polystyrene carriers were manually sieved to collect beads with diameters between 4.38 mm and 5.38 mm. Analytical grade ethanol was purchased from Sigma (Sigma-Aldrich Corp., MO, USA).

### **8.2.2. Traditional Coating of Polystyrene Beads**

Individual batches consisted of three polystyrene beads placed into a 30 mL glass vial following the addition of 5 mg of micronized drug powder. The vial was sealed and blended with a Turbula® orbital mixer (Glen Mills, NJ, USA) for 40 minutes at 46 RPM. These parameters are identical to those employed in the lactose formulation studies of Chapters 3 – 6. Following blending, the beads were dropped approximately 30 cm onto an aluminum mesh to remove any loosely adhered powder. The beads were stored in a desiccator for 3 days prior to use.

### **8.2.3. Piezo-Assisted Coating of Polystyrene Beads**

To coat the polystyrene beads, 5 mg of micronized drug powder was added to a 30 mL scintillation vial. For each coating 'batch,' three polystyrene beads with diameters between 4.38 – 5.38 mm were added to the vial containing the drug powder. The vial was sealed and the bottom half was submerged in an ultra-sonicating water bath (Fisher Scientific, NH, USA). When the vial is placed in the water bath, the energy imparted to the powder by the sonics serves to aerosolize a fraction of the powder bed, creating a sustained plume as powder is continuously aerosolized, then slowly deposits back to the powder bed via gravitational settling, and then is aerosolized once more. Throughout the coating period the beads are continuously exposed to the aerosol cloud, and as the aerosolized drug particles deposit, some will land on the bead surface where initially they adhere directly to the bead via van der Waals interactions. With continued drug deposition, particles will begin to deposit on top of other drug particles,

adhering directly to them rather than to the surface of the polystyrene. Accordingly, initial coating of the drug is an adhesive-driven process, as coating is governed by the affinity between the drug and bead surface. By contrast, subsequent coating is influenced by cohesive interactions between the drug particles.

Unless otherwise specified, the beads were coated for 2 minutes. During coating, the vial was rotated slowly from side-to-side, allowing the beads to roll across the powder, thereby exposing the entire surface to the emitted drug particles. Following coating, the beads were removed from the scintillation vial and dropped approximately 12 inches onto an aluminum mesh to remove any loosely adhered drug particles and agglomerates. The drug-coated polystyrene beads were then stored in a desiccator for 3 days prior to use.

#### **8.2.4. Scanning Electron Microscopy (SEM)**

Drug coating of the carrier particles was assessed using scanning electron microscopy (SEM; Supra 40VP, Zeiss, Germany). To accommodate the large beads, following initial bead placement onto a stage covered with double-sided conductive tape, the sides of the tape were folded against the bead and then transixed with a metal pin, piercing both the tape and the bead to allow adequate conduction. Prior to imaging, approximately 20 nm of a platinum::palladium (80::20) mixture was deposited onto the beads via sputter coating.

#### **8.2.5. In vitro Aerosol Performance**

The aerosol performance of the drug-coated polystyrene beads was evaluated in vitro using a next generation cascade impactor (NGI; MSP Corp., MN, USA) at  $60 \text{ L min}^{-1}$ , with a 4-second actuation time. For each actuation, a single bead (diameter 4.38 – 5.38 mm) was placed into the capsule chamber of either the Aerolizer™ (Plastiap S.p.A., Italy) or the Handihaler™ (Boehringer Ingelheim, CT, USA). Following actuation, the capsule, dispersion chamber, mouthpiece, mouthpiece adaptor, and induction port were each rinsed with 10 mL of EtOH, and the stages of the NGI were each rinsed with 5 mL. The amount of budesonide depositing on each component was quantified by UV-VIS spectroscopy using an Infinite M200



microplate reader equipped with a cuvette port (Tecan US, Inc., NC, USA) at 244 nm. For each impaction, the total amount of drug collected from the bead, inhaler, mouthpiece adaptor, induction port, pre-separator, and NGI stages is defined as the recovered dose. The emitted fraction (EF) is the percentage of the recovered dose collected from the mouthpiece adaptor, induction port, pre-separator, and NGI stages. The fine particle fraction (FPF) is provided as the percentage of the emitted dose collected from stage 3 – 8 of the NGI. The respirable fraction (RF) is the ratio of the drug collected from stages 3 – 8 of the NGI, over the recovered dose.

### **8.3. RESULTS AND DISCUSSION**

#### **8.3.1. Influence of Device on Performance**

The *in vitro* performance of drug-coated polystyrene beads dispersed through either the Aerolizer or Handihaler at  $60 \text{ L min}^{-1}$  is shown in Figure 8.2. As mentioned in the previous chapter, the device retention in the Aerolizer typically exceeds 50% of the total dose. This performance is repeated in the present study, as only 42% of the dose was emitted from this inhaler. By contrast, device emission from the Handihaler was very efficient, with 85% of the total dose emitted from this device. To explain this disparity in delivery efficiency, a closer examination of the respective mechanism governing bead motion within the two devices is required.

The operating mechanism of the Aerolizer was discussed in detail previously in chapter 7. In this device, the drug-coated beads collide repeatedly with the mesh and inner walls of device due to the tangential air inlets located on opposite sides of the dispersion chamber [13]. Throughout device actuation, the bead continuously rattles as it collides with multiple sections of the inner device geometry, and with the combined influence of the flow stream, detaches the drug particles from the surface of the bead. However, these physical collisions between the drug-coated beads and the device causes drug to rub-off onto the inhaler walls, where it remains adhered.

In contrast to the dual tangential inlets of the Aerolizer, the Handihaler employs a single cylindrical air inlet, 3.5 mm in diameter [14]. The air inlet opens into the dispersion chamber

(diameter = 7.6 mm) where the capsule is located. While the geometry is more straightforward than that of the Aerolizer, a unique fluid phenomena known as sudden flow stream expansion arises from this configuration.

Sudden expansion of a flow stream occurs when a small volume channel abruptly opens to a larger volume chamber (Figure 8.3). When this happens the flow stream decelerates as it enters the larger volume, detaching from the inner walls of the channel at the corner of the expansion, and reattaching downstream of this transition region [15]. However, a portion of the flow is detached, and rather than proceeding downstream with the bulk of the flow, recirculates as a turbulent eddy at the corner of the abrupt volume expansion, causing a pressure loss. Figure 8.4 depicts the static pressure profile through the dispersion chamber of the Handihaler as the volumetric flow rate is varied. It is noted that the pressure gradient that develops across the dispersion chamber increases with the volumetric flow rate. For example, pressure values range from approximately  $-2.5 \times 10^2$  to  $6 \times 10^1$  Pa at  $30 \text{ L min}^{-1}$ . When the flow rate is raised to  $60 \text{ L min}^{-1}$  the disparity in static pressure across the dispersion chamber also increases, ranging from  $-8 \times 10^2$  to  $3 \times 10^2$  Pa. As depicted in Figure 8.4, the low pressure region is located at the corner of the volume expansion.

In contrast to the Aerolizer, where the motion of the beads is similar regardless of bead diameter, the dynamic profile varies considerably with diameter in the Handihaler. When a small bead (diameter  $< 4.5 \text{ mm}$ ) is placed in the dispersion chamber of the Handihaler, the incoming flow carries the bead forward and pushes it against the mesh, where it is held stationary for the duration of the flow stream. Conversely, when a large bead (diameter  $> 6 \text{ mm}$ ) is employed, it is confined primarily to the rear of the dispersion chamber, where it oscillates weakly, repeatedly colliding against the base of the dispersion chamber adjacent to the inlet.

Based on the fluid profile that develops in the Handihaler as the inlet transitions abruptly into the dispersion chamber, it is speculated that the small diameter beads are not influenced by the low pressure region in the corner of the expansion. Accordingly, they primarily, if not exclusively, experience the force of the incoming flow stream, which carries them toward the mesh located opposite the inlet. Alternatively, the motion of the large

diameter beads in the dispersion chamber is greatly influenced by the low pressure region, to the extent that despite the incoming flow stream pushing the bead toward the mesh, the bead is retained in the region adjacent to the inlet, oscillating weakly as it is simultaneously acted upon by the two forces, though the backward force of the low pressure regions appears to be predominate.

This is supported by the observation that when a polystyrene bead with an approximate diameter between 4.5 – 5.5 mm is placed in the Handihaler, it oscillates rapidly near the center of dispersion chamber. In this case, the diameter of the bead allows it to be influenced nearly equally by the incoming flow stream, which carries it forward, and the low pressure region, which pulls it in the opposite direction. During inhalation, the forces act in unison to rapidly oscillate the low density bead. For the specific geometry of the Handihaler, the bead diameter that functions best is fixed between 4.5 – 5.5 mm. This diameter will vary according to both the diameter of the dispersion chamber, and the ratio of the dispersion chamber diameter to the diameter of the air inlet.

In light of these observations, the high emitted fraction from the Handihaler relative to the Aerolizer is better understood, as in the latter device the bead undergoes repeated physical impactions with the inhaler walls, while in the Handihaler the bead oscillates primarily in the center of the dispersion chamber, and physical collisions with the device are minimal. However, the higher emitted fractions obtained from the Handihaler did not translate into improved aerosol performance from this device relative to the Aerolizer. The fine particle fraction from beads dispersed from the Handihaler was only 40%, while the Aerolizer produced significantly higher FPF values of 64%. In contrast to the Aerolizer, where the majority of the emitted dose reaches the lower stages of the cascade impactor, approximately 48% of the emitted dose from the Handihaler deposits in the induction port. Accordingly, overall performance in terms of respirable fraction was comparable between drug-coated beads actuated from the Aerolizer and Handihaler.

The tangential inlets of the Aerolizer have been shown to produce rather large turbulence levels within the dispersion chamber, specifically in the absence of a capsule [16].

This may explain the greater powder dispersion observed from this device, where FPF values exceeded 60%. In contrast to the Aerolizer, which has been extensively studied by computational fluid dynamics, published studies examining the turbulence levels within the Handihaler are not available [16 - 19]. However, from the data it is clear that that ability of the Handihaler to detach and emit drug from the device is superior to the Aerolizer, while the Aerolizer provides more extensive powder dispersion. This trend is not exclusive to the drug-coated polystyrene beads, as similar results were observed in Chapter 5, when lactose carrier DPI formulations were dispersed from both inhalers.

While the overall drug deposition was not significantly greater through the Handihaler, the extremely high emitted fraction made it a more ideal device for the drug-coated polystyrene beads compared to the Aerolizer. As it was speculated that the high induction port deposition was primarily due to agglomerated drug particles that were not effectively dispersed following detachment, a novel method to coat drug onto the bead surface as primary particles was investigated.

### **8.3.2. Influence of Coating Method**

As previously mentioned, the very low surface area of the polystyrene beads ensures that drug particles will interact extensively during blending, and coupled with the low mass of these carriers, the aggregates that form will not be effectively disrupted. Accordingly, an alternative approach to coating the beads would be to modulate the nature of the interaction between drug particles, preventing the formation of large, stable agglomerates. To achieve this, it was proposed to coat the bead by initially aerosolizing the drug powder into primary particles, then allowing the particles to deposit onto the surface of the polystyrene bead where they may remain adhered via Van der Waals forces. In this way, the drug particles will deposit on top of each other through a random process. This contrasts with traditional blending, where repeated contact occurs between drug particles as the powder continuously cascades within the vial, allowing the drug particles repeated opportunities to encounter other particles with orientations that may yield a strong cohesive interaction.

#### 8.4. PIEZO-ASSISTED COATING (PAC)

To compensate for the diminished surface area of the polystyrene beads and decrease the extent of drug agglomerates coating the bead surface, a novel coating method was developed that employed piezoelectric energy to aerosolize micronized drug powder onto the polystyrene beads. An overview of the method is depicted in Figure 8.5, and the coating process is described in detail in the 'Experimental' section of this chapter.

As seen in the SEM micrographs in Figure 8.6, traditional coating produced patches of drug powder distributed sporadically over the bead surface. Closer examination indicated these were composed primarily of dense powder aggregates. During actuation these powder compacts may be released largely intact, and in the absence of effective particle dispersion deposit in the induction port and pre-separator. By contrast, the PAC method yielded a more uniform distribution of powder on the bead surface, where the powder appeared as distinct primary particles as opposed to the dense aggregates observed during standard blending. It is noted that the mass of budesonide coated by the PAC method (200 – 300 mcg) was on average much lower than that produced by standard blending (600 – 900 mcg). However, the coating masses from the PAC method were comparable to those found in commercial products for the pulmonary delivery of a budesonide powder, where the nominal dose can range between 100 – 400 mcg [20, 21].

The *in vitro* performance from polystyrene beads coated by either standard blending or PAC is shown in Figure 8.7. As speculated, while the EF values were similar between the two coating methods, significantly lower induction port deposition occurred using the PAC method, resulting in greater overall performance as FPF and RF was significantly higher ( $p < 0.05$ ) relative to the standard coating method. The combination of powder dispersion through the Handihaler with the PAC method improved overall drug deposition (as measured by RF) from 28% up to 45%.

## 8.5. MODULATING DRUG COATING

While the coating levels of budesonide observed with the PAC method are within the range typically delivered by commercial devices, the ability to accurately control the dose coated onto the beads is essential. Accordingly, the potential parameters that influence overall coating mass were investigated. For the initial studies the coating time was altered, and beads were coated with budesonide for 1, 2, 5 and 10 minutes and the drug depositing on their surface quantified following the standard drop from a short distance to remove any loosely adhered powder. As the beads ranged in size from 4.38 – 5.38 mm, the dose was normalized to the bead diameter, yielding a strong relationship ( $R^2 = 0.992$ ) between coating time and drug deposition (in terms of mcg of drug per bead diameter in millimeters) (Figure 8.8). It is noted that the relationship is not linear, as doubling the coating time does not double the dose. However, as coating time was increased so too did the amount of drug coated on the bead surface, with the 1-minute coating time providing the lowest overall coating levels (64 mcg/mm) and the 10 minute time the highest (128 mcg/mm), demonstrating that moderately high doses of budesonide, in excess of 500 mcg, are achievable by the PAC method when the coating time is prolonged.

In the preceding PAC examples, the beads were placed directly in the powder bed, resulting in hundreds of micrograms of drug being coated onto their surface. For situations requiring low drug doses, a different approach was examined where the beads were removed from the micronized drug and coated while being held a fixed distance above the powder bed. During the PAC method the coating vial is filled by an aerosol cloud, as the powder is continuously fluidized by the piezoelectric energy provided by the sonicating water bath. It was speculated that holding the bead above the powder bed would still allow drug deposition onto the bead surface (as the bead will be located within the aerosol cloud), but to a lesser extent relative to when the bead is directly in the powder. Examples of the low dosing ranges that are targeted include the SPIRIVA® (22 mcg of tiotropium bromide per dose) and FORADIL (12 mcg of formoterol fumarate) formulations, delivered from the Handihaler and Aerolizer, respectively [22, 23].

For this study, the beads were held either 10 mm or 25 mm above the powder bed, and compared against the coating masses attained when the bead is placed directly in the powder. As with the coating-time study, due to the minor variations in bead size the drug mass depositing on the bead surface was normalized to bead diameter (Table 8.1). When the bead is held 10 mm above the powder bed, coating levels ranged between 27 – 31 mcg, as an average of 5.6 mcg/mm were coated compared to 65 mcg/mm when the bead is directly in the powder. Elevating the bead further to 25 mm above the powder reduces drug coating to approximately half that of the 10 mm distance, with coating levels of 2.4 mcg/mm, yielding 11 – 13 mcg total per bead, comparable to the nominal dose delivered by the Aerolizer [22].

## **8.6. CONCLUSIONS**

In this chapter, the potential of an alternative dispersion mechanism to improve the emitted fraction from drug-coated polystyrene beads was evaluated. During the screening study described in Chapter 7, large drug-coated beads were dispersed in the Aerolizer DPI resulting in repeated, physical collisions between the bead and inner walls of the device. For low-density polystyrene beads, over half the dose remained adhered to the inhaler following actuation such that despite the good powder dispersion levels exhibited from this device overall drug delivery remained below 30% of the nominal dose. In contrast to the physical collisions between the bead and device in the Aerolizer, when the bead was actuated from the Handihaler it oscillated rapidly within the center of the dispersion chamber and physical collisions between the device and bead were infrequently observed. However, despite the absence of physical collisions between the bead and inhaler, it is speculated that the momentum transfers that arise due to the rapid and continuous acceleration changes of the bead as it oscillates provide sufficient detachment forces to promote effective drug delivery. This was supported by the high emitted fraction exhibited by the Handihaler, where EF values were approximately double those obtained through the Aerolizer.

Although the delivered dose obtained from the Handihaler made it better suited to optimize performance of the drug-coated polystyrene beads, the higher EF values did not yield improved overall performance, as extensive induction port deposition from the Handihaler

resulted in RF values comparable to those from the Aerolizer. To improve performance by lowering the 'throat' deposition, a coating method was developed to inhibit the extensive drug agglomerates that were formed during traditional blending of drug with the beads. The novel PAC method employed piezoelectric energy from a sonicating water bath to aerosolize the drug powder into primary particles, which were then able to deposit on the bead surface and adhere via van der Waals forces. Combined with the dispersion mechanism of the Handihaler, the PAC method produced RF values of 45%. Additionally, the ability to modulate the dose by adjusting the coating time and the bead distance from the powder bed was demonstrated, permitting a range of drug masses of approximately 10 – 500 mcg to be coated onto the bead. In the following chapter, the precise bead size to maximize oscillations and optimize performance will be assessed. Additionally, the potential of the drug-coated beads to provide flow rate independent performance through the Handihaler will be evaluated.



## 8.7. REFERENCES

1. T.M. Crowder, and Donovan, M.J. Controlled Pulmonary Drug Delivery, Springer, New York, 2011.
2. N. Islam and E. Gladki. Dry powder inhalers (DPIs)—A review of device reliability and innovation. *Int J Pharm.* 360:1-11 (2008).
3. H.W. Frijlink and A.H. De Boer. Dry powder inhalers for pulmonary drug delivery. *Expert Opin Drug Deliv.* 1:67-86 (2004).
4. T.M. Crowder, Louey, M.D., Sethuraman, V.V., Smyth, H.D.C., and Hickey, A.J. An odyssey in inhaler formulation and design. *Pharmaceutical Technology.* 7:99 - 107 (2001).
5. A.H. de Boer, Gjaltema, D., and Hagedoorn, P. Inhalation characteristics and their effects on *in vitro* drug delivery from dry powder inhalers Part 2: Effect of peak flow rate (PIFR) and inspiration time on the *in vitro* drug release from three different types of commercial dry powder inhalers. *Int J Pharm.* 138:45 - 56 (1996).
6. A.H. de Boer, Gjaltema, D., and Hagedoorn, P. Inhalation characteristics and their effects on *in vitro* drug delivery from dry powder inhalers. Part 2: Effect of peak flow rate (PIFR) and inspiration time on the *in vitro* drug release from three different types of commercial dry powder inhalers. *Int J Pharm.* 138:45 - 56 (1996).
7. A. Voss, and Finlay, W.H. Deagglomeration of dry powder pharmaceutical aerosols. *Int J Pharm.* 248:39 - 50 (2002).
8. B. Dickhoff. The effect of carrier surface and bulk properties on drug particle detachment from crystalline lactose carrier particles during inhalation, as function of carrier payload and mixing time. *Eur J Pharm Biopharm.* 56:291-302 (2003).

9. M.P. Flament, P. Leterme, and A. Gayot. The influence of carrier roughness on adhesion, content uniformity and the in vitro deposition of terbutaline sulphate from dry powder inhalers. *Int J Pharm.* 275:201-209 (2004).
10. B. Dickhoff, A. Deboer, D. Lambregts, and H. Frijlink. The interaction between carrier rugosity and carrier payload, and its effect on drug particle redispersion from adhesive mixtures during inhalation. *Eur J Pharm Biopharm.* 59:197-205 (2005).
11. P. Begat, Morton, D.A.V., Staniforth, J.N., and Price, R. The cohesive-adhesive balances in dry powder inhaler formulations I: Direct quantification by atomic force microscopy. *Pharm Res.* 21:1591 - 1597 (2004).
12. P. Begat, Morton, D.A.V., Staniforth, J.N., and Price, R. The Cohesive-Adhesive balances in dry powder inhaler formulations II: Influence on fine particle delivery characteristics. *Pharm Res.* 21:1826 - 1833 (2004).
13. M.S. Coates, H.-K. Chan, D.F. Fletcher, and J.A. Raper. Influence of Air Flow on the Performance of a Dry Powder Inhaler Using Computational and Experimental Analyses. *Pharm Res.* 22:1445-1453 (2005).
14. H. Wachtel, Ertunc, O., Koksoy, C., and Delgado, A. Aerodynamic Optimization of Handihaler and Respimat: The Roles of Computational Fluid Dynamics and Flow Visualization. *Respiratory Drug Delivery* 2008. 1:165 - 174 (2008).
15. V. Gupta, and Gupta, S.K. *Fluid Mechanics and Its Applications*, New Age International, New Delhi, 1984.
16. M.S. Coates, D.F. Fletcher, H.K. Chan, and J.A. Raper. The role of capsule on the performance of a dry powder inhaler using computational and experimental analyses. *Pharm Res.* 22:923-932 (2005).
17. M.S. Coates, D.F. Fletcher, H.K. Chan, and J.A. Raper. Effect of design on the performance of a dry powder inhaler using computational fluid dynamics. Part 1: Grid

- structure and mouthpiece length. *Journal of Pharmaceutical Sciences*. 93:2863-2876 (2004).
18. M.S. Coates, H.K. Chan, D.F. Fletcher, and J.A. Raper. Influence of air flow on the performance of a dry powder inhaler using computational and experimental analyses. *Pharm Res*. 22:1445-1453 (2005).
  19. M.S. Coates, H.K. Chan, D.F. Fletcher, and H. Chiou. Influence of mouthpiece geometry on the aerosol delivery performance of a dry powder inhaler. *Pharm Res*. 24:1450-1456 (2007).
  20. K. Wetterlin. Turbuhaler: A new powder inhaler for administration of drugs to the airways. *Pharm Res*. 5:506 - 508 (1988).
  21. H. Bisgaard, B. Klug, B.S. Sumby, and P.K.P. Burnell. Fine particle mass from the Diskus inhaler and Turbuhaler inhaler in children with asthma. *Eur Respir J*. 11:1111-1115 (1998).
  22. N.Y.K. Chew, and Chan, H.K. In Vitro Aerosol Performance and Dose Uniformity between the Foradile® Aerolizer® and the Oxis® Turbuhaler®. *Journal of Aerosol Medicine*. 14:495 - 501 (2001).
  23. S. Chodosh, Flanders, J.S., Kesten, S., Serby, C.W., Hochrainer, D., and Witek, T.J. Effective Delivery of Particles with the HandiHaler® Dry Powder Inhalation System over a Range of Chronic Obstructive Pulmonary Disease Severity. *Journal of Aerosol Medicine*. 14:309 - 315 (2001).

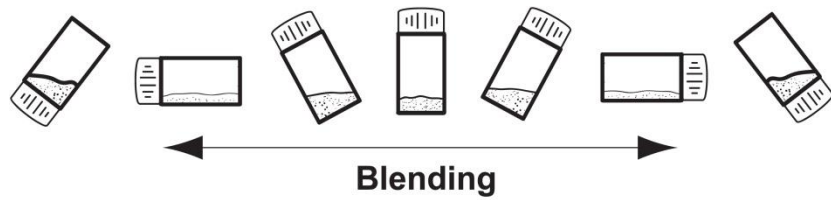


Figure 8.1. Illustration of Powder Motion during Blending in a Turbula® Orbital Mixer.

For standard blending of lactose carrier particles with micronized drug, the powders are mixed using a Turbula® orbital blender. In this method, the vial is continuously rotated, inducing the powder to cascade from one end of the vial to the other. This blending process typically exhibits excellent drug content uniformity, as the repeated abrasion of the drug powder by the coarse carriers effectively disrupts drug agglomerates.

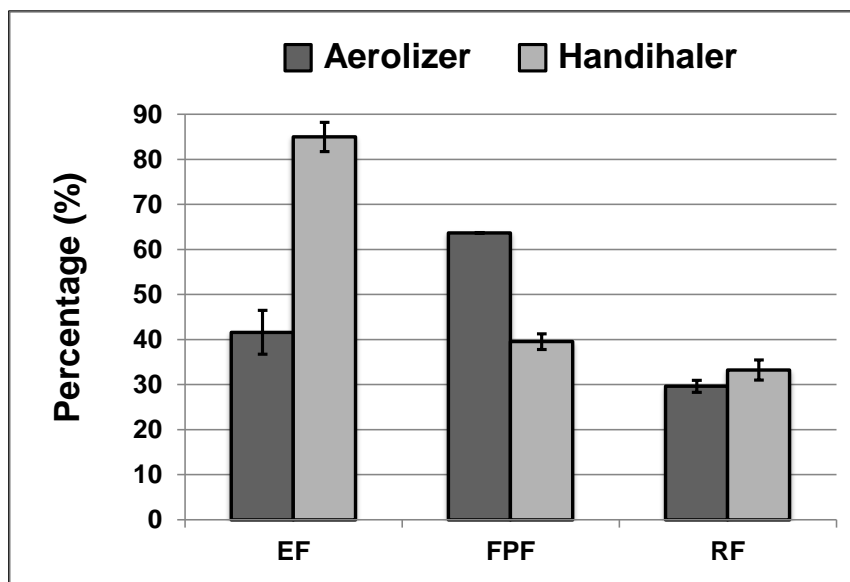


Figure 8.2. Aerosol Performance of Budesonide-Coated Polystyrene Beads from the Aerolizer and Handihaler DPIs

The *in vitro* aerosol performance of budesonide-coated polystyrene beads (diameters between 4.38 - 5.38  $\mu\text{m}$ ) was evaluated at 60 L  $\text{min}^{-1}$  through the Aerolizer<sup>TM</sup> and Handihaler<sup>TM</sup> DPIs. Opposing trends in emitted fraction (EF) and fine particle fraction (FPF) yielded comparable respirable fractions (RF) from the two inhalers. Values are provided as the mean ( $\pm$  standard deviation) for N = 3 replicates.

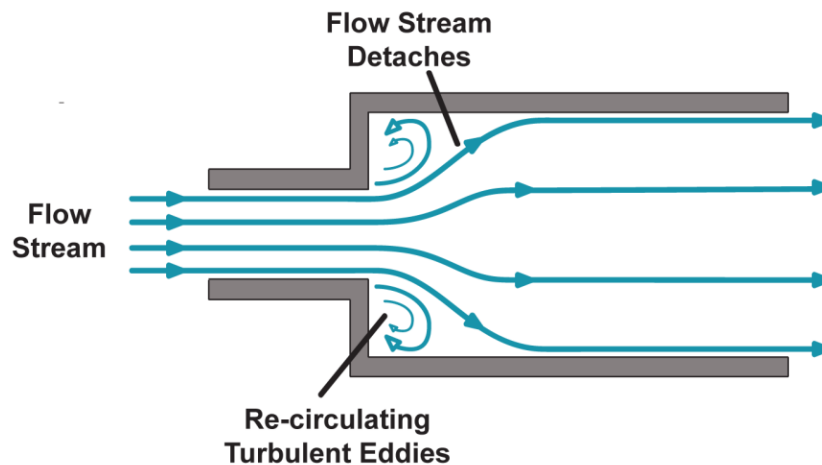


Figure 8.3. Sudden Expansion of a Flow Stream (Adapted from Gupta, et al, 1984).

In the Handihaler, the 3.5 mm diameter inlet opens abruptly to the 7.6 mm diameter dispersion chamber. When a flow stream travels through such a volume expansion, it decelerates as it flows into the larger chamber, and the boundary layer that forms in the narrow chamber detaches at the corner of the expansion. This results in an annular region developing at the corner of the volume expansion, where the fluid does not continue downstream, but recirculates as an eddy. These eddies induce a pressure loss, causing a reduction in the mechanical energy carried by the flow, and are generally avoided.

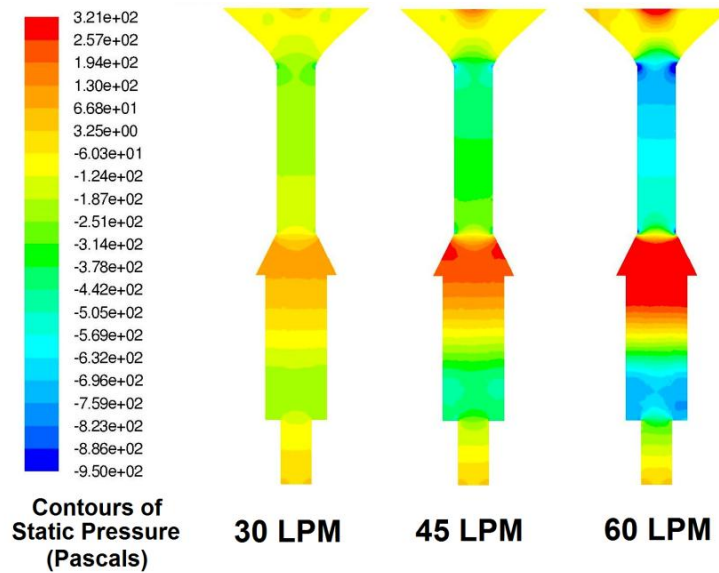


Figure 8.4. Static Pressure Contours Across the Handihaler Dispersion Chamber at 30, 45, and 60 L min<sup>-1</sup>.

When a flow stream passes from the inlet to the dispersion chamber of the Handihaler, it encounters a sudden volume expansion. This phenomenon results in a pressure gradient developing across the dispersion chamber, where the low pressure region is located at the corner of the expansion. The pressure gradient increases with increasing flow rate through the device. This image was produced using the computational fluid dynamic (CFD) software Fluent® (Fluent Inc. (2006), NH, USA). Image courtesy of Shaun Kim.

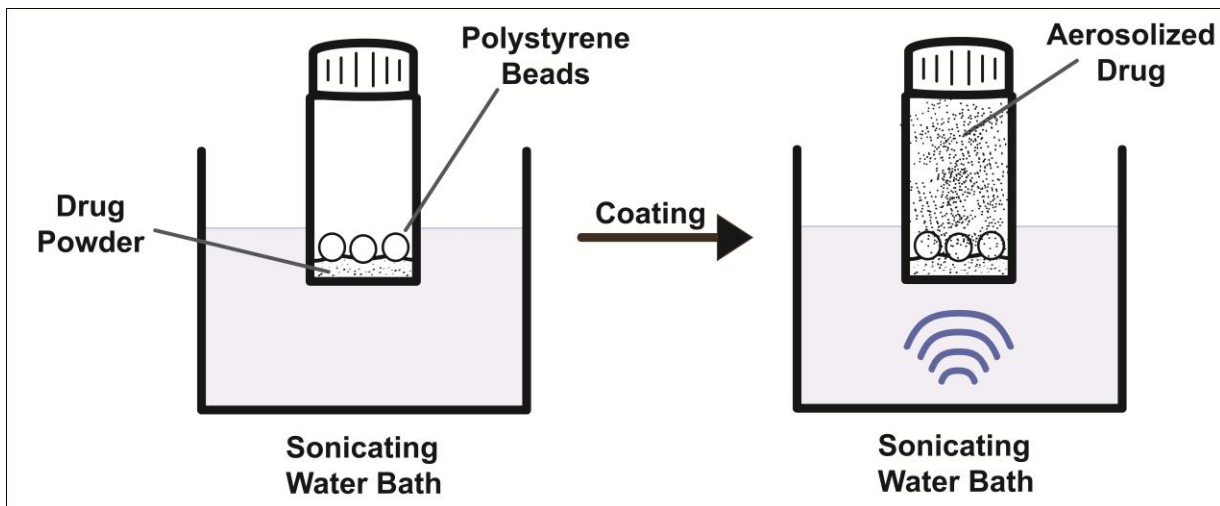


Figure 8.5. Illustration of Piezo-Assisted Coating (PAC) Process for Coating Polystyrene Beads

To limit the extent of drug agglomerates, a piezo-assisted coating (PAC) method was developed to aerosolize the drug particles and then allow them to settle onto the bead surface and remain adhered through van der Waals interactions. A vial containing the beads and micronized powder is placed within a sonicating water bath, where the energy of the sonics fluidizes a portion of the powder bed, creating a sustained aerosol plume of dispersed drug particles.



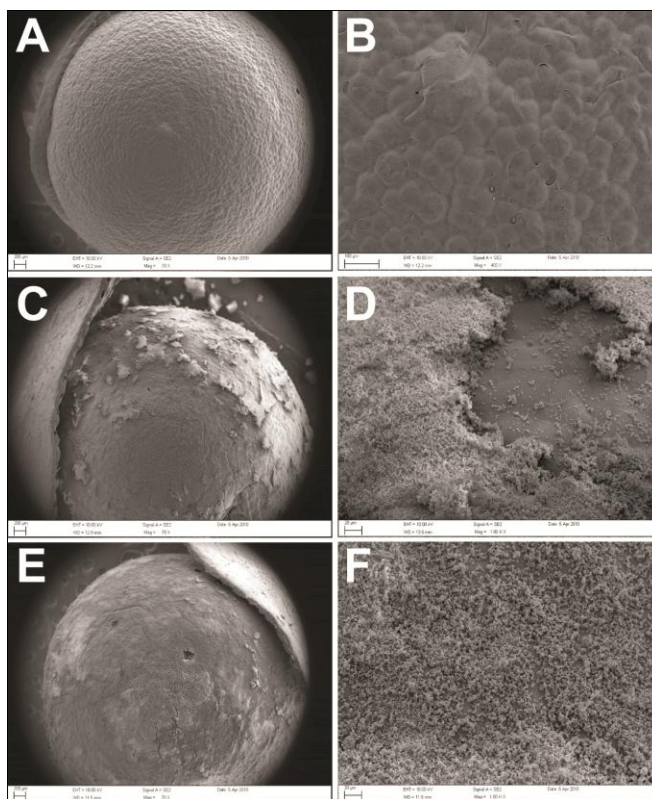


Figure 8.6. SEM Images of Uncoated Polystyrene Beads, and Beads Coated with Budesonide via Standard Blending or with the PAC Method.

Budesonide-coated polystyrene beads were imaged via SEM to evaluate the potential of the two coating methods to minimize the formation of stable drug agglomerates. SEM images of uncoated polystyrene carriers (Figures A – B) indicate that the beads are not perfectly spherical as assumed, but possess a degree of surface roughness. The beads were coated using standard blending in a Turbula® orbital mixer (Figures C – D) or via the piezo-assisted coating method (Figures E – F). To accommodate the polystyrene carriers, the beads were lightly pressed down onto a stage covered with double-sided conductive tape, and then the sides of the tape were folded against the bead and transfixed with a metal pin, piercing both the tape and the bead to permit adequate conduction.

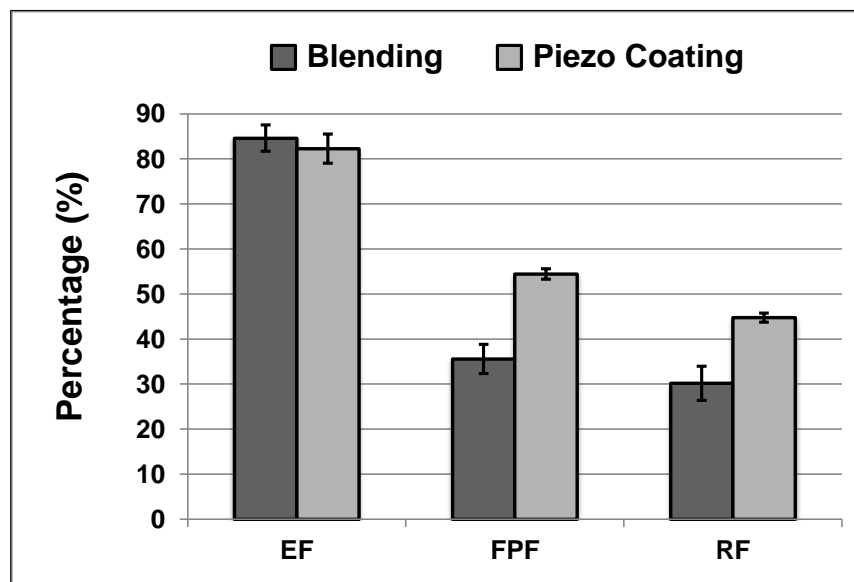


Figure 8.7. *In Vitro* Aerosol Performance of the PAC Method.

The *in vitro* aerosol performance of budesonide-coated polystyrene beads (diameters between 4.38 - 5.38 mm) at 60 L min<sup>-1</sup> through the Handihaler DPI. The beads were coated either with the standard method in a Turbula® orbital blender, or using the piezo-assisted coating (PAC) method. Values are provided as the mean (± standard deviation) for N = 3 replicates. While both methods produced comparable emitted fractions (EF), the fine particle fraction (FPF) and respirable fraction (RF) values were significantly improved by the PAC method.

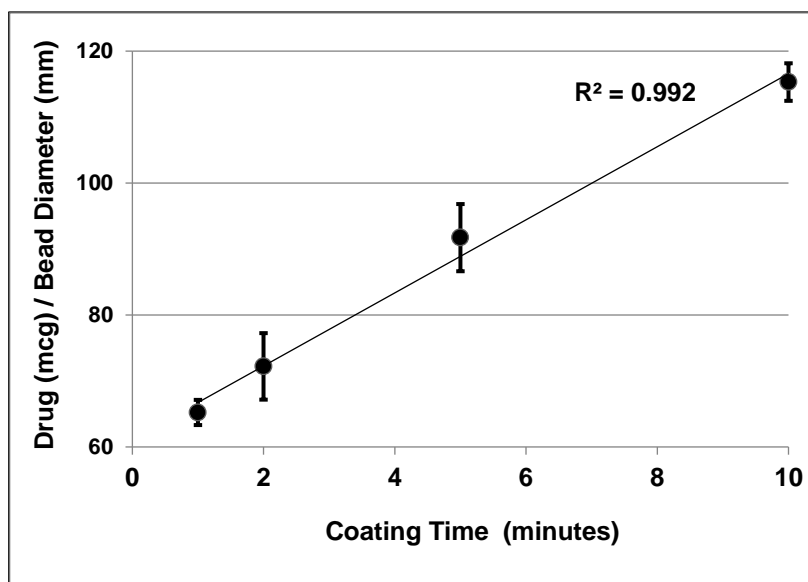


Figure 8.8. Coating Time Studies using the PAC Method

To evaluate influence of coating time using the PAC method, polystyrene beads were coated for 1, 2, 5, or 10 minutes. To normalize for bead diameter, the total drug mass recovered following coating was divided by the bead diameter as measured using calipers. Values are provided as the mean ( $\pm$  standard deviation) for N = 3 replicates.

Table 8.1. Drug Coating as a Function of Bead Distance

	<b>Bead Distance from Powder Bead (mm)</b>		
	<b>0</b>	<b>10</b>	<b>25</b>
Total drug mass per bead diameter (mcg/mm)	65.2 (1.9)	5.6 (0.3)	2.4 (0.2)
Total Drug Mass per Bead (mcg)	327 - 333	27 - 31	11 - 13

Previous studies have coated the beads while they were directly in the powder bed. To evaluate the potential to coat lower drug masses, the beads were held either 10 mm or 25 mm above the powder bed during the 2-minute coating period. The coating levels are compared to beads that were coated while directly in the powder bed. To normalize for bead diameter, the total drug mass recovered following coating was divided by the bead diameter as measured using calipers. Values are provided as the mean ( $\pm$  standard deviation) for N = 3 replicates.

## CHAPTER 9

### 9. Refinement and Optimization of Large Carrier Particle Dispersion Technology

#### 9.1. INTRODUCTION

Passive dry powder inhalers are completely dependent on the inspiratory effort generated by the patient to aerosolize and disperse the dose. However, due to marked differences between patients, particularly with regards to age and disease state, there is considerable variation in the inspiratory effort that a patient can produce through a given device. Consequently, aerosol performance varies considerably between patients. For example, patients with severe COPD were reported to inhale through the Handihaler with a median flow rate of  $35 \text{ L min}^{-1}$ , in contrast to patients with mild COPD, who generated a median flow of  $45 \text{ L min}^{-1}$  through this inhaler [1]. An additional study examining patient flow rates through the Handihaler noted that approximately one-quarter of COPD patients with a severe condition were unable to achieve a flow rate of  $20 \text{ L min}^{-1}$ [2]. *In vitro* deposition studies of tiotropium delivered from the Handihaler reported that at  $20 \text{ L min}^{-1}$  only 16% of the nominal dose is delivered, as opposed to 22% at  $28.3 \text{ L min}^{-1}$ . Accordingly, many of the patients who would most benefit from inhalation therapy are those least capable of producing sufficient flow rates to adequately disperse the powder.

In the two preceding chapters, a candidate carrier bead material was selected and matched to a dispersion mechanism that demonstrated high dose delivery from a commercial dry powder inhaler. When the beads are placed in dispersion chamber of a Handihaler, they can oscillate rapidly due to the opposing fluid forces that simultaneously act upon them. The extremely low density of the polystyrene beads could potentially enable them to oscillate at very low rates, where traditional lactose carrier particles have been shown to perform poorly, thus allowing the drug-coated bead to provide efficient drug dispersion performance independent of inspiratory effort.

### *Specific Aim*

The specific aim of this chapter is to obtain a thorough mechanistic understanding of the parameters that govern the performance of the drug-coated bead through the Handihaler. Beads were photographed during actuation within the Handihaler, and their dynamic profiles compared to that of standard capsules. In addition, as the beads emit a loud ‘rattling’ sound during actuation, their acoustic signals were recorded to assess the frequency of their oscillations. To evaluate the potential for the large carriers to function effectively independent of flow rate, the aerosol performance of the drug-coated polystyrene beads are compared to that of traditional binary blends using both a corticosteroid and a  $\beta$ -agonist at 15, 30 and 45 L  $\text{min}^{-1}$ .

## **9.2. EXPERIMENTAL**

### **9.2.1. Materials**

Budesonide and salbutamol were both purchased in bulk (Jinhua Chemical Company, China) and micronized with a high energy jet-mill with respective pusher and grinding pressures of 80 and 110 PSI (Aljet; Fluid Energy Processing and Equipment Co., PA, USA). Respitose® ML006 inhalation-grade lactose was generously provided by DMV-Fonterra (New Zealand) and used as received. Size-3 gelatin capsules were provided by Capsugel (NJ, USA).

### **9.2.2. Physical Characterization of Carrier Particles**

The size distribution and drug coating on the lactose carrier particles was visually assessed by scanning electron microscopy (SEM; Supra 40VP, Zeiss, Germany). Prior to SEM, approximately 20 nm of a platinum::palladium (80::20) mixture was deposited onto the particles via sputter coating. SEM was also performed on both uncoated and drug-coated polystyrene beads. To accommodate the polystyrene carriers, the beads were lightly pressed down onto a stage covered with double-sided conductive tape. The sides of the tape were then folded against the bead and transixed with a metal pin, piercing both the tape and the bead to permit

adequate conduction. As with the lactose particles, prior to imaging approximately 20 nm of a platinum::palladium (80::20) mixture was deposited onto the beads via sputter coating.

Powders were sized via laser diffraction using a Sympatec HELOS (Sympatec GmbH, Germany) apparatus equipped with a 6-mL cuvette dispersing system. Mineral oil was used as the dispersing fluid, which included 1% Span 85 to aid in particle de-aggregation. The powders were suspended in the mineral oil and, if physically stable, sonicated for 60 seconds to disrupt aggregates. Measurements were collected following elimination of all visible air bubbles. The ‘forced stability’ option was used to ignore the signal from errant dust or residual air bubbles.

The specific surface area of the lactose carrier particles was determined via nitrogen adsorption with a single-point BET method using a Monosorb<sup>®</sup> surface area analyzer (Quantachrome Instruments; FL, USA). Samples were outgassed under nitrogen at 40 °C for 24 hours prior to each measurement. The surface area of the polystyrene beads was approximated using the equation for the surface area of a smooth sphere.

The density of the lactose carrier particles was evaluated by helium pycnometry (Quantachrome, FL, USA). For the porous polystyrene, 10 beads were weighed individually and their respective diameters measured with calipers. The volume was assumed equal to that of a sphere.

### **9.2.3. Preparation of Binary Lactose Formulations**

Budesonide and salbutamol were each mixed in a ratio of 1:50 (w/w) with ML006 inhalation-grade lactose via geometric dilution to obtain 500 mg of a 2% binary blend. The formulations were blended with a Turbula<sup>®</sup> orbital mixer (Glen Mills, NJ, USA) for 40 min at 46 RPM. Samples were stored in a desiccator at least 5 days prior to use. Blend uniformity was determined by assessing the drug content in eight 20-mg samples selected at random from each mixture. The formulations exhibited high content uniformity, with coefficients of variation between the samples for both blends below 3%.

#### 9.2.4. Drug Coating of Polystyrene Beads

To coat the polystyrene beads, 2 mg of micronized drug powder were weighed into a 30-mL scintillation vial, followed by three 5.2 mm polystyrene beads. The vial was sealed and the bottom half was submerged in a sonicating water bath (Fisher Scientific, NH, USA) for 2 minutes. When the vial is placed in the water bath, the energy imparted to the powder by the sonics aerosolizes a fraction of the powder bed, creating a sustained plume as powder is continuously aerosolized, then deposits by gravitational settling, and then is aerosolized once more. Throughout the coating period, the beads are continuously exposed to the aerosol cloud, and as the aerosolized drug particles deposit some land on the bead surface where initially they adhere directly to the surface of the bead, and then once a monolayer has been formed, subsequent drug particles adhere directly to other drug particles via van der Waals and electrostatic interactions. Due to the small size, and thus negligible mass, of the primary drug particles, van der Waals interactions overwhelm other types of forces, including gravitational forces. During coating, the vial was rotated slowly from side-to-side, permitting the bead to roll across the powder and thereby expose the entire surface to the emitted drug particles. Following coating, the bead was removed from the scintillation vial and dropped approximately 12 inches onto an aluminum mesh to remove any loosely adhered drug particles and agglomerates. The drug-coated polystyrene beads were then stored in a desiccator for 3 days prior to use.

#### 9.2.5. Measurement of Device Resistance

To evaluate the resistance of the DPI, the pressure drop (cmH<sub>2</sub>O) across the Handihaler at multiple volumetric flow rates (20, 30, 40, 50, 60, and 70 L min<sup>-1</sup>) was measured using a digital manometer (SPER Scientific; AZ, USA). The device resistance was determined by plotting the square root of the pressure drop ( $\Delta P$ ) against the flow rate (Q), with the slope of the relationship equaling the device resistance (R), as described by Clark and Hollingworth [3]:

$$\sqrt{\Delta P} = Q \times R$$



The pressure drop across the device was initially assessed with an empty dispersion chamber, and then with either a size-3 gelatin capsule (perforated with the Handihaler's piercing mechanism), or with a 5.2 mm polystyrene bead placed within the dispersion chamber. Additionally, the flow rate corresponding to a pressure drop of 4 kPa through the inhaler was also determined for each of the three configurations.

#### **9.2.6. Bead Imaging**

Images of the beads during device actuation were shot at f/22 with a 1/8 second exposure using a strobe flash (Canon Speedlite 500EX) for the solitary light source firing five times at a rate of 199 Hz. The strobe captured the position of the gelatin capsule or polystyrene bead at five distinct locations (ca.  $5 \times 10^{-3}$  seconds between each flash) within the inhaler during actuation. Long exposure photographs were captured at f/14 and 4 s to allow the imaging of both the beads and the capsules over the course of a normal inhalation profile. This method allowed the visualization of the average location of either the bead or the capsule throughout the duration of the inhalation event.

#### **9.2.7. Acoustic Characterization of the Oscillating Polystyrene Beads**

The audio data of an oscillating bead in the Handihaler™ was recorded using a BOSS BR-600 Digital Recorder (Roland Instruments). The inhaler and microphone were placed inside a noise-isolating box which was lined with extra foam padding, to reduce the pickup of vacuum pump or other laboratory noise. The inhaler was then connected, via a USP induction port, to an NGI set outside of the box. The desired flow rate was attained, and then 300 s of audio data were captured at 44.1 kHz. The open-source software Audacity was used to visualize the waveform of the collected audio data. The distance (in time) from one peak (an audio event) to the next was measured, and 128 such measurements were performed on each recording to determine the average frequency of an audio event. One audio event was assumed to represent one virtual impaction, with two impactions occurring in one full bead oscillation cycle.

### 9.2.8. *In vitro* Aerosol Performance

The respective aerosol performance profiles of the binary blends and drug-coated large polystyrene carrier particles were evaluated *in vitro* with a next generation cascade impactor (NGI; MSP Corporation, MN, USA) at 15, 30, and 45 L min<sup>-1</sup>. The actuation times at 30 and 45 L min<sup>-1</sup> were adjusted to provide a 4 L volume through the inhaler (8 and 5.3 seconds, respectively). However, at 15 L min<sup>-1</sup>, the device was actuated for 8 seconds, corresponding to a 2 L volume. The volumetric flow rates were measured with a digital flowmeter (TSI Performance Measurement Tools, MN, USA) connected in series with the NGI, and a home-built solenoid-valve timer box ensured that the actuation times were consistent between runs. For the binary blends, 20 (±1) mg of powder were placed into size 3 gelatin capsules and punctured via the piercing mechanism of the DPI. For the drug-coated polystyrene carriers, a single bead was placed into the dispersion chamber for each impaction. To prevent particle re-entrainment, the NGI stages were coated with a 2% (v/v) solution of silicon oil in hexane and allowed to air dry prior to each impaction.

For the cascade impactions of the binary formulations at 30 and 45 L min<sup>-1</sup>, 15 mL of EtOH were added to the pre-separator prior to every run and collected following each impaction. The capsule, dispersion chamber, mouthpiece, mouthpiece adaptor, and induction port were each rinsed with 10 mL of EtOH, and the stages of the NGI were each rinsed with 5 mL. At 15 L min<sup>-1</sup> a pre-separator was not included, as recommended by the archival calibration study. Additionally, an external filter was attached downstream of the impactor as at this flow rate the MOC is not an effective final stage particle collector [4]. For the NGI experiments with the polystyrene beads, a pre-separator was not included at any flow rate, and similar to the 2% formulations an external filter was included downstream of the impactor at 15 L min<sup>-1</sup>. Following each impaction, the polystyrene bead was rinsed with 10 mL of EtOH, with the remaining rinsing volumes identical between the binary blends and polystyrene beads.

The drug content was assessed by UV-VIS spectroscopy using an Infinite M200 microplate reader equipped with a cuvette port (Tecan US, Inc., NC, USA) at 230 nm and 244 nm for salbutamol and budesonide, respectively. The emitted fraction (EF) is given as the

percentage of the total recovered dose depositing on the mouthpiece adaptor, induction port, pre-separator (for binary blends) and NGI stages; at 15 L min<sup>-1</sup> the drug depositing on the external filter was also included. The fine particle fraction (FPF) is given as the percentage of the emitted fraction depositing on stage 3 and below at 30 and 45 L min<sup>-1</sup>, and stage 4 and below (including the external filter) at 15 L min<sup>-1</sup>. The respirable fraction (RF) is calculated as the percentage of the total recovered dose depositing on stage 3 and below at 30 and 45 L min<sup>-1</sup>, and stage 4 and below (including the external filter) at 15 L min<sup>-1</sup>. For 15 and 30 L min<sup>-1</sup>, the cut-off sizes for the stages of the NGI were obtained from the literature, while at 45 L min<sup>-1</sup> the stage cut-off sizes were calculated in accordance with the guidelines described in the U.S. Pharmacopeia [4, 5]. The respective cut-off diameters of stage 2 at 30 and 45 L min<sup>-1</sup> are 6.40 µm and 5.18 µm, while that of stage 3 at 15 L min<sup>-1</sup> is 5.39 µm (Table 9.1).

#### **9.2.9. Statistics**

Statistical significance between performance values was determined with one-way ANOVA with Post Hoc tests between groups according to the Bonferroni method ( $P < 0.05$ ).

### **9.3. RESULTS AND DISCUSSION**

#### **9.3.1. Physical Characterization of Drug and Carriers**

The measured physical properties for the lactose carriers and polystyrene beads are presented in Table 9.2. The lactose population is characterized by small particle sizes and a high percentage of fine particles (diameters < 10 µm). Previous studies in our laboratory evaluating the aerosol performance of binary blends with multiple inhalation-grade lactose populations (Respitose grades: ML006, ML001, SV003 and SV010) concluded that ML006 provides the highest performance levels of the tested carriers. Accordingly, it was selected as a comparator to the drug-coated polystyrene beads.

For a 20-mg sample of ML006 lactose, the total surface area of the carrier population is approximately 0.021 m<sup>2</sup>, and thus the surface area available for drug binding in a 20-mg sample is approximately 250 times greater than the surface area available for drug attachment on a

single 5.2 mm polystyrene bead. Accordingly, for comparable drug masses, interactions between drug particles will be more extensive for the polystyrene beads. In Figure 9.1, the low concentration of drug (2% w/w) coupled with the large SSA of the lactose carriers resulted in very low surface coverage of the carrier particles. In contrast, the polystyrene beads were coated with multiple layers of drug particles (Figure 9.2). Both budesonide and salbutamol provided nearly uniform coatings on the surface of the bead, and the drug particles were observed largely as discrete particles rather than dense agglomerates.

### 9.3.2. Device Resistance

The Handihaler is a high-resistance device, with a measured resistance of approximately  $0.173 \text{ ((cmH}_2\text{O)}^{0.5} / \text{L min}^{-1})$  when a perforated, size 3 gelatin capsule is in the dispersion chamber (Table 9.3). This value matched the device resistance of the Handihaler reported in the literature, where a  $39 \text{ L min}^{-1}$  flow rate was found to correspond with a 4 kPa pressure drop [1]. When a capsule is placed within the device, the resistance increases approximately 31%, from 0.132 to  $0.173 \text{ ((cmH}_2\text{O)}^{0.5} / \text{L min}^{-1})$ . By comparison, a lower increase in device resistance (9%) was observed upon addition of a polystyrene bead to the dispersion chamber of the Handihaler, with a measured value of  $0.144 \text{ ((cmH}_2\text{O)}^{0.5} / \text{L min}^{-1})$  (Figure 9.3). Due to the lower overall resistance upon addition of the bead, the flow rate corresponding to a 4 kPa pressure drop is approximately  $44 \text{ L min}^{-1}$ , compared to  $39 \text{ L min}^{-1}$  when a capsule occupies the dispersion chamber.

Devices with resistances below  $0.07 \text{ (cmH}_2\text{O)}^{0.5} / \text{L min}^{-1}$  are classified as low resistance devices, while the demarcating value traditionally cited to distinguish intermediate and high resistance devices is  $0.12 \text{ (cmH}_2\text{O)}^{0.5} / \text{L min}^{-1}$  [6]. Accordingly, the Handihaler is a high resistance device, and aerosol performance was thus evaluated at volumetric flow rates between  $15 \text{ L min}^{-1}$  and  $45 \text{ L min}^{-1}$  to encompass the range of inspiratory efforts achievable by patients through the Handihaler [1, 2].

### 9.3.3. *In vitro* Aerosol Performance

The *in vitro* aerosol performance for both binary blends and polystyrene beads are presented in Tables 9.4 and 9.5. Studies examining the *in vitro* deposition of tiotropium from the Handihaler have reported relatively low emitted fractions, with 56 – 60% of the nominal dose delivered from the device between 20 and 60 L min<sup>-1</sup> [1]. This contrasts with the values obtained in the present study for the binary lactose blends, where the Handihaler exhibited very high emitted fractions of 84 – 90% for both drug formulations at 30 and 45 L min<sup>-1</sup>. By comparison, the emitted fractions from the polystyrene carriers at 45 L min<sup>-1</sup> were comparable to the binary formulations for both drugs, though salbutamol was slightly higher than budesonide. When the flow rate was reduced to 30 L min<sup>-1</sup>, the performance was diminished for both drugs, though the difference was only significantly ( $p < 0.05$ ) lower for budesonide. This is potentially due to the greater adhesive interaction between the budesonide particles and the polystyrene beads, as will be discussed in detail below.

Despite the high EF values for the binary lactose blends at these flow rates, much of the emitted dose was deposited in the induction port and pre-separator, particularly for budesonide, as noted by the FPF values. By comparison, the majority of the dose emitted from the device by the polystyrene beads was well dispersed, with FPF values between 66 – 68% and 76 – 82% for budesonide and salbutamol, respectively.

Although the FPF and RF values were significantly greater from salbutamol, the improvement in aerosol performance from the drug-coated beads relative to the binary blends was greater for the budesonide formulations, where the maximum disparity between RF values for the lactose blend (26%) and drug-coated-bead (58%) occurred at 45 L min<sup>-1</sup>. By comparison, performance differences between the lactose blend and the bead were less stark, as deposition increased to 69% for the latter relative to 47% from the former. These differences suggest that the ability to coat the drug onto the bead surface largely as primary particle is more advantageous for a highly cohesive powder such as budesonide. By comparison, the observed aerosol performance of salbutamol indicates it is readily dispersible powder, with FPF and RF values approximately 50% greater than those observed for the budesonide blend.

#### 9.3.4. Performance at 15 L min<sup>-1</sup>

When a capsule is placed within the dispersion chamber of the Handihaler, it vibrates and rattles during actuation, and this motion is believed to aid in ejecting powder from the capsule (Figure 9.4). By comparison, the opposing fluid forces acting on the bead cause it to oscillate rapidly within the dispersion chamber, and it is noted that the bead also spins while it oscillates. As seen in Figure 9.5, the bead does not typically collide with the mesh or extensively contact the walls of the dispersion chamber. Rather, the bead oscillates rapidly near the center, which as discussed in the previous chapter, limits the amount of drug retained in the device and promotes a high emitted fraction.

Figure 9.6 depicts long-exposure photographs of both the capsule and beads within the dispersion chamber of the Handihaler during actuation at 30 and 15 L min<sup>-1</sup>. At 30 L min<sup>-1</sup> the capsule vibrates and rattles extensively, as indicated by the blurred image representing the motion of capsule during the 4-second exposure. When the flow rate is reduced to 15 L min<sup>-1</sup>, the capsule no longer rotates or rattles, but rather rests against the mesh of the inhaler throughout actuation, as this flow rate is not sufficiently high to induce capsule vibrations, which is believed to aid in powder emission. Additionally, the low flow rate is insufficient to pull the powder through the perforations in the capsule wall, and consequently the majority of the formulation is retained in the device, specifically still within the capsule. EF values of 9% and 15% were observed for budesonide and salbutamol, respectively. For the low-density polystyrene beads, 15 L min<sup>-1</sup> reduced, but did not prevent, oscillation, as frequencies of 110 Hz were generated at this flow rate. Additionally, at 30 L min<sup>-1</sup> the bead appeared to travel a slightly greater distance within the dispersion chamber relative to the lower flow rate. However, despite the lower frequency and shorter distance traveled between oscillations, the detachment forces produced at this flow rate were sufficient to yield emitted fractions of 65% for salbutamol and 45% for budesonide.

Overall, the lactose-based formulations yielded respirable fractions below 10% for both drugs. For the drug-coated polystyrene beads, deposition of salbutamol remained significantly higher than for budesonide, with RF values of 44% and 24%, respectively. Nevertheless, for

both drugs the respirable fractions produced from the polystyrene bead carriers at 15 L min<sup>-1</sup> were comparable to those obtained from the lactose formulations at 30 and 45 L min<sup>-1</sup> (Figure 9.7)

### **9.3.5. Drug Coating**

The overall drug mass coating the surface of the polystyrene beads is governed initially by the strength of the adhesive interaction between the drug and bead to form the initial monolayer, followed by the cohesive interaction between drug particles during the formation of subsequent layers. The affinity of the drugs to the polystyrene beads was not identical, with budesonide yielding higher coating masses than salbutamol for the 2-minute coating period. This disparity may arise from the differences in the lipophilic nature of the drugs, with respective log P values of 2.18 and 0.015 for budesonide and salbutamol, which may result in greater adhesion to the hydrophobic polystyrene surface [7, 8]. Additionally, budesonide has been noted to be a relatively cohesive drug, and in combination with its greater lipophilicity, may result in the significantly higher coating masses observed for this API. This higher affinity of budesonide for the polystyrene bead surface is noted in the overall fraction of the nominal dose that is retained on the bead following actuation.

### **9.3.6. Bead Oscillations and Detachment Forces**

During actuation, the bead generates a very loud rattling sound as it oscillates within the dispersion chamber. For every oscillation of the bead, it was speculated that two 'impaction' events occur, where each 'impaction' signals an abrupt acceleration change as the bead rapidly comes to a stop and then proceeds to reverse direction, accelerate, and stop; the process is repeated for the entirety of the actuation period. The continuous nature of these 'impaction' events results in the characteristic rattling of the bead. The frequency of the 'impaction' events arising from the oscillations of the polystyrene beads ranged from 110 Hz at a flow rate of 15 L min<sup>-1</sup>, up to 225 Hz at 45 L min<sup>-1</sup> (Table 9.6). The oscillation frequency of the beads was not constant, but varied slightly as the amplitude of the oscillations varied.

### **9.3.6.1. Influence of Oscillations**

To assess the role of the oscillations in drug detachment, a polystyrene bead was held stationary within the dispersion chamber of a Handihaler during actuation at 30 L min<sup>-1</sup>. A small hole was drilled into the side of the dispersion chamber to allow a pin to enter the chamber and pierce the budesonide-coated polystyrene bead (Figure 9.8). The bead was held in the center of the chamber, approximately 2 mm from the opening of the inlet into the chamber, with a flow rate of 30 L min<sup>-1</sup> for 8 seconds. During actuation, the pin was slowly rotated to allow the entire surface area of the bead to be exposed directly to the incoming flow stream.

The performance of the stationary and oscillating beads at 30 L min<sup>-1</sup> is shown in Figure 9.9. With the bead held stationary by the pin, 72.0% of the dose remained on the bead following actuation. By comparison, when the polystyrene bead oscillates, only 5.4% remains adhered to the carrier. Overall, the respirable fraction from the stationary polystyrene bead was 8.3%, a significant decline in performance when compared to the oscillating bead, where 52.6% of the coated dose deposited in the lower stages of the cascade impactor. While the incoming flow stream does detach drug particles from the polystyrene bead, the detachment forces are not as effective as when the flow stream is coupled with the momentum transfers arising from the rapidly oscillating bead.

## **9.4. CONCLUSION**

This chapter compared the performance of traditional lactose-based binary blends with that of 5.2 mm drug-coated polystyrene beads using budesonide and salbutamol as model APIs. To evaluate the relative flow rate dependence of the formulations, dispersion performance was assessed at flow rates ranging from 15 to 45 L min<sup>-1</sup>, encompassing the range of inhalation efforts observed in COPD patients for whom the Handihaler is commonly prescribed. Overall performance for salbutamol exceeded that of budesonide for all flow rates, and is likely due to a difference in the cohesive and adhesive properties between the two drugs, as this API performance disparity was noted from both the drug-coated beads and the lactose binary blends.



At 30 and 45 L min<sup>-1</sup>, the polystyrene beads significantly outperformed the lactose blends, with bead RF values ranging from 53 – 58% for budesonide, and 67 – 69% for salbutamol. At 15 L min<sup>-1</sup>, the performance of the lactose blends was extensively inhibited, as the flow rate is too low to induce capsule vibrations, and over 80% of the dose was retained in the device. By contrast, though the frequency of the bead oscillations declined with the decreasing flow rate, they remained sufficiently high at 15 L min<sup>-1</sup> to generate detachment forces capable of emitting between 45% - 65% of the dose from the DPI. Additionally, it was observed that the respirable fractions of the polystyrene bead carriers at 15 L min<sup>-1</sup> were comparable to those obtained from the lactose formulations at 30 and 45 L min<sup>-1</sup> for both drugs.

The oscillations of the polystyrene bead during actuation appeared to play a significant role in drug detachment, as overall performance when the bead was held stationary in the dispersion chamber was approximately 16% of that when the bead oscillated. Thus, the polystyrene carriers function initially as a scaffold onto which drug particles attach in their primary particle size via the piezo-assisted coating method. During actuation, the forces generated by the rapid oscillations of the polystyrene bead within the dispersion chamber effectively detach the drug from the bead surface, producing high drug deposition levels relative to traditional lactose-based binary formulations.

In Chapters 7 – 9 the *in vitro* aerosol performance of the polystyrene beads was evaluated through a commercial DPI. However, these inhalers are not designed to optimize the performance of the drug-coated polystyrene beads, and in the previous studies the dispersion mechanism was designed around the device. Accordingly, in the last chapter of this thesis, inhaler prototypes will be designed to optimize the aerosol performance of the large, drug-coated polystyrene beads.

## 9.5. REFERENCES

1. S. Chodosh, Flanders, J.S., Kesten, S., Serby, C.W., Hochrainer, D., and Witek, T.J. Effective Delivery of Particles with the HandiHaler® Dry Powder Inhalation System over a Range of Chronic Obstructive Pulmonary Disease Severity. *Journal of Aerosol Medicine*. 14:309 - 315 (2001).
2. R.A. Al-Showair, W.Y. Tarsin, K.H. Assi, S.B. Pearson, and H. Chrystyn. Can all patients with COPD use the correct inhalation flow with all inhalers and does training help? *Respiratory Medicine*. 101:2395-2401 (2007).
3. A.R. Clark, and Hollingworth, A.M. The relationship between powder inhaler resistances and peak inspiratory conditions in healthy volunteers - implications for in vitro testing. *Journal of Aerosol Medicine*. 6:99 - 110 (1993).
4. V.A. Marple, Olson, B.A., Santhanakrishnan, K., Roberts, D.L., Mitchell J.P., and Hudson-Curtis, B.L., . Next Generation Pharmaceutical Impactor: A New Impactor for Pharmaceutical Inhaler Testing. Part III. Extension of Archival Calibration to 15 L/min. *Journal of Aerosol Medicine*. 17:335 - 343 (2005).
5. V.A. Marple, Roberts, D.L., Romay, F.J., Miller, N.C., Truman, K.G., Van Oort, M., Olsson, B., Holroyd, M.J., Mitchell, J.P., and Hochrainer, D. Next Generation Pharmaceutical Impactor (A New Impactor for Pharmaceutical Inhaler Testing). Part I: Design. *Journal of Aerosol Medicine*. 16:283 - 299 (2004).
6. C.A. Dunbar, Morgan, B., Van Oort, M., Hickey, A.J. A comparison of dry powder inhaler dose delivery characteristics using a power criterion. *Journal of Pharmaceutical Science and Technology*. 54:478 - 484 (2000).
7. J.F. Desaphy, Pierno, S., de Luca, A., Didonna, P, and Camerino, D.C. Different ability of clenbuterol and salbutamol to block sodium channels predicts their therapeutic use in muscle excitability disorders. *Molecular Pharmacology*. 63:659 - 670 (2003).

8. N. Bandi, W. Wei, C.B. Roberts, L.P. Kotra, and U.B. Kompella. Preparation of budesonide- and indomethacin-hydroxypropyl-beta-cyclodextrin (HPBCD) complexes using a single-step, organic-solvent-free supercritical fluid process. *European Journal of Pharmaceutical Science*. 23:159-168 (2004).

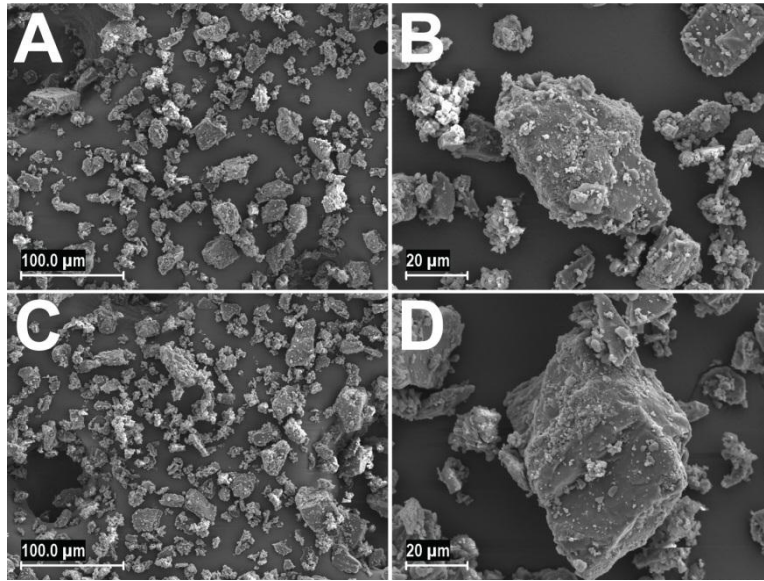


Figure 9.1. SEM Images of ML006 Lactose Binary Blends

SEM images of ML006 lactose carrier particles blended with micronized (A - B) budesonide or (C - D) salbutamol to prepare 2% (w/w) binary DPI formulations. Scale bars for images A and C denote 100 μm, while scale bars for images B and D equal 20 μm.

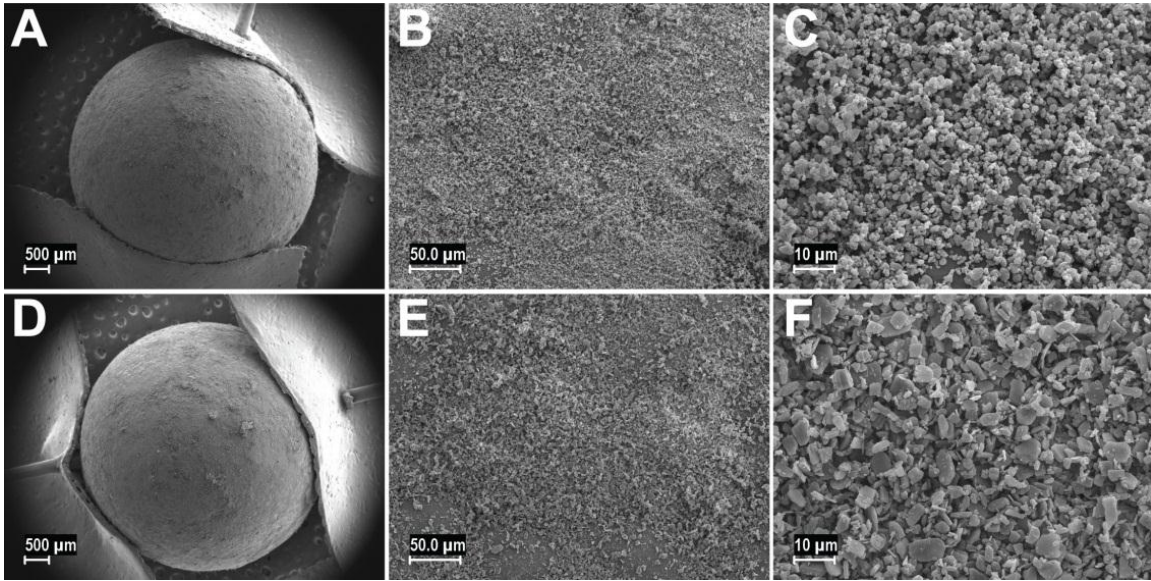


Figure 9.2. SEM Images of Drug Coated Polystyrene Beads

SEM micrographs of polystyrene beads following 2-minutes of piezo-assisted coating with either micronized (A - C) budesonide or (D – F) salbutamol. As seen in figures A and D, the double-sided tape was folded against opposite sides of the polystyrene bead and transfixed with a metal pin to hold it in place during sputter-coating and provide adequate conduction for imaging.

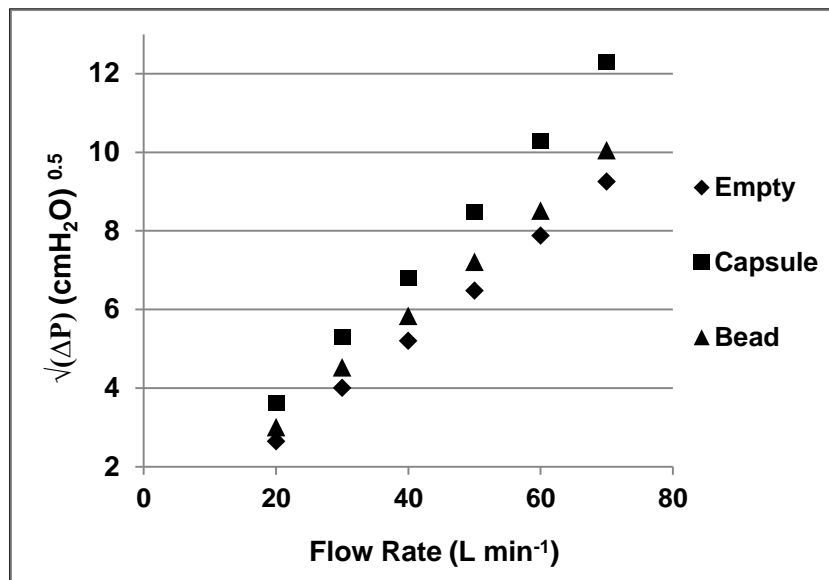


Figure 9.3. Device Resistance Measurement of the Handihaler with a Capsule or Bead

The device resistance was measured by plotting the square root of the pressure drop across the inhaler at multiple volumetric flow rates. The measurements were recorded either with an empty dispersion chamber, or with a perforated size-3 gelatin capsule or 5.2 mm polystyrene bead in the dispersion chamber. The inclusion of the capsule yielded a higher increase in device resistance relative to the bead as noted by the steeper slope of the (pressure drop)<sup>0.5</sup>-flow rate relationship.

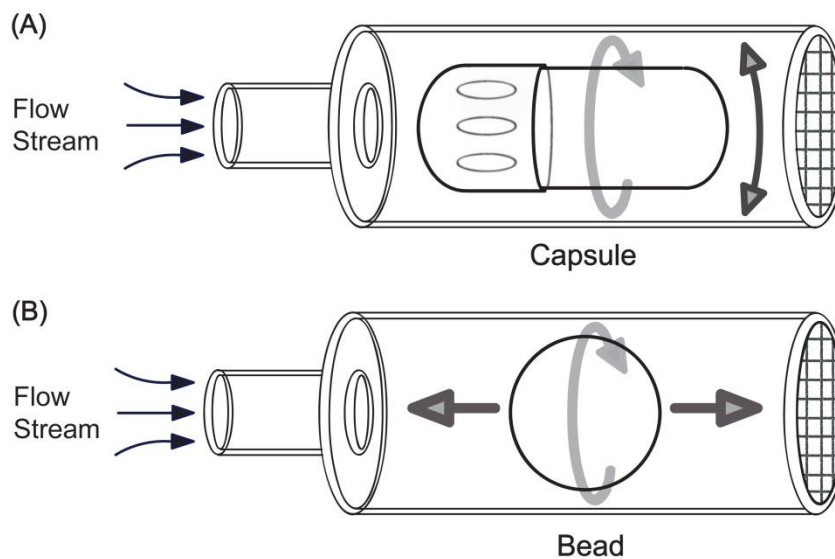


Figure 9.4. Illustration Depicting Relative Capsule and Bead Motions in the Handihaler

During actuation, the capsule will travel the length of the dispersion chamber until it contacts the mesh, where the flow stream induces it to spin and vibrate rapidly as it rattles against the walls of the devices. In contrast, the polystyrene bead oscillates rapidly near the center of the dispersion chamber, with infrequent contact against the inner walls of the DPI. Additionally, though only a single arrow is provided depicting the rotation of the polystyrene carrier, during actuation the bead may spin in three dimensions.

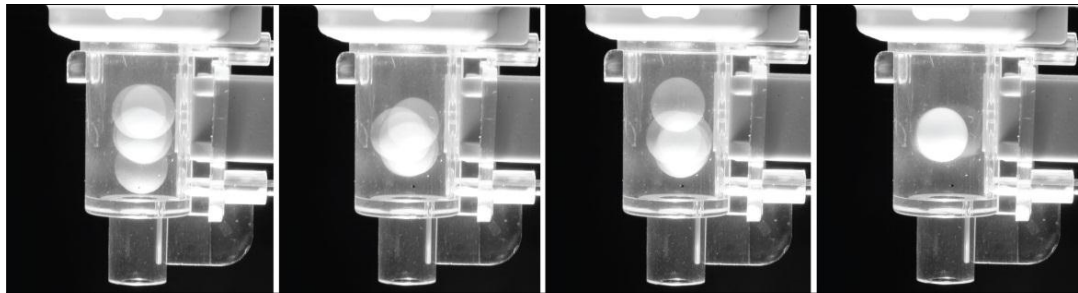


Figure 9.5. Image Series of Polystyrene Bead Oscillations.

The images depict the oscillating motion of an uncoated, 5.2 mm polystyrene bead in the dispersion chamber of the Handihaler at  $30 \text{ L min}^{-1}$ . The images were captured with a  $1/8$  second exposure using a strobe flash for the solitary light source firing five times at a rate of 199 Hz. The strobe captured the position of the polystyrene bead at five distinct locations (ca. 5 milliseconds between flashes) within the inhaler during actuation. The above images were all captured during a single, 8-second actuation period.



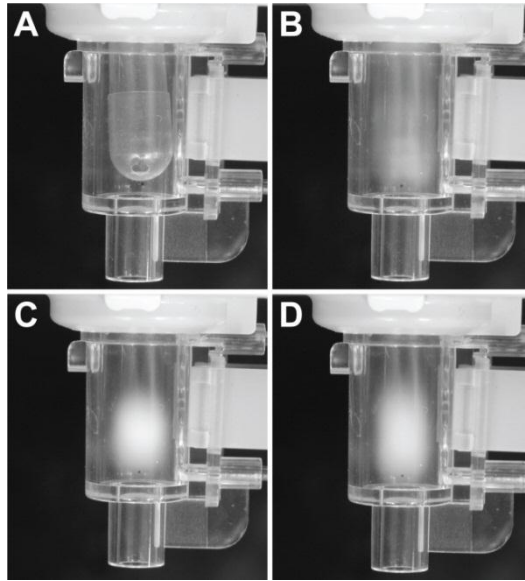


Figure 9.6. Long Exposure Photographs of Capsule and Bead Motion.

Bead and capsule motion at 15 and 30 L min<sup>-1</sup> were imaged using long exposure photographs. The images were captured at f/14 and 4-s to allow the imaging of both the beads and the capsules over the course of a typical inhalation profile. This method allowed the visualization of the average location of either the bead or the capsule throughout the duration of the inhalation event. At 15 L min<sup>-1</sup> the image of the capsule (A) is not blurred because it remained stationary throughout the 4 second exposure. By contrast, the capsule at 30 L min<sup>-1</sup> (B) produced a blurred image as it vibrated rapidly in the dispersion chamber. The polystyrene beads oscillated at both 15 L min<sup>-1</sup> (C) and 30 L min<sup>-1</sup> (D), though their respective frequencies and amplitudes differed.

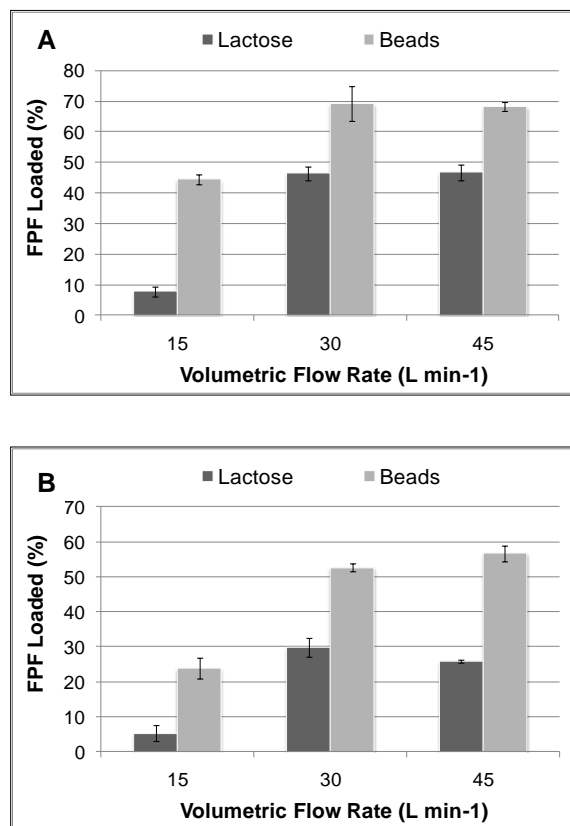


Figure 9.7. *In Vitro* Performance of Salbutamol and Budesonide Formulations

The *in vitro* aerosol performance values (RF) of (A) salbutamol sulphate and (B) budesonide formulations prepared either with lactose carrier particles or coated directly onto polystyrene beads are provided. Values are given as mean ( $\pm$  standard deviation) for N = 3 replicates. For both drugs, the polystyrene beads outperform the binary blends at all tested flow rates. Performance at 15 L min<sup>-1</sup> from the polystyrene carriers is comparable to that of the lactose blends at 30 and 45 L min<sup>-1</sup>.

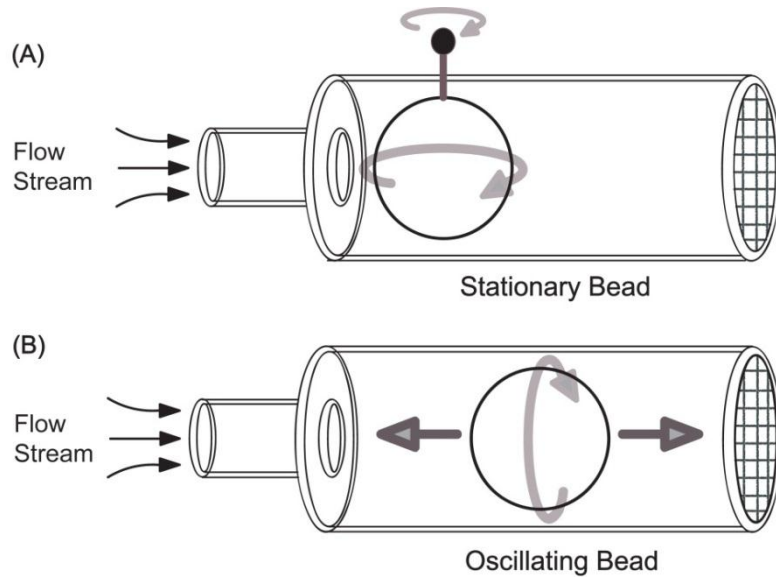


Figure 9.8. Illustration Depicting a Stationary Bead Configuration.

A small hole was drilled into the side of a Handihaler capsule chamber to allow a metal pin to transfix a budesonide-coated polystyrene bead, preventing it from oscillating. During actuation the pin was slowly rotated, turning the bead and allowing the entire surface to be directly exposed to the incoming flow stream. As noted previously, the polystyrene bead oscillates rapidly near the center of the dispersion chamber, with infrequent contact with the inner walls of the DPI. Though only a single arrow is provided depicting the rotation of the polystyrene bead, during actuation the bead spins in three dimensions.

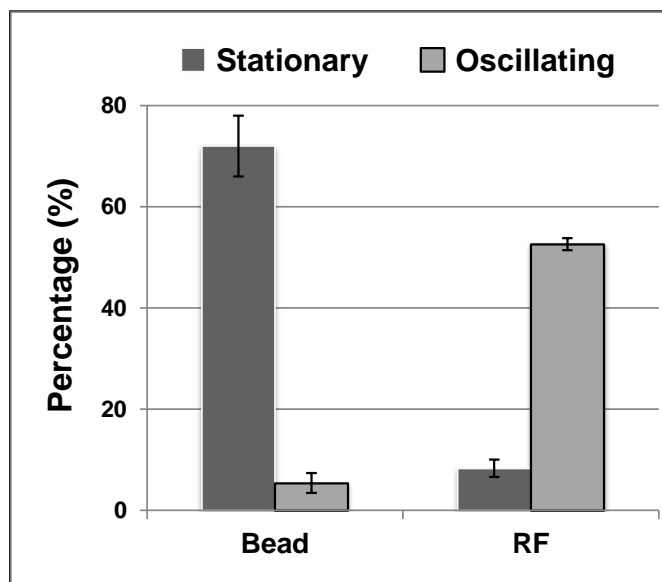


Figure 9.9. *In vitro* Performance of Stationary and Oscillating Budesonide-Coated Polystyrene Beads

The performance disparity of the stationary and oscillating beads is provided by the percentage of the nominal dose retained on the bead carrier, and the respirable fraction (RF) following a single 8-second actuation at  $30 \text{ L min}^{-1}$ . The bead was either held stationary within the dispersion chamber using a metal pin that was rotated during the 8-second actuation period to allow the entire surface of the bead to be directly exposed to the incoming flow stream. The impaired drug dispersion from the stationary bead suggests the oscillations of the bead are effective at detaching drug. The values are given as mean ( $\pm$  standard deviation) for  $N = 3$  replicates.

Table 9.1. Stage Cut-off Sizes for the NGI at 15, 30 and 45 L min<sup>-1</sup>

	<b>D<sub>50</sub> (μm) for each volumetric flow rate (L min<sup>-1</sup>)</b>		
	<b>15</b>	<b>30</b>	<b>45</b>
<b>Stage 1</b>	14.1	11.7	9.41
<b>Stage 2</b>	8.61	6.40	5.18
<b>Stage 3</b>	5.39	3.99	3.26
<b>Stage 4</b>	3.30	2.30	1.90
<b>Stage 5</b>	2.08	1.36	1.09
<b>Stage 6</b>	1.36	0.83	0.65
<b>Stage 7</b>	0.98	0.54	0.41

Table 9.2. Physical Characterization of ML006 Lactose Carrier Particles and Large Porous Polystyrene Beads

	Diameter ( $\mu\text{m}$ )			SSA ( $\text{m}^2/\text{g}$ )	Density ( $\text{g}/\text{cm}^3$ )
	$d_{10}$	$d_{50}$	$d_{90}$		
<b>LACTOSE</b>	3.5	14.3	41.0	1.04	1.54
	Diameter (mm)		Surface Area ( $\text{m}^2$ )	Density ( $\text{g}/\text{cm}^3$ )	
<b>POLYSTYRENE</b>	5.2 ( $\pm 0.1$ )		$8.5 \times 10^{-5}$	0.027	

Particle sizing, specific surface area, and density measurements for Respitose® ML006 lactose carrier particles and polystyrene beads are provided. In contrast to the lactose carriers, where specific surface area is a population measurement and provided as  $\text{m}^2/\text{g}$ , the surface area reported for the polystyrene carrier is that of a single polystyrene carrier (assuming a spherical bead) and is provided in units of  $\text{m}^2$ .

Table 9.3. Device Resistance of Handihaler with the Inclusion of a Capsule or Bead

Dispersion Chamber Configuration	Device Resistance ((cmH <sub>2</sub> O) <sup>0.5</sup> / L min <sup>-1</sup> )	Flow Rate at 4 kPa (L min <sup>-1</sup> )
Empty	0.132	49
Size 3 Gelatin Capsule	0.173	39
5.2 mm Polystyrene Bead	0.144	44

The bead provides a smaller increase in device resistance relative to the capsule, and accordingly the flow rate corresponding to a 4 kPa pressure drop is higher when a bead is in the dispersion chamber

Table 9.4. *In vitro* Aerosol Performance of Budesonide Formulations

Flow Rate (L min <sup>-1</sup> )	Lactose Carrier Particles				Macro Carrier Particles			
	EF (%)	FPF (%)	RF (%)	FPD (mcg)	EF (%)	FPF (%)	RF (%)	FPD (mcg)
15	8.9 (4.1)	52.7 (4.3)	5.2 (2.3)	11 – 24	44.8 (4.6)	55.3 (1.9)	23.8 (3.0)	64 – 78
30	84.4 (1.9)	35.3 (4.0)	29.7 (2.7)	95 – 122	78.9 (2.1)	66.7 (1.6)	52.6 (1.2)	133 – 168
45	84.1 (2.6)	30.7 (1.4)	25.8 (0.4)	97 - 114	85.9 (1.5)	67.8 (2.0)	58.2 (1.3)	142 - 172

The *in vitro* aerosol performance of 2% (w/w) formulations and budesonide-coated polystyrene beads evaluated through the Handihaler at 15, 30 and 45 L min<sup>-1</sup>. Values are given as mean (± standard deviation) for N = 3 replicates.



Table 9.5. *In vitro* Aerosol Performance of Salbutamol Formulations

Flow Rate (L min <sup>-1</sup> )	Lactose Carrier Particles				Macro Carrier Particles			
	EF (%)	FPF (%)	RF (%)	FPD (mcg)	EF (%)	FPF (%)	RF (%)	FPD (mcg)
15	15.1 (3.8)	52.4 (7.9)	7.8 (1.6)	35 – 48	65.4 (2.5)	68.2 (2.7)	44.4 (1.5)	67 – 86
30	87.6 (1.5)	53.0 (1.7)	46.5 (2.2)	181 – 209	84.9 (4.1)	81.4 (2.9)	69.2 (5.7)	108 – 128
45	90.4 (0.4)	51.7 (2.7)	46.7 (2.6)	202 - 223	89.4 (3.2)	74.6 (1.3)	66.7 (2.6)	103 - 152

The *in vitro* aerosol performance of 2% (w/w) formulations and salbutamol-coated polystyrene beads evaluated through the Handihaler at 15, 30 and 45 L min<sup>-1</sup>. Values are given as mean ( $\pm$  standard deviation) for N = 3 replicates.

Table 9.6. Acoustic Profile Data of Polystyrene Beads

	Volumetric Flow Rate (L min <sup>-1</sup> )		
	15	30	45
<b>Time Between Audio Events (ms)</b>	18.3 (0.8)	10.9 (0.9)	9.2 (0.8)
<b>Bead Oscillation Frequency (Hz)</b>	55 (4)	95 (16)	112 (20)

During actuation, the polystyrene beads generate a strong audible signal in the form of a loud rattle. The acoustic profiles at different flow rates were measured and analyzed to assess the time between 'rattles' (the audio events) and obtain the frequency at which the beads oscillate. One audio event was assumed to represent one virtual impaction, with two impactions occurring in one full bead oscillation cycle.

## CHAPTER 10

### **10.Design, Development, and Testing of Prototype Inhaler Devices to Optimize Aerosol Performance from Drug-Coated Polystyrene Carrier Particles**

#### **10.1. INTRODUCTION**

Passive dry powder inhalers rely solely on the inspiratory effort provided by the patient to fluidize, entrain and disperse the powder formulation. However, particle engineering technologies notwithstanding, simply passing the flow stream across the powder bed is insufficient to promote effective powder dispersion from standard binary formulations. As a result, DPIs incorporate a diverse array of design features to enhance particle dispersion and improve performance. Many of these features are designed to induce turbulent flow, typically just prior to where the flow stream encounters the dose. Additional device geometries including baffles, grids and spiraling flow channels are incorporated to promote particle-particle and particle-device collisions. The various mechanisms of DPI dispersion were discussed in detail in Chapter 1.

The diverse inner geometries of commercial DPIs have given rise to devices possessing a wide spectrum of resistance levels (Table 10.1). Low resistance devices are typically more comfortable for patients to use, as for two DPIs with disparate resistance values patients must exert a greater inhalation effort through the higher resistance device to achieve a sufficiently strong flow rate for adequate particle dispersion. However, it has been extensively reported that there is generally a trade-off between resistance and performance, as higher resistance devices will emit a greater fraction of fine particles, provided that a sufficient airflow can be generated by the patient through the inhaler. Accordingly, relatively high resistance devices, such as the Turbuhaler, exhibit marked flow rate dependence as many patients are incapable of producing a sufficient flow rate to adequately operate the device. By comparison, low

resistance devices offer more consistent dispersion over a wider range of flow rates, though on average performance is significantly lower relative to their high-resistance counterparts.

The relationship between device resistance and the energy passing through a DPI can be approximated as [1]:

$$E = Q(\Delta P)t$$

where  $Q$  is the volumetric flow rate ( $\text{L min}^{-1}$ ),  $\Delta P$  is the pressure drop across the device (Pa), and  $t$  is the dose emptying time (seconds). The pressure drop across the device is related to the device resistance ( $R$ ) as [2]:

$$\sqrt{\Delta P} = QR$$

An alternative approach to characterize inhaler performance is described by Dunbar and colleagues [116]. This approach is based on the power supplied by the inhalation flow stream, where power is defined as the rate at which work is done by the air flow (alternatively described as the rate of inspiratory effort):

$$\text{Power} = (\Delta P) Q$$

As power is the rate at which work is performed, it is noted that the above two methods are essentially identical. Accordingly, for a comparable flow rate, the energy/power that flows through a device and interacts with the dose is proportional to the device resistance. High flow rates through high resistance devices generally provide the greatest dispersion performance. Unfortunately, many patients cannot produce a sufficient flow stream through a high resistance inhaler, and performance is inhibited.

#### *Specific Aim*

As reported in Chapter 9, the drug-coated polystyrene beads provide effective powder dispersion even at very low flow rates where traditional binary blends essentially cease to function. The *in vitro* aerosol studies were performed using the Handihaler, a capsule-based DPI that is not designed to optimize performance of the drug-coated polystyrene beads.

Additionally, the Handihaler is a very high resistance device that many patients have reported difficulty using, and therefore the ability to lower device resistance while maintaining the high performance levels previously noted is highly desirable. Accordingly, the specific aim of this chapter is focused on the design, development and testing of inhaler prototypes to optimize the performance of the large, drug-coated polystyrene beads described in Chapters 7 through 9. To this end, prospective inhaler geometries will be designed and produced via rapid prototyping, and performance will be evaluated *in vitro* using cascade impaction.

In addition to the prototypes designed for a single bead, a DPI with two dispersion chambers in parallel will also be developed. This configuration allows the simultaneous actuation of two drug-coated beads for combination drug therapy. Additionally, a dual-chamber configuration may be employed for high doses of a single drug, such as for the delivery of vaccines or antibiotics.

#### *Rapid Prototyping*

Rapid prototyping is a solid freeform fabrication (SFF) process, and is a collection of techniques, including selective laser sintering (SLS) and stereolithography (SLA) that are employed to manufacture solid objects initially modeled with computer aided design (CAD) software [4, 5]. SLS employs a CO<sub>2</sub> laser that traces a pattern onto a hot bed of thermoplastic powder, thereby solidifying the powder where it passes. Following the completion of each individual layer, a fresh layer of powder is placed on top of the bed, repeating the process. By contrast, SLA polymerization of the resin occurs through crosslinking by a UV laser to produce a solid. As with SLS, a three-dimensional object is formed from the successive layering of thin, two-dimensional cross-sections. Generally the material properties produced by SLA are inferior to those developed by SLS, as the latter process employs actual engineering thermoplastics. However, the higher level of detail, lower cost, and faster production times of the SLA process made it well-suited to the present studies.

## **10.2. EXPERIMENTAL**

### **10.2.1. Materials**

Budesonide was purchased in bulk (Jinhua Chemical Company, China) and micronized under nitrogen using a high energy jet-mill with respective pusher and grinding pressures of 80 and 110 PSI (Aljet; Fluid Energy Processing and Equipment Co., PA, USA). Two micronization cycles were performed to produce a narrow particle size distribution of drug. Micronized salbutamol sulphate was purchased from Letco Medical (AL, USA) and used as received. Low density ( $0.027 \text{ g/cm}^3$ ) polystyrene beads were generously provided by Styrochem® (TX, USA) and sorted to obtain particle diameters between 5.1 and 5.3 mm.

### **10.2.2. Prototype Design**

The device geometries were modeled using the 3D CAD software package, Inventor® (Autodesk, CA, USA). The final designs were saved in the STL file format and submitted to the RP manufacturer.

### **10.2.3. Rapid Prototyping**

The completed prototype CAD designs were submitted to the rapid prototyping company, FineLine Prototyping (NC, USA). As discussed above, the relatively low cost, excellent dimensional accuracy and rapid development times of the SLA technology made it the ideal choice for production of the device prototypes. While numerous materials may be employed in stereolithography, DSM SOMOS 9120 was selected for our application as it most closely resembles the physical properties of a stiff polypropylene material, providing robust, durable prototypes with excellent chemical resistance and accurate features. It is noted that this material does not meet USP Class VI testing requirements for biocompatibility and cytotoxicity. However, these prototypes were not designed for clinical studies, but rather to obtain a mechanistic understanding of the geometries that would most optimize dispersion performance from the polystyrene carrier particles, and thus the selected material is well-suited for the study

objectives. The prototypes were manufactured using normal resolution stereolithography, where building proceeds in 0.004" (0.10 mm) layers.

#### **10.2.4. Measurement of Device Resistance**

To assess the resistance of the DPI, the pressure drop (cmH<sub>2</sub>O) across the Handihaler at multiple volumetric flow rates (20, 30, 40, 50, 60, and 70 L min<sup>-1</sup>) was measured using a digital manometer (SPER Scientific; AZ, USA). The base of the inhaler was kept constant through the measurements (3.5 mm inlet diameter, 8 mm inlet length, with a 15 degree taper), and only the mouthpiece designs were varied. Unless specified, each dispersion chamber contained a 5.2 mm, uncoated polystyrene bead during the pressure drop measurements. The device resistance was determined by plotting the square root of the pressure drop against the volumetric flow rate, with the slope of the relationship equaling the device resistance, as described by Clark and Hollingworth [2]. The flow rate (L min<sup>-1</sup>) corresponding to a 4 kPa pressure drop across the device was also measured for the single dispersion chamber model, the configurations incorporating flow bypass channels, and also for the dual dispersion chamber design.

#### **10.2.5. Drug Coating of Polystyrene Beads**

The polystyrene beads were coated according to the protocol detailed in Chapter 9. Briefly, 2 mg of micronized drug (either budesonide or salbutamol sulphate) were weighed into a 30-mL glass scintillation vial. Three 5.2 mm polystyrene beads were added to the vial, which was then sealed and the bottom half submerged in a sonicating water bath (Fisher Scientific, NH, USA) for 2 minutes. During coating, the vial was slowly rotated side-to-side to enable the bead to roll across the powder bed. Following coating, the bead was removed from the scintillation vial and dropped approximately 30 cm onto an aluminum mesh to remove any loosely adhered drug particles and agglomerates. The drug-coated polystyrene beads were then stored in a desiccator for 3 days prior to use.

### 10.2.6. *In vitro* Aerosol Performance

The aerosol performance profiles of the drug-coated large polystyrene carrier particles were evaluated *in vitro* with a next generation cascade impactor (NGI; MSP Corporation, MN, USA). For the Handihaler (Boehringer Ingelheim, Germany) and single chamber prototype devices, the flow rate was set to 39 L min<sup>-1</sup>, with a 4-second actuation time. For the dual chamber devices, and models incorporating flow bypass channels, the flow rate was set to correspond to a 4 kPa pressure drop across the inhaler. The volumetric flow rates were measured with a digital flowmeter (TSI Performance Measurement Tools, MN, USA). For each actuation, a single bead was placed into the dispersion chamber of the device. To prevent particle re-entrainment, the NGI stages were coated with a 2% (v/v) solution of silicon oil in hexane and allowed to air dry prior to each impaction. Following each impaction, the capsule, dispersion chamber, mouthpiece, mouthpiece adaptor, and induction port were each rinsed with 10 mL of EtOH, and the stages of the NGI were each rinsed with 5 mL. For the dual chamber studies, the individual components of the device apparatus were rinsed with the same volumes but with a mobile phase of 50 mM sodium acetate buffer.

The drug content was assessed by UV-VIS spectroscopy with an Infinite M200 microplate reader equipped with a cuvette port (Tecan US, Inc., NC, USA) at 244 nm for budesonide. Quantification of simultaneous drug deposition from the dual chamber device *in vitro* studies was performed according to a published protocol [6]. Briefly, analysis was performed using gradient elution with a 2 mL/min flow rate with an HPLC equipped with a C<sub>18</sub> column (150 x 3.9 mm, 5 µm particle size; Waters Corp., MA, USA), and a detection wavelength of 240 nm.

The emitted fraction (EF) is the percentage of the total recovered dose depositing on the mouthpiece adaptor, induction port, and NGI stages. The fine particle fraction (FPF) is given as the percentage of the delivered dose possessing an aerodynamic diameter less than 5 µm. The respirable fraction (RF) is calculated as the percentage of the total recovered dose with an aerodynamic diameter below 5 µm. As discussed in detail below, an additional performance



metric assessed was the percentage of the emitted dose collected from the USP induction port (%IP).

### **10.3. RESULTS AND DISCUSSION**

#### **10.3.1. Particle Deposition in the USP Induction Port**

In Chapter 8, the fluid flow phenomenon that occurs when a relatively narrow volume abruptly opens to a larger volume was discussed. At the corners of the volume expansion, the flow stream detaches from the inner walls, re-attaching a distance downstream of the transition region. However, a portion of the flow stream is entrapped at the corners of the expansion producing a pressure drop. It is believed that this phenomenon is responsible for the rapid bead oscillations that occur during actuation, which effectively detach drug particles from the surface of the polystyrene carrier particles.

However, similar to the abrupt volume expansion found in the transition region between the inlet (3.5 mm) and the dispersion chamber (7.6 mm) of the device, a second volume expansion occurs when the mouthpiece of the device (5 mm) transitions into the comparatively larger USP induction port (22 mm). Particle deposition in the induction port of the cascade impactor corresponds to extrathoracic particle deposition *in vivo*, and accordingly *in vitro* particle deposition in this region is commonly referred to as 'throat' deposition.

Particle deposition in the induction port is speculated to occur by inertial impaction, as coarse carrier particles and agglomerated drug particles are unable to follow the flow stream as it navigates the 90° bend in the induction port, thus colliding into the walls of this region where they remain adhered. Additionally, as the volumetric flow rate is augmented, the amount of particles that deposit in this area is also increased, as larger primary drug particles will be collected from this region due to the increased inertia resulting from their higher velocity. Accordingly, while the performance through DPIs is often classified as being flow rate dependent, particle deposition does not continually improve with flow rate until 100% FPF has been achieved. For example, a previous study examining the influence of flow rate on performance through the Aerolizer has reported that overall performance is optimized at

approximately  $65 \text{ L min}^{-1}$ , corresponding to a pressure drop well below 4 kPa through this device [7]. When the flow rate is increased from this value, any improvements to particle emission and dispersion that occur are offset by enhanced 'throat' deposition, resulting in no overall change in total drug deposition. An additional study of extrathoracic deposition from DPIs concluded that particles above  $10 \mu\text{m}$  in aerodynamic diameter may be expected to deposit in the extrathoracic region, either in the oral cavity or the larynx, while particles with aerodynamic diameters below  $2 \mu\text{m}$  (e.g. primary drug particles) would not be extensively influenced by inertial impaction [8].

Accordingly, while 'throat' deposition by impaction is problematic for particles possessing relatively high inertia, such as coarse carriers and agglomerated drug particles, this does not apply to the same extent for primary drug particles with comparatively lower masses. However, while primary particles possess relative immunity to deposition in the induction port by inertial impaction, they may be more susceptible to deposition in this region by an alternative mechanism. As discussed above, when the mouthpiece of the inhaler transitions into the induction port, an abrupt volume expansion is encountered resulting in recirculating eddies at the corner of the expansion. It is speculated that this recirculating region would most likely influence primary drug particles, as the relatively low inertias that enable them to accurately follow the flow stream through the induction port may also serve to render them more readily susceptible to deposition in this region due to the turbulent flow in this region.

We have performed dispersion studies from drug-coated polystyrene beads where drug particle collection from the induction port was separated into two fractions, corresponding to regions either adjacent to the mouthpiece or adjacent to the NGI. It was noted that upwards of 50% of the drug mass that deposits in the induction port is collected from the half of the induction port adjacent to the mouthpiece, indicating that an extensive number of fine particles deposit in this region. Indeed, following each cascade impaction a dusting of fine powder is observed in this transition area, while large drug particle aggregates are observed in the region of the induction port proximal to the NGI. It is speculated that the drug particles collected from the inhaler-induction port transition region would otherwise contribute to FPF and RF values.

Accordingly, the prototypes were designed with the primary purpose of minimizing drug loss in this region, and the two metrics primarily employed to report the performance of a given design are the %IP (percentage of the emitted dose that deposits in the induction port) and FPF (percentage of the emitted dose with an aerodynamic diameter < 5  $\mu\text{m}$ ).

### **10.3.2. In vitro Aerosol Performance from the Handihaler DPI**

For comparative purposes, three budesonide-coated beads were dispersed through the Handihaler at 39 L min<sup>-1</sup>, corresponding to a 4 kPa pressure drop through the device. The resulting %IP and FPF values are 21.3 % and 72.1 %, respectively.

### **10.3.3. Prototype Design**

The archetypal design of the prototype inhalers is shown in Figure 10.1. Overall, the base of the inhaler remained unchanged through the experiments, with a constant 15-degree taper throughout the 8 mm inlet, and a 3.5 mm exit diameter. Previous work in our laboratory has shown that this design reduces the device resistance relative to the straight air inlet configuration employed in the Handihaler while maintaining the high bead oscillation frequencies responsible for effective particle detachment from the bead surface. The measured resistance of this design (including a 5.2 mm bead in the dispersion chamber) is 0.140 (cmH<sub>2</sub>O)<sup>0.5</sup> / L min<sup>-1</sup>. Although this value falls into the category of a high-resistance device, it is only 80% the resistance value of the Handihaler [3, 9]. Accordingly, the flow rate corresponding to a 4 kPa pressure drop through the prototype is 46 L min<sup>-1</sup> as compared to 39 L min<sup>-1</sup> for the commercial device (Table 10.2).

### **10.3.4. Mouthpiece Length**

The diameter of the flow passage through the mouthpiece was kept constant at 7.6 mm (corresponding to the diameter of the dispersion chamber) as the length of the mouthpiece was varied between 20 mm, 30 mm, and 40 mm (Figure 10.2). The influence of mouthpiece length is depicted in Figure 10.3. As the length is increased from 20 mm to 30 and 40 mm a slight but significant ( $p < 0.05$ ) decrease was noted in the induction port deposition, as the 20.0% from the

20 mm length was reduced to 16.3% and 15.2% for the 30 and 40 mm configurations, respectively. This corresponded to a significant improvement in FPF for both 30 and 40 mm mouthpiece lengths relative to the 20 mm design, with values increasing from 69.4% up to 76.5% (30 mm) and 75.4% (mm). Performance between the 30 and 40 mm mouthpiece lengths were comparable, and no significant differences were observed.

These results generally match those obtained by Coates and colleagues, who examined the influence of varying the mouthpiece length of the Aerolizer DPI from 47 mm down to three-quarters and one-half the standard length [10]. CFD studies indicated that the full-length mouthpiece produces a well distributed velocity profile. By contrast, the three-quarters length mouthpiece produced a slightly greater velocity difference while the half-length mouthpiece produced a non-uniform flow profile, where high-velocity regions were observed together with lower velocity regions. It was speculated by the authors that the high velocity regions observed in the shorter mouthpiece could potentially increase throat deposition. However, no significantly increased induction port deposition was observed *in vitro*, and the authors concluded that high velocity regions may dissipate in the throat prior to particle impaction.

These conclusions match those of the present study, with the exception that the 20 mm mouthpiece length was shown to significantly lower performance (FPF), though overall differences were slight. By comparison with drug-coated beads from the Handihaler, where mouthpiece length is approximately 28 mm (5 mm diameter), overall performance was comparable with all three tested lengths, as the slightly higher performance levels from the 30 and 40 mm designs were not found to be significant.

#### **10.3.5. Mouthpiece Exit Diameter**

To evaluate the influence of the exit diameter, mouthpiece designs with tapered flow channels such that the exit diameter was twice that of diameter at the base of the mouthpiece, were compared against the standard straight channel geometry, where the flow channel diameter is constant throughout the length of the mouthpiece (Figure 10.4). The *in vitro* performance data is presented in Figure 10.5. For both mouthpiece lengths, doubling the exit

diameter significantly lowered %IP and improved FPF. At 20 mm, % IP declined from 20.0% to 11.8%, with a corresponding improvement in FPF from 69.4% to 79.7%. Likewise, %IP from the 30 mm tapered design declined from 16.3% down to 10.0%, while FPF improved from 76.5% up to 84.1%.

Interestingly, there was no significant difference between the different mouthpiece lengths of the tapered configurations. As described above for the straight flow channel designs, decreasing the mouthpiece length from 30 to 20 mm was found to significantly reduce performance by increasing the %IP and lowering FPF. However, for the tapered designs, performance was observed to be comparable between both mouthpiece lengths. A previous study by Coates and colleagues through the Aerolizer also examined performance as the exit diameter was increased. Two of the configurations included in their study were tapered to provide exit diameters 1.5 times (16 mm) and 2 times (21 mm) greater than that of the standard design (10.5 mm). The authors observed that while overall drug deposition differences between the designs were not found to be significant, a significant decline in deposition in the induction port was noted for the tapered designs. Using CFD, the authors concluded that the tapered design significantly reduces the axial component of the air flow velocity exiting the mouthpiece, thus corresponding to lower particle deposition in this region. Additionally, the study indicated that it is the axial motion of the particles that is primarily responsible for induction port deposition, and that the radial motion of the emitted aerosol was not found have a significant influence on *in vitro* 'throat' deposition. These results matched those of the present study, where reduced induction port deposition was observed when the exit diameter was doubled. However, in the present study, significant FPF values were noted for the tapered geometries with both mouthpiece lengths. Additionally, compared against the performance of the drug-coated polystyrene beads through the Handihaler, the tapered design significantly lowered % IP and improved FPF for both mouthpiece lengths.

In the Aerolizer® study, the authors concluded that the design of the mouthpiece influences 'throat' deposition by controlling the axial component of the air flow velocity exiting the mouthpiece, and lower values for this parameter were correlated with decreased throat

deposition. As noted previously, the mouthpiece transitions into the induction port, there is a sudden volume expansion. It was speculated that the flow profile in this region may be responsible for the deposition of fine particles. However, for the tapered designs, the particle-laden flow stream is expanding as it enters the induction port, and it was speculated that this may reduce the overall pressure drop in the transition region, as there is no longer the same abrupt volume expansion as with the straight-channel design. Unfortunately, in the present studies CFD simulations were not coupled with the *in vitro* performance data, and thus the precise mechanism of how the tapered designs influence performance has not been fully elucidated.

#### **10.3.6. Powder Channel Diameter**

To evaluate the influence of the diameter of the powder channel through the mouthpiece, designs were developed where the channel diameter was varied from 4, 5, 6, and 7.6 mm (Figure 10.6). The length of the mouthpiece was kept constant at 40 mm. The *in vitro* aerosol performance results are shown in Figure 10.7. As noted by Coates and colleagues in their studies of aerosol performance in the Aerolizer, the mouthpiece geometry exerts its influence on ‘throat’ deposition by modulating the axial velocity of the aerosol cloud emitted from the device. Specifically, reduced axial velocities were correlated with significantly lower levels of induction port deposition.

For a constant volumetric flow rate, decreasing the diameter of the powder channel through the mouthpiece would be expected to increase the velocity of the emitted aerosol cloud. According to the previous theory, smaller diameter devices would be expected to produce the higher %IP values. This was observed for the 4 mm design, which exhibited significantly higher deposition in the induction port (%IP = 34%), and lower FPF values (56%) compared to the 5 mm, 6 mm, and 7.6 mm channel diameter mouthpieces, where induction port deposition ranged from 23 – 26% and FPFs were between 64 – 66%. Accordingly, none of these designs provided significantly improved performance relative to that observed from the Handihaler.

### 10.3.7. Flow Bypass Channels and Sheath Flow

The mouthpiece designs incorporated flow bypass channels to lower the overall resistance of the device while providing a sheath of air flow around the powder-laden flow stream exiting the mouthpiece (Figure 10.8). For the bypass channels, eight circular inlets (diameter = 1.5 mm) were arranged circumferentially around the mouthpiece, entering perpendicular to the central axis of the powder flow channel, and connecting with the sheath flow channel; a distance of 2 mm separated the sheath flow channel from the powder flow channel. The distance between the inner and outer edge of the sheath flow channel was varied from 1.5 mm to 3 mm. A final design included a 3-mm gap between the inner and outer edge of the sheath flow channel, with a 5 mm fillet applied to the outer edge of the device, yielding a sheath flow passage that diverges from the central powder channel as it transitions into the induction port. For the sheath-flow designs, the length of the mouthpiece was kept constant (40 mm) as was the diameter of the powder flow channel (5 mm).

The measured resistances of these prototypes are listed in Table 10.3. The inclusion of flow bypass channels markedly lowered device resistance relative to the single chamber design, increasing the flow rate at a 4 kPa pressure drop from 46 L min<sup>-1</sup> up to 108 L min<sup>-1</sup>. When the distance between the inner and outer edge of the sheath flow channel is increased from the 1.5 mm to 3.0 mm, the device resistance is reduced by 30%, from 0.079 to 0.061 (cmH<sub>2</sub>O)<sup>0.5</sup> / L min<sup>-1</sup>, thus transitioning from an intermediate resistance device to a low resistance device [3]. The inclusion of a filleted outer edge with a 3.0 mm does not appreciably alter resistance, and the 4 kPa flow rate is only marginally increased, from 105 to 110 L min<sup>-1</sup>.

The *in vitro* performance of the flow bypass designs was compared against a mouthpiece without flow bypass channels, with a 5-mm powder flow channel diameter and 40-mm mouthpiece length at 39 L min<sup>-1</sup> (Figure 10.9). The inclusion of flow channels is not sufficient to effect induction port deposition, as the %IP values are not significantly different between the design without bypass channels and the mouthpieces with the 1.5 and 3.0 mm sheath flow channels. However, when the outer edge of the channel is filleted, %IP declined significantly from 26% to 18% compared to the design without flow bypass channels.

In contrast to %IP, where only the filleted 3.0 mm flow bypass design exhibited significant differences, FPF values were significantly higher for all flow bypass designs relative to the control design. FPF values for the flow bypass channels ranged from 70 – 77%, with the filleted design demonstrating the highest performance values. However, when compared to performance from the Handihaler, only the filleted design displayed significantly improved performance in terms of both lower %IP and higher FPF.

### **10.3.8. Performance of Dual Chamber Prototype**

The design of the dual chamber device is shown in Figure 10.10. To accommodate both dispersion chambers while keeping the overall device diameter fixed at 22 mm, the two channels were separated by only 1 mm. Due to the close proximity of the dispersion chambers, it was not possible to use the tapered air inlet employed in the single dispersion chamber prototypes as overlap would have occurred between the adjacent inlets. Accordingly, this design used straight air inlets similar to the Handihaler®.

The device resistance of the inhaler is provided in Table 10.4. Due to the two air inlets, the overall resistance is only  $0.079 \text{ (cmH}_2\text{O)}^{0.5} / \text{L min}^{-1}$  when two beads are included in the dispersion chamber, and is categorized as an intermediate resistance device [3]. The flow rate corresponding to a 4 kPa pressure drop across the device is  $81 \text{ L min}^{-1}$ , approximately twice that of the Handihaler. The inclusion of the polystyrene beads into each dispersion chamber produces a minimal increase in device resistance relative to the empty chambers (Figure 10.11).

*In vitro* deposition performance from the dual chamber device incorporating two beads, each coated with either budesonide or salbutamol and simultaneously actuated in parallel is shown in Figure 10.12. As discussed above, the plastics and surface finishing of the prototype devices were not optimized to maximize the emitted dose, and the device retention values were 29% for budesonide and 30% for salbutamol, compared to 20% and 13% observed when dispersion was evaluated through the Handihaler. As a result, the emitted fractions were diminished 16% (budesonide) and 21% (salbutamol) relative to the EF values obtained from the commercial device at approximately the same overall pressure drop. While it is noted that the



dispersion through the Handihaler was performed with a single bead, the device retention values through the dual chamber device are comparable to those observed with the single chamber prototypes, indicating that retention was due primarily to the prototype material as opposed to being attributable to the simultaneous actuation of two beads and a corresponding lower flow rate through each chamber. The two drugs exhibited similar deposition profiles through the NGI and aerodynamic diameters of 2.76  $\mu\text{m}$  and 2.91  $\mu\text{m}$  were calculated for budesonide and salbutamol, respectively (Figure 10.13).

As noted in the previous chapter, budesonide displayed a higher affinity for the bead relative to salbutamol, as recovered doses ranged from 230 – 280  $\mu\text{g}$  for the corticosteroid, and 100 – 180  $\mu\text{g}$  for the  $\beta$ -agonist. Additionally, bead retention for the former was between 6 – 9 % of the total dose, compared to 2 – 4% for the latter. By comparison, for the commercial combination DPI products ADVAIR<sup>®</sup> Diskus<sup>®</sup> and SYMBICORT<sup>®</sup> Turbuhaler<sup>®</sup>, *in vitro* drug delivery has been reported to range between 10 – 25% of the metered dose [11-13].

#### **10.4. CONCLUSION**

This chapter examined variations in mouthpiece design performance with the purpose of developing a prototype device to improve the aerosol performance of drug-coated polystyrene beads. To that end, designs were developed using CAD software and manufactured via stereolithography. The designs incorporated variations in mouthpiece length, mouthpiece exit diameter, and powder channel diameter, in addition to flow bypass and sheath flow configurations. Of the different designs evaluated *in vitro*, only the tapered mouthpieces and filleted sheath flow channel design significantly outperformed dispersion from the Handihaler, with FPF values ranging up to 84%, and %IP as low as 10%. Additionally, the inclusion of flow bypass channels reduced overall device resistance to approximately half the value of the Handihaler, enabling flow rates in excess of 100 L min<sup>-1</sup> at 4 kPa, demonstrating the development of a low resistance device capable of highly efficient drug delivery.

## 10.5. REFERENCES

1. N.Y.K. Chew, Chan, H.K., Bagster, D.F., and Mukhraiya, J. Characterization of pharmaceutical powder inhalers: estimation of energy input for powder dispersion and effect of capsule device configuration. *Aerosol Science*. 33:999 - 1008 (2002).
2. A.R. Clark, and Hollingworth, A.M. The relationship between powder inhaler resistances and peak inspiratory conditions in healthy volunteers - implications for in vitro testing. *Journal of Aerosol Medicine*. 6:99 - 110 (1993).
3. C.A. Dunbar, Morgan, B., Van Oort, M., Hickey, A.J. A comparison of dry powder inhaler dose delivery characteristics using a power criterion. *Journal of Pharmaceutical Science and Technology*. 54:478 - 484 (2000).
4. P.F. Jacobs. Rapid Prototyping and Manufacturing: Fundamentals of Stereolithography, 1992.
5. F.P. Melchels, J. Feijen, and D.W. Grijpma. A review on stereolithography and its applications in biomedical engineering. *Biomaterials*. 31:6121-6130 (2010).
6. A.J. Blewett, Varma, D., and Gilles, T., Butcher, R., Jacob, J., Amazan, J., and Jansen, S.A. Development and validation of a stability-indicating high-performance liquid chromatography method for the simultaneous determination of albuterol, budesonide, and ipratropium bromide in compounded nebulizer solutions. *Journal of AOAC International*. 94:110 - 117 (2011).
7. M.S. Coates, H.K. Chan, D.F. Fletcher, and J.A. Raper. Influence of air flow on the performance of a dry powder inhaler using computational and experimental analyses. *Pharmaceutical Research*. 22:1445-1453 (2005).
8. W. Dehaan and W. Finlay. Predicting extrathoracic deposition from dry powder inhalers. *Journal of Aerosol Science*. 35:309-331 (2004).

9. S. Chodosh, Flanders, J.S., Kesten, S., Serby, C.W., Hochrainer, D., and Witek, T.J. Effective Delivery of Particles with the HandiHaler® Dry Powder Inhalation System over a Range of Chronic Obstructive Pulmonary Disease Severity. *Journal of Aerosol Medicine*. 14:309 - 315 (2001).
10. M.S. Coates, D.F. Fletcher, H.K. Chan, and J.A. Raper. Effect of design on the performance of a dry powder inhaler using computational fluid dynamics. Part 1: Grid structure and mouthpiece length. *Journal of Pharmaceutical Sciences*. 93:2863-2876 (2004).
11. M. Taki, C. Marriott, X.M. Zeng, and G.P. Martin. Aerodynamic deposition of combination dry powder inhaler formulations in vitro: a comparison of three impactors. *International Journal of Pharmaceutical Sciences*. 388:40-51 (2010).
12. P.T. Daley-Yates, Parkins, D.A., Thomas, M.J., Gillett, B., House, K.W., and Ortega, H.G. Pharmacokinetic, Pharmacodynamic, Efficacy, and Safety Data From Two Randomized, Double-Blind Studies in Patients With Asthma and an In Vitro Study Comparing Two Dry-Powder Inhalers Delivering a Combination of Salmeterol 50 mcg and Fluticasone Propionate 250 mcg: Implications for Establishing Bioequivalence of Inhaled Products. *Clinical Therapeutics*. 31:370 - 385 (2009).
13. W.Y. Tarsin, S.B. Pearson, K.H. Assi, and H. Chrystyn. Emitted dose estimates from Seretide Diskus and Symbicort Turbuhaler following inhalation by severe asthmatics. *International Journal of Pharmaceutical Sciences*. 316:131-137 (2006).
14. B.J. Meakin, Ganderton, D., Panza, I., and Ventura, P. The effect of flow rate on drug delivery from the Pulvinal, a high-resistance dry powder inhaler. *Journal of Aerosol Medicine*. 11:143 - 152 (1998).
15. T. Weuthen, Roeder, S., Brand, P., Mullinger, B., and Scheuch, G. In vitro testing of two formoterol dry powder inhalers at different flow rates. *Journal of Aerosol Medicine*. 15:297 - 303 (2002).

16. G.R. Pitcairn, Lankinen, T., Seppala, O.P., and Newman, S.P. Pulmonary Drug Delivery from the Taifun Dry Powder Inhaler Is Relatively Independent of the Patient's Inspiratory Effort. *Journal of Aerosol Medicine*. 13:97 - 104 (2004).
17. M. DeLong, Wright, J., Dawson, M., Meyer, T., Sommerer, K., Dunbar, C. Dose Delivery Characteristics of the AIR® Pulmonary Delivery System Over a Range of Inspiratory Flow Rates. *Journal of Aerosol Medicine*. 18:452 - 459 (2005).
18. R. Pavkov, S. Mueller, K. Fiebich, D. Singh, F. Stowasser, G. Pignatelli, B. Walter, D. Ziegler, M. Dalvi, J. Dederichs, and I. Rietveld. Characteristics of a capsule based dry powder inhaler for the delivery of indacaterol. *Current Medical Research Opinion*. 26:2527-2533 (2010).
19. A. Palander, Mattila, T., Karhu, M., and Muttonen, E. In vitro Comparison of Three Salbutamol-Containing Multidose Dry Powder Inhalers: Buventol Easyhaler®, Inspiryl Turbuhaler® and Ventoline Diskus®. *Clinical Pharmacokinetics*. 20:25 - 33 (2000).
20. C.C. Smutney, Friedman, E.M., Polidoro, J.M., and Amin, N. Inspiratory Efforts Achieved in Use of the Technosphere® Insulin Inhalation System. *Journal of Diabetes Science and Technology*. 3:1175 - 1182 (2009).

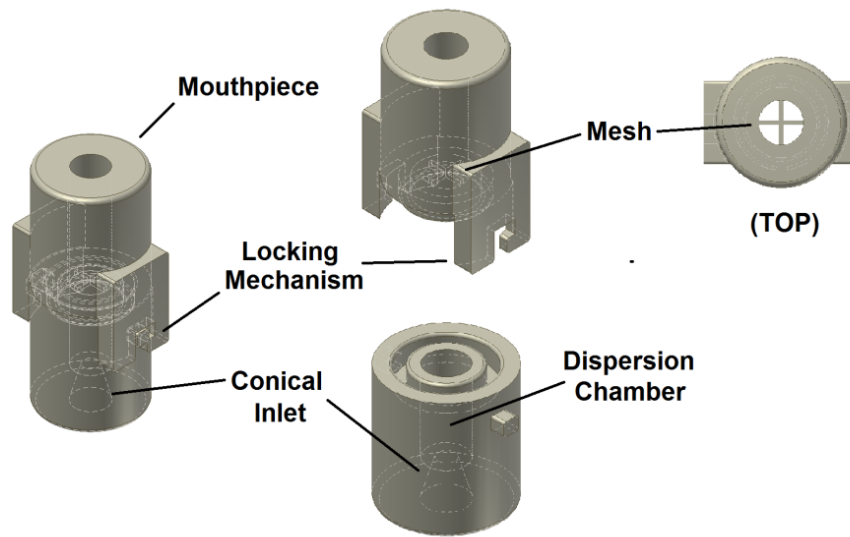


Figure 10.1. Archetypal Design of a Single Dispersion Chamber Prototype Inhaler

The inner diameters of the dispersion chamber and powder flow channel through the mouthpiece were both 7.6 mm. Providing the flow stream to the dispersion chamber was a conical inlet (8 mm length with a 15 degree taper angle) with a 3.5 mm diameter inlet. The mouthpiece contains a mesh situated directly above the dispersion chamber to prevent escape of the bead from the device. A locking mechanism on each side of the inhaler allows the mouthpiece and dispersion chambers to be sealed during actuation.

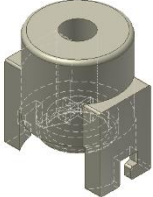
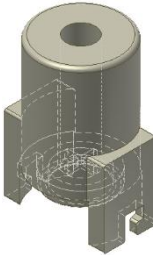
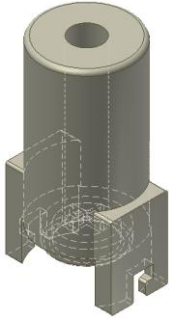
Mouthpiece Length		
20 mm	30 mm	40 mm
		

Figure 10.2. Prototype Designs with Varying Mouthpiece Length

The overall dimensions were kept constant relative to the archetype, with only the length of the mouthpiece varying to provide powder channels of 20 mm, 30 mm, and 40 mm.

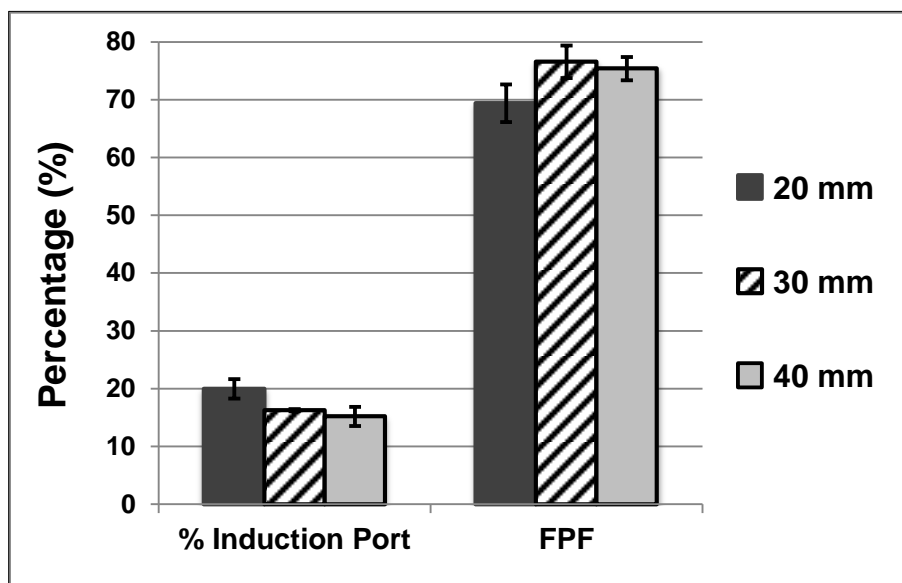


Figure 10.3. Performance of Prototypes with Varying Mouthpiece Length

*In vitro* aerosol performance was evaluated at  $39 \text{ L min}^{-1}$  as mouthpiece length was varied from 20, 30, and 40 mm. Values are provided as the mean ( $\pm$  standard deviation) for  $N = 3$  replicates.

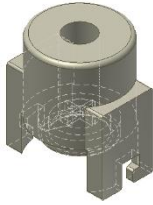
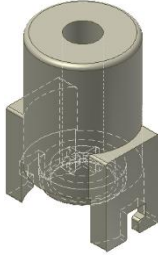
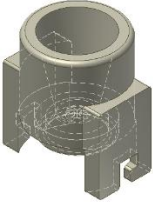

	20 mm	30 mm
STRAIGHT		
TAPERED		

Figure 10.4. Prototype Designs with Tapered Device Outlet Channels

The diameter of the channel was tapered to be 15.2 mm at the exit, corresponding to the twice the diameter at the base of the mouthpiece (7.6 mm). The length of the mouthpiece was also varied to provide powder channels of 20 mm, 30 mm and compared against straight-channel mouthpieces of similar lengths.



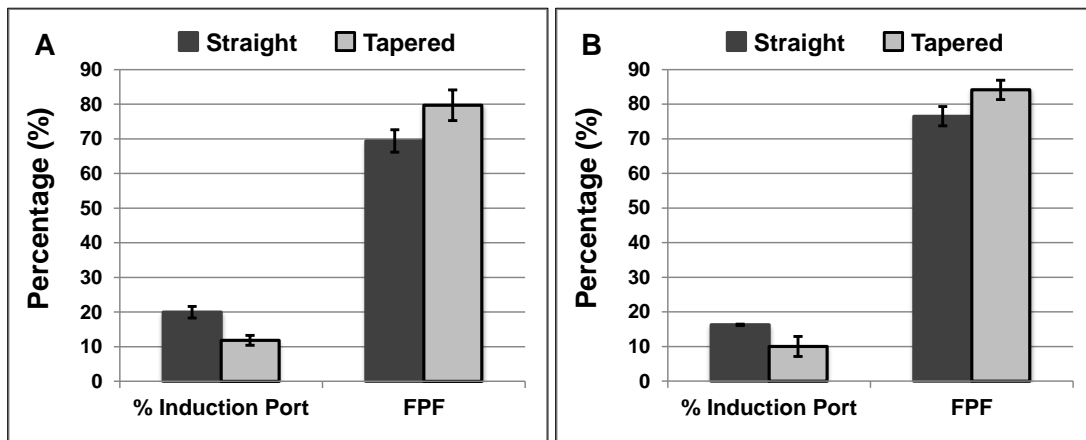


Figure 10.5. Performance of Tapered Mouthpiece Channel Prototypes

*In vitro* aerosol performance was evaluated at  $39 \text{ L min}^{-1}$  as the diameter of the mouthpiece outlet was varied from 7.6 mm to 15.2 mm for (A) 20 mm and (B) 30 mm mouthpiece lengths. Values are provided as the mean ( $\pm$  standard deviation) for  $N = 3$  replicates.


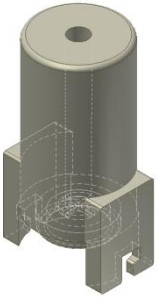
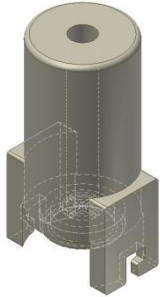
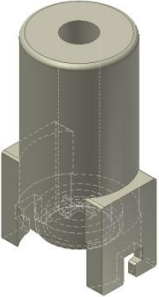
Mouthpiece Diameter			
4 mm	5 mm	6 mm	7.6 mm
			

Figure 10.6. Prototype Designs with Varying Mouthpiece Channel Diameters

The length of the mouthpiece was maintained at 40 mm while the diameter of the channel was altered from 4 mm, 5 mm, 6 mm and 7.6 mm.

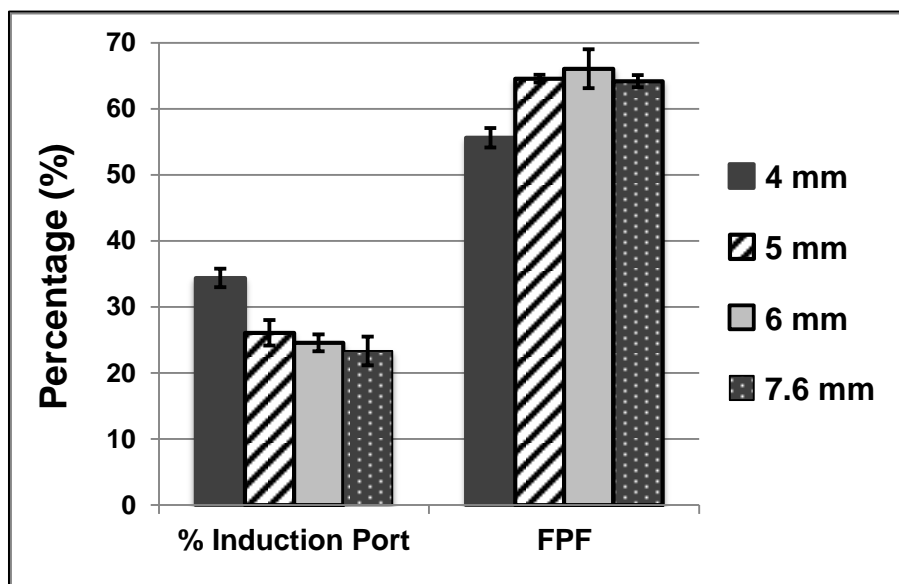


Figure 10.7. Performance of Varying Mouthpiece Channel Diameters

*In vitro* aerosol performance was evaluated at  $39 \text{ L min}^{-1}$  as the diameter of the mouthpiece outlet was varied between 4 mm, 5 mm, 6 mm, and 7.6 mm. The overall length of the channel was 40 mm. Values are provided as the mean ( $\pm$  standard deviation) for  $N = 3$  replicates.

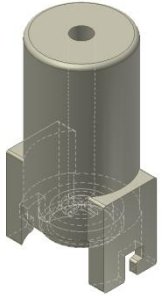
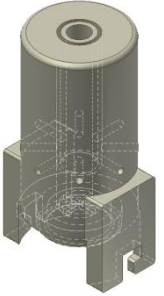
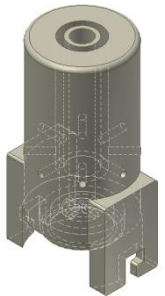

Flow Bypass Channel Configuration			
None	1.5 mm	3 mm	3 mm Filleted Edge
			

Figure 10.8. Designs Possessing Flow Bypass and Sheath Flow Channels

The length of the mouthpiece was maintained at 40 mm, and the diameter of the powder flow channel was 5 mm for all designs. Eight circular inlets (1.5 mm diameter) were arranged circumferentially around the mouthpiece. The inlets connected to a sheath flow channel whose inner edge was separated from the outer edge of the powder flow channel by a 2 mm distance. The distance between the inner and outer edge of the sheath flow channel was varied between 1.5 mm and 3.0 mm. In the latter configuration, the outer edge of the sheath flow channel was filleted by 5 mm.

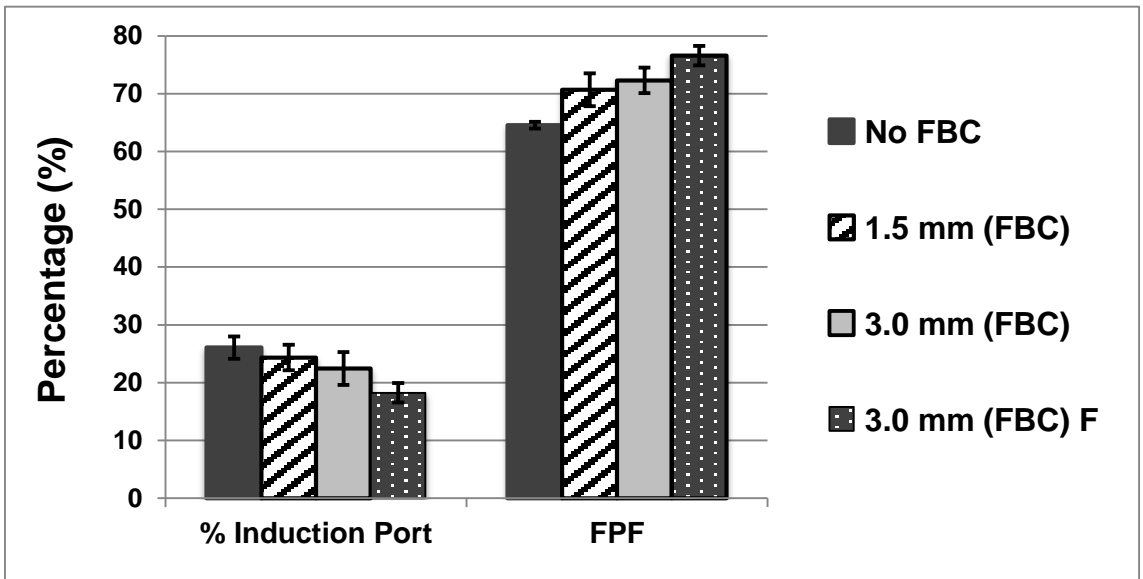


Figure 10.9. Performance of Flow Bypass and Sheath Flow Mouthpiece Designs

*In vitro* aerosol performance for the various flow bypass channel (FBC) configurations. The performance of these designs was compared against a prototype with similar mouthpiece and channel diameters (40 mm and 5 mm, respectively) but without flow bypass channels (No FBC). The designed tested included a distance between the inner and outer edge of the sheath flow channel of 1.5 mm (1.5 mm (FBC)) and 3.0 mm (3.0 mm (FBC)). Additionally, a design similar to the latter prototype but with a filleted outer edge of the sheath flow channel (3.0 mm (FBC) F) was evaluated. Values are provided as the mean ( $\pm$  standard deviation) for N = 3 replicates.

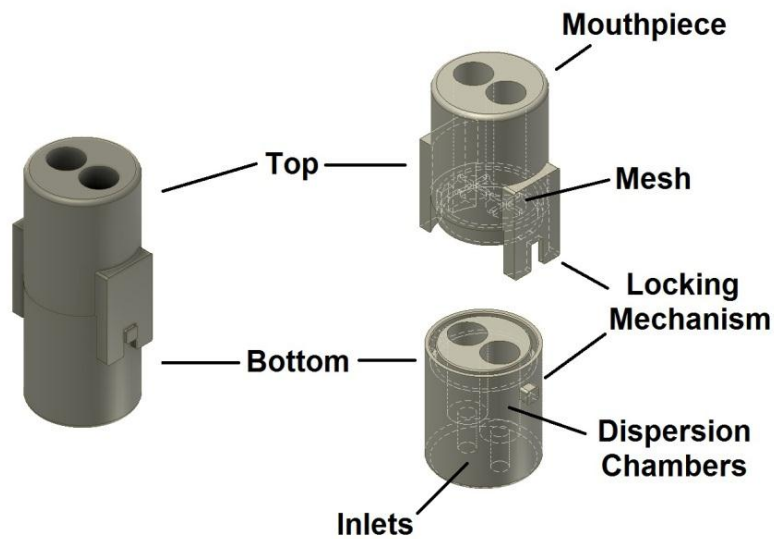


Figure 10.10. Design of a Dual Dispersion Chamber Prototype Inhaler

The inner diameters of the dispersion chamber and mouthpiece were 7.6-mm for both channels. Providing the flow stream to the dispersion chamber was a straight inlet, 8-mm in length and 3.5-mm in diameter. The mouthpiece contains two meshes, each situated directly above a dispersion chamber to prevent escape of the beads from the device. A locking mechanism on each side of the inhaler allows the mouthpiece and dispersion chambers to be maintained closed during actuation.

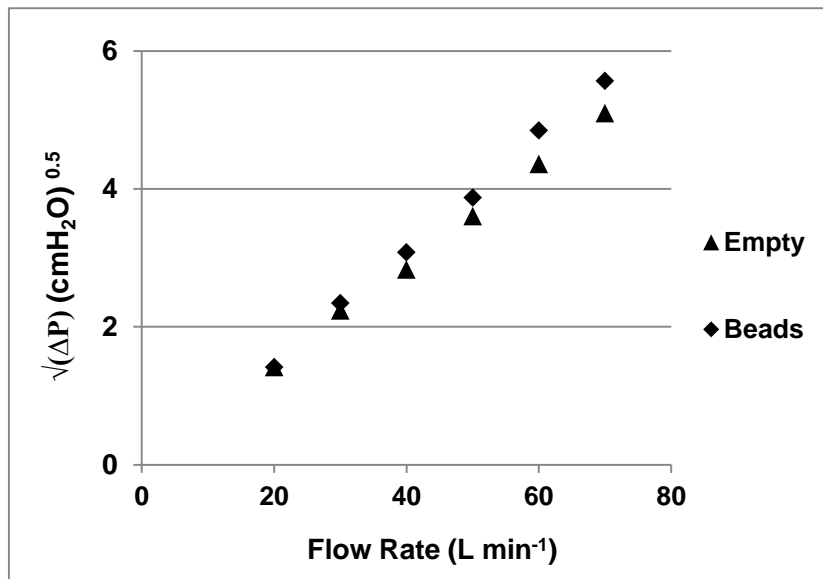


Figure 10.11. Pressure Drop Across the Dual Chamber Prototype at Various Flow Rates

The square root of the pressure drop was evaluated with both dispersion chambers empty, or with a 5.2 mm polystyrene bead included in each chamber.

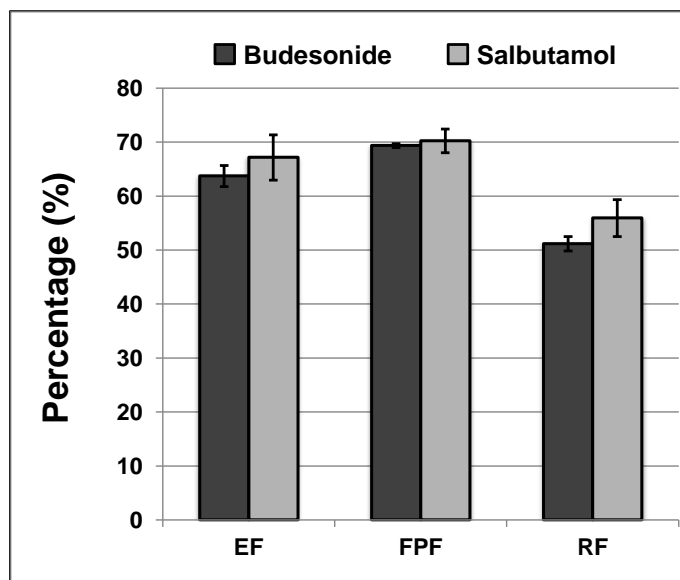


Figure 10.12. Performance of Dual Chamber Prototype Inhaler

*In vitro* aerosol performance of budesonide- and salbutamol-coated polystyrene beads dispersed simultaneously from the dual chamber prototype design. The volumetric flow rate was set to correspond to a 4 kPa pressure drop across the device ( $81 \text{ L min}^{-1}$ ) and the actuation time adjusted to provide 4 L of air flow through the device. Values are reported as the mean ( $\pm$  standard deviation) for N = 3 replicates.



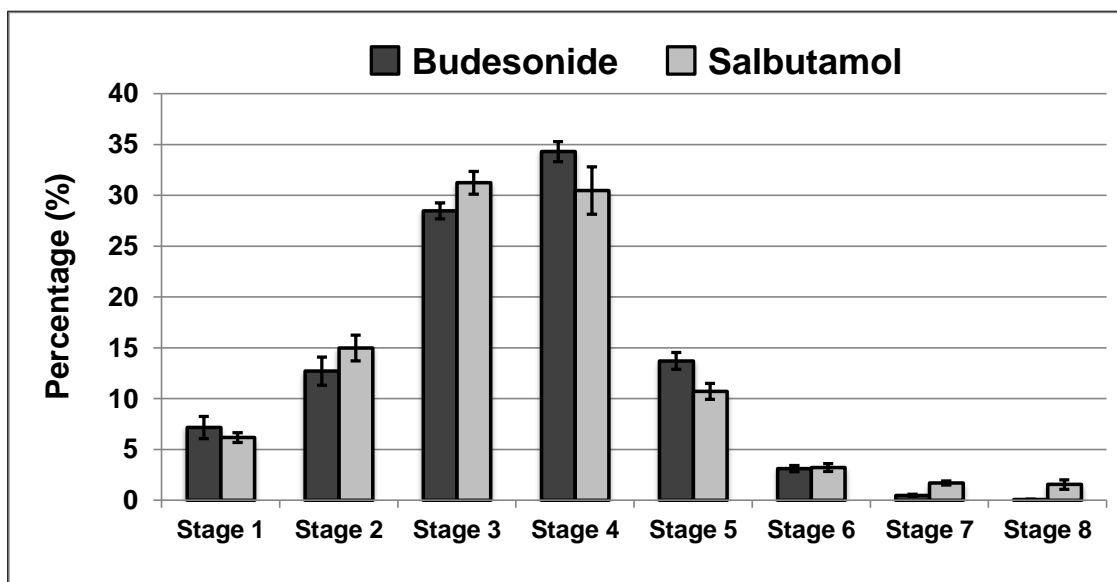


Figure 10.13. Stage Deposition from Dual Chamber Prototype

The deposition values are reported for each stage as a fraction of the cumulative dose collected from all eight NGI stages following each cascade impaction. The similarity of the stage deposition profiles indicates comparable aerosol performance, as reflected by their similar aerodynamic diameters. Values are reported as the mean ( $\pm$  standard deviation) for N = 3 replicates.

Table 10.1. Resistances of Marketed DPIs and Devices Presently in Development

Dry Powder Inhaler	Device Resistance (cmH <sub>2</sub> O) <sup>0.5</sup> / L min <sup>-1</sup>	Flow Rate @ 4 kPa (L min <sup>-1</sup> )	REF
Rotahaler	0.040	160	[2]
Spinhaler	0.051	125	[2]
Diskus	0.066	96	[13]
Diskhaler	0.067	95	[2]
Aerolizer	0.070	91	[15]
Breezhaler	0.070	91	[18]
Turbuhaler (Mark III)	0.086	74	[13]
Turbuhaler	0.100	64	[2]
AIR	0.140	46	[17]
Easyhaler	0.156	41	[19]
Handihaler	0.164	39	[9]
Inhalator	0.180	36	[2]
Taifun	0.182	35	[16]
Pulvinal	0.190	34	[14]
MedTone	0.374	17	[20]

Table 10.2. Device Resistances of Handihaler and Single Chamber Prototype

Device	Device Resistance ((cmH <sub>2</sub> O) <sup>0.5</sup> / L min <sup>-1</sup> )	Flow Rate @ 4 kPa (L min <sup>-1</sup> )
Handihaler	0.173	39
Prototype	0.140	46

Prior to resistance measurements, an empty size-3 gelatin capsule was placed into the dispersion chamber of the Handihaler and punctured via the piercing mechanism of the DPI. For the prototype, a 5.2 mm polystyrene bead (uncoated) was likewise placed into the dispersion chamber before measuring the resistance.

Table 10.3. Resistances for Flow Bypass and Sheath Flow Channel Configurations

Device	Device Resistance ((cmH <sub>2</sub> O) <sup>0.5</sup> / L min <sup>-1</sup> )	Flow Rate @ 4 kPa (L min <sup>-1</sup> )
1.5 mm	0.079	81
3.0 mm	0.061	105
3.0 mm, Filleted	0.058	110

Prior to resistance measurements, a 5.2 mm polystyrene bead (uncoated) was placed into the dispersion chamber of the prototype inhaler.

Table 10.4. Measured Device Resistance for Dual Chamber Prototype Device

Dispersion Chamber Configuration	Device Resistance ((cmH <sub>2</sub> O) <sup>0.5</sup> / L min <sup>-1</sup> )	Flow Rate at 4 kPa (L min <sup>-1</sup> )
Empty	0.073	90
5.2 mm Polystyrene Beads	0.079	81

Resistance of a prototype device with dual dispersion chambers was initially measured with both dispersion chambers empty and with each chamber containing a 5.2 mm polystyrene bead.

## CHAPTER 11

### 11. Final Conclusions

This thesis has examined the influence that the physical properties, specifically the diameter and surface roughness, of the carrier particle population can impart to the aerosol performance of binary DPI formulations.

In chapter 3, a comprehensive *in vitro* study was undertaken, examining the aerosol performance of 4 grades of lactose fractionated into 13 narrow and contiguous size fractions. In addition to the *in vitro* drug deposition profiles from these 52 formulations, many of the physicochemical parameters that have been reported to be important for the performance of binary blends, including the lactose fines concentration, specific surface area, and surface energy of the carrier particles were examined. It was noted that while the overall performance of the  $\alpha$ -lactose monohydrate carrier populations followed the expected trend where increasing the diameter of the carrier particle resulted in diminishing overall drug deposition, the performance from many of the formulations deviated from that predicted in the literature. Specifically, spray dried and granulated lactose carriers, both possessing extensive surface roughness, exhibited performance improvements with large carrier particle diameters.

Chapter 4 more closely examined the influence of carrier particle diameter and surface roughness, while simultaneously using a distinct drug and concentration than that employed in the previous chapter. Though the absolute values differed between studies, the overall trends were similar as the larger granulated carrier particles outperformed smaller size fractions. It was speculated that this may occur due to a shift in the predominant drug detachment mechanism for these larger granulated particles, as their surface roughness would diminish the influence of fluid-based drug detachment from the flow stream, thus causing them to rely more on mechanical detachment forces derived from particle collisions. Accordingly, this would favor larger carrier particles capable of producing sufficient momentum transfers between the drug and carriers during collisions.

In chapter 5 the performance of a DPI as a function of carrier particle size and surface roughness was evaluated. Specifically, formulations were delivered from two commercial inhalers (Aerolizer® and Handihaler®) and computational fluid dynamics was used to model the carrier particle trajectories within the devices. The results indicated that in the Aerolizer, carrier particles undergo more collisions with the inner walls of the DPI as their diameter increases. In contrast, the Handihaler exhibited no marked change in the frequency of particle collisions as their diameter was altered. These disparate trends were reflected in the *in vitro* studies from the granulated carriers, where increasing particle diameter improved performance from the Aerolizer but not in the Handihaler, suggesting that particle-device collisions could indeed promote drug delivery.

Chapter 6 examined the influence of flow rate on the performance of lactose carrier particles as a function of diameter and surface roughness. These studies revealed that larger diameter carrier particles benefit most from increases in flow rate. Additionally, granulated carrier particles exhibited both the greatest performance improvement as flow was increased from 30 min<sup>-1</sup> to 90 L min<sup>-1</sup>, and the best overall performance at the higher flow rate. These results suggest that mechanical detachment forces can dominate fluid forces, and carrier particles that are designed to optimize the influence of the former can yield excellent drug dispersion.

From these observations, a novel dry powder dispersion mechanism was developed based on drug detachment due to mechanical forces. Specifically, large carrier particles (> 500 μm) were employed to increase the collision forces between particle and device. These particles were designed to be much larger than the pore sizes of the meshes found in DPIs, ensuring that the particle is retained and thus allowing the use of materials other than FDA-approved lactose.

Chapter 7 focused on the selection of an appropriate carrier particle material, with low-density polystyrene beads emerging as the optimal candidate. Chapter 8 addressed the development of both a dispersion mechanism to minimize the dose retained within the device, and a novel coating method to limit the extent of drug agglomeration and optimize performance of these particles.

In Chapter 9, drug-coated polystyrene beads were compared against the performance of traditional binary formulations at multiple flow rates. At all flow rates, for both budesonide and salbutamol, the beads significantly outperformed the lactose carrier particle-based formulations. Specifically, the performance of the beads at  $15 \text{ L min}^{-1}$  was comparable to the performance of the binary lactose blends at  $30$  and  $45 \text{ L min}^{-1}$ . Additionally, the oscillating frequency of these beads as a function of flow rate was measured, enabling a better understanding of the mechanism governing their performance.

In Chapter 10, the potential of a prototype device to further improve the performance of the large, drug-coated polystyrene beads was investigated. Using rapid prototyping, diverse inhaler designs were manufactured and tested. Specifically, the inclusion of flow bypass channels enabled the production of a low resistance device demonstrating FPF values of approximately 80%. Additionally, a dual-chamber prototype was designed and tested for use in combination therapy (e.g. for delivery of a corticosteroid and a  $\beta$ -agonist), and FPF values of approximately 70% for both drugs were observed at a flow rate corresponding to a 4 kPa pressure drop across the device.

In conclusion, this project has demonstrated that large carrier particle diameters are not as detrimental to performance as initially theorized. Coupling large diameter particles possessing extensive surface roughness to both a device and flow rate that promotes mechanical detachment forces can yield excellent dispersion performance. These observations then led to the development of a novel dispersion mechanism that has reproducibly demonstrated superior performance to commercially employed formulations.



## APPENDIX

### 1. Reported Literature Values of DPI Performance

The following table lists the *in vitro* and *in vivo* aerosol performance data reported in the literature for various dry powder inhalers. For commercial devices, such as the Diskus™ and Turbuhaler™, only the dispersion performance of each DPI's marketed formulation is provided, as opposed to experimental formulations that were dispersed through a commercial device.

For clarity, the table is sorted by inhaler, then by whether the study occurred *in vitro* or *in vivo*, and then according to the API delivered. Multiple flow rates that were investigated in the same study are reported together. The values reported represent the lung deposition of the metered dose, except where only the deposition of the emitted dose was provided, which is denoted by an asterisk (\*). For the *in vivo* studies, the mean volumetric flow rate measured for the patient population was reported.

Inhaler	Study	REF	API / Formulation	Flow Rate (L min <sup>-1</sup> )	FPF Mean (StDev)			
AEROLIZER	<i>In vitro</i>	(1)	Formoterol	28.3	~ 17 %			
				40	~ 23 %			
				60	~ 27 %			
				80	~ 27 %			
				(2)	30	~ 13 %		
					60	~ 15 %		
					90	~ 31 %		
					120	~ 31 %		
				(3)	28.3	~ 18 %		
					80	~ 19 %		
				(4)	60	25.7 %		
				<i>In vivo</i>	(3)	Formoterol		20 %
AIR	<i>In vitro</i>	(5)	Placebo Large Porous Particles	20	67 % (4)			
				28.3	71 % (3)			
				60	74 % (4)			
				<i>In vivo</i>	(5)	Placebo Large Porous Particles	38*	51 %
	AIRMAX	<i>In vitro</i>	(6)	Budesonide	60 – 70	47 %		
60 – 70					48 %			
60 - 70					61 %			
(7)					70	42.7 % (1.9)		
<i>In vivo</i>					(7)	Budesonide	37*	28.3 % (5.6)
		71*	25.8 % (6.5)					
ASPIRAIR	<i>In vitro</i>	(8)	Neuro-active Compound	60	77 %			

<b>BREEZHALER</b>					
	<i>In vitro</i>				
		<b>Indacaterol</b>			
	(9)		30	18.0 %	(1.4)
			40	22.7 %	(1.1)
			50	25.3 %	(0.9)
			60	28.0 %	(0.6)
			70	28.7 %	(0.5)
			80	30.0 %	(0.5)
			90	31.3 %	(1.1)
			100	32.0 %	(0.7)
	(9)		30	18.0 %	(1.1)
			40	24.0 %	(1.2)
			50	28.3 %	(1.3)
			60	30.0 %	(2.0)
			70	31.0 %	(2.2)
			80	33.7 %	(1.8)
			90	35.3 %	(1.5)
			100	34.3 %	(1.2)
<b>CERTIHALER</b>					
	<i>In vitro</i>				
		<b>Novel Anti-inflammatory Agent</b>			
	(10)		60	45.0 %	
			60	53.9 %	
	(11)	<b>Formoterol</b>	60	32 – 49%	
<b>CLICKHALER</b>					
	<i>In vitro</i>				
		<b>Beclomethasone</b>			
	(12)		60	24.2 %	(3.6)
		<b>Budesonide</b>			
	(13)		60	34.6 %	(2.5)
		<b>Salbutamol Sulphate</b>			
	(14)		28.3	31.4 %	
	(12)		60	40.7 %	(4.5)
	<i>In vivo</i>				
		<b>Budesonide</b>			
	(13)		60	26.8 %	(6.8)
<b>DISKHALER</b>					
	<i>In vitro</i>				
		<b>Beclomethasone</b>			
	(15)		60	23.0 %	
		<b>Salbutamol Sulphate</b>			
	(16)		30	14.4 %	(2.3)
			55	15.3 %	(1.1)
			80	30.4 %	(1.9)
	(16)		30	11.4 %	(1.2)
			55	27.0 %	(2.1)

<b>DISKHALER</b>					
<b>(Cont'd)</b>	(17)	28.3	20.4 %	(8.6)	
		60	26.9 %	(5.7)	
	(18)	30	26.7 %		
		60	40.3 %		
	(19)	60	35.1 %	(1.0)	
<b>DISKUS</b>					
	<i>In vitro</i>				
		<b>Fluticasone</b>			
	(20)	30	13.3 %		
		60	18.5 %		
		90	16.1 %		
	(21)	30	19.2 %	(2.6)	
		60	22.4 %	(1.4)	
		90	36.9 %	(3.4)	
	(22)	28.3	16 %		
		60	21 %		
	(23)	60	20.1 %	(1.4)	
	(19)	60	29.9 %	(0.6)	
	(24)	87	25.1 %	(0.4)	
	(25)	PIF?	15 %	(2)	
		PIF?	18 %	(2)	
		<b>Salbutamol Sulphate</b>			
	(26)	30	14.5 %		
		60	20.7 %		
		90	20.1 %		
	(17)	28.3	23.3 %	(0.9)	
		60	31.6 %	(0.9)	
	(18)	---	26 %		
	(27)	PIF	36.8 %	(9.8)	
		<b>Salmeterol Xinafoate</b>			
	(23)	60	23.4 %	(0.8)	
		<b>Comination (Advair)</b>			
	(28)	Fluticasone	30	10.7 %	(0.3)
		Salmeterol		8.5 %	(0.2)
	(28)	Fluticasone	30	16.1 %	(0.5)
		Salmeterol		13.3 %	(0.03)
	(28)	Fluticasone	67	22.5 %	(0.9)
		Salmeterol		24.0 %	(1.0)
	(28)	Fluticasone	71	26.4 %	(1.1)
		Salmeterol		25.1 %	(1.3)

<b>DISKUS (Cont'd)</b>		(29)	Fluticasone Salmeterol	60	26.5 % 25.6 %		
		(30)	Fluticasone Salmeterol	PIFs	20.4 % 18.4 %	(4.8) (4.4)	
<b>DRYHALER</b>	<i>In vitro</i>		<b>Salbutamol Sulphate</b>				
		(31)		28.3	20 %	(3.3)	
<b>EASYHALER</b>	<i>In vitro</i>		<b>Beclomethasone</b>				
		(19)		60	23.3 %	(0.6)	
			<b>Budesonide</b>				
		(32)		58	35.9 %	(4.6)	
	<i>In vivo</i>		<b>Salbutamol Sulphate</b>				
		(26)		30 40 60	15.6 % 20.9 % 23.2 %		
			<b>Beclomethasone</b>				
		(33)		-----	18.9 %	(9.5)	
	<b>Budesonide</b>						
(32)		63*	18.5 %	(7.8)			
	<b>Salbutamol Sulphate</b>						
(34)		32 - 65	24 %	(6)			
<b>FLOWCAPS</b>	<i>In vitro</i>		<b>Budesonide</b>				
		(35)		30	20.8 %		
			<b>Salbutamol</b>				
(35)		30	43.6 %				
<b>GENUAIR</b>	<i>In vitro</i>		<b>Acridinium Bromide</b>				
		(36)		Not specified Not specified	23.2 % 37.1 %		
		(37)		90	40.3 %	(5.6)	
	<i>In vivo</i>		<b>Acridinium Bromide</b>				
	(37)		79*	30.1 %	(7.3)		

<b>HANDIHALER</b>	<i>In vitro</i>	<b>Ipratropium</b>	(38)	20	16.3 %		
				28.3	21.8 %		
				40	23.4 %		
				50	25.3 %		
				60	24.3 %		
	<i>In vivo</i>	<b>Tiotropium</b>	(39)	Healthy	18 %		
				Mild COPD	19 %		
				Moderate COPD	22 %		
				Severe COPD	18 %		
<b>INHALATOR</b>	<i>In vitro</i>	<b>Salbutamol Sulphate</b>	(40)	28.3	9.6 %		
				60	21.9 %		
		<b>Tiotropium</b>	(19)		60	34.7 %	
<b>MAGHALER</b>	<i>In vitro</i>	<b>Salbutamol</b>	(41)	60	46.7 %		
	<i>In vivo</i>	<b>Salbutamol</b>	(41)	36.3*	21.1 %	(5.1)	
				62.1*	26.4 %	(4.3)	
<b>MEDTONE</b>	<i>In vivo</i>	<b>Insulin (Technosphere)</b>	(42)	Not Measured	39.5 %		
<b>MICRODOSE DPI</b>	<i>In vitro</i>	<b>Unspecified API</b>	(43)	28.3	84 %		
<b>MONODOSE</b>	<i>In vitro</i>	<b>Budesonide</b>	(44)	60	33.1 %	(1.8)	
	<i>In vivo</i>	<b>Budesonide</b>	(44)	47*	21.4 %	(7.5)	
				96*	21.4 %	(4.3)	

<b>NOVOLIZER</b>	<i>In vitro</i>	<b>Budesonide</b>	(45)	35	~ 15 %		
				60	~ 34 %		
				100	~ 48 %		
	<i>In vivo</i>	<b>Budesonide</b>	(46)	54	19.9 %		
				65	25.0 %		
				99	32.1 %		
<b>PULVINAL</b>	<i>In vitro</i>	<b>Beclomethasone</b>	(47)	28	22 %		
				63	34 %		
	<i>In vivo</i>	<b>Salbutamol</b>	(48)	27.8*	11.7 %	(2.3)	
				46.0*	14.1 %	(3.2)	
	<b>ROTAHALER</b>	<i>In vitro</i>	<b>Beclomethasone</b>	(21)	30	10.6 %	(1.2)
					60	15.2 %	(1.0)
				90	24.3 %	(2.3)	
(49)				60	12.6 %	(1.8)	
(50)				60	16 %	(2.3)	
<b>Salbutamol Sulphate</b>			(16)	30	12.2 %	(1.1)	
				55	15.1 %	(1.2)	
				80	18.2 %	(3.1)	
(40)			28.3	3.7 %			
			60	14.2 %			
(16)			30	8.6 %	(1.1)		
			55	22.6 %	(4.2)		
(47)			34	~ 8 %			
			107	~ 17 %			
(51, 52)	74	12.9 %					
	144	18.8 %					
(53)	60	16.6 %	(0.3)				
(54)	60	27.1 %	(2.0)				
<i>In vivo</i>	<b>Salbutamol Sulphate</b>	(55)	Unspec.	9.1 %	(0.6)		

<b>SPINHALER</b>	<i>In vitro</i>	<b>Cromolyn Sodium</b>	(19)	60	4.2 %	(0.7)		
			(15)	60	7.8 %			
			(56)	60	8.6 %			
			(57)	60	12.5 %			
			(58)	60	15 %			
			(59)	100	14.1 %	(1.4)		
			<b>SPIROS</b>	<i>In vitro</i>	<b>Salbutamol Sulphate</b>	(60)	15	25.8 %
	60	19.3 %				(7.3)		
<b>TAIFUN</b>	<i>In vitro</i>	<b>Budesonide</b>	(61)	28.3	30.2 %			
			(62)	28.3	45 %			
				28.3	35 %			
			(63)	33	27.6 %	(2.6)		
				33	30.6 %	(1.3)		
		<i>In vivo</i>	<b>Budesonide</b>	(61)	20.6* (2.2)	29.6 %	(5.9)	
					35.8* (4.5)	34.3 %	(5.8)	
		<b>TURBUHALER</b>	<i>In vitro</i>	<b>Budesonide</b>	(21)	30	12.4 %	(2.8)
						60	28.4 %	(2.3)
	90				40.7 %	(5.5)		
(22)	28.3				6 %			
	60				18 %			
(64)	60				27.3 %			
(13)	60				29.8 %	(5.5)		
(65)	60				34 %	(2.5)		
(32)	60				34.4 %	(2.6)		
(44)	60				36.2 %	(1.0)		
(15)	60				37.5 %			
(66)	60				38.7 %			
(19)	60				39.3 %	(2.0)		
(25)					21 %	(10)		
					32 %	(9)		



TURBUHALER (Cont'd)				
		<b>Formoterol</b>		
(1)		28.3	~ 18 %	
		40	~ 35 %	
		60	~ 41 %	
		80	~ 40 %	
(2)		30	~ 5 %	
		60	~ 13 %	
		90	~ 33 %	
		120	~ 34 %	
		<b>Salbutamol Sulphate</b>		
(17)		28.3	9.7 %	(3.2)
		60	23.3 %	(3.0)
(17)		28.3	13.3 %	(1.6)
		60	27.6 %	(8.0)
(26)		30	11.5 %	
		60	23.8 %	
(51, 52)		30	25.2 %	
		60	41.8 %	
(27)			28.7 %	(7.7)
		<b>Terbutaline Sulphate</b>		
(16)		30	14.8 %	(1.7)
		55	18.7 %	(3.2)
		80	28.0 %	(3.8)
(67)		28.3	12 %	
		60	42 %	
(16)		30	8.8 %	(1.1)
		55	27.1 %	(7.6)
(57)		60	34.6 %	
(19)		60	35.4 %	(1.4)
		<b>Combination (Symbicort)</b>		
(30)		Budesonide	23.1 %	(12.9)
		Formoterol	20.7 %	(11.1)
	<i>In vivo</i>	<b>Budesonide</b>		
(66)		29*	17.8 %	
		58*	28.5 %	
(7)		31*	22.7 %	(5.6)
		59*	29.8 %	(6.9)
(44)		33*	18.5 %	(6.5)
		66*	25.1 %	(6.1)
(64)		36*	14.8 %	(3.3)
		58*	27.7 %	(9.5)

<b>TURBUHALER (Cont'd)</b>		(46)	58	21.4 %		
		(32)	64*	21.8 %	(8.2)	
		(68)	??	20.8 %		
		(64)	57*	27.0 %	(7.7)	
<b>TWISTHALER</b>	<i>In vitro</i>					
		(69)	60	35.6 %	(3.4)	
			60	39.9 %	(2.5)	
<b>ULTRAHALER</b>	<i>In vitro</i>					
			(70)	60	18.6 %	(1.6)
			(71)	60	34.6 %	(4.3)
			(72)	60	44.7 %	
	<i>In vivo</i>					
		(71)	60**	24.6 %	(7.3)	
		(70)	42.5* (8.6)	9.8 %	(3.5)	
			75.3* (19)	13.3 %	(4.8)	

### 1.1. APPENDIX REFERENCES

1. T. Weuthen, Roeder, S., Brand, P., Mullinger, B., and Scheuch, G. In vitro testing of two formoterol dry powder inhalers at different flow rates. *Journal of Aerosol Medicine*. 15:297 - 303 (2002).
2. N.Y.K. Chew, and Chan, H.K. In Vitro Aerosol Performance and Dose Uniformity between the Foradile® Aerolizer® and the Oxis® Turbuhaler®. *Journal of Aerosol Medicine*. 14:495 - 501 (2001).
3. T. Meyer, Brand, P., Ehlich, H., Kobrich, R., Meyer, G., Riedinger, F., Sommerer, K., Weuthen, T., and Scheuch, G. . Deposition of Foradil P in Human Lungs: Comparison of In Vitro and In Vivo Data. *Journal of Aerosol Medicine*. 17:43 - 49 (2004).
4. C.P. Criece, Meyer, T., Petro, W., Sommerer, K., and Zeising, P. In Vitro Comparison of Two Delivery Devices for Administering Formoterol: Foradil® P and Formoterol Ratiopharm Single-Dose Capsule Inhaler. *Journal of Aerosol Medicine*. 19:466 - 472 (2006).
5. M. DeLong, Wright, J., Dawson, M., Meyer, T., Sommerer, K., Dunbar, C. Dose Delivery Characteristics of the AIR® Pulmonary Delivery System Over a Range of Inspiratory Flow Rates. *Journal of Aerosol Medicine*. 18:452 - 459 (2005).
6. X. Zeng. Delivery of salbutamol and of budesonide from a novel multi-dose inhaler Airmax™. *Respiratory Medicine*. 96:404-411 (2002).
7. P. Hirst, Newman, S.P., Clark, D.A., and Hertog, M.G.L. Lung deposition of budesonide from the novel dry powder inhaler Airmax™. *Respiratory Medicine*. 96:389-396 (2002).
8. Y. Kamlag, and Morton, D.A.V. Intelligent formulation by design: a case study for systemic delivery, *Respiratory Drug Delievery (2006)*, 2006, pp. 935 - 938.

9. R. Pavkov, S. Mueller, K. Fiebich, D. Singh, F. Stowasser, G. Pignatelli, B. Walter, D. Ziegler, M. Dalvi, J. Dederichs, and I. Rietveld. Characteristics of a capsule based dry powder inhaler for the delivery of indacaterol. *Curr Med Res Opin.* 26:2527-2533 (2010).
10. T. Eggimann, Fueg, L.M., Mueller-Walz, R., and Venthoye, G. In vitro aerosol performance of the next generation Skyehaler™ delivering a high drug payload powder. In e.a. R.N. Dalby (ed.), *Respiratory Drug Delivery*, 2006, pp. 781 - 783.
11. R. Guchardi, M. Frei, E. John, and J.S. Kaerger. Influence of fine lactose and magnesium stearate on low dose dry powder inhaler formulations. *Int J Pharm.* 348:10 - 17 (2008).
12. T. Ehtezazi, D.R. Allanson, I.D. Jenkinson, I. Shrubbs, and C. O'Callaghan. Investigating improving powder deagglomeration via dry powder inhalers at a low inspiratory flow rate by employing add-on spacers. *Journal of Pharmaceutical Sciences.* 97:5212-5221 (2008).
13. S. Warren, Taylor, G., Smith, J., Buck, H., and Parry-Billings, M. Gamma Scintigraphic Evaluation of a Novel Budesonide Dry Powder Inhaler Using a Validated Radiolabeling Technique. *Journal of Aerosol Medicine.* 15:15 - 25 (2002).
14. C.H. Richardson, M. de Matas, H. Hosker, R. Mukherjee, I. Wong, and H. Chrystyn. Determination of the relative bioavailability of salbutamol to the lungs following inhalation from dry powder inhaler formulations containing drug substance manufactured by supercritical fluids and micronization. *Pharm Res.* 24:2008-2017 (2007).
15. A.H. de Boer, Gjaltema, D., and Hagedoorn, P. Inhalation characteristics and their effects on in vitro drug delivery from dry powder inhalers. Part 2: Effect of peak flow rate (PIFR) and inspiration time on the *in vitro* drug release from three different types of commercial dry powder inhalers. *Int J Pharm.* 138:45 - 56 (1996).

16. K.J. Smith, Chan, H.K., and Brown, K.F. Influence of flow rate on aerosol particle size distributions from pressurized and breath-actuated inhalers. *Journal of Aerosol Medicine*. 11:231 - 245 (1998).
17. D. Prime, Grant, A.C., Slater, A.L., and Woodhouse, R.N. A critical comparison of the dose delivery characteristics of four alternative inhalation devices delivering salbutamol: Pressurized metered dose inhaler, *Diskus* inhaler, *Diskhaler* inhaler, and *Turbuhaler* inhaler. *Journal of Aerosol Medicine*. 12:75 - 84 (1999).
18. T. Srichana, Martin, G.P., and Marriott, C. Dry powder inhalers: The influence of device resistance and powder formulation on drug and lactose deposition in vitro. *European Journal of Pharmaceutical Sciences*. 7:73 - 80 (1998).
19. H. Steckel, and Muller, B.W. In vitro evaluation of dry powder inhalers I: drug deposition of commonly used devices. *Int J Pharm*. 154:19 - 29 (1997).
20. W.E.S. Kamin, Genz, T., Roeder, S., Scheuch, G., Trammer, T., Juenemann, R., and Cloes, R.M. Mass output and particle size distribution of glucocorticosteroids emitted from different inhalation devices depending on various inspiratory parameters. *Journal of Aerosol Medicine*. 15:65 - 73 (2002).
21. M.R. Feddah, Brown, K.F., Gipps, E.M., Davies, N.M. In vitro characterization of metered dose inhaler versus dry powder inhaler glucocorticoid products: influence of inspiratory flow rates. *Journal of Pharmacy and Pharmaceutical Sciences*. 3:317 - 324 (2000).
22. L.S. Hill, and Slater, A.L. A comparison of the performance of two modern multidose dry powder asthma inhalers. *Respiratory Medicine*. 92:105 - 110 (1998).
23. M. Taki, S. Ahmed, C. Marriott, X.M. Zeng, and G.P. Martin. The 'stage-by-stage' deposition of drugs from commercial single-active and combination dry powder inhaler formulations. *European journal of pharmaceutical sciences*. 43:225 - 235 (2011).

24. H. Steckel. In vitro characterization of jet-milled and in-situ-micronized fluticasone-17-propionate. *Int J Pharm.* 258:65-75 (2003).
25. H. Bisgaard, B. Klug, B.S. Sumby, and P.K.P. Burnell. Fine particle mass from the Diskus inhaler and Turbuhaler inhaler in children with asthma. *European Respiratory Journal.* 11:1111-1115 (1998).
26. A. Palander, Mattila, T., Karhu, M., and Muttonen, E. In vitro Comparison of Three Salbutamol-Containing Multidose Dry Powder Inhalers: Buventol Easyhaler®, Inspiryl Turbuhaler® and Ventoline Diskus®. *Clinical Pharmacokinetics.* 20:25 - 33 (2000).
27. M.E.A.C. Broeders, Molema, J., Burnell, P.K.P., and Folgering H.T.M. Ventolin diskus and inspiryl turbuhaler: an in vitro comparison. *Journal of Aerosol Medicine.* 18:74 - 82 (2005).
28. M. Taki, C. Marriott, X.M. Zeng, and G.P. Martin. Aerodynamic deposition of combination dry powder inhaler formulations in vitro: a comparison of three impactors. *Int J Pharm.* 388:40-51 (2010).
29. P.T. Daley-Yates, Parkins, D.A., Thomas, M.J., Gillett, B., House, K.W., and Ortega, H.G. Pharmacokinetic, Pharmacodynamic, Efficacy, and Safety Data From Two Randomized, Double-Blind Studies in Patients With Asthma and an In Vitro Study Comparing Two Dry-Powder Inhalers Delivering a Combination of Salmeterol 50 mcg and Fluticasone Propionate 250 mcg: Implications for Establishing Bioequivalence of Inhaled Products. *Clinical Therapeutics.* 31:370 - 385 (2009).
30. W.Y. Tarsin, S.B. Pearson, K.H. Assi, and H. Chrystyn. Emitted dose estimates from Seretide Diskus and Symbicort Turbuhaler following inhalation by severe asthmatics. *Int J Pharm.* 316:131-137 (2006).
31. J.P. Kemp, Hill, M.R., Vaughan, L.M., Meltzer, E.O., Welch, M.J., and Ostrom, N.K. Pilot Study of Bronchodilator Response to Inhaled Albuterol Delivered by Metered-Dose

- Inhaler and a Novel Dry Powder Inhaler *Annals of Allergy, Asthma, and Immunology*. 79:322 - 326 (1997).
32. P. Hirst, Bacon, R.E., Pitcairn, G.R., Silvasti, M., and Newman, S.P. A comparison of the lung deposition of budesonide from Easyhaler®, Turbuhaler® and pMDI plus spacer in asthmatic patients. *Respiratory Medicine*. 95:720-727 (2001).
  33. S.P. Newman, Pitcairn, G.R., Adkin, D.A., Vidgren, M.T., and Silvasti, M. Comparison of Beclomethasone Dipropionate Delivery by Easyhaler® Dry Powder Inhaler and pMDI Plus Large Volume Spacer. *Journal of Aerosol Medicine*. 14:217 - 225 (2001).
  34. M. Vidgren, Arppe, J., Vidgren, P., Hyvärinen, L., Vainio, P., Silvasti, M., and Tukiainen, H. Pulmonary Deposition and Clinical Response of <sup>99m</sup>Tc-Labelled Salbutamol Delivered from a Novel Multiple Dose Powder Inhaler *Pharm Res*. 11:1320 - 1324 (1994).
  35. H. Steckel, Villax, P., Eskandar, F., and Borowski, M. Selecting Lactose for a Capsule-Based Dry Powder Inhaler. *Pharmaceutical Technology Europe*. 16:23 - 35 (2004).
  36. K. Block, and Fynys, B. Different inhalation volumes do not impact on the aerodynamics of acclidinium bromide delivered using the Genuair® inhaler, *European Respiratory Society*, Barcelona, 2010.
  37. S.P. Newman, D.J. Sutton, R. Segarra, R. Lamarca, and G. de Miquel. Lung deposition of acclidinium bromide from Genuair, a multidose dry powder inhaler. *Respiration*. 78:322-328 (2009).
  38. S. Chodosh, Flanders, J.S., Kesten, S., Serby, C.W., Hochrainer, D., and Witek, T.J. Effective Delivery of Particles with the HandiHaler® Dry Powder Inhalation System over a Range of Chronic Obstructive Pulmonary Disease Severity. *Journal of Aerosol Medicine*. 14:309 - 315 (2001).

39. P. Brand, T. Meyer, T. Weuthen, W. Timmer, E. Berkel, G. Wallenstein, and G. Scheuch. Lung deposition of radiolabeled tiotropium in healthy subjects and patients with chronic obstructive pulmonary disease. *J Clin Pharmacol.* 47:1335-1341 (2007).
40. M. Louey, M. Vanoort, and A. Hickey. Standardized entrainment tubes for the evaluation of pharmaceutical dry powder dispersion. *Journal of Aerosol Science.* 37:1520-1531 (2006).
41. S. Newman, Malik, S., Hirst, P., Pitcairn, G., Heide, A., Pabst, J., Dinkelaker, A., and Fleischer, W. Lung deposition of salbutamol in healthy human subjects from the MAGhaler dry powder inhaler. *Respiratory Medicine.* 96:1026 - 1032 (2002).
42. J.P. Cassidy, N. Amin, M. Marino, M. Gotfried, T. Meyer, K. Sommerer, and R.A. Baughman. Insulin Lung Deposition and Clearance Following Technosphere((R)) Insulin Inhalation Powder Administration. *Pharm Res* (2011).
43. B. Brown, Rasmussen, J., Becker, D., and Friend, D.R. A piezo-electronic inhaler for local and systemic applications. *Drug Delivery Technology.* 4:1 - 8 (2004).
44. D.J. Ball, P.H. Hirst, S.P. Newman, B. Sonet, B. Streel, and F. Vanderbist. Deposition and pharmacokinetics of budesonide from the Miat Monodose inhaler, a simple dry powder device. *Int J Pharm.* 245:123-132 (2002).
45. U. Munzel, Marschall, K., Fyrnys, B., and Wedel, M. Variability of fine particle dose and lung deposition of budesonide delivered through two multidose dry powder inhalers. *Curr Med Res Opin.* 21:827 - 833 (2005).
46. S.P. Newman, Pitcairn, G.R., Hirst, P.H., Bacon, R.E., O'Keefe, E., Reiners, M., and Hermann, R. Scintigraphic comparison of budesonide deposition from two dry powder inhalers. *European Respiratory Journal.* 16:178 - 183 (2000).



47. B.J. Meakin, Ganderton, D., Panza, I., and Ventura, P. The effect of flow rate on drug delivery from the Pulvinal, a high-resistance dry powder inhaler. *Journal of Aerosol Medicine*. 11:143 - 152 (1998).
48. G. Pitcairn, Lunghetti, G., Ventura, P., and Newman, S. A comparison of the lung deposition of salbutamol inhaled from a new dry powder inhaler, at two inhaled flow rates *Int J Pharm*. 102:11 - 18 (1994).
49. H. Cabral-Marques and R. Almeida. Optimisation of spray-drying process variables for dry powder inhalation (DPI) formulations of corticosteroid/cyclodextrin inclusion complexes. *European journal of pharmaceuticals and biopharmaceutics*. 73:121-129 (2009).
50. M. Weda, Geuns, E.R.M., Vermeer, R.C.R., Buiten, N.R.A., Hendriks-de Jong, K., Bult, A., Zanen, P., and Barends, D.M. Equivalence testing and equivalence limits of metered-dose inhalers and dry powder inhalers measured by in vitro impaction. *European Journal of Pharmaceutics and Biopharmaceutics*. 4:295 - 302 (2000).
51. S.P. Newman, Wilding, I.R., and Hirst, P.H. Human lung deposition data: the bridge between in vitro and clinical evaluations for inhaled drug products? *Int J Pharm*. 208:49 - 60 (2000).
52. L. Borgstrom. In vitro, ex vivo, in vivo veritas. *Allergy*. 54:88 - 92 (1999).
53. X.M. Zeng, Martin, G.P., Marriott, C., and Pritchard, J. Lactose as a Carrier in Dry Powder Formulations: The Influence of Surface Characteristics on Drug Delivery. *Journal of Pharmaceutical Sciences*. 90:1424 - 1434 (2001).
54. S.P. Shah, and Misra, A. Liposomal Amikacin Dry Powder Inhaler: Effect of Fines on In Vitro Performance. *AAPS PharmSciTech*. 5:1 - 7 (2004).

55. B.M.Z. Zainudin, Biddiscombe, M., Tolfree, S.E.J., Short, M., Spiro, S.G. Comparison of bronchodilator responses and deposition patterns of salbutamol inhaled from a pressurised metered dose inhaler, as a dry powder, and as a nebulised solution. *Thorax*. 45:469 - 473 (1990).
56. L.M. Nolan, J. Li, L. Tajber, O.I. Corrigan, and A.M. Healy. Particle engineering of materials for oral inhalation by dry powder inhalers. II-Sodium cromoglicate. *Int J Pharm*. 405:36-46 (2011).
57. M. Hindle, Byron, P.R., and Miller, N.C. Cascade impaction methods for dry powder inhalers using the high flowrate Marple-Miller Impactor. *Int J Pharm*. 134:137 - 146 (1996).
58. M. Hindle, and Makinen, G.M. Effects of humidity on the in-vitro aerosol performance aerodynamic size distribution of cromolyn sodium for inhalation *European Journal of Pharmaceutical Sciences*. 4:S142 (1996).
59. H. Steckel. In-situ-micronization of disodium cromoglycate for pulmonary delivery. *European Journal of Pharmaceutics and Biopharmaceutics*. 55:173-180 (2003).
60. H. Chrystyn. Is inhalation rate important for a dry powder inhaler? using the In-Check Dial to identify these rates. *Respiratory Medicine*. 97:181 - 187 (2003).
61. G.R. Pitcairn, Lankinen, T., Seppala, O.P., and Newman, S.P. Pulmonary Drug Delivery from the Taifun Dry Powder Inhaler Is Relatively Independent of the Patient's Inspiratory Effort. *Journal of Aerosol Medicine*. 13:97 - 104 (2004).
62. T. Kinnarinen, P. Jarho, K. Järvinen, and T. Järvinen. Pulmonary deposition of a budesonide/ $\gamma$ -cyclodextrin complex in vitro. *Journal of Controlled Release*. 90:197-205 (2003).

63. K.A. Overhoff, R. Clayborough, and M. Crowley. Review of the TAIFUN multidose dry powder inhaler technology. *Drug Dev Ind Pharm.* 34:960-965 (2008).
64. L. Borgström, E. Bondesson, F. Morén, E. Trofast, and S.P. Newman. Lung deposition of budesonide inhaled via Turbuhaler®: a comparison with terbutaline sulphate in normal subjects. *European Respiratory Journal.* 7:69-73 (1994).
65. T. Sebti and K. Amighi. Preparation and in vitro evaluation of lipidic carriers and fillers for inhalation. *Eur J Pharm Biopharm.* 63:51-58 (2006).
66. G. Pitcairn, Reader, S., Pavia, D., and Newman, S. Deposition of Corticosteroid Aerosol in the Human Lung by RespiMat® Soft Mist™ Inhaler Compared to Deposition by Metered Dose Inhaler or by Turbuhaler® Dry Powder Inhaler. *Journal of Aerosol Medicine.* 18: (2005).
67. B.J. Meakin, Caine, J.M, and Woodcock, P.M. Drug delivery characteristics of Bricanyl Turbuhaler® dry powder inhalers. *Int J Pharm.* 119:91 - 102 (1995).
68. L. Borgstrom, Bengtsson, T., Derom, E., and Pauwels, R. Variability in lung deposition of inhaled drug, within and between asthmatic patients, with a pMDI and a dry powder inhaler, Turbuhaler®. *Int J Pharm.* 193:227 - 230 (2000).
69. T.T. Yang, Li, S., Wyka, B., and Kenyon, D. Drug Delivery Performance of the Mometasone Furoate Dry Powder Inhaler. *Journal of Aerosol Medicine.* 14:487 - 494 (2001).
70. G.R. Pitcairn, Lim, J., Hollingworth, A., and Newman, S.P. Scintigraphic Assessment of Drug Delivery from the Ultrahaler Dry Powder Inhaler. *Journal of Aerosol Medicine.* 10:295 - 306 (1997).
71. S. Rohatagi, Chapel, S., Kirkesseli, S., Newman, S., Zhang, J., Paccaly, D., Randall, L., Wray, H., Wellington, S., Shah, B., and Jensen, B.K. Pharmacoscintigraphic Comparison

- of HMR 1031, a VLA-4 Antagonist, in Healthy Volunteers Following Delivery Via a Nebulizer and a Dry Powder Inhaler. *American Journal of Therapeutics*. 11:103 - 113 (2004).
72. J.G.P. Lim, Shah, B., Rohatagi, S., and Bell, A. Development of a Dry Powder Inhaler, the Ultrahaler, Containing Triamcinolone Acetonide Using In Vitro–In Vivo Relationships. *American Journal of Therapeutics*. 13:32 - 42 (2006).

## REFERENCES

- ALSHOWAIR, R., TARSIN, W., ASSI, K., PEARSON, S. & CHRYSTYN, H. 2007. Can all patients with COPD use the correct inhalation flow with all inhalers and does training help? *Respiratory Medicine*, 101, 2395-2401.
- ASHURST, I., MALTON, A., PRIME, D. & SUMBY, B. 2000. Latest advances in the development of dry powder inhalers. *Pharmaceutical Science & Technology Today*, 3, 246-256.
- AYDIN, M., AKOUKA, H., MERRILL, T., REYNOLDS, E., BECKER, D., SHUKLA, R., WEITZEL, D., AND BYRON, D. Application of synthetic jetting for pulmonary delivery of drug candidates.
- BEGAT, P., MORTON, D.A.V., STANIFORTH, J.N., AND PRICE, R. 2004. Dry powder inhaler formulations I: Direct quantification by atomic force microscopy. *Pharmaceutical Research*, 21, 1591 - 1597.
- BISGAARD, H., KLUG, B., SUMBY, B. S. & BURNELL, P. K. P. 1998. Fine particle mass from the Diskus inhaler and Turbuhaler inhaler in children with asthma. *European Respiratory Journal*, 11, 1111-1115.
- BRAMBILLA, G., COCCONI, D., ARMANNI, A., SMITH, S., LYE, E., AND BURGE, S. 2006. Designing a novel dry powder inhaler: The NEXTTM DPI (Part 1). *Respiratory Drug Delivery*, 2, 553 - 555.
- BRONSKY, E. A., GROSSMAN, J., HENIS, M. J., GALLO, P. P., YEGEN, Ü., CIOPPA, G. D., KOTTAKIS, J. & MEHRA, S. 2004. Inspiratory flow rates and volumes with the Aerolizer dry powder inhaler in asthmatic children and adults. *Current Medical Research and Opinion*, 20, 131-137.
- BROWN, B., RASMUSSEN, J., BECKER, D., AND FRIEND, D.R. 2004. A piezo-electronic inhaler for local and systemic applications. *Drug Delivery Technology*, 4, 90 - 93.

- CHEW, N. Y. K., CHAN, H.K., BAGSTER, D.F., AND MUKHRAIYA 2002. Characterization of pharmaceutical powder inhalers: estimation of energy input for powder dispersion and effect of capsule device configuration. *Aerosol Science*, 33, 999 - 1008.
- CHODOSH, S., FLANDERS, J. S., KESTEN, S., SERBY, C. W., HOCHRAINER, D. & WITEK, T. J. 2001. Effective Delivery of Particles with the HandiHaler® Dry Powder Inhalation System over a Range of Chronic Obstructive Pulmonary Disease Severity. *Journal of Aerosol Medicine*, 14, 309-315.
- CHOW, A., TONG, H., CHATTOPADHYAY, P. & SHEKUNOV, B. 2007. Particle Engineering for Pulmonary Drug Delivery. *Pharmaceutical Research*, 24, 411-437.
- CLARK, A. R., AND HOLLINGWORTH, A.M. 1993. The relationship between powder inhaler resistance and peak inspiratory conditions in healthy volunteers - implications for in vitro testing. *Journal of Aerosol Medicine*, 6, 99 - 110.
- CLINE, D., AND DALBY, R. 2002. Predicting the quality of powder for inhalation from surface energy and area. *Pharmaceutical Research*, 19, 1274 - 1277.
- COATES, M. S., CHAN, H.-K., FLETCHER, D. F. & CHIOU, H. 2007. Influence of Mouthpiece Geometry on the Aerosol Delivery Performance of a Dry Powder Inhaler. *Pharmaceutical Research*, 24, 1450-1456.
- COATES, M. S., CHAN, H.-K., FLETCHER, D. F. & RAPER, J. A. 2005a. Influence of Air Flow on the Performance of a Dry Powder Inhaler Using Computational and Experimental Analyses. *Pharmaceutical Research*, 22, 1445-1453.
- COATES, M. S., CHAN, H.-K., FLETCHER, D. F. & RAPER, J. A. 2006. Effect of design on the performance of a dry powder inhaler using computational fluid dynamics. Part 2: Air inlet size. *Journal of Pharmaceutical Sciences*, 95, 1382-1392.

- COATES, M. S., FLETCHER, D. F., CHAN, H.-K. & RAPER, J. A. 2004. Effect of design on the performance of a dry powder inhaler using computational fluid dynamics. Part 1: Grid structure and mouthpiece length. *Journal of Pharmaceutical Sciences*, 93, 2863-2876.
- COATES, M. S., FLETCHER, D. F., CHAN, H.-K. & RAPER, J. A. 2005b. The Role of Capsule on the Performance of a Dry Powder Inhaler Using Computational and Experimental Analyses. *Pharmaceutical Research*, 22, 923-932.
- CROWDER, T. & HICKEY, A. 2006. Powder specific active dispersion for generation of pharmaceutical aerosols. *International Journal of Pharmaceutics*, 327, 65-72.
- CROWDER, T. M., LOUEY, M.D., SETHURAMAN, V.V., SMYTH, H.D.C., AND HICKEY, A.J 2001. An odyssey in inhaler formulation and design. *Pharmaceutical Technology*, 7, 99 - 107.
- DE BOER, A., HAGEDOORN, P., GJALTEMA, D., GOEDE, J. & FRIJLINK, H. 2003a. Air classifier technology (ACT) in dry powder inhalation Part 1. Introduction of a novel force distribution concept (FDC) explaining the performance of a basic air classifier on adhesive mixtures. *International Journal of Pharmaceutics*, 260, 187-200.
- DE BOER, A., HAGEDOORN, P., GJALTEMA, D., GOEDE, J. & FRIJLINK, H. 2006a. Air classifier technology (ACT) in dry powder inhalation Part 3. Design and development of an air classifier family for the Novolizer® multi-dose dry powder inhaler. *International Journal of Pharmaceutics*, 310, 72-80.
- DE BOER, A., HAGEDOORN, P., GJALTEMA, D., GOEDE, J., KUSSENDRAGER, K. & FRIJLINK, H. 2003b. Air classifier technology (ACT) in dry powder inhalation Part 2. The effect of lactose carrier surface properties on the drug-to-carrier interaction in adhesive mixtures for inhalation. *International Journal of Pharmaceutics*, 260, 201-216.
- DE BOER, A., HAGEDOORN, P., WESTERMAN, E., LEBRUN, P., HEIJERMAN, H. & FRIJLINK, H. 2006b. Design and in vitro performance testing of multiple air classifier technology in a

- new disposable inhaler concept (Twincer®) for high powder doses. *European Journal of Pharmaceutical Sciences*, 28, 171-178.
- DE BOER, A. H., GJALTEMA, D., AND HAGEDOORN, P. 1996. Inhalation characteristics and their effects on in vitro drug delivery from dry powder inhalers Part 2: Effect of peak flow rate (PIFR) and inspiration time on the in vitro drug release from three different types of commercial dry powder inhalers. *International Journal of Pharmaceutics*, 138, 45 - 56.
- DE BOER, A. H., HAGEDOORN, P., GJALTEMA, D., LAMBREGTS, D., IRNGARTINGER, M. & FRIJLINK, H. W. 2004. The Mode of Drug Particle Detachment from Carrier Crystals in an Air Classifier-Based Inhaler. *Pharmaceutical Research*, 21, 2167-2174.
- DE BOER, A. H., HAGEDOORN, P., GJALTEMA, D., LAMBREGTS, D., IRNGARTINGER, M., AND FRIJLINK, H.W. 2004. The rate of drug particle detachment from carrier crystals in an air classifier-based inhaler. *Pharmaceutical Research*, 21, 2158 - 2166.
- DICKHOFF, B. 2003. The effect of carrier surface and bulk properties on drug particle detachment from crystalline lactose carrier particles during inhalation, as function of carrier payload and mixing time. *European Journal of Pharmaceutics and Biopharmaceutics*, 56, 291-302.
- DICKHOFF, B., DEBOER, A., LAMBREGTS, D. & FRIJLINK, H. 2005. The interaction between carrier rugosity and carrier payload, and its effect on drug particle redispersion from adhesive mixtures during inhalation. *European Journal of Pharmaceutics and Biopharmaceutics*, 59, 197-205.
- DONOVAN, M. J. & SMYTH, H. D. C. 2010. Influence of size and surface roughness of large lactose carrier particles in dry powder inhaler formulations. *International Journal of Pharmaceutics*, 402, 1 - 9.



- EDWARDS, D. A., HANES, J., CAPONETTI, G., HRKACH, J., BEN-JEBRIA, A., ESKEW, M. L., MINTZES, J., DEEVER, D., LOTAN, N. & LANGER, R. 1997. Large Porous Particles for Pulmonary Drug Delivery. *Science*, 276, 1868-1872.
- EGGINS, B. R. 2002. *Chemical Sensors and Biosensors*, West Sussex, England, John Wiley & Sons Ltd.
- FINLAY, W. H. 2001. *The Mechanics of Inhaled Pharmaceutical Aerosols*, London, UK, Academic Press.
- FLAMENT, M. 2004. The influence of carrier roughness on adhesion, content uniformity and the in vitro deposition of terbutaline sulphate from dry powder inhalers. *International Journal of Pharmaceutics*, 275, 201-209.
- FRENCH, D. L., EDWARDS, D.A., AND NIVEN, R.W. 1996. The influence of formulation on emission, deaggregation and deposition of dry powders for inhalation. *Journal of Aerosol Science*, 27, 769 - 783.
- FRIJLINK, H. W. & DE BOER, A. H. 2004. Dry powder inhalers for pulmonary drug delivery. *Expert Opinion on Drug Delivery*, 1, 67-86.
- FRIJLINK, H. W. & DE BOER, A. H. 2005. Trends in the technology-driven development of new inhalation devices. *Drug Discovery Today: Technologies*, 2, 47-57.
- GUENETTE, E., BARRETT, A., KRAUS, D., BRODY, R., HARDING, L. & MAGEE, G. 2009. Understanding the effect of lactose particle size on the properties of DPI formulations using experimental design. *International Journal of Pharmaceutics*, 380, 80-88.
- GUPTA, V., AND GUPTA, S.K. 1984. *Fluid Mechanics and Its Applications*, New Delhi, New Age International.
- HICKEY, A. J. (ed.) 2004. *Pharmaceutical Inhalation Aerosol Technology*, New York, NY: Marcel Dekker, Inc.

- HICKEY, A. J., MANSOUR, H. M., TELKO, M. J., XU, Z., SMYTH, H. D. C., MULDER, T., MCLEAN, R., LANGRIDGE, J. & PAPADOPOULOS, D. 2007. Physical characterization of component particles included in dry powder inhalers. I. Strategy review and static characteristics. *Journal of Pharmaceutical Sciences*, 96, 1282-1301.
- HOOTON, J. C., JONES, M. D. & PRICE, R. 2006. Predicting the behavior of novel sugar carriers for dry powder inhaler formulations via the use of a cohesive–adhesive force balance approach. *Journal of Pharmaceutical Sciences*, 95, 1288-1297.
- ISLAM, N. & GLADKI, E. 2008. Dry powder inhalers (DPIs)—A review of device reliability and innovation. *International Journal of Pharmaceutics*, 360, 1-11.
- ISLAM, N., STEWART, P., LARSON, I. & HARTLEY, P. 2005. Surface roughness contribution to the adhesion force distribution of salmeterol xinafoate on lactose carriers by atomic force microscopy. *Journal of Pharmaceutical Sciences*, 94, 1500-1511.
- ISLAM, N., STEWART, P., LARSON, I., AND HARTLEY, P. 2004. Lactose surface modification by decantation: are drug-fine lactose ratios the key to better dispersion of salmeterol xinafoate from lactose-interactive mixtures? *Pharmaceutical Research*, 21, 492 - 499.
- JOHANNES, H. W., NIGEL, D. D., JOYCE, M. W., SUNALENE, G. D. & PETER, N. L. 1999. Inhalation therapy in asthma: Nebulizer or pressurized metered-dose inhaler with holding chamber? In vivo comparison of lung deposition in children. *The Journal of pediatrics*, 135, 28-33.
- JONES, M. D. & PRICE, R. 2006. The Influence of Fine Excipient Particles on the Performance of Carrier-Based Dry Powder Inhalation Formulations. *Pharmaceutical Research*, 23, 1665-1674.
- KARHU, M., KUIKKA, J., KAUPPINEN, T., BERGSTROM, K., AND VIDGREN, M. 2000. Pulmonary deposition of lactose carriers used in inhalation powders. *International Journal of Pharmaceutics*, 196, 95 - 103.

- KAWASHIMA, Y., SERIGANO, T., HINO, T., YAMAMOTO, H., AND TAKEUCHI, H. 1998. Effect of surface morphology of carrier lactose on dry powder inhalation property of pranlukast hydrate. *International Journal of Pharmaceutics*, 172, 179 - 188.
- LARHRIB, H. 2003. Characterisation and deposition studies of engineered lactose crystals with potential for use as a carrier for aerosolised salbutamol sulfate from dry powder inhalers. *European Journal of Pharmaceutical Sciences*, 19, 211-221.
- LARHRIB, H., ZENG, X.M., MARTIN, G.P., MARRIOTT, C., AND PRITCHARD, J. 1999. The use of different grades of lactose as a carrier for aerosolised salbutamol sulphate. *International Journal of Pharmaceutics*, 191, 1 - 14.
- LAWS, E. M., AND LIVESEY, J.L. 1978. Flow through screens. *Annual Reviews in Fluid Mechanics*, 10, 247 - 266.
- LOUEY, M. D., AND STEWART, P.J. 2002. Particle interactions involved in aerosol dispersion of ternary interactive mixtures. *Pharmaceutical Research*, 19, 1524 - 1531.
- LOUEY, M. D., MULVANEY, P., AND STEWART, P.J. 2001. Characterisation of adhesional properties of lactose carriers using atomic force microscopy. *Journal of Pharmaceutical and Biomedical Analysis*, 25, 559 - 567.
- LOUEY, M. D., RAZIA, S., AND STEWART, P.J. 2003. Influence of physico-chemical carrier properties on the in vitro aerosol deposition from interactive mixtures. *International Journal of Pharmaceutics*, 252, 87 - 98.
- LUCAS, P., ANDERSON, K., AND STANIFORTH, J.N. 1998. Protein Deposition from Dry Powder Inhalers: Fine Particle Multiplets as Performance Modifiers. *Pharmaceutical Research*, 15, 562 - 69.

- MARPLE, V. A., ROBERTS, D.L., ROMAY, F.J. AND HOCHRAINER, D. 2003. Next generation pharmaceutical impactor (A new impactor for pharmaceutical inhaler testing). Part I: Design. *Journal of Aerosol Medicine*, 16, 283 - 299.
- MEAKIN, B. J., GANDERTON, D., PANZA, I. & VENTURA, P. 1998. The Effect of Flow Rate on Drug Delivery from the Pulvinal, a High-Resistance Dry Powder Inhaler. *Journal of Aerosol Medicine*, 11, 143-152.
- MENDES, P., PINTO, J. & SOUSA, J. 2007. A non-dimensional functional relationship for the fine particle fraction produced by dry powder inhalers. *Journal of Aerosol Science*, 38, 612-624.
- NEEDHAM, M., FRADLEY, G., AND COCKS, P. 2010. Investigating the efficiency of reverse cyclone technology for DPI drug delivery. *Respiratory Drug Delivery*, 2, 369 - 372.
- NICHOLS, S. C., AND WYNN, E. 2008. New Approaches to Optimizing Dispersion in Dry Powder Inhalers – Dispersion Force Mapping and Adhesion Measurements. *Respiratory Drug Delivery 2008*, 1, 175 - 184.
- NIELSEN, K. G., SKOV, M., KLUG, B., IFVERSEN, M. & BISGAARD, H. 1997. Flow-dependent effect of formoterol dry-powder inhaled from the Aerolizerfi. *European Respiratory Journal*, 10, 2105-2109.
- PITCHAYAJITTIPONG, C., PRICE, R., SHUR, J., KAERGER, J. S. & EDGE, S. 2010. Characterisation and functionality of inhalation anhydrous lactose. *International Journal of Pharmaceutics*, 390, 134-141.
- PODCZECK, F. 1998a. Evaluation of the Adhesion Properties of Salbutamol Sulphate to Inhaler Materials. *Pharmaceutical Research*, 15, 806-808.

- PODCZEK, F. 1998b. The relationship between physical properties of lactose monohydrate and the aerodynamic behaviour of adhered drug particles. *International Journal of Pharmaceutics*, 160, 119 - 130.
- POPE, S. B. 2000. *Turbulent Flows*, Cambridge University Press.
- SAINTLORANT, G., LETERME, P., GAYOT, A. & FLAMENT, M. 2007. Influence of carrier on the performance of dry powder inhalers. *International Journal of Pharmaceutics*, 334, 85-91.
- SALEEM, I., SMYTH, H. & TELKO, M. 2008. Prediction of Dry Powder Inhaler Formulation Performance From Surface Energetics and Blending Dynamics. *Drug Development and Industrial Pharmacy*, 34, 1002-1010.
- SELVAM, P., MAREK, S., TRUMAN, C. R., MCNAIR, D. & SMYTH, H. 2011. Micronized Drug Adhesion and Detachment from Surfaces: Effect of Loading Conditions. *Aerosol Science and Technology*, 45, 81-87.
- SELVAM, P., MCNAIR, D., TRUMAN, R. & SMYTH, H. D. C. 2010. A novel dry powder inhaler: Effect of device design on dispersion performance. *International Journal of Pharmaceutics*, 401, 1-6.
- SHUR, J., HARRIS, H., JONES, M. D., KAERGER, J. S. & PRICE, R. 2008. The Role of Fines in the Modification of the Fluidization and Dispersion Mechanism Within Dry Powder Inhaler Formulations. *Pharmaceutical Research*, 25, 1631-1640.
- SMYTH, H. D. C., AND LEACH, C.L. 2005. Alternative propellant aerosol delivery systems. *Critical Reviews in Therapeutic Drug Carrier Systems*, 22, 493 - 534.
- SRICHANA, T., MARTIN, G. P. & MARRIOTT, C. 1998. Dry powder inhalers: The influence of device resistance and powder formulation on drug and lactose deposition in vitro. *European Journal of Pharmaceutical Sciences*, 7, 73-80.

- SRICHANA, T., MARTIN, G.P, AND MARRIOTT, C. 1998. On the relationship between drug and carrier deposition from dry powder inhalers in vitro. *International Journal of Pharmaceutics*, 167, 13 - 23.
- STANIFORTH, J. N. 1995. Performance-modifying influences in dry powder inhalation systems. *Aerosol Science and Technology*, 22, 346 - 353.
- STECKEL, H. 2004. Alternative sugars as potential carriers for dry powder inhalations. *International Journal of Pharmaceutics*, 270, 297-306.
- STECKEL, H., AND MULLER, B.W. 1997. In vitro evaluation of dry powder inhalers II: influence of carrier particle size and concentration on in vitro deposition. *International Journal of Pharmaceutics*, 154, 31 - 37.
- STEIN, S., HODSON, D., ALBAND, T., SITZ, R., ROBISON, T., WANG, Z., CHIOU, H., SIMONS, J., MCNALLY, R., AND GANSER, J. 2010. The 3M™ taper dry powder inhaler device. *Respiratory Drug Delivery*, 2, 377 - 380.
- TEE, S. K., MARRIOTT, C., ZENG, X.M., AND MARTIN, G.P. 2000. The use of different sugars as fine and coarse carriers for aerosolised salbutamol sulphate. *International Journal of Pharmaceutics*, 208, 111 - 123.
- TELKO, M. J. & HICKEY, A. J. 2007. Critical assessment of inverse gas chromatography as means of assessing surface free energy and acid-base interaction of pharmaceutical powders. *Journal of Pharmaceutical Sciences*, 96, 2647-2654.
- TULEY, R., SHRIMPTON, J., JONES, M., PRICE, R., PALMER, M. & PRIME, D. 2008. Experimental observations of dry powder inhaler dose fluidisation. *International Journal of Pharmaceutics*, 358, 238-247.
- VOSS, A., AND FINLAY, W.H. 2002. Deagglomeration of dry powder pharmaceutical aerosols. *International Journal of Pharmaceutics*, 248, 39 - 50.

- WACHTEL, H., ERTUNC, O., KOKSOY, C., AND DELGADO, A. 2008. Aerodynamic Optimization of Handihaler and Respimat: The Roles of Computational Fluid Dynamics and Flow Visualization. *Respiratory Drug Delivery 2008*, 1, 165 - 174.
- WATLING, C. P., ELLIOTT, J. A. & CAMERON, R. E. 2010. Entrainment of lactose inhalation powders: A study using laser diffraction. *European Journal of Pharmaceutical Sciences*, 40, 352-358.
- WETTERLIN, K. 1988. Turbuhaler: A new powder inhaler for administration of drugs to the airways. *Pharmaceutical Research*, 5, 506 - 508.
- ZENG, X. M., MARTIN, G.P., MARRIOTT, C., AND PRITCHARD, J. 2000. The influence of carrier morphology on drug delivery by dry powder inhalers. *International Journal of Pharmaceutics*, 200, 93 - 106.
- ZENG, X. M., MARTIN, G.P., MARRIOTT, C., AND PRITCHARD, J. 2001. Lactose as a carrier in dry powder formulations: The influence of surface characteristics on drug delivery. *Journal of Pharmaceutical Sciences*, 90, 1424 - 1434.
- ZENG, X. M., MARTIN, G.P., TEE, S.K., AND MARRIOTT, C. 1998. The role of fine particle lactose on the dispersion and deaggregation of salbutamol sulphate in an air stream in vitro. *International Journal of Pharmaceutics*, 176, 99 - 110.
- ZENG, X. M., MARTIN, G.P., TEE, S.K., GHOUSH, A.A., AND MARRIOTT, C. 1999. Effects of particle size and adding sequence of fine lactose on the deposition of salbutamol sulphate from a dry powder formulation. *International Journal of Pharmaceutics*, 182, 133 - 144.

## VITA

Martin Joseph Donovan was born and raised in Texas. He pursued his undergraduate studies at the University of Texas at El Paso, where he graduated summa cum laude with a Bachelor of Science in Chemistry in 2004. Following completion of his bachelor's degree, Martin enrolled in the Biomedical Sciences graduate program at the University of New Mexico, where he performed research in laboratory of Hugh Smyth. In 2009, Martin accompanied his advisor to The University of Texas at Austin, enrolling in the Pharmaceutics Division in the College of Pharmacy. He is currently residing in Austin, Texas.

Email Address: [mjdonovan@utexas.edu](mailto:mjdonovan@utexas.edu)

This dissertation was typed by the author.